Synthetic Investigations of Molecular *s*-block Organometallic Chemistry Supported by Singlet Carbenes

Lucas A. Freeman

B.S. Chemistry, College of Charleston, 2017

A Dissertation presented to the Graduate Faculty
of the University of Virginia in Candidacy for the degree of
Doctor of Philosophy

Department of Chemistry

University of Virginia
October 2021

Abstract.

Singlet *N*-heterocyclic carbenes and cyclic(alkyl)(amino) carbenes have transformed many aspects of modern organic and organometallic chemistry. These ligands have been used to support and stabilize a wide array of highly reactive molecular fragments. Carbenes have proven especially useful in stabilizing electron-rich or hydridic main group organometallic compounds that would be otherwise inaccessible. In the *s*-block, the isolation and study of such compounds is a highly sought-after goal at the forefront of the field. As such, much effort has been placed on developing appropriate ligand platforms to allow for reliable synthetic chemistry with *s*-block elements under mild conditions. Success toward this goal has been achieved when a strongly coordinating, anionic supporting ligand was used, as will be discussed in Chapter 1. These ligands afford a high degree of control over the many decomposition pathways known for alkaline earth compounds; however, this stability comes at the price of somewhat restricting the chemistry that can occur at the metal center. By contrast, carbene-supported systems allow for a high degree of coordinative flexibility at the metal center, but using singlet carbenes to support alkali and alkaline earth chemistry has proved difficult. A number of synthetic challenges remain in this area, but solving these difficulties with well-designed synthetic protocols is critical to unlocking new reaction motifs for alkaline earth systems.

The doctoral research presented herein covers a multi-year effort to expand the known coordination chemistry of carbene-supported alkaline earth fragments. In work presented in chapter 2, the reduction chemistry of carbene–magnesium complexes was studied in detail. This effort resulted in a series of magnesium–diimine compounds that can be reduced in a stepwise fashion to yield highly sought-after electron-rich alkaline earth compounds with unusual electronic structures. Moreover, these reduced compounds were compared with their beryllium

analogs, yielding a rare opportunity to comparatively study the first two alkaline earth elements in a combined synthetic and computational investigation.

Described in chapter 3, a reliable and high-yielding synthetic method was discovered for obtaining hydrocarbon-soluble, low-nuclearity, carbene-supported magnesium hydride complexes. Despite their high synthetic utility, it is notoriously challenging to synthesize alkaline earth hydride compounds which can be studied in solution and maintain discrete stable molecular structures without ligand dissociation or exchange. This is especially true when using neutral donor ligands such as carbenes, so there is substantial value associated with reliable synthetic procedures like those presented in chapter 3.

Chapter 4 details the investigation of direct reduction chemistry of carbene–CO_2 adducts, known as carbene-2-carboxylates, resulting in both metal-free and alkali-mediated reduction of C═O bonds of carbon dioxide. In electrochemical systems, a CAAC-2-carboxylate can accept on electron to form a radical anion which itself can undergo further reaction with free CO_2. The result of this transformation is the reductive disproportionation of two units of CO_2 to CO and CO_3^{2-}. When alkali metal reductants were used in place of electrochemical reduction, one- and two-electron reduced CAAC–CO_2 clusters incorporating alkali cations were obtained. Notably, these reduced compounds were soluble, crystalline, and thermally stable thanks to the presence of the carbene fragment. These results represent a substantial addition to the known chemistry of these popular synthetic reagents. Prior to this study, no reports existed focused on solely on the electron-acceptor capabilities of carbene-2-carboxylates, despite their common use in systems focused on CO_2 reduction.

Copyright Information

Chapters 1–4 contain modified versions of published work which have been reproduced in accordance with the American Chemical Society Journal Publishing Agreement (ACS.org), John Wiley and Sons Publication Agreement (chemistry-europe.onlinelibrary.wiley.com), and Royal Society of Chemistry Publication Agreement (RSC.org). Proper citation for each chapter is given below and on the first page of each of the chapters within this thesis.

Chapter 1.

Freeman, L. A.; Walley, J. E.; Obi, A. D.; Wang, G.; Dickie, D. A.; Molino, A.; Wilson, D. J. D.; Gilliard, R. J., Stepwise Reduction at Magnesium and Beryllium: Cooperative Effects of Carbenes with Redox Non-Innocent α-Diimines. *Inorg. Chem.* **2019,** *58* (16), 10554-10568.

https://doi.org/10.1021/acs.inorgchem.9b01058

Freeman, L. A.; Walley, J. E.; Dickie, D. A.; Gilliard, R. J., Low-nuclearity magnesium hydride complexes stabilized by N-heterocyclic carbenes. *Dalton Trans.* **2019,** *48*, 17174-17178. https://doi.org/10.1039/C9DT03915E

Lieske, L. E.; Freeman, L. A.; Wang, G.; Dickie, D. A.; Gilliard, R. J., Jr.; Machan, C. W., Metal-Free Electrochemical Reduction of Carbon Dioxide Mediated by Cyclic(Alkyl)(Amino) Carbenes. *Chem. Eur. J.* **2019**, *25*, 6098-6101.

https://doi.org/10.1002/chem.201900316

Freeman, L. A.; Obi, A. D.; Machost, H. R.; Molino, A.; Nichols, A. W.; Dickie, D. A.; Wilson, D. J. D.; Machan, C. W.; Gilliard, R. J., Soluble, crystalline, and thermally stable alkali $CO2^{-}$ and carbonite ($CO2^{2-}$) clusters supported by cyclic(alkyl)(amino) carbenes. *Chem. Sci.* **2021,** *12*, 3544-3550.

https://doi.org/10.1039/D0SC06851A

Chapter 2.

Freeman, L. A.; Walley, J. E.; Obi, A. D.; Wang, G.; Dickie, D. A.; Molino, A.; Wilson, D. J. D.; Gilliard, R. J., Stepwise Reduction at Magnesium and Beryllium: Cooperative Effects of Carbenes with Redox Non-Innocent α-Diimines. *Inorg. Chem.* **2019,** *58*, 10554-10568.

https://doi.org/10.1021/acs.inorgchem.9b01058

Wong, Y. O.; Freeman, L. A.; Agakidou, A. D.; Dickie, D. A.; Webster, C. E.; Gilliard, R. J., Two Carbenes versus One in Magnesium Chemistry: Synthesis of Terminal Dihalide, Dialkyl, and Grignard Reagents. *Organometallics* **2019,** *38*, 688-696.

https://doi.org/10.1021/acs.organomet.8b00866

Chapter 3.

Freeman, L. A.; Walley, J. E.; Dickie, D. A.; Gilliard, R. J., Low-nuclearity magnesium hydride complexes stabilized by N-heterocyclic carbenes. *Dalton Trans.* **2019,** *48*, 17174-17178.

https://doi.org/10.1039/C9DT03915E

Chapter 4.

Lieske, L. E.; Freeman, L. A.; Wang, G.; Dickie, D. A.; Gilliard, R. J., Jr.; Machan, C. W., Metal-Free Electrochemical Reduction of Carbon Dioxide Mediated by Cyclic(Alkyl)(Amino) Carbenes. *Chem. Eur. J.* **2019**, *25*, 6098-6101.

https://doi.org/10.1002/chem.201900316

Freeman, L. A.; Obi, A. D.; Machost, H. R.; Molino, A.; Nichols, A. W.; Dickie, D. A.; Wilson, D. J. D.; Machan, C. W.; Gilliard, R. J., Soluble, crystalline, and thermally stable alkali $CO2^{-}$ and carbonite ($CO2^{2-}$) clusters supported by cyclic(alkyl)(amino) carbenes. *Chem. Sci.* **2021,** *12*, 3544-3550.

https://doi.org/10.1039/D0SC06851A

Acknowledgements.

To my incredible and irreplaceable wife, Emily, thank you for your unwavering support, encouragement, and motivation on the difficult days, and thank you for celebrating with me on the good days. Moreover, thank you for still at least pretending to be interested when I talk about some interesting science thing after 9+ years of me taking chemistry classes.

To my parents, Allen and Jenny, thank you for always encouraging me to pursue my passions, and for instilling in me a sense of personal accountability and responsibility to always follow through on my commitments. I am so grateful to have had two such excellent examples to emulate while finding my way in this world.

To my parents-in-law, Kim and Jerry, thanks for always treating me as one of your own, and for always supporting Emily and I at every opportunity. Thank you also for instilling in us a subtle appreciation for wines which we have found valuable amongst the flourishing vineyards around Charlottesville.

To all of my past and present lab mates, it was a joy working with you and growing together as chemists and people. Through lots of the failed experiments, broken glassware, and reagents on back-order, our friendships and debriefing sessions helped me to stay sane and try the recrystallization one more time.

To Kelsie and Jacob, my longest-standing cohort and closest companions in the Gilliard group, I am so grateful to have gone through graduate school with you both from start to finish. From our first days in lab unpacking boxes, to working out at the AFC after our evening class, to all of the innumerable coffee runs – I will cherish our memories and these experiences for a lifetime. I am so excited to follow your journeys as scientists and people. Most of all, I am glad that I get to defend first, because you two will set the bar incredibly high for anyone that follows.

To my collaborators outside of the Gilliard group – Andrew, Nathan, Lauren, Asa, Prof. Machan, Prof. Webster, and Prof. Wilson – thank you so much for making each collaboration unique and exciting, and for teaching me so much about your areas of expertise. I am a better scientist because of each of our projects together.

To all my chemistry teachers and professors through my many years of formal education, thank you for fostering in me a passion for the chemical sciences, and for giving me the knowledge needed to appreciate the beauty of nature at the molecular level.

To my high school chemistry teacher, Mrs. Noyes, thank you so much for putting up with my attitude as a high schooler that could not be bothered with homework assignments, making me take AP chemistry my senior year, and most of all for not letting me waste my potential on the easy and lazy ways out. I owe you so much gratitude for setting me on the path to where I find my self today.

To my undergraduate academic and research advisors at the College of Charleston and the University of Bristol – Profs. Rogers, Himes, Boucher, and Bedford – thank you all for your thoughtful guidance, for trusting me to conduct your research, and for assuring me that a Ph.D. was accessible for someone like me.

Lastly to my doctoral advisor, Robert: Thank you for letting me take part in founding your research program, for teaching me (us) so many lessons, for your patience with me during hard times, for pushing me to be my best, for not letting me settle for good enough, for all of your imparted wisdom, and for making jokes only we South Carolinians can fully appreciate.

Table of Contents

List of Abbreviations

Ae	any alkaline earth element
Li	lithium
Na	sodium
K	potassium
Be	beryllium
Mg	magnesium
Ca	calcium
H	hydrogen
Ar	argon
Si	silicon
Cl	chlorine
O	oxygen
O_2	dioxygen
CAAC	cyclic(alkyl)(amino) carbene
^{Et2}CAAC	3,3-diethyl CAAC
^{Cy}CAAC	3-spirocyclohexyl CAAC
NHC	*N*-heterocyclic carbene
IPr	1,3-*bis*(2,6-diisopropylphenyl)imidazole-2-ylidine

$\mathrm{I^{i}Pr^{Me2}}$	*N*,*N′*-diisopropyl-2,3-dimethylimidazol-2-ylidine
SIPr	1,3-bis(2,6-diisopropylphenyl)-4,5-dihydroimidazole-2-ylidene
Dipp	2,6-diisopropylphenyl
Mes	2,4,6-trimethylphenyl
*i*Pr	*iso*-propyl
THF	tetrahydrofuran
THF-d_8	perdeuterated tetrahydrofuran-d_8
MeCN	acetonitrile
C_6H_6	benzene
C_6D_6	perdeuterated benzene or benzene-d_6
CD_2Cl_2	perdeuterated dichloromethane or dichloromethane-d_2
$CDCl_3$	deuterated chloroform or chloroform-*d*
Et_2O	diethyl ether
H_2	dihydrogen
H_2O	water
CO_2	carbon dioxide
CO	carbon monoxide
CO_3^{2-}	carbonate

N_2O	nitrous oxide
KC_8	potassium graphite (intercalation compound)
5% Na/NaCl	dispersion of elemental sodium (5% mass) on sodium chloride
HOMO	highest occupied molecular orbital
LUMO	lowest occupied molecular orbital
SOMO	singly occupied molecular orbital
$^{\mathrm{Dipp}}$BIAN	1,2-bis[(2,6-diisopropylphenyl)imino]acenaphthene
$^{\mathrm{Dipp}}$DAB	*N*,*N*-bis(2,6-diisopropylphenyl)-1,4-diaza-1,3-butadiene
DAB	1,4-diazabutadienes, generally
BIAN	*bis*-imino acenaphthenes, generally
Bpy	2,2-bipyridine
CAAC–CO_2	adduct of CAAC and CO_2, also CAAC-2-carboxylate
carbene–CO_2	general abbreviation for a carbene-2-carboxylate compound
wt.%	weight percentage or gravimetric percentage
CaO	calcium oxide
MgO	magnesium oxide
CaH_2	calcium dihydride
MgH_2	magnesium dihydride

RMgCl	general alkyl magnesium chloride where R = alkyl
$CaCl_2$	calcium chloride
ASCP	2,2,5,5-tetramethyl-2,5-disila-1-azacyclopent-1-yl
HMDS	hexamethyldisilazide
$K[N(SiMe_3)_2]$	potassium hexamethyldisilazide or potassium *bis*(trimethylsilyl)amide
KHMDS	potassium hexamethyldisilazide or potassium *bis*(trimethylsilyl)amide
nBuLi	*n*-butyllithium
DFT	density functional theory
TD-DFT	time-dependent density functional theory
NBO	natural bond orbital
EDA	energy decomposition analysis
NRT	Natural Resonance Theory
QM	quantum mechanics/quantum mechanical
QT-AIM	quantum theory of atoms in molecules
Å	Ångstroms
deg.	degrees (°)
ppm	parts per million

cm^{-1}	inverse centimeters or wavenumbers (ν)
nm	nanometers
cm	centimeters
UV-Vis	ultraviolet-visible
FTIR	Fourier-transform infrared
NMR	nuclear magnetic resonance
^{1}H NMR	proton nuclear magnetic resonance
^{13}C NMR	carbon-13 nuclear magnetic resonance
EPR/ESR	electron paramagnetic resonance/electron spin resonance
CW	continuous wave
CV	cyclic voltammetry
IR-SEC	infrared-spectroelectrochemistry
Fc^{+}/Fc	ferrocenium/ferrocene
SC-XRD	single crystal-X-ray diffraction
COD	cyclooctadienyl
Rh	rhodium
$TBA(HCO_3)$	tetrabutylammonium bicarbonate
Ag/AgCl	silver/silver chloride

TBA(PF_6)	tetrabutylammonium hexafluorophosphate
TBA(ox)	tetrabutylammonium oxalate

List of Figures

Br1: 2.4642(14); Mg1–N2: 2.097(4); Mg1–N3: 2.140(5); C35–N2: 1.341(7); C36–N3: 1.347(4); C35–C36: 1.404(7); C1–Mg1–Br1: 114.68(12); C35–N2–Mg1: 105.6(3). **2.8**: Mg1–C1: 2.246(4); C1–N1: 1.301(5); Mg1–Br1: 2.4724(15); Mg1–N2: 2.073(4); Mg1–N3: 2.069(4); C27–N2: 1.383(5); C28–N3: 1.389(5); C27–C28: 1.409(6); C1–Mg1–Br1: 108.92(11); C27–N2–Mg1: 112.8(3).

Figure 2.4. Plot of frontier molecular orbitals for singly-reduced magnesium complexes.

Figure 2.7. Molecular structure of **2.9** (H atoms omitted for clarity). Selected bond distances (Å) and angles (°): Mg1–C1: 2.194(2); Mg1–N2: 1.9644(16); Mg1–N3: 1.9682(16); C23–N2: 1.410(2); C24–N3: 1.410(2); C23–C24: 1.342(3); C1–Mg1–N2: 144.38(7); N2–Mg1–N3: 90.79(7).

Figure 2.8. Plot of HOMO (left) and HOMO-1 (right) for compound **2.9^{NMe}**.

Figure 2.9. Molecular structure of **2.10** (H atoms and Dipp-isopropyl groups omitted for clarity). Selected bond distances (Å) and angles (°): Mg1–N2: 2.000(2); Mg1–N1: 2.157(2); Mg1–C1: 2.138(3); Mg1–C1’: 2.284(3); Mg1–C2: 2.629(3); Mg1–Mg1’: 3.1017(16); N2–Mg1–N1: 85.02(8); N2–Mg1–C1: 120.65(9).

Figure 3.1. Syntheses of carbene-coordinated magnesium hydride complexes.

Figure 3.2. Molecular structure of **3.2** (a) and **3.3** (b) (thermal ellipsoids at 50% probability; H atoms omitted for clarity with the exception of those located on C10 in **3.3**); only the major occupied position is shown for disordered *N*-isopropyl substituents in (b). Selected bond distances (Å) and angles (deg): **3.2**: Mg1–C1: 2.2120(19); Mg1–N3: 1.9920(16); Mg1–N4: 1.9944(16); C1–N1: 1.360(2); C1–N2: 1.361(2); N3–Mg1–C1: 111.75(7); N4–Mg1–C1: 117.82(7); N4–Mg1–N3: 130.27(7). **3.3**: Mg1–C1: 2.2118(13); Mg1–H10A: 2.429(16); Mg1–N3: 1.9855(10); Mg1–N4: 1.9755(11); C1–N1: 1.3572(16); C1–N2: 1.3583(15); N3–Mg1–C1: 113.92(4); N4–Mg1–C1: 115.06(4); N4–Mg1–N3: 130.62(4); C1–Mg1–H10A: 78.4(4); C10–H10A–Mg1: 121.1(11).

Figure 3.3. Molecular structures of **3.4** (a) and **3.5** (b) [thermal ellipsoids set at 50%; H atoms omitted for clarity with the exception of H1 and H2 which were isotropically refined; only the major occupied position is shown for disordered *N*-isopropyl substituents in (b)]. Selected bond distances (Å) and angles (deg): **3.4**: Mg1–C1: 2.2239(17); Mg2–C18: 2.2250(16); Mg1–H1: 1.828(18); Mg1–H2: 1.933(18); Mg2–H1: 1.861(17); Mg2–H2: 1.865(18); Mg1–Mg2 2.8269(9); Mg1–N3: 2.0098(14); Mg2–N6: 2.0144(14); N3–Mg1–C1: 118.02(6); C1–Mg1–H1: 105.3(6); H1–Mg1–H2: 81.4(8). **3.5**: Mg1–C1: 2.230(4); Mg2–C12: 2.228(4); Mg1–H1: 1.93(4); Mg1–H2: 1.93(4); Mg2–H1: 1.97(4); Mg2–H2: 1.82(4); Mg1–Mg2; 2.8163(19); Mg1–N3: 1.994(4); Mg2–N6: 2.000(4); N3–Mg1–C1: 119.27(16); C1–Mg1–H1: 107.1(12); H1–Mg1–H2: 84.4(17).

Figure 4.1. (A) Molecular structure of compound **4.1** (thermal ellipsoids at 40% probability; only one of the two chemically equivalent but crystallographically distinct molecules is shown). H atoms and co-crystallized THF solvent molecules omitted for clarity. Selected bond distances (Å) bond angles (°) and torsion angles (°): C1–C24: 1.526(4); C1–N1: 1.297(4); O1–C24 1.236(4); O2–C24: 1.234(4); N1–C1–C24: 123.9(3); O2–C24–O1: 131.5(3); O1–C24–C1: 113.7(3); N1–C1–C24–O2: 101.2(4). (B) Stick representations of the DFT optimized structures of **4.1** (gray, blue and red) and **[4.1]**$^{-}$ (light blue). ORCA 4.0.1 B3LYP/G, def2-TZVP, CPCM(THF).

Figure 4.2. CV response of **4.1** at reducing potentials under an inert atmosphere (black) and CO_2 saturation (red) in THF. Conditions: 5 mM **4.1**, 0.1 M $TBAPF_6$/THF glassy carbon working electrode, glassy carbon counter electrode, Ag/AgCl pseudoreference electrode, referenced to internal ferrocene standard.

Figure 4.3. (A) Disappearance of the CO_2 adduct at 1670 cm^{-1} as the reduced species **[4.1]**$^{-}$ grows in and disappears at 1531 cm^{-1} at reducing conditions under Ar saturation monitored by IR-SEC. Presumptive ketene **4.2** degradation products appear at 1660 and 1603 cm^{-1}. (B) Comparable experiments under CO_2 saturation conditions show the loss of the CO_2 adduct upon the formation of CO_3^{2-} (1690 and 1635 cm^{-1}).

Figure 4.4. Previous methods used to study highly reactive alkali-CO_2 salts (Top). Method of synthesizing stable alkali CO_2 salts utilizing carbene stabilization reported herein (Bottom); Dipp = 2,6-diisopropylphenyl.

Figure 4.5. Solid state molecular structures of **4.4** (A), **4.5** (B), and **4.6** (C). All H atoms and carbon atoms not directly attached to the CAAC core ring are omitted for clarity. Selected bond distances (Å) and angles (deg): **4.4**: O1–C1: 1.2732(12); O2–C1: 1.2778(12); C1–C2: 1.4533(13); N1–C2: 1.3802(12); O1–C1–O2: 123.71(9); O1–C1–C2: 119.84(9); O2–C1–C2: 116.45(9); N1–C2–C1: 124.85(9); N1–C2–C3: 110.81(8). **4.5**: O1–C1: 1.286(3); O2–C1: 1.266(3); C1–C2: 1.458(3); N1–C2: 1.385(3); O2–C1–O1: 122.9(2); O2–C1–C2: 118.7(2); O1–C1–C2: 118.3(2); N1–C2–C1: 124.7(2); N1–C2–C3: 109.7(2). **4.6**: O1–C1: 1.276(6); O2–C1: 1.265(7); C1–C2: 1.451(7); N1–C2: 1.384(6); O2–C1–O1: 123.0(5); O2–C1–C2: 119.1(5); O1–C1–C2: 117.9(5); N1–C2–C1: 123.3(5); N1–C2–C3: 110.2(4).

Figure 4.6. Continuous Wave X-band EPR spectra of **4.4-4.6** taken on a 250 μM toluene solution at RT.

Figure 4.7. Plots of the SOMOs of **4.4** (A), **4.5** (B), and **4.6** (C). H atoms and THF (in B and C) omitted for clarity.

Figure 4.8. Digital image of the mixture of compounds **4.7** (red crystals) and **4.8** (yellow crystals) (A), **4.9** (B), and **4.10** (C) viewed at 40x magnification on an optical microscope.

Figure 4.9. Solid state molecular structure of **4.7** (A) and **4.8** (B). All H atoms and carbon atoms not directly attached to the CAAC core ring are omitted for clarity. Selected bond distances (Å) and angles (deg): **4.7**: O1–C1: 1.354(7); O2–C1: 1.332(7); C1–C2: 1.379(8); N1–C2: 1.463(7); O2–C1–O1: 114.1(5); O1–C1–C2: 121.2(5); O2–C1–C2: 124.6(5); C1–C2–N1: 120.0(5); N1–C2–C3: 109.6(5). **4.8**: O1–C1: 1.365(2); O2–C1: 1.360(2); C1–C2: 1.343(3); N1–C2: 1.452(2); O2–C1–O1: 114.20(15); C2–C1–O1: 120.63(16); C2–C1–O2: 125.16(16); C1–C2–N1: 121.20(16); N1–C2–C3: 110.58(15).

Figure 4.10. Solid state molecular structures of **4.9** (A) and **4.10** (B). All H atoms and all carbon atoms not directly attached to the CAAC core ring are omitted for clarity. Selected bond distances (Å) and angles (deg): **4.9**: O1–C1: 1.364(4); O2–C1: 1.336(4); C1–C2: 1.365(5); N1–C2: 1.452(4); O2–C1–O1: 113.4(3); O1–C1–C2: 124.0(3); C1–C2–N1: 122.9(3); N1–C2–C3: 107.9(3). **4.10**: O9–C93: 1.342(10); O10–C93: 1.304(9); C93–C94: 1.385(11); N5–C94: 1.455(9); O10–C93–O9: 115.8(7); O9–C93–C94: 120.0(7); C93–C94–N5: 119.5(6); N5–C94–C95: 108.7(6).

List of Schemes

Scheme 2.1. Reactions of ^{Et2}CAAC with MgCl$_2$.

Scheme 2.2. Reactions of IPr with MgCl$_2$.

Scheme 2.3. Reactions of SIPr and ^{Et2}CAAC with MgBr$_2$.

Chapter One: Introduction and Overview

1.1. Overview of Group 2 Organometallic Chemistry – Historical to Modern-Day

Over the past two decades, the field of main group chemistry has received dramatic growth as chemists the world over have made a concerted effort to more fully develop the synthetic chemistry that is possible with main group elements (i.e., the *s*- and *p*-blocks). One of the primary reasons for this growth – aside from the goal of expanding the known chemistry of the entire periodic table – has been a paradigm shift in modern chemistry towards a set of principles and practices known as "Green Chemistry."[1] This core set of tenets has become a necessary framework around which to redesign the chemical academia and industry in order to build a more sustainable system. Many main group elements are inexpensive, non-toxic and Earth-abundant – desirable characteristics around which to build a robust modern synthetic platform. This is especially true of the alkaline earth elements. The elements of group 2 are inexpensive, earth-abundant, and non-toxic (with the notable exceptions of Be and Ra). Magnesium (2.33 wt.%) and calcium (4.15 wt.%) are the #5 and #7 most abundant elements in the Earth's crust, and magnesium oxide (MgO, 35.07%) and calcium oxide (CaO, 4.37%) place at #2 and #5 respectively in the 10 most abundant compounds in the Earth's crust.[2] Despite their natural predisposition towards being "green" elements for chemical synthesis, common compounds of group 2 elements are either extremely inert (e.g., $CaCO_3$, $MgSO_4$, $CaCl_2$, etc.) or highly reactive (e.g., CaH_2,[3] RMgCl,[4] etc.) under ambient conditions, which has made their chemistry relatively daunting to study. As such, applications of alkaline earth metals have historically been confined to stoichiometric reagents for reductive nucleophilic substitutions with organic electrophiles.[4-8] These more traditional applications are discussed briefly in the following section. Thereafter a glimpse is given of how group 2 chemistry of the past two decades has built upon the foundation of the 20th century and unlocked completely new frontiers of reactivity with the elements first favored by German chemists in the late 1800's/early 1900's.

Organometallic compounds of *s*-block elements have been studied since as early as the mid 1800's, when pioneering chemists such as E. Frankland, and J. A. Wanklyn were pursuing alkyl radicals by reacting ethyl iodide first with alkali metals before, famously, choosing less reactive zinc metal.[9, 10] These initial discoveries were followed shortly thereafter by the important studies of alkyllithium and alkylmagnesium compounds by V. Grignard, W. Schlenk,[11, 12] and their protégés. *s*-Block organometallic compounds are now among the most fundamental and ubiquitous tools in chemical synthesis. Indeed, the molecular compounds of groups 1 and 2 have substantially impacted each of the other "blocks" of the periodic table. These reagents serve as some of the most potent bases and reducing agents used in organic synthesis,[13, 14] substrates in transition metal-catalyzed coupling reactions,[15-19] and templates for expanding our understanding of divalent *f*-block organometallic compounds.[20] In the past two decades, as the global chemical community has made a concerted push towards more sustainable chemical practices, alkaline earth compounds have reestablished themselves as popular targets for intensive synthetic investigation.[21, 22] The renewed interest in these compounds has additionally been fueled by the potential of light *s*-block hydrides to serve as solid-state hydrogen storage materials.[3, 23-26] The recent resurgence in the chemistry of group 2 has precipitated several dramatic shifts in the traditional paradigms associated with the compounds, including most notably the isolation of thermally stable molecular group 2 hydrides,[3, 27-35] low valent alkaline earth complexes,[36-41] and the use of these compounds as molecular catalysts in organic transformations.[42-50] Much of the recent work in the field of molecular group 2 chemistry has focused on exploiting the high reactivity of the metal centers in the aforementioned new structural paradigms to activate and functionalize energy-relevant targets such as O_2,[51] H_2,[52] CO,[53] CO_2[30, 54-57] and even recently to achieve the unprecedented nucleophilic alkylation of benzene.[34, 58] The majority of the work presented in this dissertation will be focused on group 2 hydrides, reduced group 2 complexes, their corresponding synthons, and related reactivity products.

1.2. Important Atomic Properties of Group 2 Elements and their Effects on Molecular Chemistry

When comparing the known coordination chemistry of organometallic alkaline earth compounds, it becomes abundantly clear that the first three elements, Be, Mg, and Ca, exhibit substantial variances in their bonding and structural characteristics, consequently giving them markedly different reactivity profiles. It is worth noting that the heaviest non-radioactive elements, Ca, Sr, and Ba, tend to behave more similarly to one another, and exhibit more consistent trends in accordance with the changes in size between them. As a result, the first three elements are often treated separately in synthetic investigations, and few comparative studies exist. The striking differences in the chemistry of the alkaline earth elements is attributable to notable variances in several important properties: atomic radius and electronegativity, reduction potential, and the resulting "preferred" chemical bonding (Figure 1.1).

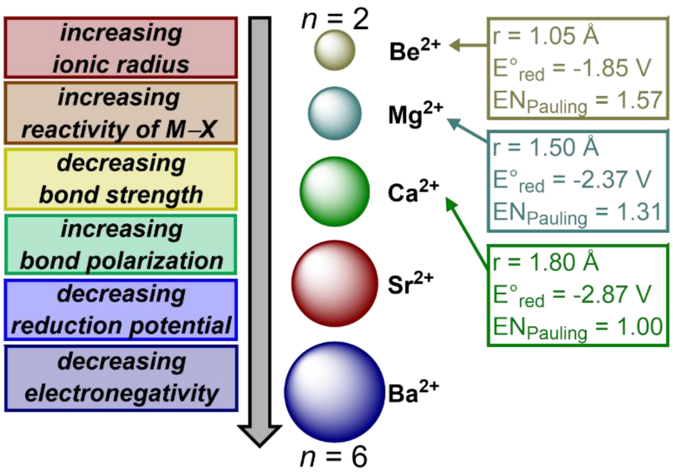

Figure 1.1. Overview of important atomic trends in the alkaline earth group. Cartoon atomic orbitals (colored spheres) represent their relative sizes, but they are not drawn to scale.

1.2.1. Atomic Radius and Electronegativity.

First and foremost, the atomic radii of the group 2 elements exhibit a dramatic increase from beryllium to calcium, followed by only moderate changes in size from calcium to barium (Be, 1.05 Å; Mg, 1.50 Å; Ca, 1.80 Å; Sr, 2.00 Å; Ba, 2.15 Å). Two major changes in the core electron configurations leading to a large difference in the effective nuclear charge, Z_{eff}, are primarily responsible for this trend. Filled 2*p* and 3*s* shells are added from Be to Mg, and a full 4s and 4p shell is added from Mg to Ca. This change from the smallest and most charge-dense metal (Be) to one of the largest and least charge-dense (Ca) has a dramatic effect on how these elements form chemical bonds with other atoms. Specifically, the distance of a typical M–X bond (M = metal, X = halide, O_{alkoxide}, N_{amide}, C_{alkyl}) increases substantially down the group, concomitantly decreasing the strengths (and increasing the lability in reactions) of these bonds. The remarkably different electronegativity values for the alkaline earth metals also have an impact upon the bonding behavior (Be, 1.57; Mg, 1.31; Ca, 1.00; Sr, 0.95; Ba, 0.89). If the difference in electronegativity (ΔEN) between two bonded atoms is between 0 and 1.6, the bond is considered predominantly covalent in character, e.g., formally M–X. However, a bond between two atoms with an electronegativity difference greater than 1.6 is considered ionic in character, e.g., $[M]^+[X]^-$. The high electronegativity of beryllium relative to the other group 2 elements, allows it to participate in covalent bonding with organic fragments bound through either a nitrogen atom ($\Delta EN_{\text{BeN}} = 1.47$) or especially with a carbon atom ($\Delta EN_{\text{BeC}} = 0.98$). In contrast, Mg and Ca both form ionic bonds with nitrogen and highly polar covalent bonds with carbon, (ΔEN_{MN} = 1.73(Mg) and 2.04(Ca), ΔEN_{MC} = 1.24 and 1.55, respectively).

1.2.2. Reduction Potentials and Redox Properties.

Many modern catalytic processes have key steps involving a facile redox process at a metal center, such as the oxidative addition of an alkylhalide to a Pd^0 complex or the reductive elimination of adjacent alkyl ligands to form a new C–C bond.[59] The metals involved in such processes must have the ability to easily (and reversibly) undergo changes to their oxidation state (e.g., Pd(0)/Pd(II)).[60-64] This type of behavior, which is relatively easy to achieve with transition metals, is considerably more difficult to elicit from main-group elements, with reversible redox processes at *s*-block elements being by far the most challenging.[65] As a result of their extremely low reduction potentials (Be: −1.85, Mg: −2.37, Ca: −2.87, Sr: −2.90, Ba: −2.91),[66] the alkaline earth metals heavily favor the +2 oxidation state. For this reason, group 2 metals (i.e., M^0) are highly active reducing agents, second only to the alkali group. With a few notable exceptions,[37, 67, 68] nearly all stable (isolable) group 2 complexes exhibit a metal center in its +2 oxidation state. Therefore, one major effort in modern main-group organometallic chemistry is stabilizing alkaline earth metals in low oxidation states ("subvalent" or "low-valent," i.e., M^{1+} and M^0). In correlation with the trend in reduction potentials, this challenge becomes increasingly more difficult with larger group 2 elements.

1.2.3. Bonding and Structural Trends.

The properties of the M^{2+} ion have a substantial effect on the molecular geometry that the atom adopts when bonding to ligands. Useful examples are bulky alkaline earth metal *bis*(hexamethyldisilazide) (hexamethyldisilazide = HMDS) compounds, which are shown in Figure 2. $Be(HMDS)_2$ has a *linear* geometry and does not exhibit any coordination by ethereal solvents.[69] $Mg(HMDS)_2$ crystalizes as a dimer in the solid state in the absence of donor solvents, and can accommodate two ethereal donors, adopting a *tetrahedral* geometry.[70-72] $Ca(HMDS)_2$

crystalizes as a dimer in the absence of donor solvents and accommodates two coordinated ethereal solvent molecules as well.[73-75] Detailed studies of these compounds have revealed that the small size of the beryllium center along with favorable symmetry for orbital overlap allows for multiple bonding character across the N–Be–N moiety.[76] In contrast, the M–N bonds for $Mg[N(SiMe_3)_2]_2$ and $Ca[N(SiMe_3)_2]_2$ are predominately ionic and exhibit negligible π-character. These observations agree with the change in the M–N bond lengths, which increase from 1.56 Å in $Be[N(SiMe_3)_2]_2$ to 1.98–2.15 Å and 2.27–2.52 Å for the magnesium and calcium analogs, respectively. This trend in bonding can be explained by the atomic radii and electronegativity values for the metals. The smaller, more electronegative Be atom is capable of forming shorter, stronger bonds with each HMDS ligand, whereas the Mg and Ca atoms engage in the ionic bonding we typically expect for *s*-block elements.

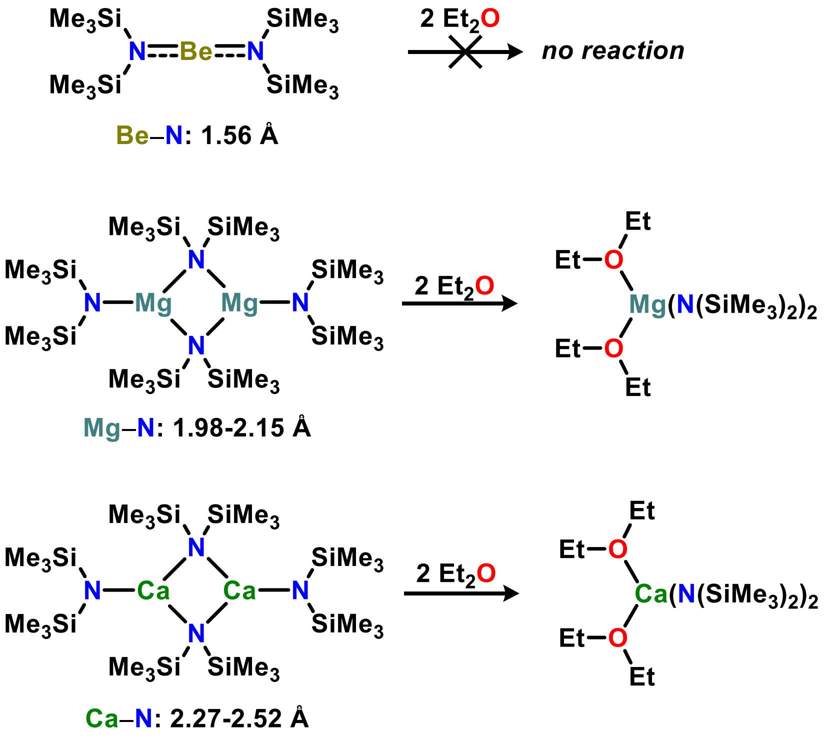

Figure 1.2. Structure of solvent-free and diethyl ether-coordinated alkaline earth *bis*-silylamides.

In addition to structural characteristics in group 2 compounds, the nature of the M–X bond is highly dependent on the atomic properties of the M^{2+} ion. For instance, compared to the ionic compounds $MgCl_2$ and $CaCl_2$, which readily dissociate into their component ions in water, $BeCl_2$ is considered a polar covalent compound and reacts *violently* with water to form $Be(OH)_2$ and gaseous HCl. Alkaline earth metal compounds of the type MX_2 also exhibit extremely high lattice energies. These lattice energies are dependent on the size of the M^{2+} ion, as larger M^{2+} ions generally result in weaker lattice energies. Alkaline earth dihydrides, for example, have overall high lattice energies (BeH_2, 3205 KJ/mol; MgH_2, 2791 KJ/mol; CaH_2, 2410 KJ/mol; SrH_2, 2250 KJ/mol; BaH_2, 2171 KJ/mol)[66] which decrease substantially after beryllium and magnesium. This property makes AeH_2 compounds (Ae = alkaline earth metal) insoluble in most organic solvents. The high lattice energies and resultant thermodynamic stabilities of alkaline earth MX_2 compounds, coupled with mostly ionic character of the M–X bonds (excepting beryllium) give rise to notorious ligand exchange and decomposition pathways for group 2 compounds, driven by precipitation of $[MX_2]_\infty$.

1.3. Stabilizing Ligands for Reactive Molecular Group 2 Chemistry

Arguably the most critical component of preparing an *isolable* complex of any reactive organometallic fragment is the stabilizing ligand. Good stabilizing ligands for reactive complexes typically exhibit have two main properties: (a) relatively high steric demand for kinetic stabilization, and (b) “correct” electronic structure for stabilization. Which ligand electronic structure is “correct” for stabilization depends on the fragment to which the ligand is bound. For electron-deficient complexes, as most divalent group 2 compounds are, an electron-rich ligand is typically preferred (strong $2e^-$ or $4e^-$ donors, e.g. RO^-, R_2N^-, etc.). For electron-rich fragments, including a low valent group 2 fragment such as Be^0 or $[Mg_2]^{2+}$, a combination of σ-basicity and π-acidity is usually ideal (e.g., CO, RCN, NHCs, CAACs, etc.). Since these high-energy ground state fragments, usually favored for their synthetic utility, are more reactive even with relatively inert molecules (e.g., the surrounding solvent, coproducts, or the complex itself), the ligand system around this center *must* have sufficiently high steric demand to prevent meaningful interactions between frontier orbitals and any potential substrates that could cause unwanted reactivity. For group 2 elements, this kinetic stabilization is also crucial to prevent Schlenk equilibria or oxidation state disproportionation among both the starting materials and target species. The electronic stabilization afforded by the ligand typically comes in the form of (a) strong bonds to the metal center, preventing ligand dissociation, and (b) lowering the energy of the dominant frontier orbital (i.e. the HOMO and LUMO for electron-rich and -deficient species, respectively), which typically both drives decomposition pathways and makes them such useful reagents.

With these general considerations in mind, two broad categories of ligand can be imagined for successful attempts at isolating reactive group 2 fragments: those which are either neutral or monoanionic. Within these two broad groupings there is an immense degree of diversity, however, a few specific classes of ligand (not including donor solvents) have emerged as the most frequently successful choices for group 2 chemistry: chelating, monoanionic *N*-donors (e.g., β-diketiminate, guanidinate, etc.) and neutral, monodentate *C*-donors [e.g., N-heterocyclic carbenes and cyclic (alkyl)(amino)carbenes]. A third, slightly different class of ligand from those listed above are redox-noninnocent ligands such as bipyridine, α-diimines, or azo compounds. As an alternative to stabilizing a reduced alkaline earth center, for example, in which the bulk of the electron density resides on the metal itself, these ligands can easily undergo multiple complete redox events using unoccupied, low-energy π-systems. These redox events shift the electron density from being predominantly metal-localized to predominately ligand-localized, dramatically increasing the overall stability and still maintaining a large degree of the behavior desirable from electron-rich complexes.

Overall, there are drastically more known complexes of group 2 elements supported by anionic stabilizing ligands than supported by neutral carbon donors. The clear advantage in binding strength and the kinetic stabilization that results from anionic ligands have led to more stable – and more synthetically viable – molecular platforms around which group 2 chemistry has grown. However, there are a number of cases in which a neutral carbon donor ligand must be used to stabilize certain group 2 species (e.g., neutral zero valent compounds) and still more potential applications that are yet to be discovered. As such, there is much work to be done towards understanding the chemistry of neutral carbon donors with the elements of group 2. The following sections will discuss these scenarios in detail.

1.4. Singlet Carbenes and Their Applications in Modern Main Group Chemistry

Since the discovery of stable *N*-Heterocyclic Carbenes (NHCs) by Arduengo, *et al.* in 1991 and cyclic (alkyl)(amino) carbenes (CAACs) by Bertrand, *et al.* in 2005, these two closely related classes of ligand have since proliferated across all areas of chemical synthesis and have affected most of modern chemistry. Within the field of “main group” chemistry, i.e., the study of elements in the *s*- and *p*-blocks of the periodic table, these ligands have completely transformed the types of bonding, reactivity, and structures that were thought possible for these elements.

By definition, a “carbene” is a divalent carbon atom (i.e., covalently bonded to two other atoms) which has six valence electrons instead of the usual eight. As a specific subclass of carbene, NHCs and CAACs have unique structural features which give the carbene center some important chemical properties. Most importantly, these two types of carbenes have N atoms bound to the carbene carbon, and these atoms are all part of a ring, locking the relative geometries in place. The adjacent N atoms stabilize the reactive carbene center via both σ-induction through the N-C σ bond and π-donation from N_{2p} nonbonding electrons into the empty C_{2p} orbital. The result is that NHCs and CAACs are – generally speaking – much more stable than their predecessors (classical Fischer and Schrock carbenes) which could not be isolated in their "free" form, i.e., not bound to a metal center.

The combination of the forward-facing, nonbonding pair of electrons and orthogonally oriented, vacant C_{2p} orbital gives the carbene carbon an ambiphilic nature, i.e., both nucleophilic and electrophilic in character. Between NHCs and CAACs the subtle change in the carbene-adjacent atoms (i.e., N versus C) leads to important differences in the energy of the two orbitals that drive the chemistry of these species. The replacement of one N atom of a classical NHC with a tertiary C atom, as seen in CAACs, both *raises* the energy of the HOMO (lone pair) and *lowers* the energy of the LUMO (the vacant C_{2p}). This makes CAACs both stronger σ donors (more nucleophilic) and stronger π acids (more electrophilic). Because of these differences, there are often markedly distinct reaction outcomes when using NHCs compared to CAACs in otherwise identical syntheses.

The degree of synthetic versatility allowed by carbene's unique frontier orbitals, especially in such a highly tunable ligand framework, has led to a wide variety of applications for both NHCs and CAACs. Through the Lewis basic lone pair, the carbene carbon can coordinate to Lewis acidic metal complexes or other electrophilic non-metallic species. In any instance where an energetically accessible vacant orbital is available for bonding, an NHC or CAAC can form strong covalent bonds thereto using its lone pair electrons. Due to the relatively high energy of these electrons, even some typically inaccessible molecular orbitals can become potential σ-bond acceptors with certain types of free singlet carbenes (the H–H and N–H σ* orbitals of H_2 and NH_3, for example). In addition to their reactivity through the carbenic lone pair, NHCs and CAACs can use their vacant C_{2p} orbital – to varying degrees depending on the specific ligand – to stabilize electron-*rich* species as well. To a large extent, the improved electrophilicity of NHCs and CAACs has been the primary advantage of these ligands as a gold-standard neutral donor ligand, as opposed to trisubstituted phosphines (PR_3) which have comparatively limited electrophilicity through their P–R σ* orbitals.

In main group chemistry, the advent of singlet carbenes allowed for a complete rewriting of established stability and reactivity rules through the isolation of dozens of complexes which would be unobservable using other ligands. Specifically, the synthesis and isolation of main group complexes with either unusual valence shell configurations and/or highly reactive functional groups was revolutionized with the use of carbenes as stabilizing ligands. In the *s*- and *p*-blocks, there is very little natural flexibility in oxidation states compared to the *d*- and *f*- block elements, due to the high energy of incomplete *s* and *p*-subshells. There is great synthetic utility for a complex having two or more valence configurations that are close in energy [e.g. Pd(0)/Pd(II) or Rh(I)/Rh(III)], and the ability to achieve this redox flexibility in stable main group complexes would open up a completely new landscape of "transition metal-like" reactivity for these elements, e.g., catalytic bond activations.[77] Indeed, singlet carbenes were the key component in isolating many new complexes featuring formally "reduced" molecular fragments, i.e. a complex wherein the central element(s) exhibit(s) an oxidation state lower than that in its predominant natural compounds. In the *p*-block, for example, multiply bonded homometallic (or "homometalloidic") molecules such as (L)Si=Si(L)[78] and (L)B≡B(L)[79] were isolable at room temperature where L=NHCs. In group 15, examples include a number of pnictinidenes [i.e. E(I)–

R, E = P,[80] As,[81] Sb,[82] Bi[83]] which were found to form highly stable adducts with carbenes [i.e. (L)E–R, L = CAAC, NHC]. Current research in this area is focused on isolating new reduced species of *p*-block elements and studying the potential electron transfer reactivity of currently known complexes, such as those discussed above.

When compared to the proliferation of singlet carbenes as stabilizing ligands for *p*-block chemistry, NHCs and CAACs have been markedly slower to establish themselves in synthetic *s*-block chemistry. This is largely due to the combined effect of inherent ligand exchange processes of group 2 compounds (e.g. Schlenk equilibria) and thermodynamically weak carbene–metal bonds making it difficult to isolate well-defined complexes (as discussed in section 1.2.). However, steady progress has been made in the past decade, specifically in the isolation of hydridic, subvalent, or cationic molecular group 2 fragments.

1.5. Molecular Alkaline Earth Hydride Chemistry

Metal–hydride bonds are of fundamental importance to numerous synthetic processes, usually as on-cycle catalytic intermediates which can readily facilitate hydrogen transfer reactions involving organic substrates. In addition, there can be an incredible degree of variability in the M–H bond polarization from $[M^+][H^-]$ to $[M^-][H^+]$ depending upon the nature of M and its ancillary ligands. As a result, hydridic organometallic complexes have been shown to exhibit remarkably diverse reactivities and physical properties and remain a critical focus of synthetic organometallic chemistry. The isolation of molecular main-group hydride complexes has become an important point of focus for researchers, due to a renewed interest in these compounds as earth-abundant molecular catalysts and candidates for chemical storage of hydrogen. For example, some of the popular candidates being studied for solid-state hydrogen storage include the main-group compounds MgH_2, $Mg(BH_4)_2$, and $Ca(NH_2BH_3)_2$ because of their high gravimetric hydrogen contents (7.6%, 15.0%, 10.1%, respectively). These compounds in their unadulterated, bulk states are plagued by extremely high lattice energies which give the compounds a correspondingly high thermodynamic stability to H_2 elimination (described by the value of the "enthalpy of decomposition"). One possible method of lowering the required desorption temperature is by decreasing the cluster size, i.e., the number of connected units of MX_2, through forcing the bulk material into smaller discrete clusters using carefully selected supporting ligands. For example, prior reports have proposed that extremely small clusters of MgH_2 ($n_{Mg} < 19$) should have a substantially decreased enthalpy of decomposition, such that as the cluster size is further decreased, the H_2 elimination temperature decreases dramatically. For this reason, low nuclearity "molecular" group 2 hydrides, borohydrides and amidotrihydroborates have recently become high-value synthetic targets. To create thermodynamically stable and isolable low nuclearity group 2 hydrides, synthetic chemists select strong, kinetically stabilizing supporting ligands which can force the formation of smaller cluster sizes of $[M_nX_m]^{(2n-m)+}$ ($X = H^-$, H_4B^-, $(H_3B)(H)_2N^-$) and prevent decomposition to insoluble MgH_2 *via* ligand exchange (*i.e.* Schlenk equilibrium). By far the largest number of isolable small cluster-size group 2 hydride complexes have been supported by strongly-binding, usually chelating, anionic ligands with extreme steric demand. Common examples include – but are not limited to – β-diketiminate (NacNac), tris(pyrazolyl)methanide, tris[((1-isopropylbenzimidazol-2-yl)-dimethylsilyl)]methanide, or macrocyclic amidopolyamine ligands. There are also some examples in which polydentate neutral ligands such as pentamethyldiethylenediamine were used to stabilize heavier s-block hydrides. It is clear that kinetic stabilization afforded by the ligands due to their physical size along with a strong L–M bond strength are the most critical factors controlling the stability and structures of the complexes.

1.6 Molecular Alkaline Earth Reduction Chemistry

The isolation and study of subvalent alkaline earth complexes has led to new reaction archetypes for these elements as soluble organometallic reducing agents for both organic and inorganic compounds. The members of group 2 strongly favor the 2+ oxidation state, and molecular alkaline earth complexes containing a reduced metal center were unknown until the synthesis of amidinate and guanidinate-stabilized Mg(I) dimers by Jones and Stasch in 2007.[37] Since this seminal report, diligent synthetic research has yielded more other examples of stable, dimeric Mg(I) compounds. Despite their relative scarcity in number, Mg(I) species have proven to be robust synthetic reagents which can insert olefinic bonds,[39] cleave C–H bonds,[84] and reduce both organic and inorganic substrates.[36] In addition to Mg(I) dimers – by far the most numerous class of reduced group 2 complexes – landmark discoveries of isolable Be(0),[68, 83] Be(I),[85, 86] Mg(I),[37] Mg(0)[87] and subvalent Ca compounds[67] have also been published.

The development of highly stabilizing neutral ligands such as Arduengo's *N*-heterocyclic carbenes (NHCs) and Bertrand's cyclic(alkyl)(amino) carbenes (CAACs) have allowed synthetic chemists to isolate a variety of low-valent main group compounds. Thus far, CAACs have proven sufficient to stabilize formally zero-valent *s*-block complexes as well. The first such complex, of the formula $(CAAC)_2Be$,[68] was reported in 2016 by Braunschweig, and exhibits strong multiple bonding between the Be center and the highly π-acidic carbene ligands. This initial discovery has been extended to allow the isolation of the first Be(I) radical cation[85] and a neutral Be(I) radical.[86] It is notable that the heavier analog containing Mg (i.e. $CAAC_2Mg$) has thus far eluded chemists.

As an alternative to the aforementioned low-valent alkaline earth complexes, which contain a highly reactive formally reduced metal center, substantial progress has been achieved in the study of alkaline earth complexes containing redox non-innocent ligands including α-diimines and azobenzene. The use of redox active proxy ligands allows the metal center to maintain its strongly preferred 2+ oxidation state while allowing facile, reversible electron transfers at the ligand. The ability to shuttle between multiple redox states under mild conditions is an important characteristic of many catalytically active metal complexes and is a primary goal for contemporary main group chemistry. Thus far, redox-active alkaline earth compounds featuring non-innocent ligands have exhibited promising reactivity including C–H[88] bond activation, C–C bond formation,[88, 89] and O_2 reduction.[51]

1.7. Overview of Synthetic Chemistry with CO_2 Anions (CO_2^{-} and CO_2^{2-})

Carbon dioxide is one of the primary greenhouse gases present in the Earth's atmosphere, and, in addition to methane, is one of the main drivers of the anthropogenic climate change of the 20th and 21st centuries. From a chemical perspective, CO_2 is a naturally abundant and relatively inexpensive C_1 synthon, however it is difficult to utilize when compared to industrial favorite C_1 sources such as methanol, formic acid, or formaldehyde, because it is gaseous and chemically inert to many common synthetic transformations. As such, there has been a concerted effort by modern chemists to unlock inexpensive, robust processes to utilize CO_2 as an organic building block that can be carried out at near-ambient conditions (i.e. low pressures and temperatures).

Because of their unique electronic structures (discussed in sec. 1.4.), NHCs and CAACs have been found to be well-suited for CO_2 activation and functionalization chemistry at ambient temperature and pressure.[90-92] A number of synthetic investigations have been reported in which the carbene reacts with CO_2 at room temperature and 1 atm of pressure, forming a carbene–CO_2 zwitterion (i.e. carbene carboxylate). Carbene-carboxylates have a distinct predisposition toward energy-relevant applications in CO_2 reduction and conversion chemistry, and a number of reported studies have focused on functionalizing or selectively transferring the carboxylate motif. However, little is known about the ability of carbene-2-carboxylates to accept electrons in "direct" reductions. In Chapter 4, results from this doctoral research toward understanding the reduction chemistry of carbene–CO_2 adducts is discussed.

Chapter 2: Carbene-Coordinated Magnesium Halides and Reduction Chemistry

Containing work that was originally published in the following:

Wong, Y. O.; Freeman, L. A.; Agakidou, A. D.; Dickie, D. A.; Webster, C. E.; Gilliard, R. J., *Organometallics* **2019**, *38*, 688-696.

Freeman, L. A.; Walley, J. E.; Obi, A. D.; Wang, G.; Dickie, D. A.; Molino, A.; Wilson, D. J. D.; Gilliard, R. J., *Inorg. Chem.* **2019,** *58*, 10554-10568.

2.1 Background on carbene-group 2 coordination chemistry.

The majority of results achieved thus far in the study of molecular alkaline earth complexes have used chelating anionic ancillary ligands such as guanidinates,[93] amidinates,[33, 94] or diketiminates[36, 95-97] to stabilize a wide variety of organometallic alkaline earth fragments. These ligand classes are desirable primarily for their strong binding and highly tunable steric environment and have proved extremely useful in advancing our understanding of group 2 coordination chemistry. However, the use of a formally anionic stabilizing ligand comes with the primary drawback of limiting the possible redox chemistry of a group 2 complex to only single-electron reductions, whether the reduction is occurring at the metal center or at a redox active ligand. Formally neutral ligands such as *N*-heterocyclic carbenes and cyclic(alkyl)(amino) carbenes are relatively scarce in group 2 chemistry, but have been shown to stabilize a number of polar group 2 fragments.[28, 98-105] Recently, we reported the first series of compounds where two NHCs are bound to a single Mg center, resulting in a range of molecular magnesium reagents such as a carbene-stabilized terminal Grignard, $(I^{i}Pr^{Me2})_2Mg(Me)Br$.[106] Additionally, Mulvey, Hevia and others have extensively studied the roles of mesoionic and dianionic carbenes in support of *s*-block bimetallic systems.[107-111]

Thiele reported that the treatment of beryllium chloride with diazadiene (DAD) and sodium produced the highly stable $[Be(DAD)_2]$, where each DAD has been singly reduced.[112] Wang showed that the reaction of beryllium chloride with an unsymmetrical 2-(2-pyridyl)indole ligand and butyllithium produces a diamagnetic bis(*N,N′*-chelating)beryllium complex, where the indole *N* atom is bound as an amide and *N′* is a pendant datively bound pyridine.[113] Interestingly, Hill noted that heating $(IMes)Be(CH_3)_2$ (IMes = 1,3-bis(2,4,6-trimethylphenyl)imidazol-2-ylidene) with excess phenylsilane yields (IMes)Be(^{Mes}DAB) (^{Mes}DAB = *bis*(2,4,6-trimethylphenyl)-1,4-diazabutadiene), where ^{Mes}DAB is a doubly-reduced diamine ligand.[114]

Magnesium complexes containing reduced diimines such as 1,2-bis[(2,6-diisopropylphenyl)imino]acenaphthene (^{Dipp}BIAN) and 1,4-diazabutadienes have been the subjects of a number of investigations.[88, 89, 115-119] Yang, e*t al* reported that one- and two-electron reductions of various *N,N*-diaryldiazabutadienes followed by reaction with $MgCl_2$ gave highly varied magnesium-diimine complexes depending on the ligand steric demand and reagent stoichiometry.[120] Among the isolated products was the Mg–Mg bonded species $K_2[(L^{iPr})MgMg(L^{iPr})]$ (L^{iPr} = $[(2,6\text{-}^iPr_2C_6H_3)NC(Me)]_2$. The chemistry of group 2–(^{R}BIAN) complexes has been studied extensively in the literature. Fedushkin, *et al.* demonstrated that a magnesium salt of ^{Dipp}BIAN, [Mg(^{Dipp}BIAN)(THF)$_3$] can act as a reducing agent for unsaturated organic substrates, as well as mediate a remarkable C_{sp}–H bond cleavage and C–C bond formation in the coupling of PhC≡CH with Ph_2CO.[88] It is notable, however, that in this system the coordination number of magnesium is at least four throughout the entire reaction sequence due to the coordination of multiple THF molecules. If donor solvents are avoided, the coordination sphere is filled either by dimerization or by ligand exchange to form a homoleptic (^{Dipp}BIAN)$_2$Mg complex, in which each ligand is singly reduced.[116] These examples highlight a significant challenge in molecular group 2 chemistry: the preparation and isolation of monomeric and solvent-free group 2 complexes. As such, our group has begun to explore the synthesis of well-defined, solvent-free carbene–alkaline earth complexes as molecular precursors.[106, 121] Based on the existing work with both Mg and Be, we sought to support a redox-active Ae–diimine fragment with a neutral donor ligand in order to obtain well-defined, solvent-free, monomeric reduced alkaline earth complexes.

2.2 Carbene coordination to group 2 halides

The synthesis of low oxidation state main group complexes typically utilizes a radical-based halide abstraction promoted by an alkali metal reducing agent such as potassium graphite (KC_8). For this type of reaction, a ligand-coordinated main group element halide is needed.[31, 68, 122] For the chemical reduction of magnesium complexes, this requires a ligand-coordinated MgX_2 complex (X = halide). The isolation of a CAAC-supported Mg halide complex had not yet been reported in the chemical literature at the time of this investigation. Initial attempts to prepare the first CAAC magnesium halide complexes focused on the reactions of a 3,3-diethyl-substituted CAAC (^{Et2}CAAC) with $MgCl_2$ in both the coordinating solvent THF and non-coordinating toluene (scheme 2.1).

Scheme 2.1. Reactions of ^{Et2}CAAC with $MgCl_2$.

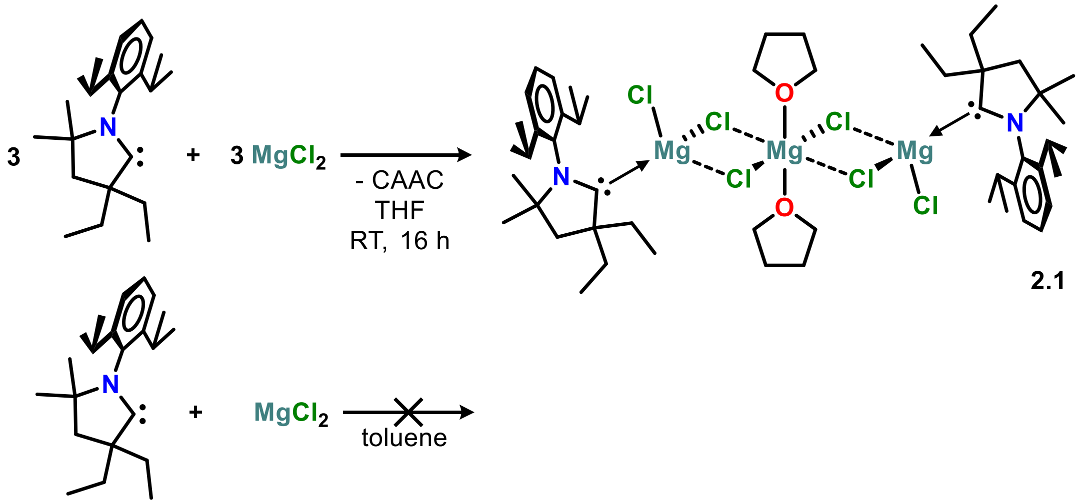

Surprisingly, an excess of THF completely inhibits the coordination of the CAAC ligand (determined via ^{1}H NMR in THF-d_8), and a complex can only be obtained by removal of the donor solvent under vacuum. Upon removal of excess THF, compound **2.1** was obtained as a bright white solid. Recrystallization of the product from a saturated toluene solution yielded colorless block-like crystals of compound **2.1** suitable for X-ray diffraction. The molecular structure of **2.1** (Figure 2.1.) shows that even after extended periods (days) under reduced pressure, THF coordination persists. Additionally, attempts to isolate a pure sample of **2.1** were unsuccessful due to the presence of THF-coordinated products of the type $(THF)_nMgCl_2$ which exhibited similar solubility to the desired product.

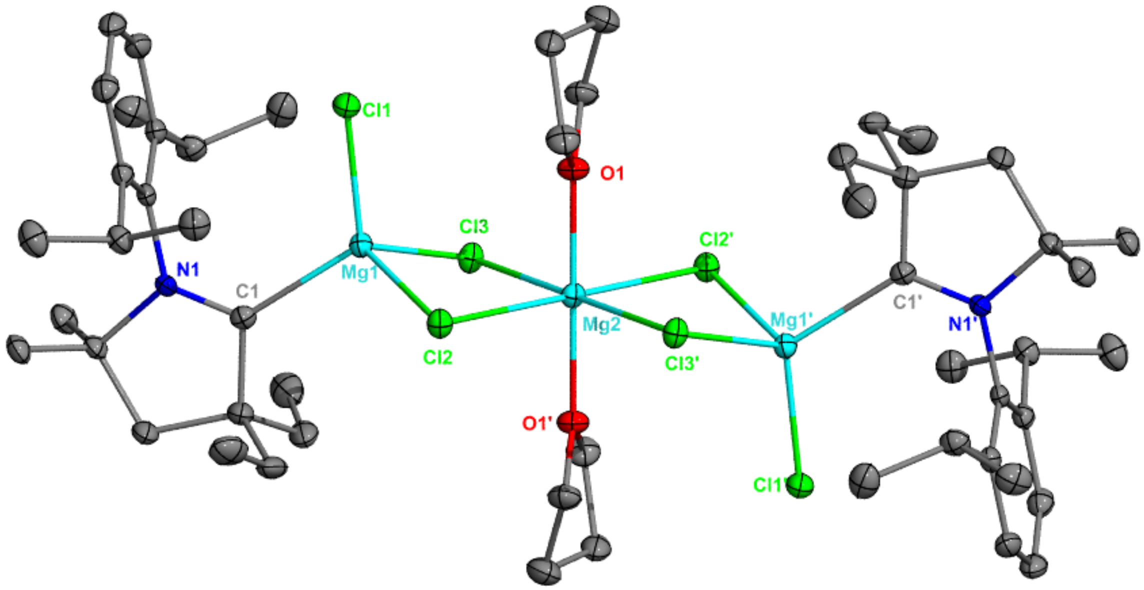

Figure 2.1. Molecular structure of compound **2.1** (thermal ellipsoids set at 50% probability, H atoms omitted for clarity). Selected bond distances (Å) and angles (deg): Cl1-Mg1: 2.2772(9); Cl2-Mg1: 2.3767(9); Cl2-Mg2: 2.5489(6); Mg1-C1: 2.234(2); Mg2-O1: 2.0573(15); N1-C1: 1.301(3); Mg1-Cl2-Mg2: 86.91(2); C1-Mg1-Cl1: 118.67(7); C1-Mg1-Cl2: 110.85(7); Cl2-Mg1-Cl3: 93.75(3).

Although two of the $MgCl_2$ units in the structure are coordinated by ^{Et2}CAAC ligands, the center unit of $MgCl_2$ does not have a coordinated CAAC, which is critical to stabilize a potential reduced product. To circumvent the complications created by the presence of THF, the same reaction was carried out in toluene, which yielded no reaction after 14 days, due to the extremely poor solubility of $MgCl_2$ in the solvent.

For comparison to this CAAC–$MgCl_2$ system, the reaction of the ubiquitous 1,3-*bis*(2,6-diisopropylphenyl)imidazole-2-ylidine (IPr) with $MgCl_2$ was also studied in both THF and toluene. In THF, the reaction of $MgCl_2$ with IPr proceeds cleanly at room temperature to yield a homogeneous, pale-yellow solution after 16 h (Scheme 2.2.). Upon removal of the solvent under vacuum and trituration with hexanes, compound **2.2** is obtained in 80% yield as a white solid. However, in toluene, the reaction requires 5 days of vigorous stirring to yield a heterogeneous mixture of **2.3** After the removal of toluene under vacuum and washing with hexanes, **2.3** is obtained as a white solid in 96% yield. Compound **2.3** exhibits a high affinity for THF and is readily converted to **2.2** in the presence of the donor solvent.

Scheme 2.2. Reactions of IPr with $MgCl_2$.

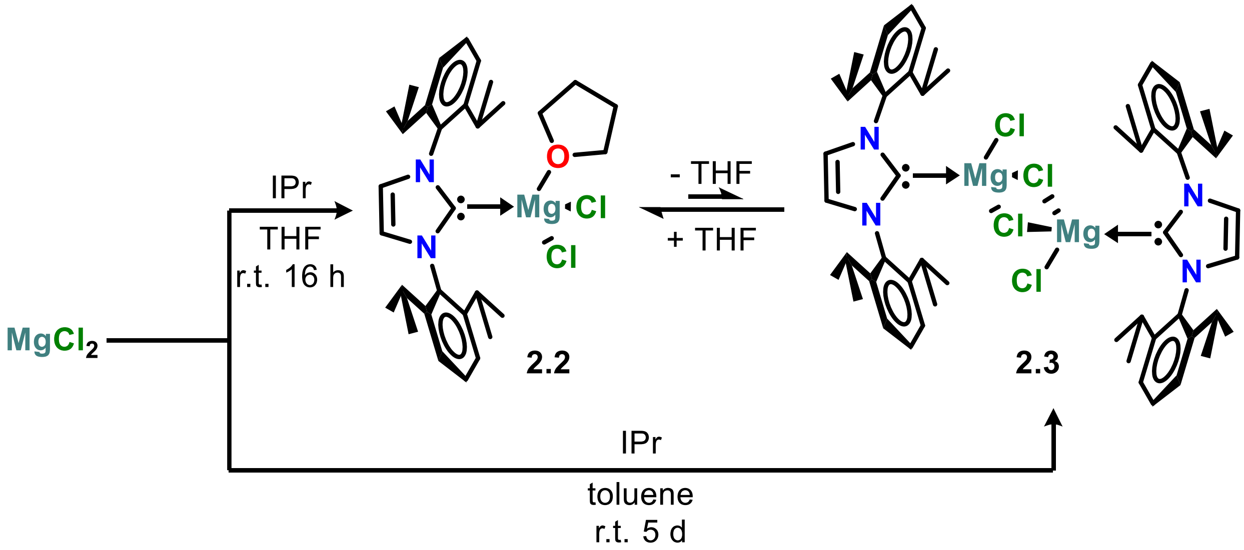

An analysis of compound **2.2** via ^{1}H NMR in THF-d_8 shows only slight shifts in the characteristic resonances of the IPr ligand. The methine protons on the diisopropylphenyl substituents shift from 2.82 ppm in the free ligand to 2.81 ppm for compound **2.2** A similar change was observed in the ^{1}H NMR resonance for the imidazolium backbone protons, which shifted from 7.17 to 7.18 ppm and exhibited slight broadening relative to the same peak for free IPr. Even at 0 °C, ^{1}H NMR analysis of **2.2** in THF-d_8 showed only slight changes (methine, 2.79 ppm; backbone protons, 7.29 ppm). These small shifts indicate that there is, at best, an extremely weak interaction between the carbene and metal center in solution and, at worst, that competitive THF coordination is predominant. An analysis of **2.3** via ^{1}H NMR proved difficult because of the poor solubility of the dimeric complex in noncoordinating solvents. Once the complex is formed, it cannot be dissolved in C_6D_6 in sufficient concentrations to obtain a ^{1}H NMR spectrum. If THF-d_8 is used, then the complex immediately converts to **2.3**, which exhibits coordination of the deuterated solvent and thus yields only resonances for **2.2** in the ^{1}H NMR spectrum. Trituration in hexanes and removal of the solvent gives partial conversion to a C_6D_6-insoluble white solid, which was attributed to compound **2.3** A disadvantage to **2.2** and **2.3** is that it can be difficult to quantify and control dynamic THF coordination.

Colorless block-shaped air- and moisture-sensitive crystals of **2.2** suitable for a single-crystal X-ray diffraction study were obtained from a saturated THF solution of the complex layered with hexanes (2:1 THF/hexanes) at room temperature. The four-coordinate magnesium center exhibits a distorted tetrahedral coordination environment with a THF molecule occupying the fourth coordination site (Figure A2.2). The Mg–O_{THF} distance of this interaction [2.018(5) Å] is only marginally longer than the IMes analogue [2.014(2) Å] and is shorter than the bis-THF analogue, $(THF)_2MgCl_2$ (2.129 Å). The nature of the bonding around magnesium in these complexes, along with the observed difficulty in removing coordinated THF, indicates that the Mg center is highly electron-deficient with only a single carbene ligand, and as a result, the Mg–THF interaction is relatively strong. When THF is removed, the complex dimerizes to yield **2.3** instead of existing as the tricoordinate (IPr)$MgCl_2$ adduct.

Colorless block-shaped crystals of **2.3** suitable for X-ray diffraction studies were obtained from refluxing a toluene suspension of the product and cooling the filtrate to room temperature. The molecular structure of **2.3** (Figure A2.3) is isostructural with the iodinated analog, [(IPr)MgI_2]$_2$ and shows a dimer with two (IPr)$MgCl_2$ units containing two tetravalent magnesium centers in distorted tetrahedral coordination environments. Three coordination sites are occupied by chlorine atoms – one terminal and two bridging – and one coordination site is occupied by the carbene carbon of an IPr ligand. The Cl–Mg1 bond [2.213(4) Å] is only marginally longer than that in **2.2** [2.202(6) Å], indicating that the replacement of the THF in **2.2** with a bridging chloride has little effect on the carbene–magnesium interaction. The coordination behavior of the sterically demanding NHC used in **2.2.** and **2.3.** was compared to a smaller NHC, $I^{i}Pr^{Me2}$ ($I^{i}Pr^{Me2}$ = *N*,*N′*-diisopropyl-2,3-dimethylimidazol-2-ylidine), in this report from our group.[106]

These results strongly suggest that $MgCl_2$ is not an easily accessible and viable halide precursor for magnesium reduction chemistry supported by neutral carbene-type ligands. A viable starting material would need to be prepared in a non-coordinating solvent such as toluene to eliminate competitive coordination from THF, so both the CAAC complex and the bulk magnesium halide must be at least moderately soluble in such solvents. Following the results obtained with $MgCl_2$, it was hypothesized that the heavier congeners $MgBr_2$ or MgI_2, which have generally higher solubility in hydrocarbon solvents than $MgCl_2$, might allow the preparation of CAAC and NHC complexes that were soluble in non-donor hydrocarbon solvents such as toluene. Indeed, the reaction of $MgBr_2$ with either free ^{Et2}CAAC or 1,3-bis(2,6-diisopropylphenyl)-4,5-dihydroimidazole-2-ylidene (SIPr) in toluene gives the desired products

2.4 and **2.5** in 74% and 68% yield respectively after only 16 hours at room temperature (scheme 2.3.).

Scheme 2.3. Reactions of SIPr and ^{Et2}CAAC with $MgBr_2$.

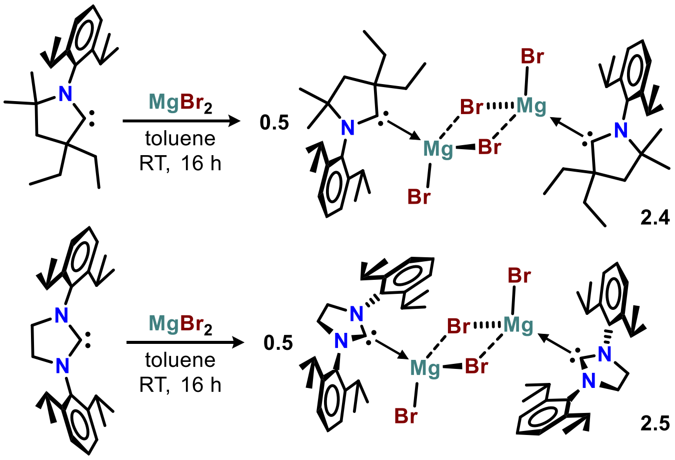

The ^{1}H NMR spectrum of **2.4** in C_6D_6 showed a shift in the characteristic resonance of the Dipp methine protons from 3.17 to 2.78 ppm, indicating a substantial change to the chemical environment of the ligand. Further evidence of coordination was given by the change to the diastereotopic methylene protons of the CAAC from two distinguishable multiplets of two protons each (δ = 1.88, 1.80 ppm) to a single overlapping multiplet signal (δ = 2.23 ppm) integrating to four protons. The ^{13}C NMR of the product showed a characteristically weak signal for the carbene carbon at 257.5 ppm, which is significantly upfield from the carbene resonance in the spectrum of free ^{Et2}CAAC at 317.5 ppm. Similarly, the ^{1}H NMR spectrum of **2.5** in C_6D_6 showed a shift in the methine resonance from 3.29 to 3.27 ppm, as well as a shift in the singlet resonance for the protons of the imidazole backbone from 3.37 to 3.48 ppm. These small shifts are consistent with those observed in other instances of coordination of NHCs to magnesium dihalides.

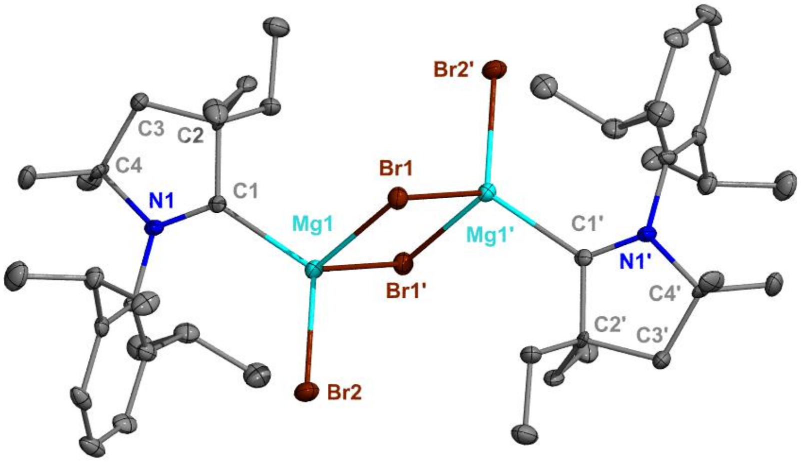

Figure 2.2. Molecular structure of 2.4. (thermal ellipsoids set at 50% probability, H atoms omitted for clarity). Selected bond distances (Å) and angles (deg): C1–Mg1:2.231(3); C1–N1:1.293(4); Mg1–Br1:2.5531(12); Mg1–Br2:2.4249(12); Mg1–Br1′: 2.5800(12); C1–Mg1–Br1:110.90(10); C1–Mg1–Br2:123.19(9); Br1–Mg1–Br2:107.82(5); Br1–Mg1–Br1′: 93.16(4).

Single crystals of **2.4** and **2.5** suitable for X-ray diffraction were grown at −37 °C from saturated solutions of the product in a 5:1 toluene/hexane mixture. The molecular structure of **2.4** (Figure 2.2.) revealed a dimer composed of two (^{Et2}CAAC)$MgBr_2$ units linked by two bridging bromide ligands. The C1–Mg1 bond distance of 2.231(3) Å is within the range of known CAAC–Mg complexes. To the best of our knowledge, **2.4** was the first structurally characterized CAAC–magnesium halide complex. The shortened C1–N1 bond in **2.4** [1.293(4) Å] is indicative of significant donation of the N1 lone pair into the unoccupied 2p orbital of C1. The DFT (B3LYP-D3(BJ)/def2-TZVP) optimized structure of **2.4** (modeled with N-Me in place of N-Dipp) is consistent with the crystal structure, with a C1–Mg1 distance of 2.193 Å (for further details see original manuscript[123]).

2.3 Attempts at Direct Reduction of Carbene Magnesium Halides

Complex **2.4** was used in attempts to synthesize a magnesium analog of the first structurally characterized Ae(0) complex, (^{Me}CAAC)$_2$Be.[68] The reaction of **2.4** with a second equivalent ^{Et2}CAAC as well as 2.2 equivalents of KC_8 in toluene consistently yielded a deeply red-orange solution under a variety of temperatures and reaction times (scheme 2.4.). Recrystallization of this product from hexanes at -37 °C yielded red-orange crystals suitable for X-ray diffraction. The molecular structure of these crystals showed the ligand activation product **2.6** (Figure A2.6).

Scheme 2.4. Attempted reductions of 2.4 with KC_8

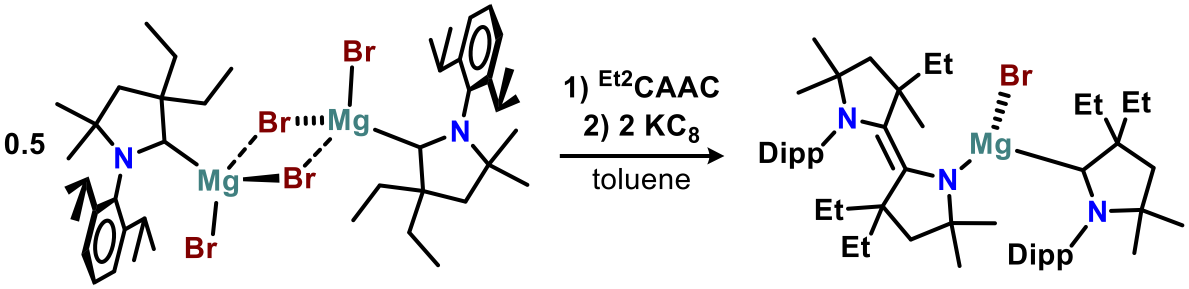

In this product, two ^{Et2}CAAC ligands have been coupled at the former carbene carbons to form a C–C double bond. Product **2.6** is similar in structure to the ligand activation products reported when using ^{Me2}CAAC by Turner, *et al.*,[100] indicating that ^{Et2}CAAC may be simply incapable of stabilizing the highly reactive magnesium species involved in these reactions.

2.4. Stepwise Reduction at Magnesium and Beryllium: Cooperative Effects of Carbenes with Redox Non-Innocent α-Diimines

Based on the results of the direct reductions of (^{Et2}CAAC)$MgBr_2$, attention was shifted to the reactions of **2.4** and **2.5** with the redox-active ligands 2,2-bipyridine (bpy) and *N*,*N*-bis(2,6-diisopropylphenyl)-1,4-diaza-1,3-butadiene (^{Dipp}DAB). Both ligand subclasses are ubiquitous in main-group and transition metal chemistry,[112, 124-129] and are highly variable scaffolds which can be prepared with a variety of *N*-substituted groups and backbone substituents. In bpy, the diimine moiety is contained within the aromatic system of the bipyridine core, and the steric demand around a bound metal center is relatively low. The diimine moiety of $^{\mathrm{Dipp}}$DAB, by contrast, is not part of an aromatic core, and has much higher steric demand when bound to a metal center. The use of these two ligands allows us to quickly and comprehensively elucidate the effect of ligand sterics and backbone electronic structure on the properties of the resulting reduced complexes.

2.4.1. Reaction of Carbene–Group 2 Dihalides with Singly-Reduced α-Diimines

Complexes **2.7** and **2.8** were prepared via the addition of the appropriate diimine to a solution of **2.4**, yielding a homogenous solution colored by the free diimine (yellow for $^{\mathrm{Dipp}}$DAB, faintly pink for bpy). The addition of one equivalent of KC_8 to these solutions at room temperature yielded a rapid change in color to that of the resulting singly reduced products whose structures are shown in scheme 2.5. Compounds **2.7** and **2.8** were obtained in 28 and 67% yields, respectively.

Scheme 2.5. Synthesis of Singly-Reduced Magnesium Complexes.

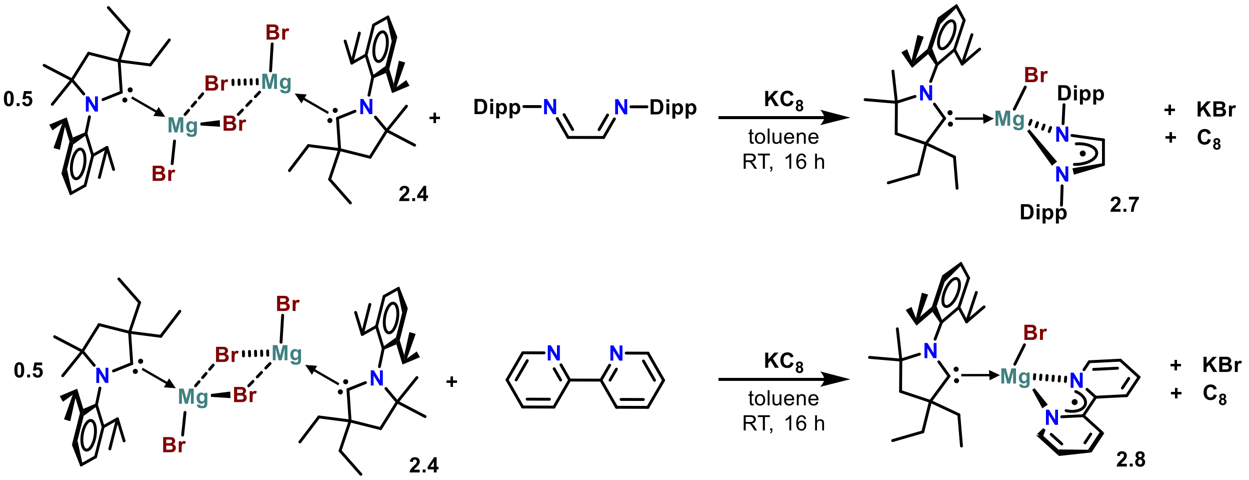

In contrast to the colorless magnesium starting material, the singly-reduced products were vibrantly colored. Complex **2.7** was bright orange in color, and compound **2.8** was dark red. Interestingly, while the reaction of **2.4** with either redox-active ligand and one equivalent of KC_8 gave clean conversions to the thermally stable **2.7** and **2.8**, singly-reduced products stabilized by SIPr could not be obtained. The reactions of **2.5** with KC_8 and either ^{Dipp}DAB or bpy under a variety of reaction conditions consistently yielded intractable product mixtures containing both diamagnetic and paramagnetic species. This is most likely a result of the differences in binding of SIPr to magnesium when compared with ^{Et2}CAAC. In this case, it appears that the subtle change in the binding behaviors leads to the formation of a mixture of products and precludes the isolation of the desired compounds.

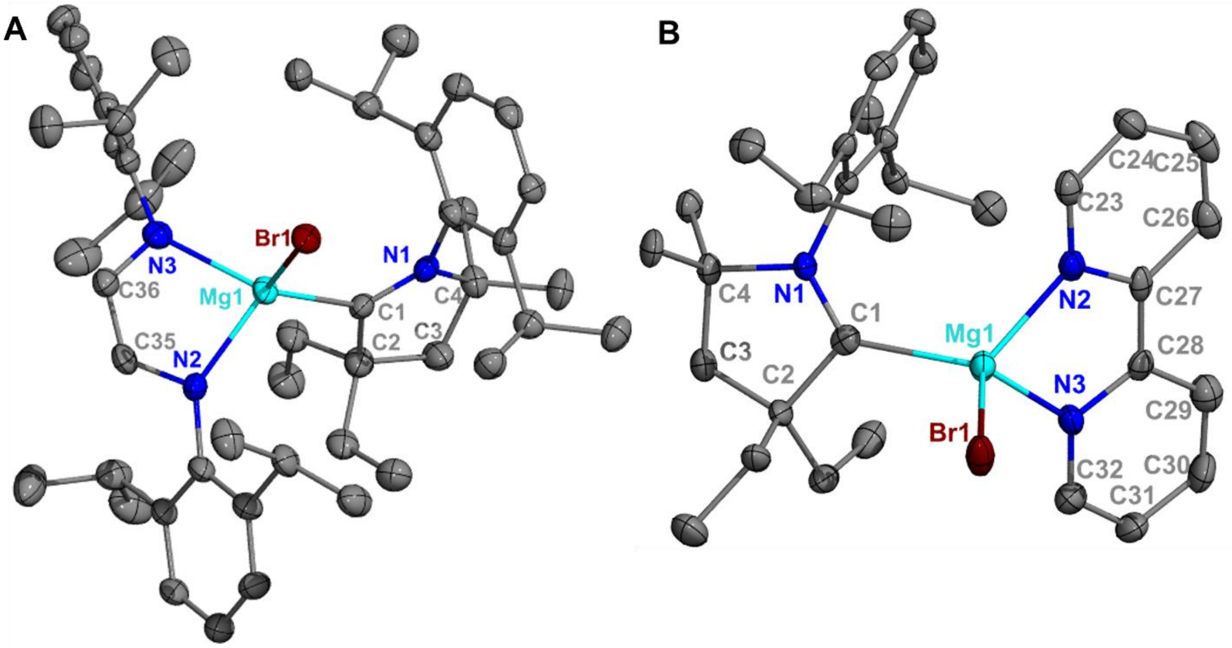

Figure 2.3. Molecular structures of **2.7** (A) and **2.8** (B) with H atoms omitted for clarity. Selected bond distances (Å) and angles (°) – **2.7**: Mg1–C1: 2.293(5); C1–N1: 1.3000(6); Mg1–Br1: 2.4642(14); Mg1–N2: 2.097(4); Mg1–N3: 2.140(5); C35–N2: 1.341(7); C36–N3: 1.347(4);

C35–C36: 1.404(7); C1–Mg1–Br1: 114.68(12); C35–N2–Mg1: 105.6(3). **2.8**: Mg1–C1: 2.246(4); C1–N1: 1.301(5); Mg1–Br1: 2.4724(15); Mg1–N2: 2.073(4); Mg1–N3: 2.069(4); C27–N2: 1.383(5); C28–N3: 1.389(5); C27–C28: 1.409(6); C1–Mg1–Br1: 108.92(11); C27–N2–Mg1: 112.8(3).

The reduction of α-diimines decreases the bond order of both backbone C–N bonds, as the added electrons occupy a C–N antibonding molecular orbital. The addition of electrons to $^{\text{Dipp}}$DAB and bpy concomitantly increases the bond order of the backbone C–C bond. The sensitivity of these bonds allows the reduction to be monitored structurally through changes in bond length around the N2–C35–C36–N3 backbone of the diimine. The backbone C–C bond changes from a formal single bond in the free diimine to a formal double bond in the dianionic form. The molecular structure of compound **2.7** (Figure 2.3A) reveals that a monoanionic [$^{\text{Dipp}}$DAB]$^{\bullet-}$ ligand has displaced a bromide from compound **2.4**, giving the desired singly-reduced product. The magnesium center is now contained within a five-membered metallacycle, however the metal center is positioned slightly out of the N2–C35–C36–N3 plane [Mg1–N2–C35–C36: 14.6(6)°]. This distortion is observable in some cases for similar Mg(II)–DAB$^{\bullet-}$ complexes.[120] Compound **2.8** (Figure 2.3B) exhibits an analogous core structure to **2.7**, with [bpy]$^{\bullet-}$ replacing [$^{\text{Dipp}}$DAB]$^{\bullet-}$. There is a shortening of the C27–C28 bond from 1.483 Å for free bpy[130] to 1.409(6) Å in **6**, indicating the expected increase in bond order resulting from reduction of the diimine core. As previously noted, the magnesium atom in **2.7** does not lie in the plane of the diimine core, but slightly above it. This contrasts with the magnesacycle of **2.8**, in which all of the bpy atoms are coplanar with the magnesium center.

The B3LYP-D3(BJ)/def2-TZVP optimized geometries of model **2.7**$^{\textbf{NMe}}$ and **2.8**$^{\textbf{NMe}}$ compounds (with N-Me substituents, see original manuscript for details[123]) both yield planar 5-

membered magnesacycles, with C-C-N-Mg dihedral angles of only 1-2°. There are insignificant differences in key bond distances (Mg-C, Mg-N, Mg-Br) between **2.7**$^{\mathbf{NMe}}$ and **2.8**$^{\mathbf{NMe}}$. Calculations with the full compounds (N-Dipp substituents) provided longer Mg-N and Mg-C bond distances, which suggests that the N-Me model compounds will yield a lower-bound to the geometries of the full complex (with greater steric bulk). Modeling the experimental structure for **2.7** (N-Dipp) yielded a larger dihedral angle of 7°, which suggests that the non-planarity results from steric effects due to the bulky Dipp groups.

Analysis of the DFT-calculated frontier molecular orbitals (MOs) indicates that the singly-occupied MOs (SOMO) for both complexes are π-symmetric MOs centered on the diimine ligand (Figure 2.4). However, the doubly-occupied SOMO-1 differs between **2.7** and **2.8**; it is a π-symmetric MO located on the bpy ligand in **2.8**, while in **2.7** it is a lone-pair orbital on the Br atom. The SOMO-2 for both compounds is a lone-pair Br orbital. This suggests that the doubly-occupied SOMO-1 (the highest doubly occupied MO) influences the planarity of the 5-membered magnesacycles; the extended bpy π-system in **2.8** results in greater planarity, while the absence of such a π-symmetric MO in **2.7** allows the Mg atom to reside above the plane of the diimine core.

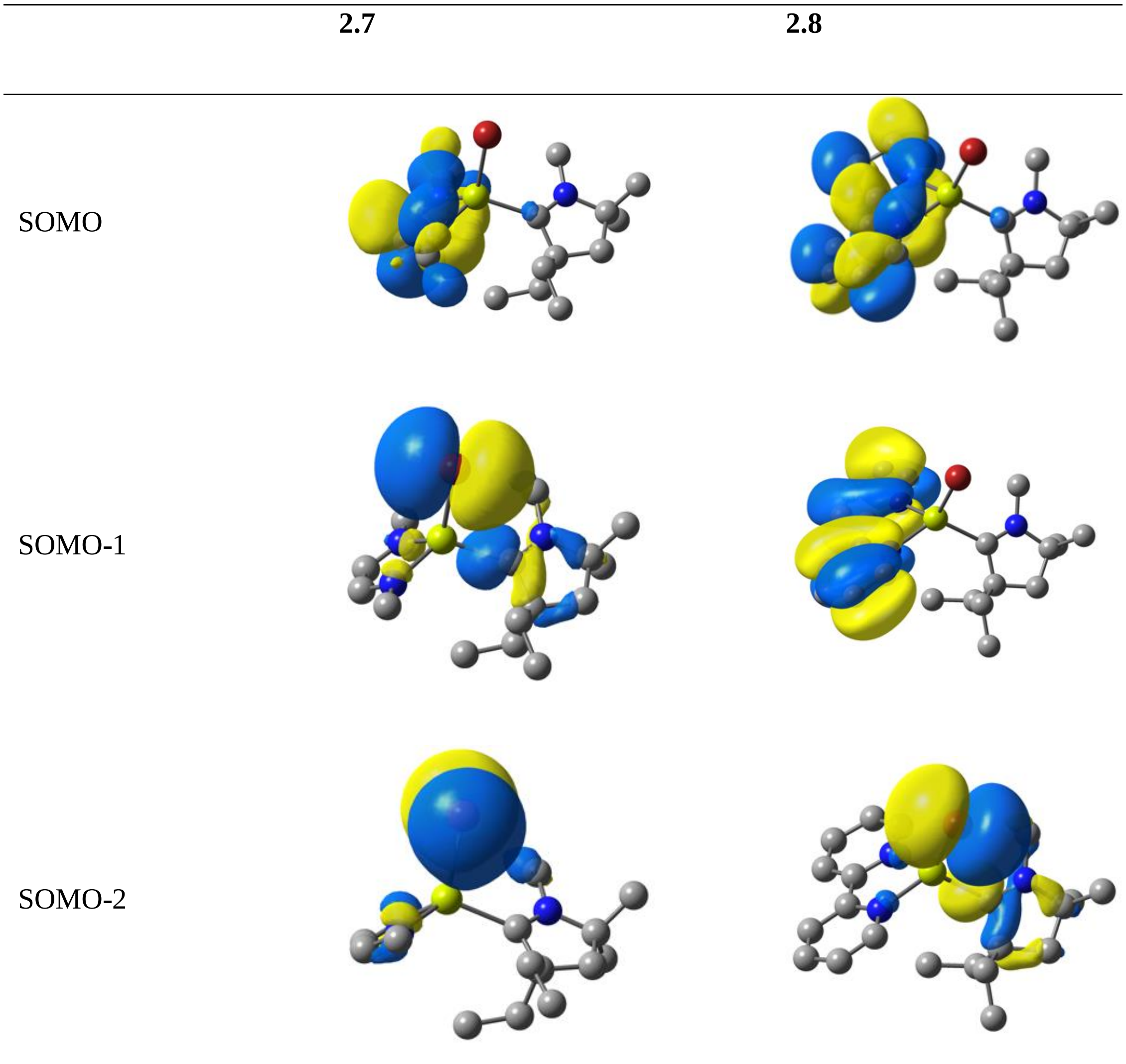

Figure 2.4. Plot of frontier molecular orbitals for singly-reduced magnesium complexes.

Each of the paramagnetic complexes **2.7** and **2.8** contained a persistent ligand-based radical electron. To determine the chemical environment of these unpaired electrons, the continuous-wave X-band EPR spectrum was obtained at room temperature of each compound in toluene. (Figure 2.5).

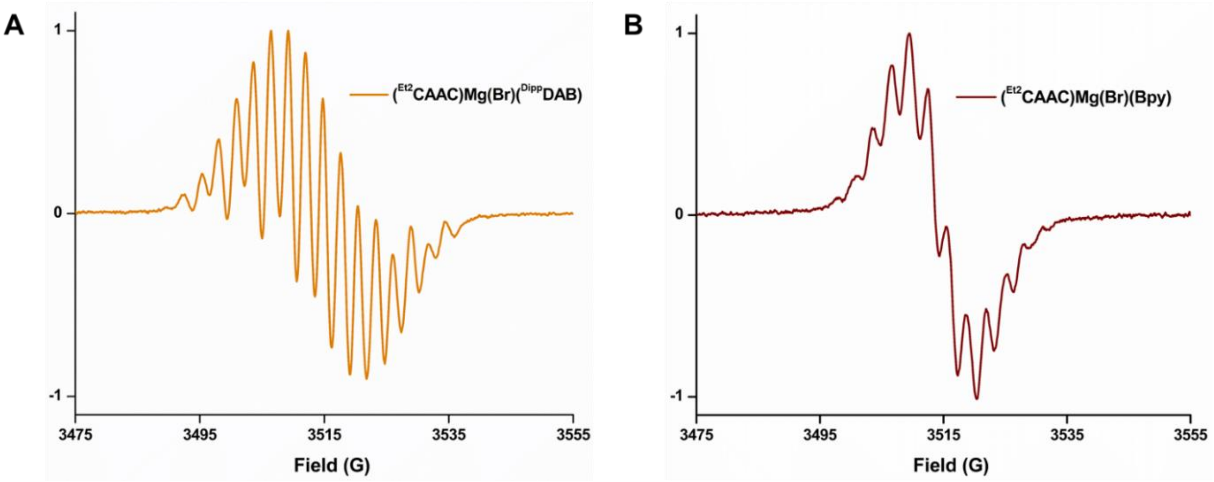

Figure 2.5. Room temperature CW X-band EPR spectra of complexes **2.7** (A) and **2.8** (B) in toluene (250 µM, 5 scans averaged).

The EPR spectrum of **2.7** (Figure 2.5A) shows a single resonance with observable hyperfine splitting by two ^{14}N and two backbone ^{1}H nuclei, yielding a 15-line spectrum with equal ^{1}H and ^{14}N hyperfine splitting constants. This data further confirms the delocalization of this electron across the four nuclei of the DAB backbone but not onto the *N*-aryl groups. There is no observable hyperfine interaction with ^{25}Mg (I = 5/2, 10% natural abundance). As such the absence of this interaction in the EPR spectrum suggests that there is minimal delocalization of the electron across the Mg center. Similar behavior was observed in the EPR spectrum of **2.8** (Figure 2.5B) in toluene at 298 K. A hyperfine interaction was observed between the unpaired electron and two ^{14}N nuclei, as well as a slightly weaker ^{1}H hyperfine interaction with two ^{1}H atoms on C26 and C29. Because of this weak coupling, the full number of theoretical lines (15) could not be observed.

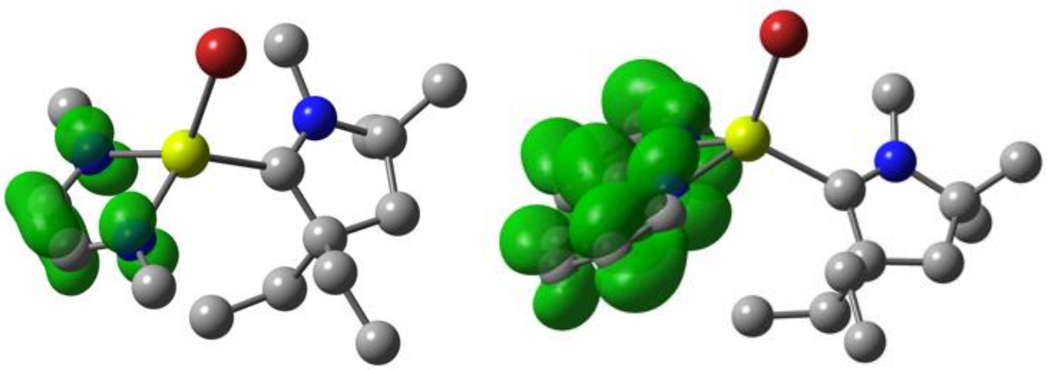

Figure 2.6. Spin density contour plots of **2.7^{NMe}** and **2.8^{NMe}**.

B3LYP-D3(BJ)/def2-TZVP DFT calculations indicate that the spin density of the unpaired electron in **2.7^{NMe}** (Figure 2.6, left) is predominantly limited to the N2–C27–C28–N3 backbone (89% of spin density), while in **2.8^{NMe}** (Figure 2.6, right) the N3-C28-C27-N2 backbone contains only 49% of the spin density. An additional 37% is located on bipyridyl C24, C25, C30, C31 atoms. This suggests some delocalization of the unpaired electron in the bipyridyl system in **2.8** but not on the Dipp substituents of **2.7** In both cases less than 3% of the spin density is located on the Mg atom, which is consistent with the lack of an observable hyperfine interaction with ^{25}Mg in the EPR spectra.

On account of the strong absorption of visible light by compounds **2.7** and **2.8**, the UV-Vis spectrum of each product was obtained in toluene (0.1 mg/mL, Figures A3.42-43). The UV-Vis spectrum of **2.7** (Figure A3.42) gives a narrow absorbance band at 458 nm (ε = 3167 M^{-1}cm^{-1}) corresponding to a ΔE of 62.4 kcal mol^{-1}. Compound **2.8** (Figure A3.43) exhibited multiple absorbances at 388 nm (ΔE = 73.7 kcal mol^{-1}, ε = 11902 M^{-1}cm^{-1}), 513 nm (ΔE = 55.7 kcal mol^{-1}, ε = 3963 M^{-1}cm^{-1}), 541 nm (ΔE = 52.8 kcal mol^{-1}, ε = 3740 M^{-1}cm^{-1}), and 830 nm (ΔE = 34.4 kcal mol^{-1}, ε = 449 M^{-1}cm^{-1}).

MO analysis and TD-DFT (ωB97XD/def2-TZVP) results illustrate the difference in absorbance between **2.7** and **2.8**. The SOMO and LUMO of both compounds are similar (diimine-based π SOMO and Mg-C based π-symmetric LUMO), however **2.8** possesses a bipyridyl system with low-lying π* MOs located on the bpy ligand that are not present in **2.7**. As a result, ligand-centered (LC) π-π* transitions are only present in **2.8**, which are calculated to occur at longer wavelengths (SOMO to LUMO+1 and LUMO+2 transitions at 799 and 702 nm, respectively). Transitions from SOMO to LUMO are calculated at 368 and 449 nm for **2.7** and **2.8**, respectively, and may be matched with the experimental absorbances at 458 (**2.7**) and 541 nm (**2.8**). The TD-DFT absorbance wavelengths are consistently shorter than the experimentally observed values.

2.4.2. Reaction of Carbene–Group 2 Dihalides with Doubly-Reduced α-Diimines

We next sought to obtain tricoordinate, doubly-reduced magnesium and beryllium compounds containing only a cyclic carbene and a dianionic diimine ligand. The reaction of either ^{Dipp}DAB or bpy with complex **2.4** and two equivalents of KC_8, yielded the doubly-reduced product (**2.9**) in 60% yield as a dark green solid (Scheme 2.7).

Scheme 2.7. Synthesis of Doubly-Reduced Magnesium Complexes.

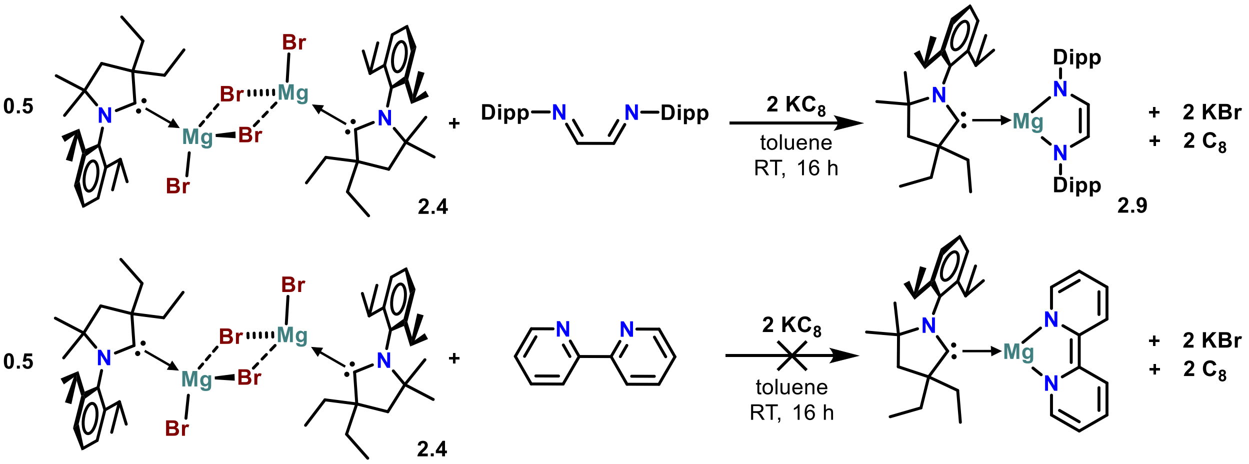

Notably, multiple attempts to obtain (^{Et2}CAAC)Mg(bpy) were unsuccessful. When 2.2 eq of KC_8 were used, the singly-reduced compound **2.8** was the only product obtained. Regardless of the stoichiometric ratio of KC_8 used, the reaction mixtures consistently showed an intractable mix of products, including free ^{Et2}CAAC. While the exact reason(s) for this result is unknown, it clearly indicates that the formation of the Mg–bpy^{2-} complex is less favorable than the Mg–DAB^{2-} compound.

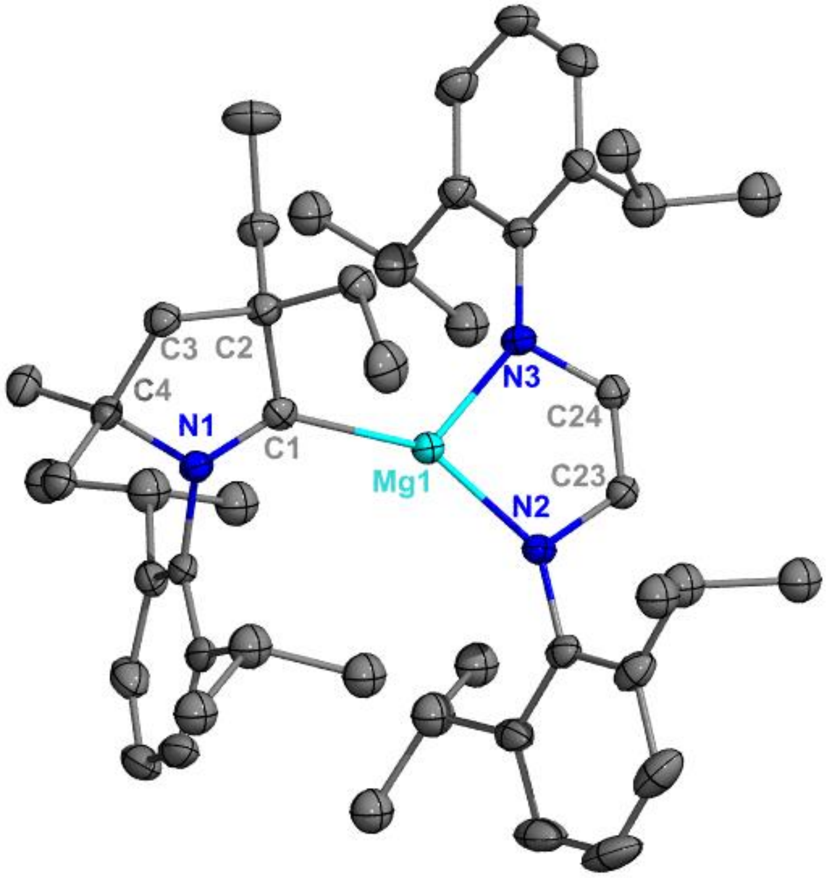

Figure 2.7. Molecular structure of **2.9** (H atoms omitted for clarity). Selected bond distances (Å) and angles (°): Mg1–C1: 2.194(2); Mg1–N2: 1.9644(16); Mg1–N3: 1.9682(16); C23–N2: 1.410(2); C24–N3: 1.410(2); C23–C24: 1.342(3); C1–Mg1–N2: 144.38(7); N2–Mg1–N3: 90.79(7).

The molecular structure of **2.9** (Figure 2.7) exhibits a tricoordinate magnesium in a highly distorted trigonal planar geometry enabled by the combined steric demand of the ^{Et2}CAAC and ^{Dipp}DAB *N*-aryl groups. This steric repulsion manifests itself in the 144.38(7)° C1–Mg1–N2 bond angle, a deviation of 24.38(7)° from the ideal 120°. In the ^{Dipp}DAB complexes **2.7** and **2.9**, the backbone C–C bond distance exhibits an incremental shortening from 1.467(5) Å for the free diimine[131] to 1.404(7) Å in compound **2.7**, to 1.342(3) Å in compound **7**. This provides further evidence that the ligand is reduced by two electrons in compound **2.9** and one electron in compound **2.7**.

DFT results yield a tricoordinate magnesium atom with co-planar rings for **2.9**$^{\mathbf{NMe}}$ with a Mg-C bond distance of 2.161 Å (WBI 0.19), which is suggestive of some double-bond character. Calculated MOs (shown in Figure 2.8) are consistent with partial double-bond Mg-C character, with the π-symmetry HOMO delocalized over the diimine N atoms, Mg, and carbene C (for further details see appendix III and original manuscript).[123]

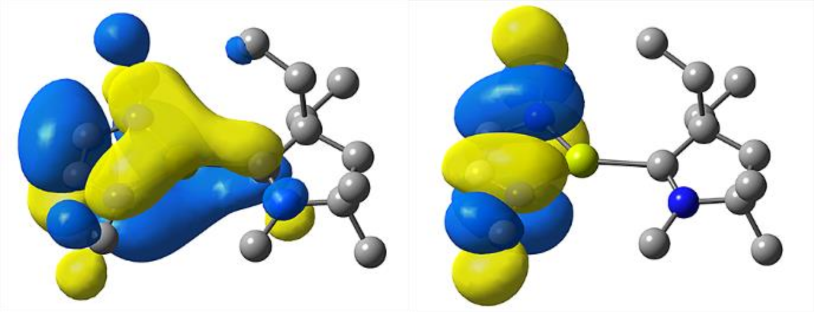

Figure 2.8. Plot of HOMO (left) and HOMO-1 (right) for compound **2.9**$^{\mathbf{NMe}}$.

The UV-Vis spectrum of **2.9** (Figure A3.44) in toluene showed an extremely broad, weak absorption band (ε = 540.0 $M^{-1}cm^{-1}$) at 783 nm, corresponding to a π-π* transition. TD-DFT (ωB97XD/def2-TZVP) calculations also yield a long wavelength band (676 nm), characterized as ligand-centered charge-transfer (LCT) from DAB to CAAC. The band is associated almost exclusively with a HOMO-LUMO π-π* transition. The corresponding energy of this electronic transition is exceptionally low at 36.5 kcal mol^{-1}. The HOMO, HOMO-1 and HOMO-2 of **2.9** are centered on DAB, and hence most absorbance bands correspond to charge transfer from the DAB ligand. In addition to the long wavelength LCT transition, TD-DFT results give two low-intensity transitions (444 and 311 nm) characterized as ligand-to-metal charge-transfer (LMCT) from DAB to Mg, while shorter wavelength bands are characterized as π-π* LCT transitions and have greater oscillator strength. The large difference between the electronic transitions between the singly- and doubly-reduced complexes of the same metal and ligand combination indicates that small changes to the ligand redox state by the addition or removal of one electron can drastically change the nature of the frontier orbitals and thus affect the potential reactivity of the complexes.

2.4.3. Insights into Reactivity of Doubly-Reduced Carbene–Mg–diimine Complexes

Scheme 2.8. Reactivity Screening of Singly- and Doubly-Reduced Magnesium Complexes.

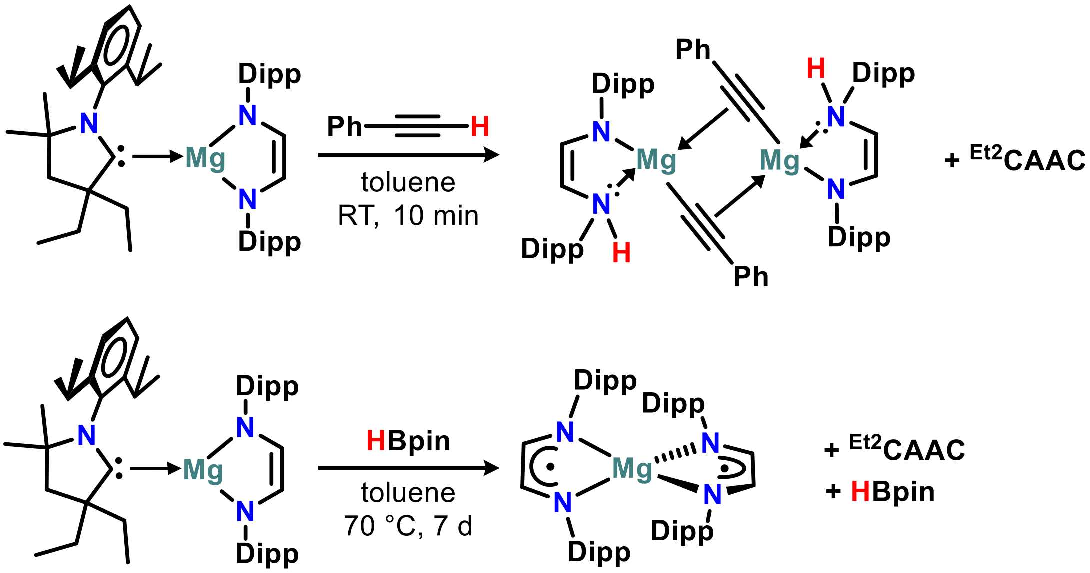

To begin to understand the reactivity of this molecular scaffold (CAAC–Mg–diimine), compounds **2.7** and **2.9** [(CAAC)Mg(Br)(DAB) and (CAAC)Mg(DAB)] were investigated in reactions with various E-H bonds (E = B, C_{sp}, C_{sp2}, C_{sp3}) or electron acceptors (e.g. benzophenone). The summary of these reactivity studies are shown in Scheme 2.8. The first substrate that was screened was the phenyl-substituted terminal alkyne, phenylacetylene (pK_a = 28.7 in DMSO).[132] When phenylacetylene was added to a toluene solution of compound **2.9** at RT, the dark green solution turned rapidly to orange as an immediate reaction occurred. Single crystals of the product of this reaction were obtained from a saturated toluene solution at –39 °C.

The molecular structure of compound **2.10** (Figure 2.9) shows a dimerized molecule connected via two $\pi_{C\equiv C}$–Mg contacts in which the terminal C–H bond of phenylacetylene has been heterolytically cleaved by one of the Mg–N bonds of the starting material, resulting in a new Mg–C and N–H covalent bonds. The N–Mg bond across which the C–H was added is now a donor-acceptor bond between the nitrogen lone pair and electropositive Mg center. The difference in the Mg–N bonding is supported experimentally by the difference in bond distance between N1–Mg1 [2.157(2) Å] and N2–Mg2 [2.000(2) Å].

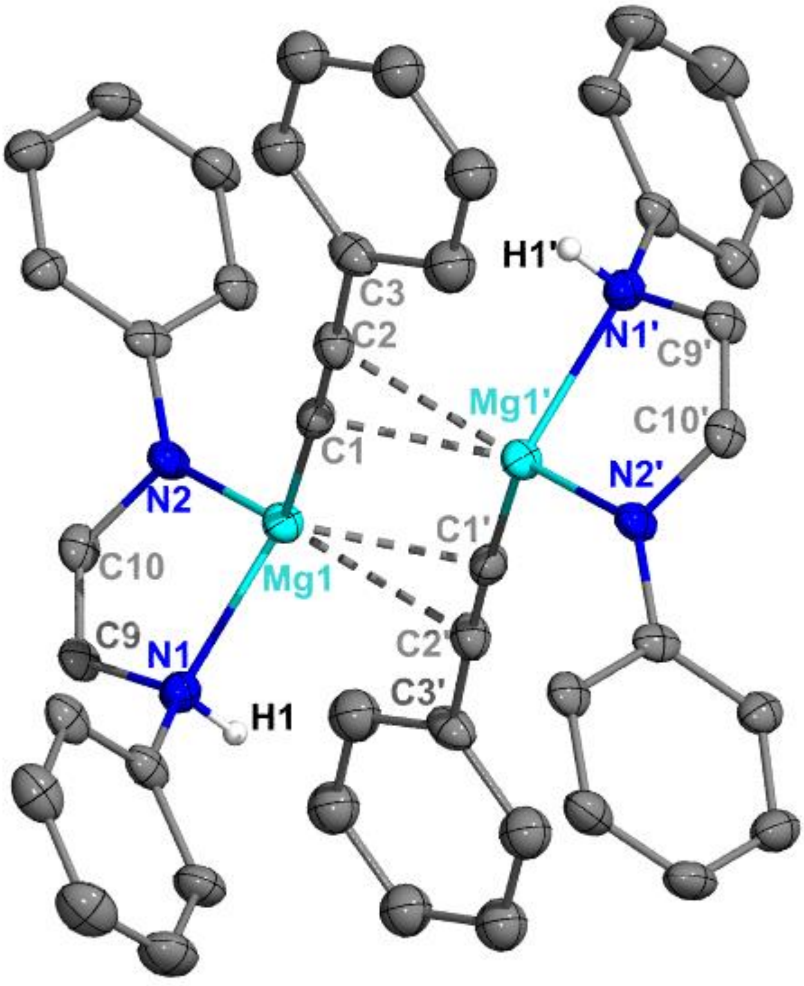

Figure 2.9. Molecular structure of **2.10** (H atoms and Dipp-isopropyl groups omitted for clarity). Selected bond distances (Å) and angles (°): Mg1–N2: 2.000(2); Mg1–N1: 2.157(2); Mg1–C1: 2.138(3); Mg1–C1’: 2.284(3); Mg1–C2: 2.629(3); Mg1–Mg1’: 3.1017(16); N2–Mg1–N1: 85.02(8); N2–Mg1–C1: 120.65(9).

Based upon the evidence (discussed above) of compound **2.9**’s potential to heterolytically cleave weakly acidic E–H bonds, this reactivity was further investigated. The reaction of **2.9** with a neutral substrate containing a sterically accessible B–H bond, pinacolborane (HBpin), was carried out (Scheme 2.8). After a solution of **2.9** and HBpin in toluene was heated at 70 °C for 7 days, a dark brown solution was observed. When this solution was allowed to slowly cool to room temperature, deeply red, block-like single crystals suitable for X-ray diffraction were obtained. The molecular structure of the product revealed a neutral molecule featuring one tetrahedral magnesium center coordinated by two monoanionic DAB ligands (Figure A2.11). This structural motif – e.g. $(DAB)_2Mg$ – is well-known for alkaline complexes coordinated by α-diimines and is often seen as a Schlenk equilibrium side product in solutions containing alkaline earth elements coordinated by doubly reduced diimine ligands. The result of this experiment indicates that the dissociation of CAAC and redistribution of the DAB ligands to form **2.11** is favored instead of the heterolytic cleavage of the B–H bond in HBpin.

To conclude, we have reported the synthesis and characterization of a series of new carbene-coordinated magnesium and beryllium dihalides, including the first structurally characterized CAAC–magnesium halide complex. We used these compounds to obtain reduced magnesium and beryllium species coordinated by a carbene and either a singly-reduced or doubly-reduced α-diimine. Interestingly, the doubly-reduced magnesium and beryllium species exhibit strong π-bonding interactions across the entire carbene–metal–diimine core. This represents a rare example of alkaline earth metals participating in π-bonding in an *s*-block heterocycle. Additionally, diverse structural and electronic characteristics were observed in the reduced products which varied in accordance with the specific combination of α-diimine, carbene, and metal center that was chosen. The relationship between ligand steric demand, ligand electronic structure, and metal identity was thoroughly investigated. We expect that the high variability of the structural and electronic properties of this ligand system will greatly expand the redox chemistry of group 2 elements. The reactivity of these systems toward bond activations and reoxidation was explored. The propensity of the CAAC to dissociate from the metal center upon reaction with labile substrates such as terminal alkynes limits the utility of **2.9** for further bond activation systems, so future studies will focus on developing a similar scaffold (i.e. carbene–Mg–diimine) with less sterically demanding ligands.[133] Additionally, future work should explore the reactivity of **2.9** with oxidizing substrates such as O_2, O_3, etc. towards obtaining useful Mg–O bonded molecular species.

Chapter 3: Low-Nuclearity Magnesium Hydride Complexes Stabilized by N-heterocyclic Carbenes

Containing work that was originally published in the following:

Freeman, L. A.; Walley, J. E.; Dickie, D. A.; Gilliard, R. J. *Dalton Trans.* **2019,** *48*, 17174-17178.

The isolation of molecular main-group hydride complexes has become an important point of focus for researchers, due to a renewed interest in these compounds as earth-abundant molecular catalysts and candidates for chemical storage of hydrogen.[3, 23, 25, 26, 29, 30, 43, 50, 134-139] One popular candidate for solid-state hydrogen storage is MgH_2, because of its high gravimetric hydrogen content (7.66% by mass). The extremely high lattice energy of bulk MgH_2 (α–MgH_2), however, gives the compound a correspondingly high thermodynamic stability to H_2 elimination.[25, 134, 140-142] One possible method of lowering the required desorption temperature is by decreasing the Mg–H cluster size. For this reason, low nuclearity "molecular" magnesium hydride clusters have recently become high-value synthetic targets. Prior reports have highlighted that extremely small clusters of MgH_2 ($n_{Mg}<19$) should have a substantially decreased enthalpy of decomposition, such that as the cluster size is further decreased, the H_2 elimination temperature decreases dramatically.[134, 143, 144] For this reason, synthetic chemists select strong, kinetically stabilizing supporting ligands which can force the formation of smaller cluster sizes of $[Mg_nH_m]^{(2n-m)+}$ and prevent decomposition to insoluble MgH_2 via ligand exchange (i.e. Schlenk equilibrium). By far the largest proportion of isolated group 2 hydrides have been supported by strongly-binding, usually chelating, anionic ligands with extreme steric demand. Common examples include – but are not limited to – β-diketiminate (NacNac), *tris*(pyrazolyl)methanide, *tris*[(1-isopropylbenzimidazol-2-yl)-dimethylsilyl)]methanide, or macrocyclic amidopolyamine ligands.[145] There are also some examples in which polydentate neutral ligands such as pentamethyldiethylenediamine were used to stabilize heavier *s*-block hydrides.[32] The kinetic stabilization afforded by the ligands due to their physical size is arguably the *most critical* characteristic controlling the stability and structure of the complex.[29, 146] These stringent stabilization requirements have made monodentate, neutral *N*-heterocyclic carbenes (NHCs) substantially less common in group 2, because these neutral donors generally exhibit much weaker coordination than a chelating anionic ligand of the same size. Despite this, the number of isolated NHC-magnesium complexes has recently begun to grow.[98, 101, 108, 110, 147-149]

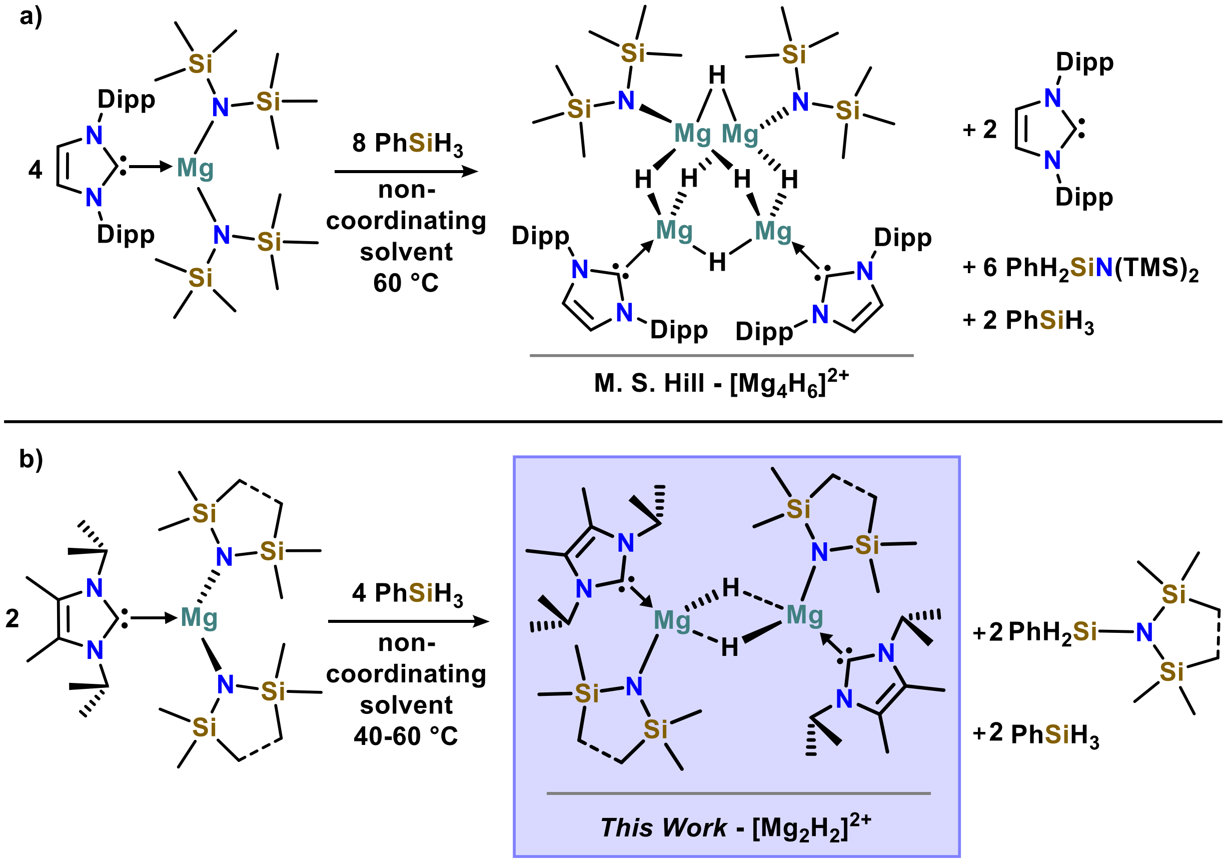

Figure 3.1. Syntheses of carbene-coordinated magnesium hydride complexes.

Thus far, there has only been one reported example of a magnesium hydride complex which utilizes a neutral donor as the *primary* source of kinetic stabilization for the complex (Fig. 1a, *vide supra*).[28] This remarkable work utilized the sterically demanding *bis*(2,6-diisopropylphenyl)imidazol-2-ylidine (IPr) to kinetically stabilize a $[Mg_4H_6]^{2+}$ cluster which still (10 years later) exhibits the highest H:Mg ratio (1.5:1) of any molecular magnesium hydride compound reported to date. This result clearly highlights the value of strongly donating carbenes to magnesium hydride chemistry. However, the formation of this complex requires a stoichiometric loss of 0.5 eq of the carbene ligand, and two of the four magnesium centers are not coordinated by a carbene. We were inspired by this report to further explore the role of ligand steric demand on the structure of carbene-stabilized magnesium hydride complexes, as we have recently found that smaller carbenes can yield more persistent binding to magnesium centers than their larger counterparts.[106, 123] Herein, we report the synthesis and characterization of two $[Mg_2(\mu\text{-}H)_2]^{2+}$ species, $[(I^iPr^{Me2})Mg(\mu\text{-}H)(HMDS)]_2$ [**3.4**, I^iPr^{Me2} = *N,N'*-diisopropyl-2,3-dimethylimidazol-2-ylidine, HMDS = hexamethyldisilazide] and $[(I^iPr^{Me2})Mg(\mu\text{-}H)(ASCP)]_2$ (**3.5**, ASCP = 2,2,5,5-tetramethyl-2,5-disila-1-azacyclopent-1-yl), supported by a monodentate silyl amide and an NHC (Fig. 1b, *vide supra*). Notably, these are only the second and third examples of a carbene-coordinated magnesium-hydride complex and are the lowest nuclearity Mg–H complexes stabilized by carbenes to date.

Traditionally successful routes to access magnesium hydride compounds utilize a bond metathesis reaction between a Mg–Y bond (e.g., Y = NR_2 or CH_2R) and a covalent hydride source such as $PhSiH_3$.[29] For the investigations reported herein, the anionic amides ASCP and HMDS were selected as the metathesis precursor, as they are practically electronically identical but have significantly different cone angles (ASCP = 123°, HMDS = 145°). The difference in the steric profile of these two ligands has been shown to elicit divergent reactivities in other divalent main group complexes.[150, 151] We therefore synthesized solvent-free, dimeric magnesium *bis*-amides, $[Mg(HMDS)_2]_2$,[152-154] and the previously unreported $[Mg(ASCP)_2]_2$ (**3.1**, molecular structure given in Fig. A2.13). These compounds were prepared via the reaction of 2 eq of the respective free silylamine with di-*n*-butyl magnesium in heptanes. The subsequent combination of 1 eq of I^{i}Pr^{Me2} with either [Mg(HMDS)$_2$]$_2$ or **3.1** in *n*-hexane gave the desired coordination complexes **3.2** and **3.3** in 86% and 89% yields as bright white amorphous solids (Scheme 3.1).

Scheme 3.1. Syntheses of I^{i}Pr^{Me2}-coordinated magnesium *bis*-amides.

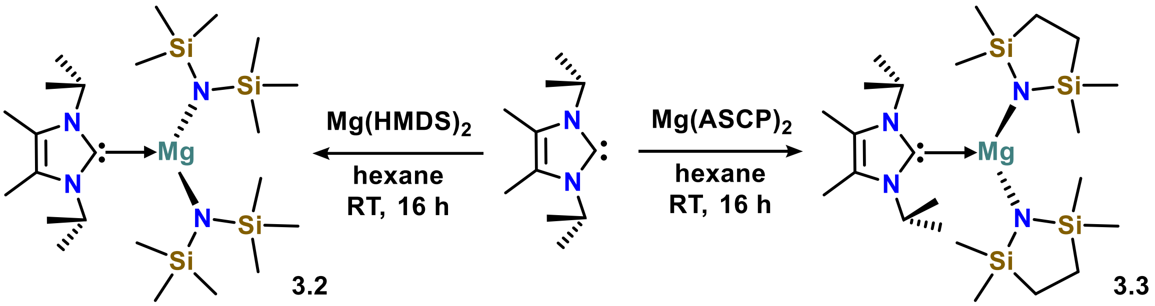

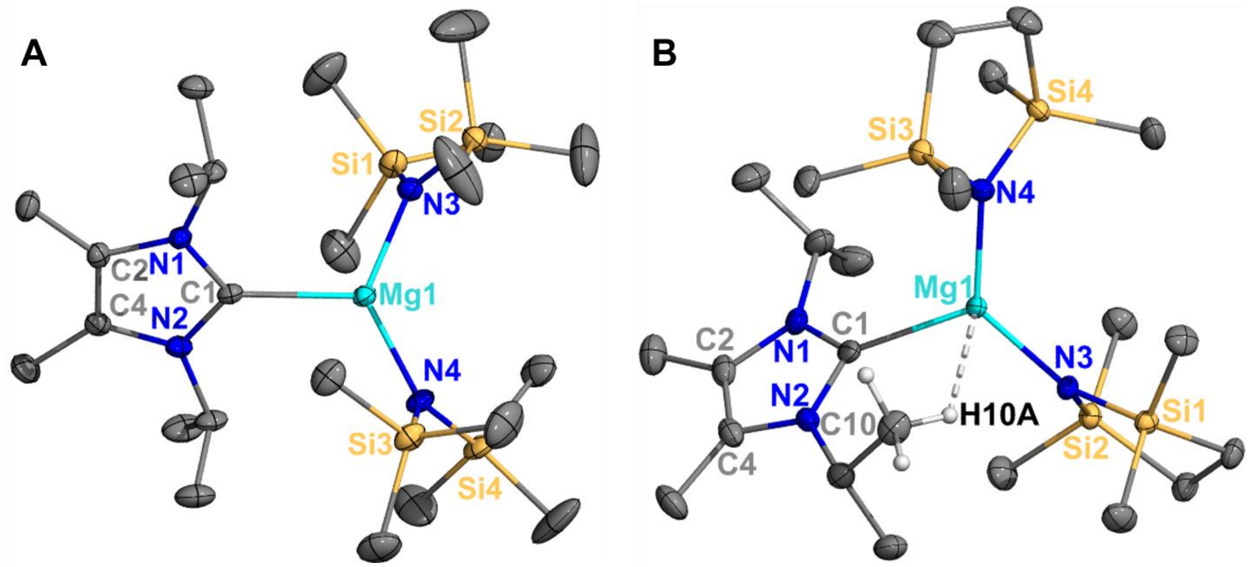

Figure 3.2. Molecular structure of **3.2** (a) and **3.3** (b) (thermal ellipsoids at 50% probability; H atoms omitted for clarity with the exception of those located on C10 in **3.3**); only the major occupied position is shown for disordered *N*-isopropyl substituents in (b). Selected bond distances (Å) and angles (deg): **3.2**: Mg1–C1: 2.2120(19); Mg1–N3: 1.9920(16); Mg1–N4: 1.9944(16); C1–N1: 1.360(2); C1–N2: 1.361(2); N3–Mg1–C1: 111.75(7); N4–Mg1–C1: 117.82(7); N4–Mg1–N3: 130.27(7). **3.3**: Mg1–C1: 2.2118(13); Mg1–H10A: 2.429(16); Mg1–N3: 1.9855(10); Mg1–N4: 1.9755(11); C1–N1: 1.3572(16); C1–N2: 1.3583(15); N3–Mg1–C1:

113.92(4); N4–Mg1–C1: 115.06(4); N4–Mg1–N3: 130.62(4); C1–Mg1–H10A: 78.4(4); C10–H10A–Mg1: 121.1(11).

Single crystals of **3.2** and **3.3** suitable for X-ray diffraction studies were obtained from a saturated solution of the respective complex in *n*-hexane at –39 °C. The molecular structure of **3.2** (Fig. 3.2a) shows the desired carbene-coordinated product, which exhibits a tricoordinate magnesium center ligated by one $I^{i}Pr^{Me2}$ and two silylamides. In the solid-state structure of **3.2**, the coordinatively unsaturated magnesium center does not exhibit dimerization or intramolecular anagostic interactions.

The molecular structure of **3.3** (Fig. 3.2b), the "tied-back" analog of **3.2**, shows an intriguing deviation from the structures of other NHC–Mg(HMDS)$_2$ complexes. The magnesium center is coordinated by two silylamides and one carbene, and the sum of the angles between these three ligands equals 359.6 deg. However, the reduced steric demand from the silylamides allow the *N*-isopropyl substituent of $I^{i}Pr^{Me2}$ to "flip" forward, resulting in a substantial electrostatic (i.e. anagostic) interaction in the solid-state structure between the ^{methyl}C–H bond and the highly Lewis acidic Mg center. The H10A–Mg1 distance [2.429(16) Å] and C10–H10A–Mg1 angle [121.1(11)] fall well within the typical range for anagostic interactions of C–H bonds with electron-deficient metal centers proposed by Brookhart, Green and Parkin (2.3-2.9 Å, 110-170 deg).[155] The ^{1}H NMR spectrum of **3.3** shows only one resonance for the *N*-isopropyl methyl groups of the $I^{i}Pr^{Me2}$ ligand; a well-resolved doublet at 1.30 ppm. This peak is shifted slightly downfield from the analogous peak in the ^{1}H NMR spectrum of **3.2** (1.19 ppm) which agrees with the expected behavior for a time-averaged signal of eleven non-anagostic protons and one anagostic proton. These data indicate that if indeed there is an anagostic interaction in solution at RT, the exchange of the anagostic protons through rotation is a rapid fluxional process in solution on the NMR timescale. VT-NMR experiments were carried out in toluene-d_8 to resolve the anagostic proton resonance, however no peak separation was observed down to –35 C.

We next sought to investigate the propensity of **3.2** and **3.3** to react with a hydride source to yield magnesium hydride clusters. Heating a benzene-d_6 solution of 4 eq of $PhSiH_3$ with either **3.2** or **3.3** in a J. Young-tap NMR tube for 16 h showed gradual formation of the desired σ-metathesis product. Similar to the reactivity observed for Hill's (IPr)Mg$(HMDS)_2$,[28] the reaction of $PhSiH_3$ with **3.2** yielded no conversion below 60 °C. The metathesis of one Mg–N bond with a Si–H bond to form a complex of the type $(I^iPr^{Me2})Mg(NR_2)(H)$ was subsequently characterized by the appearance of a new Si–^{1}H resonance at 5.17 ppm [$^1J_{SiH}$ = 102 Hz, attributable to $(SiMe_3)_2N$–Si(Ph)$(H)_2$], along with the appearance of a sharp singlet for an Mg–^{1}H resonance at 4.29 ppm. Relative integrations of the resonances indicated that there was one Mg–^{1}H moiety per I^iPr^{Me2} ligand, and no further conversion to a more hydride rich compound could be induced. An analogous NMR experiment with **3.3** showed a substantially more facile conversion to a similar Mg–H complex. In this case, substantial conversion to the expected hydride product was observed after just 30 minutes at room temperature. Subsequent heating to 40 °C for 16 h gave complete conversion to a *mono*hydride complex exhibiting a sharp Mg–^{1}H resonance at 4.31 ppm. As in the previous experiment, no further conversion to a higher order complex could be induced.

Scheme 3.2. Syntheses of $I^{i}Pr^{Me2}$-coordinated heteroleptic magnesium hydrido complexes.

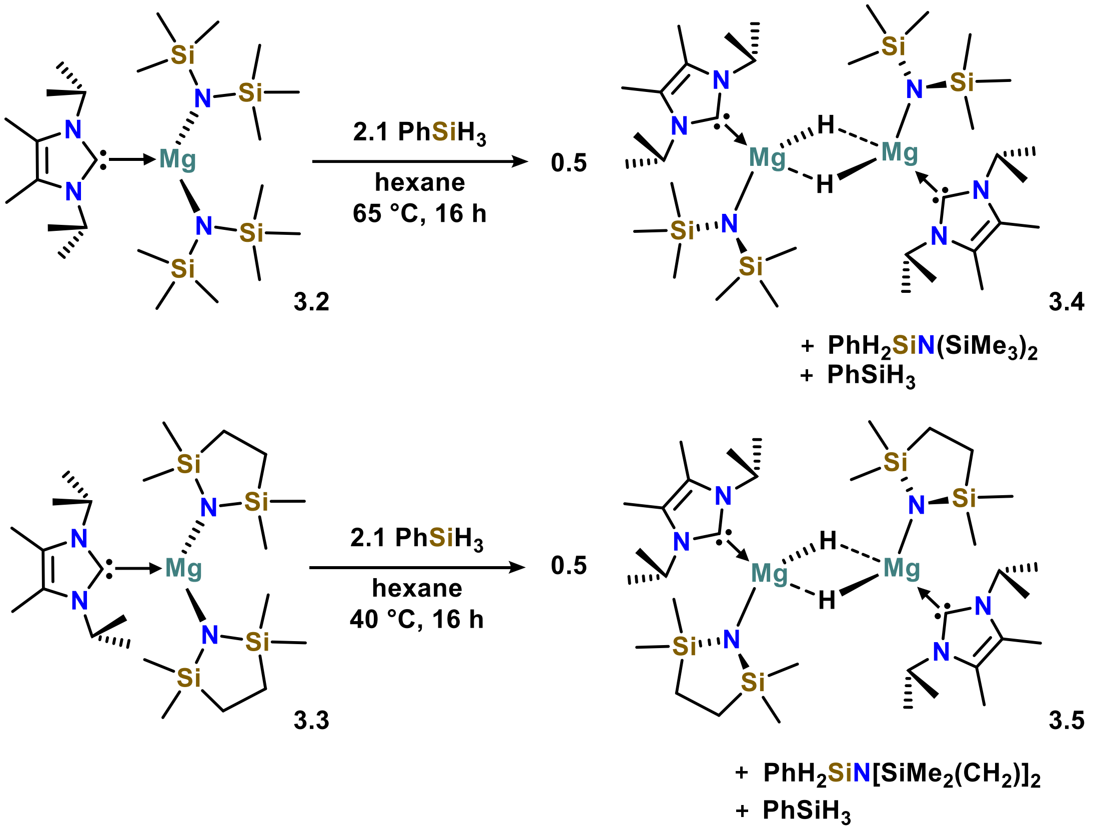

Based on the results of these NMR experiments, the carbene coordinated magnesium hydrides **3.4**[156] and **3.5** were prepared in 73% and 66% yields, respectively, via the reaction of **3.2** and **3.3** with 2 eq of $PhSiH_3$ in *n*-hexane at 65 °C (**3.4**) and 45 °C (**3.5**) for 16 h (Scheme 3.2). Colorless, block-like single crystals of **3.4** and **3.5** suitable for X-ray diffraction were obtained from saturated *n*-hexane solutions at –39 °C, which vigorously emit H_2 gas when exposed to trace amounts of moisture. The solid-state molecular structures of **3.4** and **3.5** (Fig. 3.3a-b) proved to be the same *mono*(hydrido) magnesium species observed in NMR experiments. These compounds exist in the solid state as centrosymmetric dimers which may be regarded as a $[Mg_2(\mu\text{-}H)_2]^{2+}$ core in which each of the magnesium centers is stabilized by one NHC and one silylamide. This is in stark contrast to the first NHC-stabilized magnesium hydride cluster, Hill's

$[Mg_4H_6]^{2+}$ in which half of the magnesium atoms did not exhibit any interaction with an NHC ligand.[28] The ^{carbene}C–Mg bond lengths in **3.4** [C1–Mg1: 2.2239(17) Å, C18–Mg2: 2.2250(16) Å] are similar in length to the starting material, **3.2** [C1–Mg1: 2.2120(19) Å]. The Mg–H [1.828(18)-1.933(18) Å] and Mg–Mg [2.8269(9)] interatomic distances in **3.4** are consistent with other structurally similar $[Mg_2(\mu\text{-}H)_2]^{2+}$ complexes that have been reported.[31, 94, 157-160]

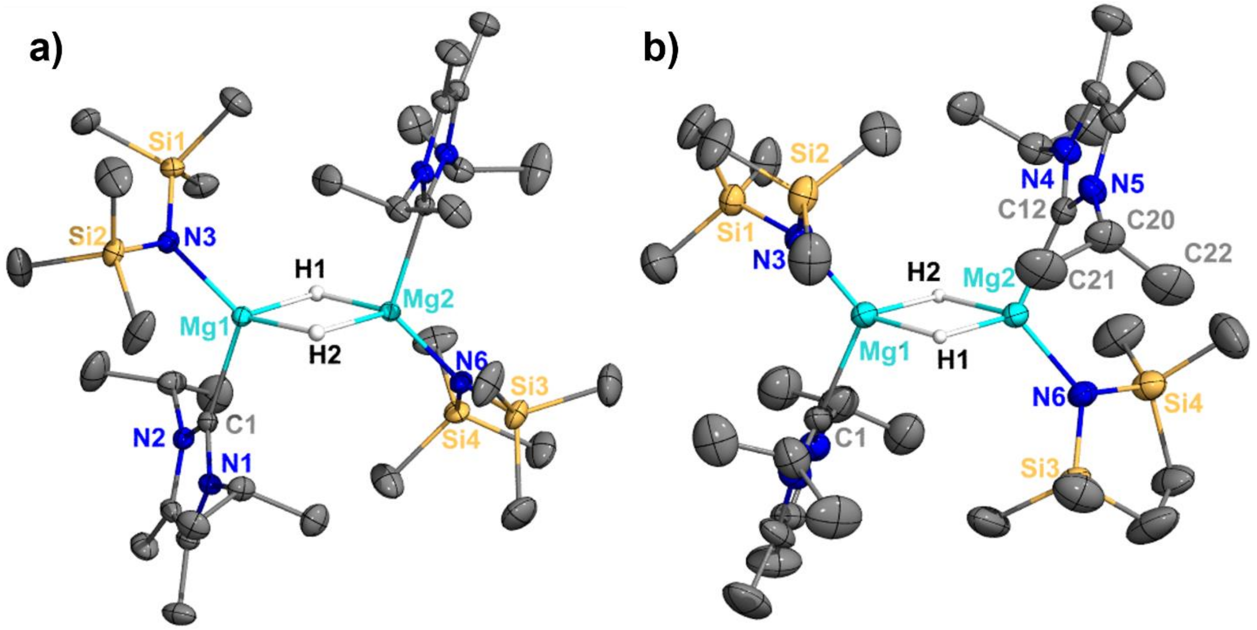

Figure 3.3. Molecular structures of **3.4** (a) and **3.5** (b) [thermal ellipsoids set at 50%; H atoms omitted for clarity with the exception of H1 and H2 which were isotropically refined; only the major occupied position is shown for disordered *N*-isopropyl substituents in (b)]. Selected bond distances (Å) and angles (deg): **3.4**: Mg1–C1: 2.2239(17); Mg2–C18: 2.2250(16); Mg1–H1: 1.828(18); Mg1–H2: 1.933(18); Mg2–H1: 1.861(17); Mg2–H2: 1.865(18); Mg1–Mg2 2.8269(9); Mg1–N3: 2.0098(14); Mg2–N6: 2.0144(14); N3–Mg1–C1: 118.02(6); C1–Mg1–H1: 105.3(6); H1–Mg1–H2: 81.4(8). **3.5**: Mg1–C1: 2.230(4); Mg2–C12: 2.228(4); Mg1–H1: 1.93(4); Mg1–H2: 1.93(4); Mg2–H1: 1.97(4); Mg2–H2: 1.82(4); Mg1–Mg2; 2.8163(19); Mg1–N3: 1.994(4); Mg2–N6: 2.000(4); N3–Mg1–C1: 119.27(16); C1–Mg1–H1: 107.1(12); H1–Mg1–H2: 84.4(17).

The molecular structure of **3.5** exhibits largely the same bonding and structural characteristics as its HMDS analog. The $C_{carbene}$–Mg interatomic distances [Mg1-C1: 2.230(4) Å, Mg2–C12: 2.228(4) Å] are similar to the same bonds in **3.4** [C1–Mg1: 2.2239(17) Å, C18–Mg2: 2.2250(16) Å]. As with compound **3.4**, the Mg–H distances of **5** are within range of a typical Mg–H bond,[31, 94, 157-160] and the Mg–Mg distance in **3.5** [2.8163(19) Å] is only marginally shorter than in **3.4** [2.8269(9) Å]. These data clearly indicate that reducing the steric demand of the *amide* has a significant impact on the reactivity of the compounds, but imparts a negligible impact on the structure of the resulting hydride. One notable structural anomaly in **3.5** is the partial orientation of the $I^{i}Pr^{Me2}$ *N*-isopropyl groups toward the core, instead of all four pointing away. As observed in **3.3**, there is a fluxional anagostic interaction between the $I^{i}Pr^{Me2}$ sidearms and the electropositive magnesium center. This interaction appears to be weaker in **3.5** than in **3.3**, and the mixture of anagostic (*N*-isopropyl pointing forward) and non-contacted (*N*-isopropyl pointing away) isomers contributes to a significant degree of disorder in the crystal lattice.

With the exception of the anagostic interactions in **3.5**, the hydride complexes **3.4** and **3.5** appear to be remarkably static in solution insofar as ligand coordination and oligomerization is concerned. The carbene-coordinated dimers appear stable in solutions of C_6D_6 up to 70 °C, above which temperature discoloration and an intractable mixture of products was observed.

In summary, we have isolated stable $I^{i}Pr^{Me2}$-coordinated magnesium hydride dimers **3.4** and **3.5**, which are the lowest nuclearity carbene-stabilized Mg–H complexes reported thus far. Furthermore, the formation of **3.4** and **3.5** does not result in stoichiometric loss of the neutral stabilizing ligand during the formation of the product. Taken in this context, we expect the results of this investigation will guide ligand selection in future studies of molecular group 2 hydride complexes. Further investigations into the reactivity of these compounds and the effect of the carbene on the H_2 release properties of the $[Mg_2H_2]^{2+}$ core are currently underway.

Chapter 4: Reduction Chemistry of Cyclic (Alkyl)(Amino) Carbene-2-Carboxylates

Containing work that was originally published in the following:

Lieske, L. E.; Freeman, L. A.; Wang, G.; Dickie, D. A.; Gilliard, R. J., Jr.; Machan, C. W. *Chem. Eur. J.* 2019, *25*, 6098-6101.

Freeman, L. A.; Obi, A. D.; Machost, H. R.; Molino, A.; Nichols, A. W.; Dickie, D. A.; Wilson, D. J. D.; Machan, C. W.; Gilliard, R. J. *Chem. Sci.* **2021,** *12*, 3544-3550.

4.1. Metal-Free Electrochemical Reduction of CO_2 Mediated by Cyclic(Alkyl)(Amino) Carbenes

Carbenes, particularly cyclic(alkyl)(amino) carbenes (CAACs), have unique reactivity with transition metals, organic small molecules and main-group elements.[161-170] These properties have been harnessed to stabilize low-coordinate organic and inorganic species, and mediate organocatalytic transformations.[147, 167, 168] While both N-heterocyclic carbenes (NHCs) and cyclic(alkyl)(amino) carbenes (CAACs) are known to stabilize carbon dioxide (CO_2) adducts as a zwitterion, only the more nucleophilic and electrophilic CAAC forms a ketene species with carbon monoxide (CO).[171] Previous reports have demonstrated that NHC-CO_2 complexes can act as a source of activated CO_2 for electrocatalytic reduction by transition metal compounds.[172] Additionally, NHC-CO_2 adducts can participate in organically-mediated transformations of CO_2 to form methanol equivalents, further hinting at the potential utility of these molecules for CO_2 reduction chemistry.[173, 174] Roesky et al. reacted a Zn biradicaloid with CO_2 to form CAAC-CO_2 and Zn metal, however, the reactivity of the adduct toward reduction was not investigated.[175] Based on these precedents, we were interested in examining the electrochemical behavior of CAAC-CO_2 adducts. Herein, we describe the synthesis, molecular structure, and electrochemical behavior of ^{Cy}CAAC-CO_2 adduct (**4.1**). Notably, compound **4.1** demonstrates reversible one-electron redox properties at $E_{1/2} = -2.15$ V vs Fc^+/Fc under Ar saturation conditions and can mediate the stoichiometric reductive disproportionation to CO and carbonate (CO_3^{2-}) under CO_2 saturation *without any additional organic or inorganic reagents*.

Bubbling CO_2 through a solution of ^{Cy}CAAC[169] in anhydrous THF or Et_2O resulted in immediate precipitation of a white solid which was isolated via filtration and determined to be the zwitterionic CO_2 adduct, compound **4.1** (Scheme 4.1). Characterization by ^1H and ^{13}C NMR

(Figure A3.19-20) were consistent with the molecular structure in Scheme 4.1. Colorless block-shaped crystals of **4.1** suitable for a single crystal X-ray diffraction study were grown from a saturated THF solution at −37 °C (Figure 4.2A).

Scheme 4.1. Complexes observed and proposed electrochemical reaction pathway.

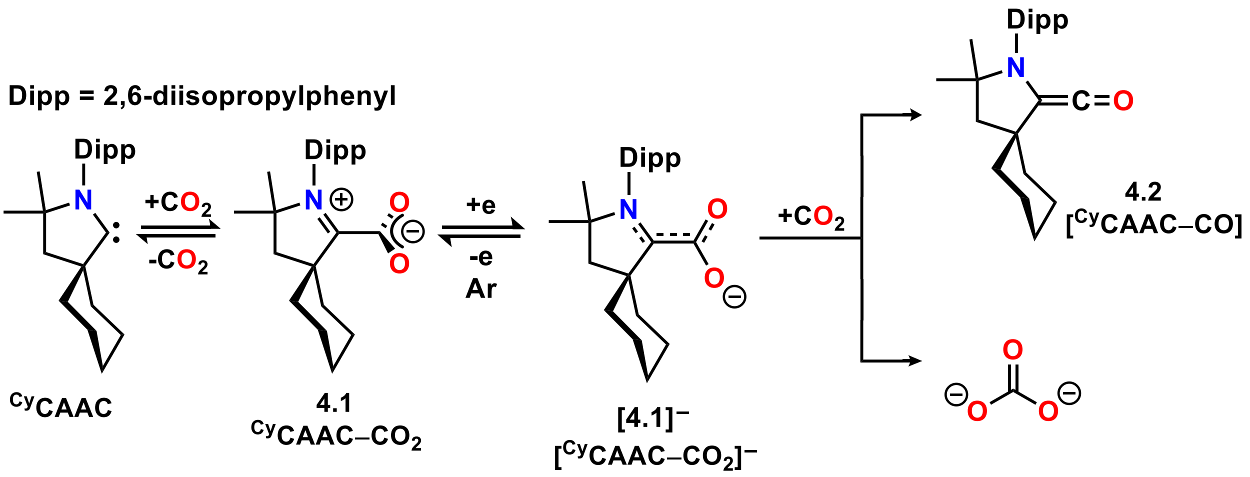

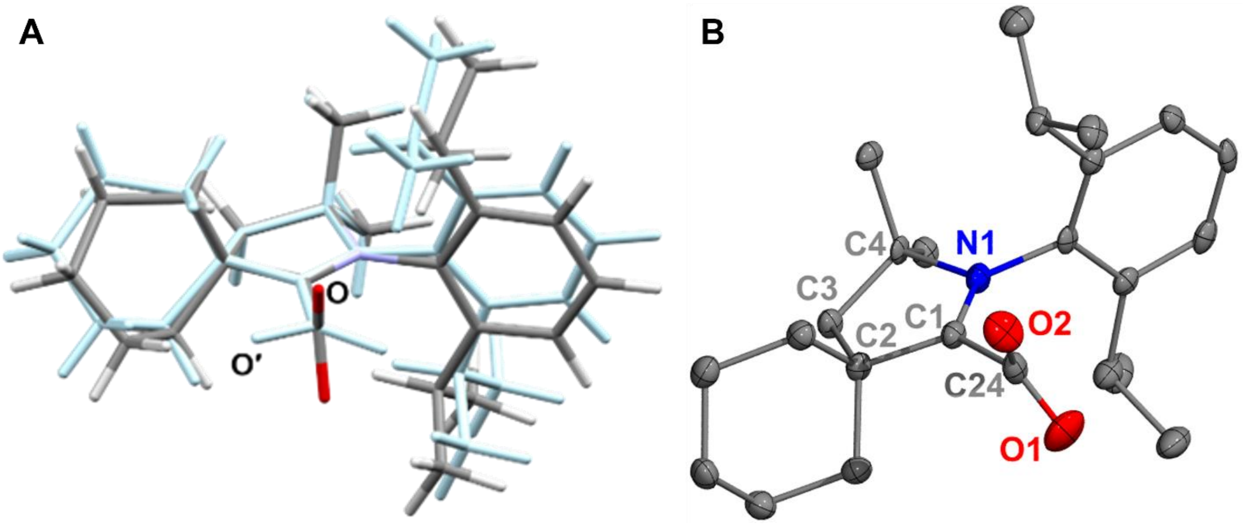

Figure 4.1. (A) Molecular structure of compound **4.1** (thermal ellipsoids at 40% probability; only one of the two chemically equivalent but crystallographically distinct molecules is shown). H atoms and co-crystallized THF solvent molecules omitted for clarity. Selected bond distances (Å) bond angles (°) and torsion angles (°): C1–C24: 1.526(4); C1–N1: 1.297(4); O1–C24

1.236(4); O2–C24: 1.234(4); N1–C1–C24: 123.9(3); O2–C24–O1: 131.5(3); O1–C24–C1: 113.7(3); N1–C1–C24–O2: 101.2(4). (B) Stick representations of the DFT optimized structures of **4.1** (gray, blue and red) and **[4.1]**$^-$ (light blue). ORCA 4.0.1 B3LYP/G, def2-TZVP, CPCM(THF).

Cyclic voltammetry (CV) experiments conducted in acetonitrile (MeCN) and tetrahydrofuran (THF; Figure 4.2) showed reversible one-electron redox behavior under Ar saturation (Figure 4.2, black trace) with $E_{1/2}$ at -2.08 V and -2.15 V vs Fc^+/Fc, respectively. Under CO_2 saturation conditions (Figure 4.2 red trace), this reduction wave became irreversible, and a new oxidation feature was observed on the return sweep at E_{pa} = -1.50 V vs Fc^+/Fc in THF and -1.40 V vs Fc^+/Fc in MeCN. The shift to irreversible redox behavior is suggestive of an *EC* mechanism, with an initial reduction of **4.1** preceding a chemical reaction step with free CO_2.[176] Importantly, these results also suggest that in the absence of inorganic components, the organic CO_2 adduct was capable of electrochemically mediating a reduction reaction of unquantified efficiency. CVs taken in blank solutions show no redox response in under either Ar or CO_2 saturation in the absence of **4.1** in this potential range for both MeCN and THF. For full data sets and analyses of electrochemical experiments see original publication and supporting information package therein.[177]

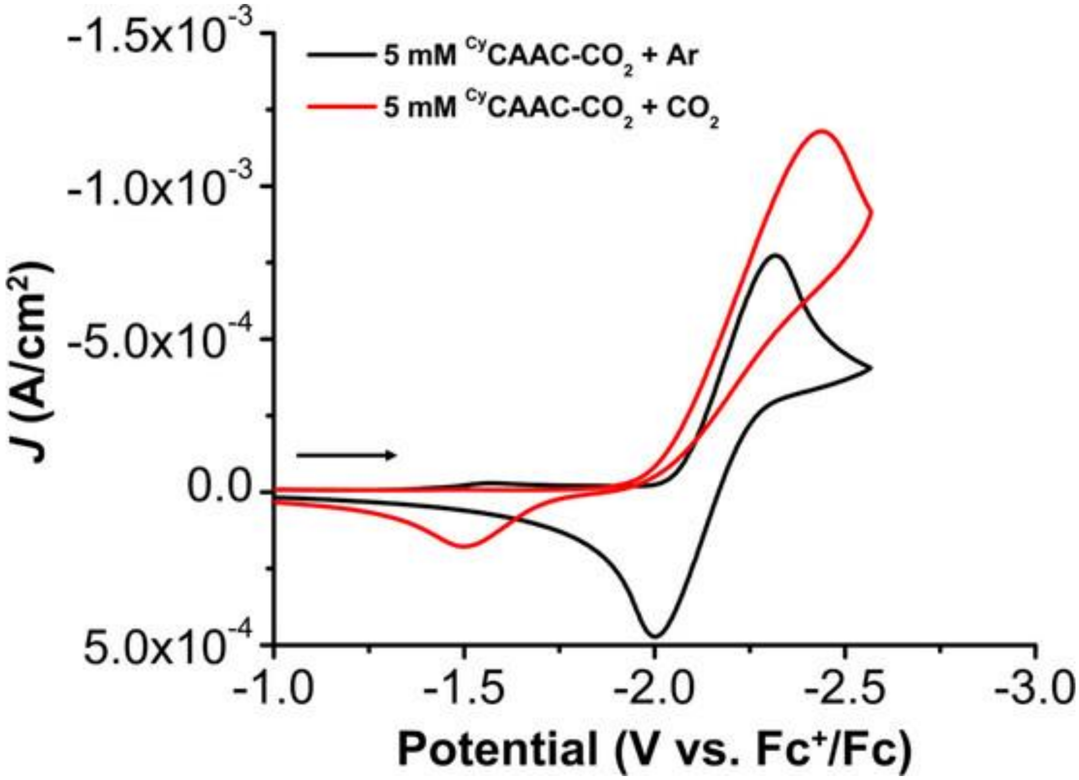

Figure 4.2. CV response of **4.1** at reducing potentials under an inert atmosphere (black) and CO_2 saturation (red) in THF. Conditions: 5 mM **4.1**, 0.1 M $TBAPF_6$/THF glassy carbon working electrode, glassy carbon counter electrode, Ag/AgCl pseudoreference electrode, referenced to internal ferrocene standard.

Infrared spectroelectrochemical[178, 179] (IR-SEC) and electrolysis experiments were undertaken to elucidate the products of this electrochemical reaction under Ar and CO_2 saturation (Figure 4.2; For full data sets and analyses of IR-SEC experiments see original publication and supporting information package therein[177]). At resting potentials under Ar saturation in THF, a strong IR absorbance mode corresponding to the CO_2 adduct is observed at 1670 cm^{-1}. If the cell potential is moved stepwise to more reducing potentials, this absorbance mode disappears with the concomitant appearance of weaker modes at 1660 and 1603 cm^{-1}, which peak in intensity around -1.9 V vs Fc^+/Fc. A weaker absorbance mode at 1531 cm^{-1} also forms upon the initial reduction of **4.1**, but disappears at potentials more negative than -1.8 V vs Fc^+/Fc. Although the CV data are consistent with a reversible redox process, on the relatively longer timeframe of the microscale electrolysis occurring during IR-SEC, there is sufficient time for the reduced species to undergo a chemical reaction. To analyze and quantify any gaseous products produced, controlled potential electrolysis experiments were conducted. Applying a potential of -2.4 V vs Fc^+/Fc with 5 mM of **4.1** in THF under Ar saturation showed CO in the headspace when analyzed by GC, corresponding to a Faradaic efficiency of 0.44% with the passage of 0.83 per electron equivalents per molecule of **4.1**. These results suggest that the electrochemical reduction reaction is stoichiometric in nature under Ar saturation conditions.

Assignment of the new species is possible through literature precedent[180] and DFT calculations. The calculated IR spectrum at the same level of theory for the one-electron reduction product **[4.1]**$^-$ in THF predicts a value of 1525 cm^{-1} for an asymmetric vibration mode of the bent CO_2 moiety, in agreement with the absorbance mode observed experimentally at 1531 cm^{-1} (Figure 4.3A). New IR absorbance modes are observed experimentally at 1660 and 1603 cm^{-1}, which are not predicted by DFT calculations for **[4.1]**$^-$. One possible product of the reduction reaction is the ketene **4.2** (Scheme 4.1). DFT calculations predict an intense absorbance mode at 2127 cm^{-1} in THF (2097 cm^{-1}, 0.986 scaling factor)[181] for **4.2**, corresponding to the CO group. Direct synthesis of **4.2** showed an *in situ* IR absorbance of 2064 cm^{-1} in THF. No IR absorbance more consistent with the ketene species is observed under Ar saturation experimentally. Given the observed instability of **4.2**, it is possible that the CO moiety is more activated in THF than predicted in the DFT methods using CPCM. Direct synthesis of tetrabutylammonium oxalate [$(TBA)_2(ox)$] as an additional experimental control shows two absorbance modes at 1550 and 1286 cm^{-1}; we propose that the absence of a correlation with the experimentally observed modes at 1660 and 1603 cm^{-1} is consistent with these absorbances corresponding to degradation products of **[4.1]**$^{–}$ or **4.2**.

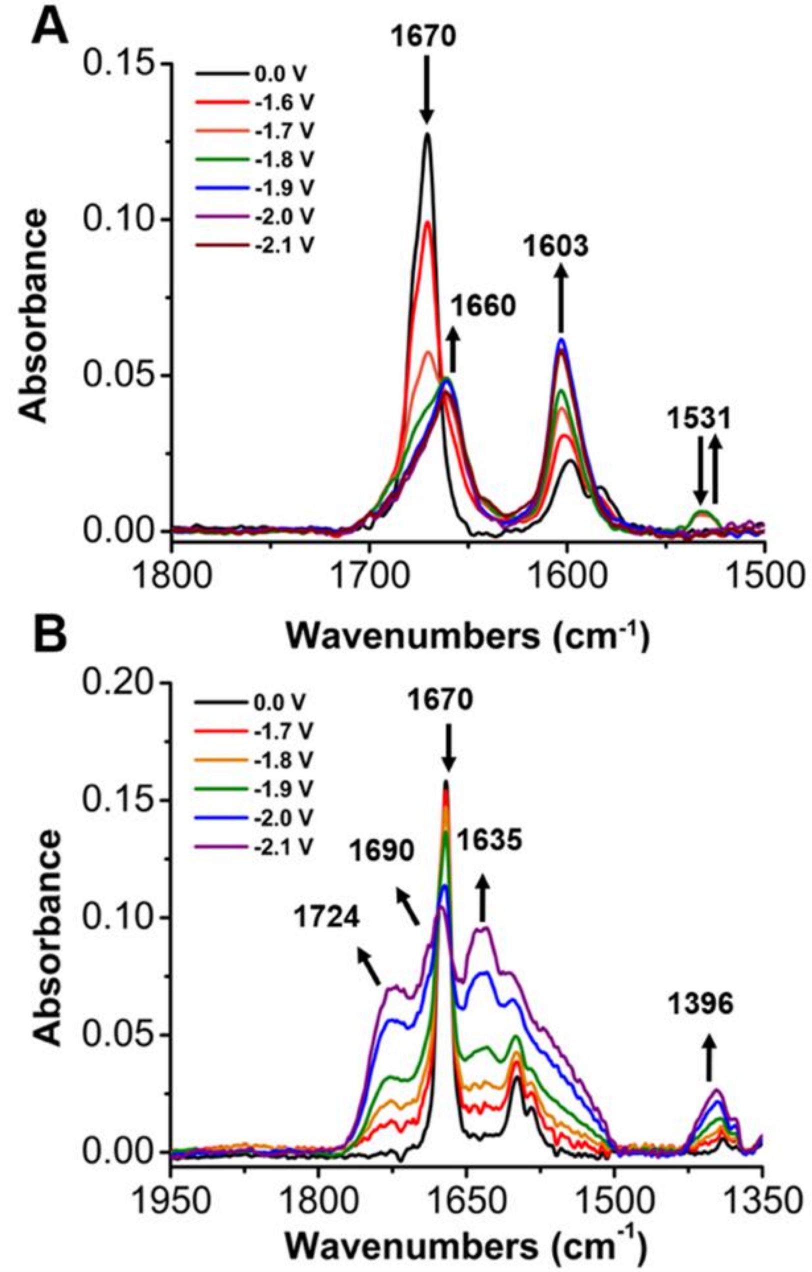

Figure 4.3. (A) Disappearance of the CO_2 adduct at 1670 cm^{-1} as the reduced species **[4.1]**$^{–}$ grows in and disappears at 1531 cm^{-1} at reducing conditions under Ar saturation monitored by IR-SEC. Presumptive ketene **4.2** degradation products appear at 1660 and 1603 cm^{-1}. (B)

Comparable experiments under CO_2 saturation conditions show the loss of the CO_2 adduct upon the formation of CO_3^{2-} (1690 and 1635 cm^{-1}).

In MeCN, the loss of the zwitterionic CO_2 adduct **4.1** also occurs at reducing potentials under Ar saturation conditions, similar to the results obtained in THF. An absorbance mode consistent with the radical intermediate **[4.1]**$^{-}$ is observed at 1224 cm^{-1} upon initial reduction in the IR-SEC experiment, with subsequent loss in absorbance intensity with the appearance of the presumptive ketene product **4.2** at 2118 cm^{-1} (2121 cm^{-1} predicted). Although an asymmetric wagging IR absorption mode is predicted at ~1500 cm^{-1}, similar to the transient species observed and predicted in THF above, the strong background solvent absorbances in MeCN preclude its observation. DFT calculations suggest this experimentally absorbance mode at 1224 cm^{-1} (1227 cm^{-1} predicted) corresponds to weak symmetric rocking by the CO_2 group, with contributions from scissoring of the ^{Cy}CAAC core. An IR absorption mode suggestive of the decomposition of **[4.1]**$^{-}$ or **4.2** is again observed at 1603 cm^{-1}.

Repeating IR-SEC experiments under CO_2 saturation conditions in THF resulted in several noteworthy differences from the data obtained with Ar. Neither the radical anion intermediate **[4.1]**$^{-}$, nor the ketene **4.2** were observed; instead, two bands at 1635 and 1690 cm^{-1} appeared and grew in intensity upon the disappearance of the symmetric CO_2 stretch of **4.1** at 1670 cm^{-1} (Figure 4.3B). Electrolysis experiments at -2.4 V vs. Fc^{+}/Fc showed CO with 0.2% Faradaic efficiency for the passage of charge corresponding to 0.95 electron equivalents per **4.1.** Although CO dissociation from **4.2** could facilitate additional CO_2 binding and electrochemical reduction cycles, it is clear that the degradation products of **4.2** do not involve regeneration of the free carbene or CO release, rendering the process stoichiometric in nature. The control compound TBA(HCO_3) shows good agreement with the IR absorption bands at 1635 and 1690 cm^{-1}, suggesting carbonate/bicarbonate formation is occurring with CO_2 present; the basicity of carbonate is such that protonation from adventitious water is feasible. Analogous IR-SEC and electrolysis experiments in MeCN under CO_2 saturation show that carbonate is again observed at 1686 and 1647 cm^{-1} across the same potential range. If $^{13}CO_2$ is introduced to a THF solution of **4.1**, rapid exchange of the predominantly $^{12}CO_2$ from the as-synthesized adduct with the isotopically labeled substrate occurs; upon reduction, the decomposition products are shifted to lower wavenumbers as well, confirming that these arise from reactions involving the CO_2 moiety.

To better understand the results of the IR-SEC and electrolysis studies, spectrochemical experiments with the *in situ* generated carbene-CO adduct were conducted. In order to prepare ^{Cy}CAAC–CO, a THF solution of free ^{Cy}CAAC was generated in a Schlenk pressure tube under an Ar atmosphere. The headspace of the reaction vessel was evacuated and subsequently refilled with $CO_{(g)}$, immediately generating an intensely-colored royal blue solution. The color of this solution is consistent with the distinctive color observed for the ^{Menthyl}CAAC–CO adduct reported by Bertrand *et al.*[171, 182] In contrast to the stability observed for the bulkier menthyl-analog, the diminished steric protection afforded by ^{Cy}CAAC (absence of iPr and Me groups) was insufficient to stabilize the ketene, and this blue product was observed to decompose rapidly above -78 °C. Rapid decomposition was observed in all attempts to isolate **4.2** in the solid-state, even under rigorously air-free conditions under a headspace of CO (Figure A1.1). As a result, the putative ketene species could only be studied *in situ* immediately after preparation. Monitoring a solution of ^{Cy}CAAC–CO by IR spectroscopy over the course of an hour revealed that the IR absorbance band corresponding to **4.2** at 2064 cm^{-1} diminishes in intensity, with an estimated half-life of ~8 mins.

The DFT-optimized structure of **[4.1]**$^{-}$ showed several important differences with the starting species **4.1**. There is a lengthening of the N–C bond distance of the carbene core (1.292 to 1.388 Å), consistent with a decrease in double-bond character. The bent CO_2 is predicted to rotate ~90° to be in plane with the central ring of the CAAC (NCCO dihedral 94.98 to 171.17). A shortening of the $^{CAAC}C{-}CO_2$ bond length also occurs with this rotation (1.518 to 1.462 Å), suggestive of a π-symmetric interaction. Significant radical character is also predicted on the central C atom of the carbene in **[4.1]**$^{-}$ (Figure 4.1B). Natural Bond Order (NBO) analysis[183, 184] is consistent with double bond character between the N–C atoms of the carbene in **4.1**, which diminishes to a single bond upon reduction to **[4.1]**$^{-}$. A lengthening of both C–O bond distances is also predicted for **[4.1]**$^{-}$ relative to **4.1** (1.242 to 1.270 Å), consistent with increased C–O antibonding character. NBO analyses in MeCN show a minimal difference with the results obtained for THF. For complete computational details, analysis, and data sets, see original manuscript.[177]

These data allow us to propose a mechanism for the electrochemical reduction of CO_2 mediated by ^{Cy}CAAC. The electronic structure of the CO_2 adduct is best described as a zwitterion, with double bond character between the carbene N and C atoms and anionic charge on the O atoms of the CO_2 moiety, made equivalent by resonance. Upon one electron reduction, the added electron density populates the vacant *p* orbital on the carbene C atom. The net result predicted by DFT methods is a lengthening of the N–C bond distance and a shortening of the carbene-CO_2 bond distance. There is a concomitant shift in the N–C–C–O dihedral bond angle as the activated CO_2 group rotates in plane with the carbene core from the starting perpendicular arrangement. The radical anion **[4.1]**$^{-}$ is observable by IR-SEC at reducing potentials. Conceptually, it is useful to think of this species as a carbene-stabilized pseudo-CO_2 radical anion, as this explains the observed products: (free CO), ketene **4.2**, and CO_3^{2-}. The net reaction results in a reductive disproportionation of two equivalents of **4.1**, generating one equivalent each of CO and CO_3^{2-}. The propensity of the ketene **4.2** to decompose via further side reactions is reflected in the observation of minimal CO in the reaction headspace.

NBO analysis of the ketene **4.2** suggests that this instability is the result of two different contributing resonance structures. Natural Resonance Theory (NRT) calculations show a 2:1 contribution of structures, with the larger contributor best described as a ketene. The lesser contributor is best described as the carbene accepting the CO lone pair, with triple bond character retained; the electron balance is satisfied by a π-symmetric lone pair on the carbene C atom. The ^{Cy}CAAC–CO adduct is intensely colored, the lowest energy absorbance is predicted to correspond to a HOMO-LUMO transition according to TD-DFT; the LUMO is anti-bonding with respect to the carbene-CO interaction.

This system represents a promising example of CAACs acting as organic mediators for a stoichiometric electrochemical reduction of CO_2. The observed instability of the resulting reaction products suggests further development may access a catalytic system in future studies. New derivatives and co-catalysts are currently being explored to control the destabilization of the CO adduct and decrease the required reduction potential.

4.2. Soluble, Crystalline, and Thermally Stable Alkali CO_2^{-} and Carbonite (CO_2^{2-}) Clusters Supported by cyclic(Alkyl)(Amino) carbenes.

Oxycarbanions, polyatomic ions of the general formula $[C_xO_y]^{z-}$, are some of the most fundamentally important chemical entities in chemistry, with applications ranging from organic synthesis to battery technologies.[185-188] Among the most important oxycarbanions are the anions of carbon dioxide, CO_2^- and CO_2^{2-} (i.e. carbonite), due to their critical relevance in CO_2 reduction/conversion chemistry and chemical synthesis. Due the high instability of CO_2^- and

CO_2^{2-}, stable compounds featuring these moieties are exceedingly rare, and typically involve metalation of the reactive anion to stabilize the electron-rich CO_2 fragment.[189, 190] In contrast to the extremely stable alkali carbonates (M_2CO_3 M = alkali metal), alkali salts of carbon dioxide (i.e. MCO_2 and M_2CO_2) formed via the reduction of $CO_{2(g)}$ by alkali metals are highly reactive species that have only been detected under specialized conditions. The Li, Na, K and Cs salts of CO_2^- and CO_2^{2-} were previously detected using matrix isolation IR spectroscopy, where they were observed to decompose to more stable alkali oxalates ($M_2C_2O_4$) at temperatures above 15 K (Figure 4.4, top).[191-193] We hypothesized that to synthesize isolable alkali-CO_2 compounds containing CO_2^- and CO_2^{2-}, the metalloxycarbene resonance forms of the anions could be stabilized using a singlet carbene (Figure 4.4, bottom).

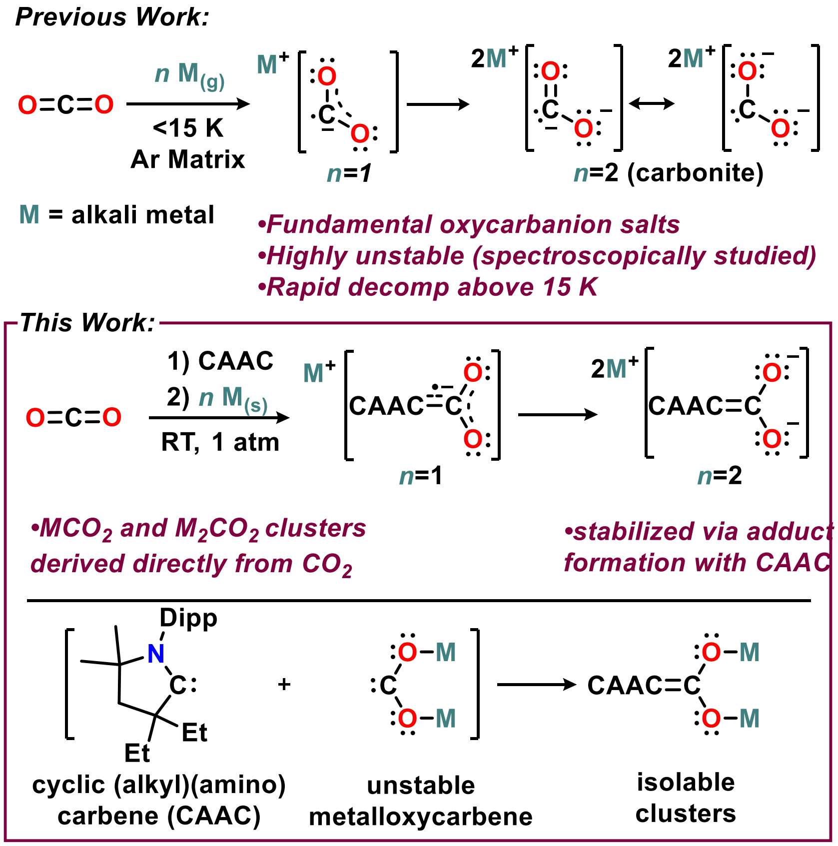

Figure 4.4. Previous methods used to study highly reactive alkali-CO_2 salts (Top). Method of synthesizing stable alkali CO_2 salts utilizing carbene stabilization reported herein (Bottom); Dipp = 2,6-diisopropylphenyl.

Since the isolation of stable N-heterocyclic carbenes (NHCs) by Arduengo,[194] and cyclic (alkyl)(amino)carbenes (CAACs) by Bertrand,[195] these ligands have had a profound impact on synthetic chemistry.[147, 167, 196-200] Notably, the ambiphilic nature of stable singlet carbenes has allowed the development of a rich body of organic chemistry which is distinct from their utility in metal-based systems.[201-208] In such transformations, a common reaction step involves the carbene functioning as a neutral carbon nucleophile with the desired electrophilic substrate(s). A significant example of this class of reaction is the behavior of free carbenes in the presence of CO_2, where the carbene lone pair forms a covalent bond with the electrophilic carbon atom of CO_2. This results in the formation of highly stable zwitterionic adducts (i.e. N,N'-disubstituted imidazolium-2-carboxylates or, more generally, carbene-2-carboxylates). It is noteworthy that although CO_2 is estimated to be a comparable electrophile to benzaldehyde, similar products of electrophilic reactivity are generally thermodynamically unfavored.[209] These adducts have become an important subclass of "masked" carbene due to their high air and moisture stability compared to the free carbene.[210] Indeed, a substantial number of imidazolium-2-carboxylate compounds are known, and their reactivity has been studied with organic nucleophiles,[201] organic electrophiles,[211, 212] and organometallic complexes {e.g. $[Rh(COD)Cl]_2$}.[210]

Carbene-carboxylates have a distinct predisposition toward energy-relevant applications in CO_2 reduction/conversion chemistry, and a number of reported studies have focused on functionalizing or selectively transferring the carboxylate motif.[92, 175, 177, 201, 213-220] However, the ability of carbene-carboxylates to participate in direct electron transfer reactions with reducing metals (e.g. the alkali elements) in order to access stable compounds with CO_2 anions is hitherto unknown. To begin studying the potential redox chemistry of CAAC–CO_2 adducts, we published the first evidence that carbene–CO_2 adducts display redox activity under electrochemically reducing conditions (see chapter 4, section 1).[177] In this initial report, we studied the electrochemical reduction of a CAAC–CO_2 adduct under both argon and CO_2 saturation conditions, and found spectroscopic evidence of reductive chemistry centered around the CAAC–CO_2 species at potentials where free CO_2 is inert. Most importantly, reduction of CAAC–CO_2 under argon saturation showed that the CAAC–CO_2 adduct is not only able to readily accept electrons, but that this electron transfer is a reversible redox couple on the CV timescale at –2.15 V (vs. Fc^+/Fc). This promising result led us to investigate the ability of carbenes to induce the reaction of CO_2 with main group elements under mild conditions.

Herein we report that CAAC adducts of CO_2 can undergo a facile reaction with alkali metals at ambient temperature and pressure. A diverse array of both singly reduced and doubly reduced CAAC–CO_2 complexes have been synthesized. These compounds may also be prepared via the one-pot reaction of free CO_2, alkali metal, and free CAAC. Compounds **4.4-4.10** were isolated as structurally diverse organoalkali metal clusters, which exhibited high stability and solubility at room temperature in both polar and non-polar solvents. The reaction sequence consists of the carboxylation of a carbene at room temperature and 1 atm of pressure, followed by the stepwise reduction of CAAC-carboxylate to a CAAC-diolate dianion using two electrons from alkali metals. In contrast to established CO_2 reduction reactions which require anionic organic nucleophiles and alkali elements to reduce CO_2,[221, 222] the reactions reported herein are the first examples of a reductive synthetic protocol which results in the cleavage of CO_2 π-bonds at atmospheric pressures and room temperature by elemental alkali metals without using carbanions, organometallic reagents, or catalysts.

We selected the ($^{\text{diethyl}}$CAAC)-2-carboxylate zwitterion, **4.3**, as the subject of this synthetic investigation due to the improved solubility and ease of preparation compared to the spirocyclic ($^{\text{cyclohexyl}}$CAAC)-2-carboxylate we previously reported.[177] Compound **4.3** possesses an isostructural CAAC-carboxylate core geometry in the solid-state molecular structure (Figure S1) along with nearly identical electronic properties.

Our initial studies focused on the isolation and structural characterization of the chemical reduction products resulting from the reaction of **4.3** with Li, Na, and K. Upon the addition of one equivalent of metal shavings (or KC_8 in the case of **4.6**) to a vigorously stirring solution of **4.3**, an immediate coloring of the mixture was observed (Li, Na, or K reducing agent yielded bright red, orange, or red colors, respectively). With vigorous stirring under inert conditions, the time necessary for complete consumption of the metal shavings scaled with the relative activity of the alkali metals (Li: 36 h; Na: 16 h; K: 6 h). The isolation of the products of these reactions via recrystallization from saturated THF or THF/hexane solutions at –39 °C yielded single crystals suitable for X-ray diffraction studies. The crystallographically determined structures of the monoanionic products $(THF)_3Li_2(CAAC–CO_2)_2$ (**4.4**), $(THF)_4Na_4(CAAC–CO_2)_4$ (**4.5**), and $(THF)_4K_4(CAAC–CO_2)_4$ (**4.6**) (Scheme 4.2, Dipp = 2,6-diisopropylphenyl) revealed a series of ion-contacted clusters incorporating the respective alkali metal cations in a $CAAC–CO_2$:M ratio of 1:1 (M = Li, Na, or K).

Scheme 4.2. Synthesis of singly-reduced $CAAC–CO_2$ compounds 4.4-4.6.

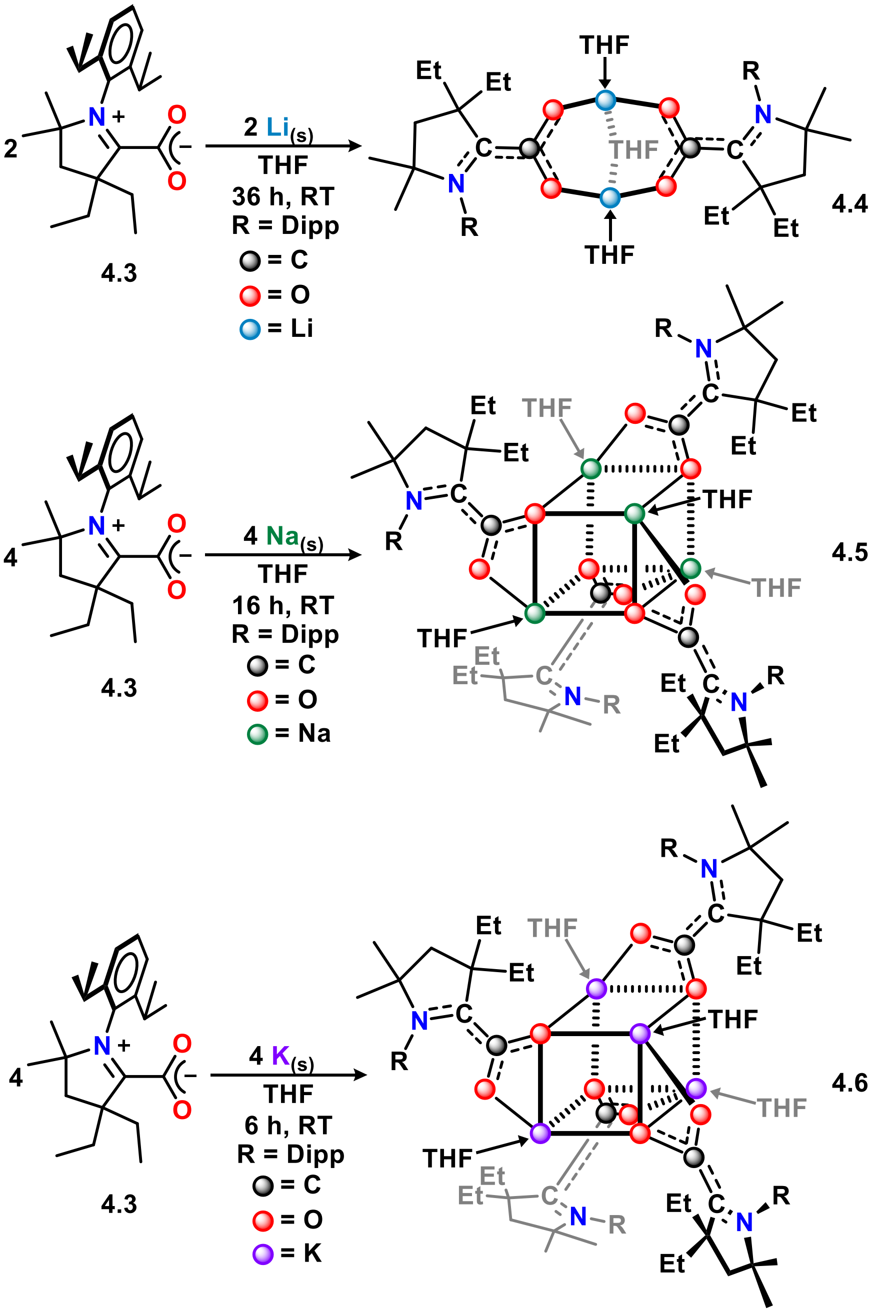

In all three cases, precise control of reaction stoichiometry and times were critical, as reactions were frequently complicated by the presence of either residual CAAC–CO_2 starting material which co-crystallizes with the desired products, or overreduction to a doubly-reduced complex.

Single crystals of compounds **4.4-4.6** suitable for X-ray diffraction studies were grown from saturated solutions of the complexes in either THF (**4.5**) or saturated THF/hexane mixtures (**4.4**, **4.6**) the molecular structures obtained from these data are shown in Figure 4.5. Interestingly, the CAAC–CO_2 core is completely planar in each singly-reduced species, which matches the predictions of our previously reported DFT calculations.[177] The N2–C2 bonds [1.3802(12), 1.385(3), and 1.384(6) Å for **4.4-4.6** respectively] and C1–O bonds [1.2732(12) Å, **4.4**; 1.286(3) Å, **4.5**; 1.276(6), **4.6**] in each species are significantly longer than those of the neutral zwitterion [C1–N2 = 1.282(5) Å, C1–O1 = 1.236(5) Å]. Concomitantly, there is a substantial contraction of the C1–C2 bond from 1.516(5) Å in **4.3** to 1.4533(13) Å, 1.458(3) Å, and 1.451(7) Å in **4.4-4.6**, respectively. These changes are consistent with the addition of one electron from the alkali metal into a π-symmetric molecular orbital, increasing the bonding character between C1 and C2, and decreasing the bond order of the C2–N1, C1–O1, and C1–O2 bonds. Notably, the CAAC nitrogen atom remains planar in its geometry, indicating that the $N_{\text{non-bonding}}$ electrons are still involved in a π-symmetric interaction with the C2 center. The cumulative effects of these bonding metrics explain the observed planarity across the CAAC–CO_2 core. It is worth noting that the solid-state structures of **4.4-4.6** exhibit similar geometries and binding modes to those known for isoelectronic metal-carbamate compounds $(R_2NCO_2M_2)_n$.[223] For example, in the case of the lithium carbamate $[(TMPCO_2)\ Li\cdot TMEDA]_2$ (TMP = 2,2,6,6-tetramethylpiperidide), similar binding and C–O bond lengths [1.261(2) and 1.255(2) Å][224] were observed compared to those in **4.4** [1.2732(12) and 1.2778(12) Å].

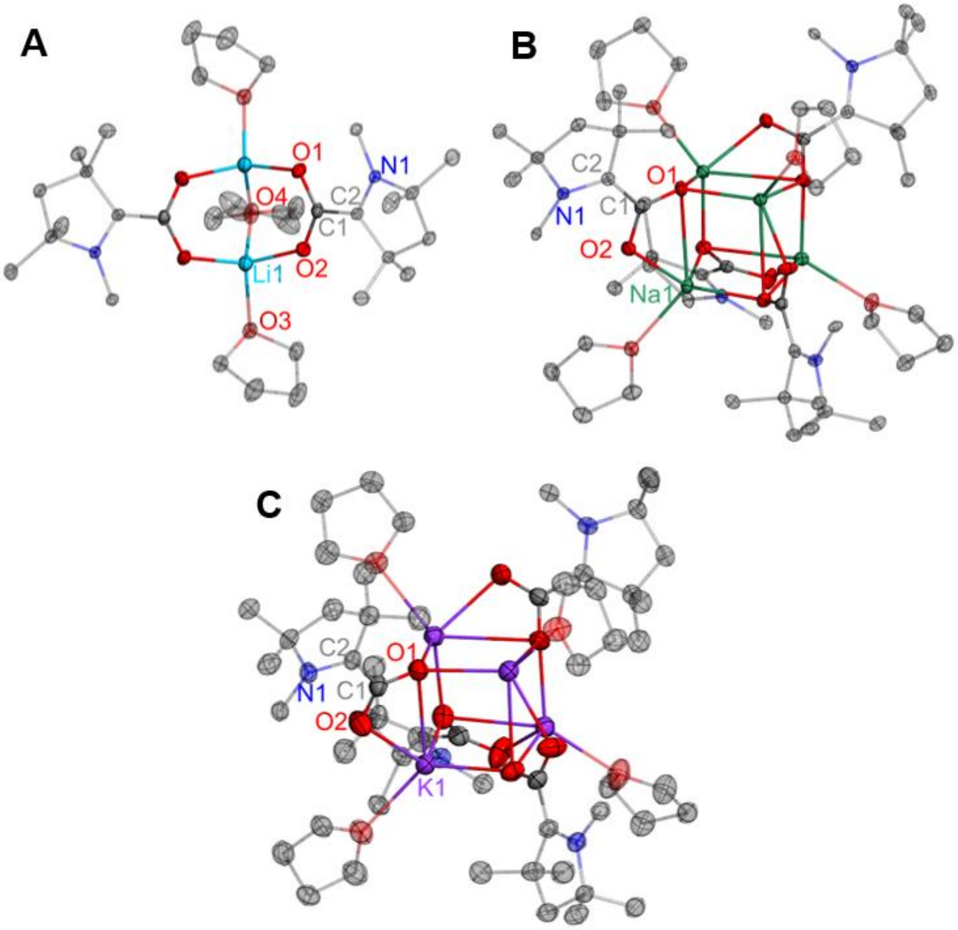

Figure 4.5. Solid state molecular structures of **4.4** (A), **4.5** (B), and **4.6** (C). All H atoms and carbon atoms not directly attached to the CAAC core ring are omitted for clarity. Selected bond distances (Å) and angles (deg): **4.4**: O1–C1: 1.2732(12); O2–C1: 1.2778(12); C1–C2: 1.4533(13); N1–C2: 1.3802(12); O1–C1–O2: 123.71(9); O1–C1–C2: 119.84(9); O2–C1–C2: 116.45(9); N1–C2–C1: 124.85(9); N1–C2–C3: 110.81(8). **4.5**: O1–C1: 1.286(3); O2–C1: 1.266(3); C1–C2: 1.458(3); N1–C2: 1.385(3); O2–C1–O1: 122.9(2); O2–C1–C2: 118.7(2); O1–C1–C2: 118.3(2); N1–C2–C1: 124.7(2); N1–C2–C3: 109.7(2). **4.6**: O1–C1: 1.276(6); O2–C1: 1.265(7); C1–C2: 1.451(7); N1–C2: 1.384(6); O2–C1–O1: 123.0(5); O2–C1–C2: 119.1(5); O1–C1–C2: 117.9(5); N1–C2–C1: 123.3(5); N1–C2–C3: 110.2(4).

In order to further probe the electronic structure of the reduced CAAC–CO2 species, CW X-band EPR data were collected for compounds **4.4-4.6** in toluene solutions at RT (Figure 4.6). In spite of the differences in their solid-state molecular structures, the EPR spectra were all nearly identical exhibiting weak splitting by two ^{13}C nuclei, with little to no observable ^{14}N interactions.

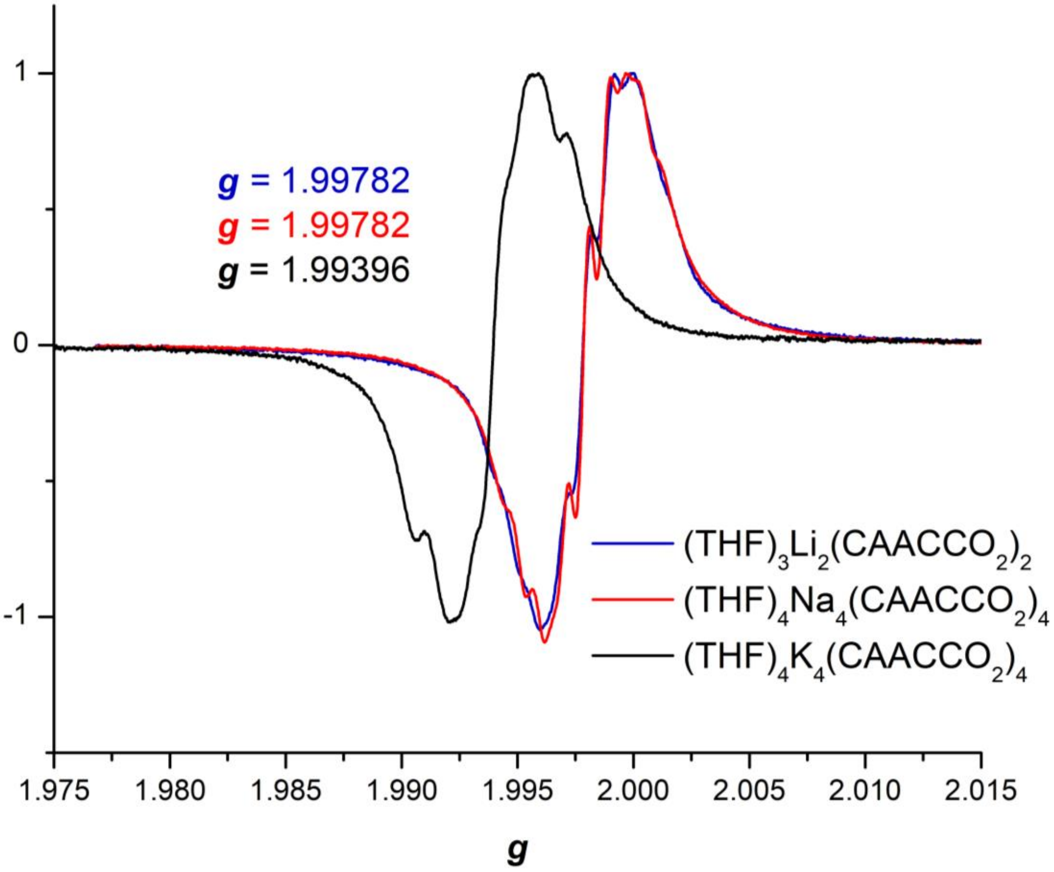

Figure 4.6. Continuous Wave X-band EPR spectra of **4.4-4.6** taken on a 250 μM toluene solution at RT.

Theoretical calculations were carried out for compounds **4.4-4.6**, with geometries optimized using a QM/MM approach including a solvent model for THF (see original publication for complete details of computational investigation).[225] Key bond distances and angles of the QM domain are consistent with SC-XRD studies (C1-C2 1.447, 1.469, 1.471 Å for **4.4-4.6**, respectively). The CAAC–CO_2 core is planar, with optimized N1-C2-C1-O1 dihedral angles are 5.4°, 3.6°, and 2.6° for compounds **4.4-4.6**, respectively, with N_{CAAC} planar in all three singly reduced compounds.

B3LYP-D3(BJ)/def2-SVP (THF solvent) calculations were carried out at the QM/MM optimized geometries for the full complexes. Molecular orbital (MO) plots of **4.4-4.6** indicate that the singly occupied MO (SOMO) largely resides on the carbon atoms that bond the CO_2 and carbene units while the LUMO is concentrated on the Dipp substituents of CAAC (Figure 4.7). The calculated spin density (see Figure A4.4-5) is mostly located on C_{CAAC}, with smaller contributions from C_{CO2}, N_{CAAC}, and O_{CO2}. X-band EPR simulations of **4.4-4.6** were found to be in good agreement with experiment (See Appendix IV). Calculated hyperfine coupling constants (a_{iso}) were notably weaker for N_{CAAC} relative to C_{CAAC} (**4.4** N_{CAAC} a_{iso} = 5.55 MHz, C_{CAAC} a_{iso} = 26.36 MHz), indicating that spin density is localized to the C_{CAAC}.

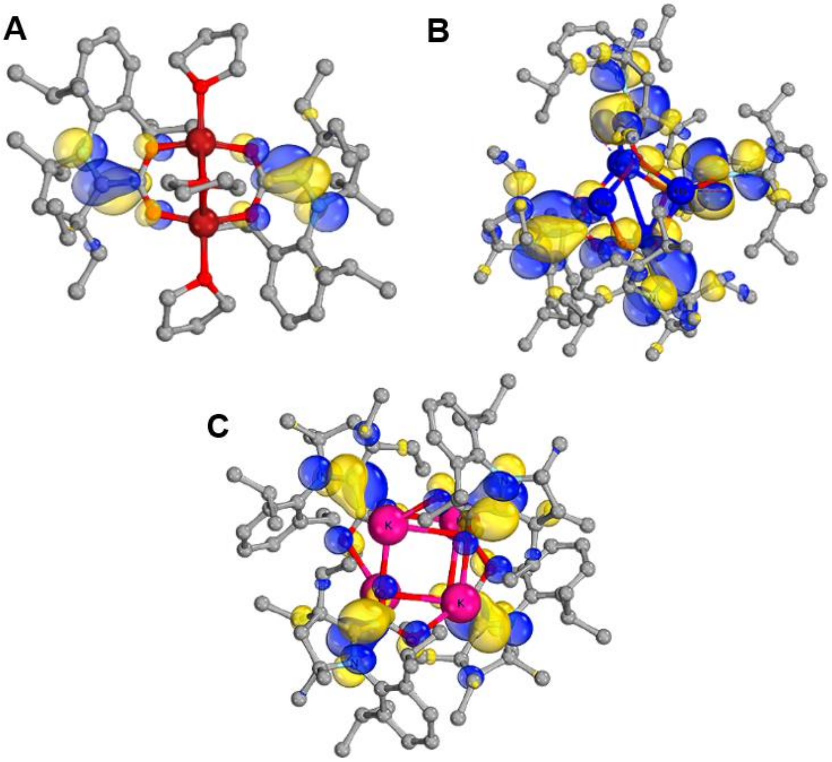

Figure 4.7. Plots of the SOMOs of **4.4** (A), **4.5** (B), and **4.6** (C). H atoms and THF (in B and C) omitted for clarity.

The addition of two or more equivalents of metal to a THF suspension of **4.3** gave gradual conversion (Li: 3 d, Na: 16 h, K: 6 h) to deeply colored, strongly absorbing (i.e. relatively high absorptivity values), homogeneous mixtures containing new reduced species. Completely evaporating this solution under reduced pressure, followed by extraction and recrystallization in hexanes produced single crystals suitable for X-ray diffraction studies. These revealed the respective solid-state structures of the doubly-reduced complexes $(THF)_2Li_6(CAAC–CO_2)_3$ (**4.7**), $Li_{12}(CAAC–CO_2)_6$ (**4.8**), $Na_{12}(CAAC–CO_2)_6$ (**4.9**), $K_{10}(CAAC–CO_2)_5$ (**4.10**) in high yields (Li: 70%;[226] Na: 86%; K: 96%), which were observed to be highly stable, crystalline, analytically pure solids at room temperature under inert atmosphere (Scheme 4.3). Interestingly, as was observed in compounds **4.4-4.6**, the identity of the alkali metal used for reduction had a dramatic effect on reaction time, color, and solid-state structure of the products. This behavior corroborates the observations reported in other investigations of alkali metal reductions which have recently been reviewed.[227]

Scheme 4.3. Synthesis of doubly reduced CAAC–CO_2 compounds 4.7-4.10.

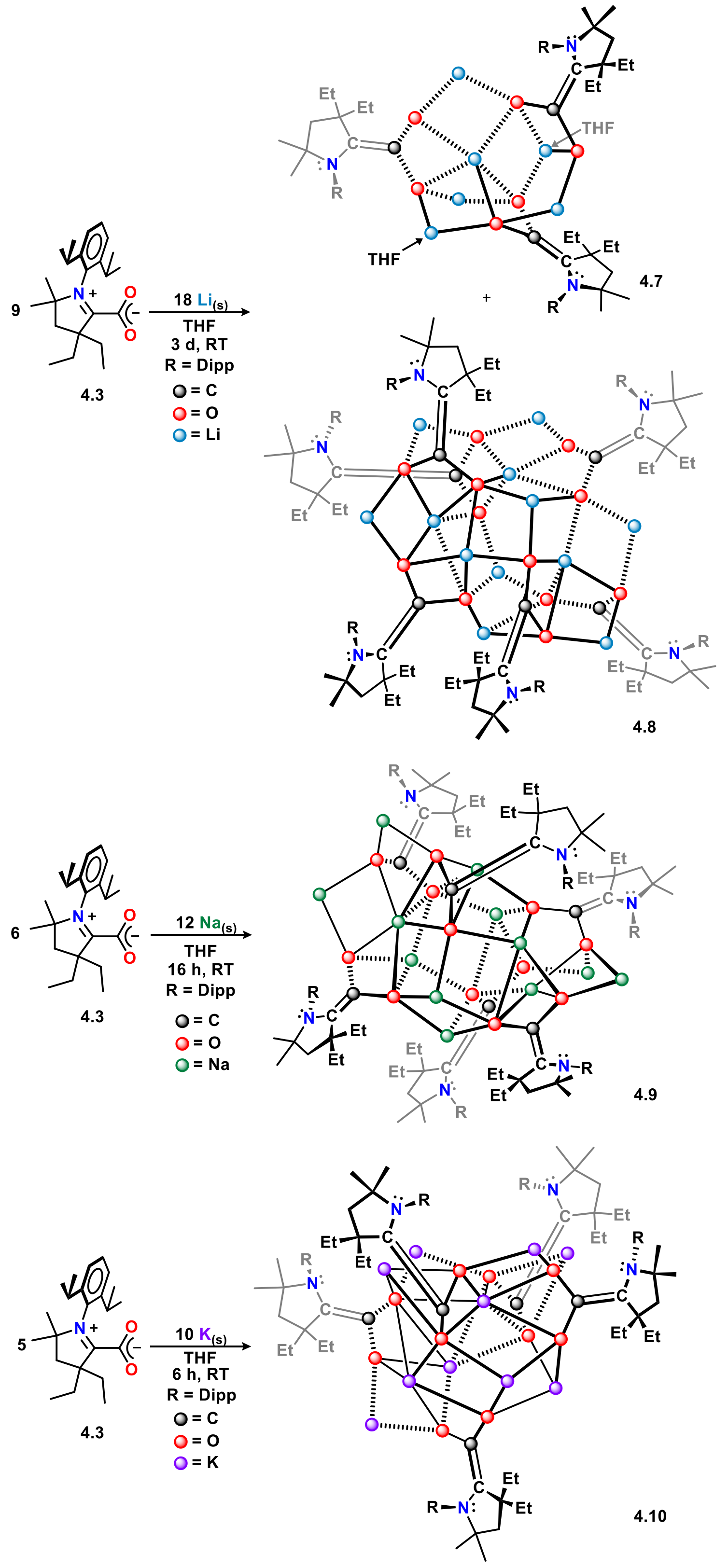

Notably, when lithium metal is used, the complete removal of THF from the crude reaction residue proved difficult. Even after multiple triturations with hexanes and prolonged drying under reduced pressure, a sticky red-orange semi-solid was obtained. Upon recrystallization of the highly soluble, red-orange bulk material from hexanes, two distinguishable crystalline species – one dark red and one bright yellow – were observed which crystallized from the same solution (Figure 4.8A). Surprisingly, similar behavior was not observed when Na or K was used, for which only one crystalline product was obtained in multiple trials [Figure 4.8B (Na) and 4C (K)].

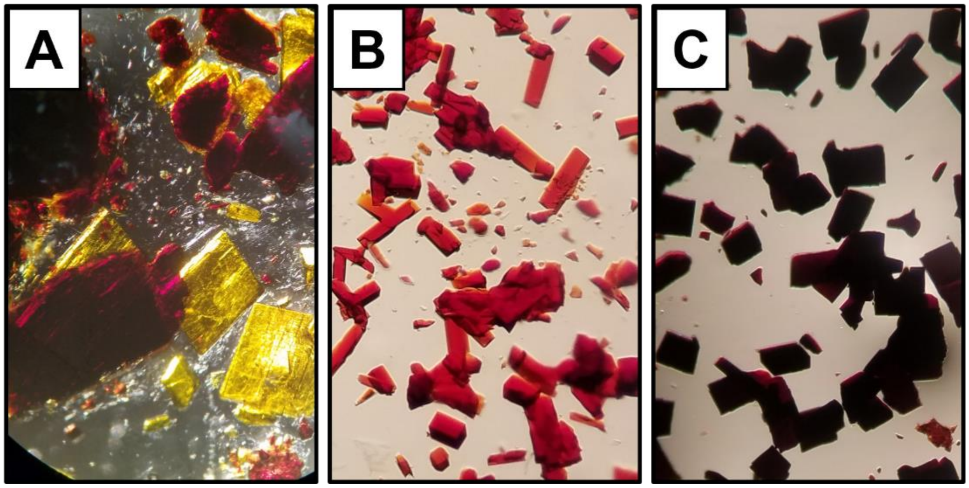

Figure 4.8. Digital image of the mixture of compounds **4.7** (red crystals) and **4.8** (yellow crystals) (A), **4.9** (B), and **4.10** (C) viewed at 40x magnification on an optical microscope.

From the mixture of crystals obtained from the Li reduction, two distinct dilithiated CAAC–CO_2 clusters (**4.7**, Figure 4.8A; **4.8**, Figure 4.8B) were structurally characterized. Despite exhibiting drastically different crystal habits and colors, both compounds contained an equal ratio of lithium ions to CAAC–CO_2 units (2:1). However, the size of the cluster varies. Compound **4.7** can be described as a hexanuclear cluster in the solid state, while compound **4.8** crystallizes as a dodecanuclear cluster. Also, compound **4.7** is the only doubly reduced species observed in this study which exhibited THF coordination in the solid-state. Combustion microanalysis performed on a bulk sample of this mixture more closely matched the calculated CHN content for **4.7**, suggesting this is the major species present in the bulk material.

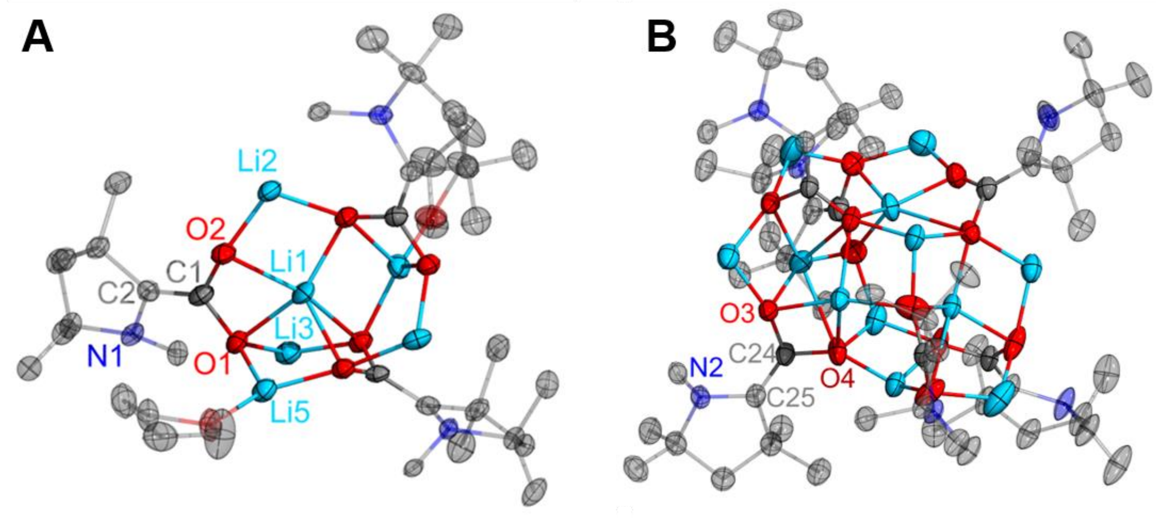

Figure 4.9. Solid state molecular structure of **4.7** (A) and **4.8** (B). All H atoms and carbon atoms not directly attached to the CAAC core ring are omitted for clarity. Selected bond distances (Å) and angles (deg): **4.7**: O1–C1: 1.354(7); O2–C1: 1.332(7); C1–C2: 1.379(8); N1–C2: 1.463(7); O2–C1–O1: 114.1(5); O1–C1–C2: 121.2(5); O2–C1–C2: 124.6(5); C1–C2–N1: 120.0(5); N1–C2–C3: 109.6(5). **4.8**: O1–C1: 1.365(2); O2–C1: 1.360(2); C1–C2: 1.343(3); N1–C2: 1.452(2); O2–C1–O1: 114.20(15); C2–C1–O1: 120.63(16); C2–C1–O2: 125.16(16); C1–C2–N1: 121.20(16); N1–C2–C3: 110.58(15).

As in the cases of the singly-reduced species, the structural features of the CAAC–CO_2 core yield information about the extent of reduction. Perhaps the most notable structural change between **4.4** and **4.7**/**4.8** is the pyramidal geometry of the CAAC nitrogen atom in the doubly-reduced complexes. This geometric change, along with a shortening of the C1–C2 bonds from 1.4533(13) Å in **4.4** to 1.379(8) Å (**4.7**) and 1.343(3) Å (**4.8**) clearly supports the existence of a nonbonding lone pair on the N_{CAAC} atom and a formal π-bond between C1 and C2. Moreover, the C1–O1 and C1–O2 bond distances in **4.7** [1.354(7) Å, 1.332(7) Å] and **4.8** [1.365(2) Å, 1.360(2) Å] indicate C–O bond orders of 1. The only major structural differences between **4.7** and **4.8** are in the nature of the non-covalent ion contacts between the electron-rich π-system of the CAAC–CO_2 core and nearby lithium cations. Perturbations in the π-π* energy gap by these nearby charges presumably lead to the observed differences in the absorption of visible light by complexes **4.7** and **4.8** (UV-Vis spectroscopic data for the bulk mixture are given in Appendix III).

Similar reactions conducted with sodium and potassium yielded highly pure single crystals suitable for X-ray diffraction studies from a saturated hexane extract of the crude product mixture. SC-XRD data collected on crystals of the Na and K products revealed the structures shown in Figure 4.6A and 4.6B.

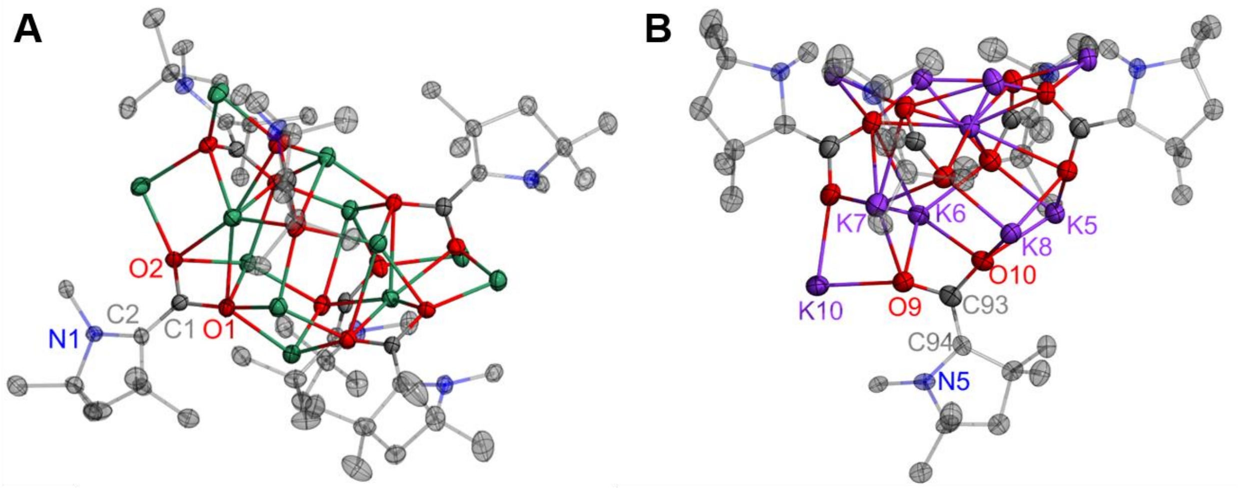

Figure 4.10. Solid state molecular structures of **4.9** (A) and **4.10** (B). All H atoms and all carbon atoms not directly attached to the CAAC core ring are omitted for clarity. Selected bond distances (Å) and angles (deg): **4.9**: O1–C1: 1.364(4); O2–C1: 1.336(4); C1–C2: 1.365(5); N1–

C2: 1.452(4); O2–C1–O1: 113.4(3); O1–C1–C2: 124.0(3); C1–C2–N1: 122.9(3); N1–C2–C3: 107.9(3). **4.10**: O9–C93: 1.342(10); O10–C93: 1.304(9); C93–C94: 1.385(11); N5–C94: 1.455(9); O10–C93–O9: 115.8(7); O9–C93–C94: 120.0(7); C93–C94–N5: 119.5(6); N5–C94–C95: 108.7(6).

The solid-state molecular structure of **4.9** shows an oblong $Na_{12}(CO_2)_6$ core "capped" by six bound CAACs, which is pseudo-S4 symmetric (S_4 axis containing Na2 and Na9). The ratio of Na ions to CAAC–CO_2 units (2:1) and the bond distances across the CAAC–CO_2 core [N1–C2: 1.452(4) Å; C1-C2: 1.365(5) Å; O1-C1: 1.364(4) Å; O2-C1: 1.336(4) Å] indicate that each unit is doubly-reduced, analogous to **4.7** and **4.8**. This description is further supported by pyramidal geometries exhibited by all N_{CAAC} atoms in the cluster. In the solid-state structure of **4.10**, a C_1-symmetric $K_{10}(CO_2)_5$ core was observed. All of the core structural features noted for complexes **4.7-4.9** were also observed in **4.10**, however all five Dipp substituents in this complex exhibited substantial K–(η^6-Dipp) interactions with externally oriented K ions. These interactions were present in **4.9** but weak, and not observed in **4.7** or **4.8**. Notably, the products **4.7-4.10** were observed to be NMR silent, and gave no signal in a parallel mode EPR experiment (which only detects species with S=1/2, 3/2, …, etc.). These experimental data are consistent with the possibility of a significant population of an S=1 (i.e. non-Kramers') paramagnetic electronic state for all doubly reduced compounds, which is supported by computational analysis (*vide infra*) and indicates some degree of chemical fluxionality at room temperature.[228-231]

Theoretically optimized geometries of **4.7-4.10** follow the trends observed of the crystal structures, with the optimized bond distances in general slightly greater than in the crystal structures. In all doubly reduced species, the N_{CAAC} is pyramidal and the C1–C2 bond distance is shorter than in the singly reduced analogue. The pyramidal geometry of N_{CAAC} is suggestive of a non-bonding lone-pair on the nitrogen atom and a C1–C2 π-bond, which is supported by intrinsic bonding orbital (IBO) results (Figure 4.11). The $\mathrm{N_{CAAC}}$ atom of the doubly-reduced species each possess a π lone pair and a N1–C2 σ bond. There is no N1–C2 π-bond observed in **4.7-4.10**, unlike the singly-reduced species **4.4-4.6**.

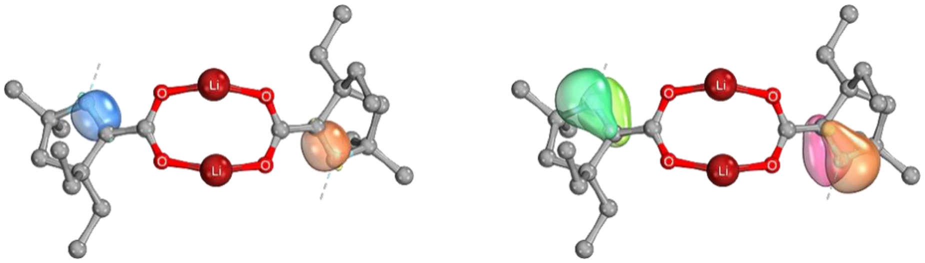

4.4 N1-C2 *σ*-bond

(N1 = 1.169; C2 = 0.813)

4.4 N1-C2 *π*-bond

(N1 = 1.603 C2 = 0.180)

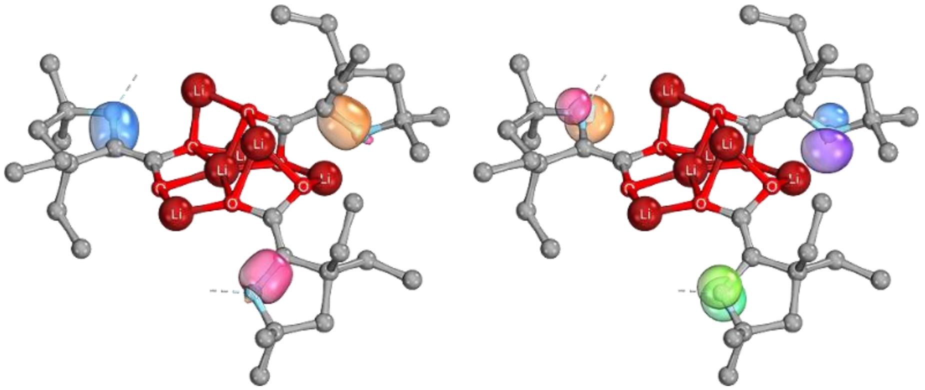

4.7 N1-C2 *σ*-bond

(N1 = 1.147; C2 = 0.822)

4.7 N1 *p* lone-pair

(N1 = 1.866 C2 = 0.00)

Figure 4.11. B3LYP-D3(BJ)/def2-SVP intrinsic bonding orbitals (IBOs) of **4.4** (top) and **4.7** (bottom). Numbers in parentheses indicate the partial charge distribution of the IBO. Orbital *iso*-surfaces enclose 80% of the integrated electron densities of the orbital. H atoms, Dipp and THF substituents omitted for clarity.

The synthetic protocols reported herein result in the carboxylation of CAAC at RT and 1 atm of pressure, followed by the stepwise one- and two-electron alkali metal reduction of CAAC-carboxylate to monoanionic radical clusters and dianionic diolate clusters. The reduced products are isolable as soluble, crystalline products with diverse electronic properties dependent on the nature of the cation and cluster topology. Notably, this represents the first example of the chemical reduction of a carbene-CO_2 adduct, and provides a facile method for the cleavage of CO_2 π-bonds by alkali metals. Moreover, this work highlights the ability of CAAC to mediate a reductive process between base alkali metals and CO_2−a reaction that does not occur in the absence of carbene. The newfound redox behavior of carbene-carboxylates will facilitate the development of new chemistries using these compounds as simple and efficient electron-transfer platforms in both stoichiometric and catalytic CO_2 conversion chemistry.

Chapter 5: Summary and Outlook

5.1. Overview of Completed Research

Chapter two of the research described in this dissertation detailed the expansion of the known coordination chemistry of NHCs and CAACs with magnesium halides, as well as progress towards reduction chemistry at magnesium supported by these ligands. The behavior of novel carbene–Mg–halides under both “direct” reduction conditions (section 2.3) and via the reduction of a coordinated redox-noninnocent diimine ligands (2.4) was studied in detail and reported herein. Detailed investigation into the coordination of singlet cyclic carbenes to magnesium halides indicated that in coordinating solvents such as THF, it is difficult to obtain the desired carbene–Mg–halide due to competition from the donor solvent.[106] As such, non-donor solvents were chosen for further syntheses. However, the poor solubility of $MgCl_2$ in non-donor solvents led to the selection of $MgBr_2$ as the halide precursor of choice, as it allowed for the isolation of both NHC- and CAAC-coordinated $MgBr_2$ complexes which were soluble in toluene.

Attempts at the direct reduction of CAAC–$MgBr_2$ consistently resulted in the reduction of the carbene ligand giving a CAAC activation/rearrangement product in which the Mg center was still in its 2+ oxidation state. Various combinations of reaction conditions still gave this species as the only isolable product. As an alternative to this “direct” reduction (i.e., at the metal center), the reduction of a mixture of redox active ligands and carbene–Mg–halides yielded a series of redox-flexible carbene–Mg–diimine complexes which were stable in solution at room temperature, soluble in hydrocarbon solvents and isolable as crystalline solids. The series of singly- and doubly-reduced complexes bearing the carbene–metal–diimine structural motif was studied in detail using experimental and computational methods, and compared to the beryllium analogs.[123] Interestingly, it was found that the electrons occupying the π system of the diimine upon reduction are delocalized across the magnesium center to interact with the π system of the

CAAC. This cooperativity between the diimine and carbene cores is an unusual and notable feature of the specific structural motif developed during this dissertation work.

The third chapter of the research presented in this dissertation focused on the convenient preparation of low nuclearity, carbene-coordinated magnesium hydride compounds. The utility of group 2 hydrides is expansive, and the synthesis of structurally discrete, hydrocarbon-soluble magnesium hydride compounds is highly desirable. The dissertation work in this area focused on the use of "small" NHCs (i.e., NHCs with a low steric demand at the metal center) and magnesium amide precursors with varied amide steric demand towards preparing structurally unique carbene–Mg–hydride complexes. The results of this investigation[232] gave a convenient synthesis for carbene–magnesium(amido)hydride dimers. Furthermore, this work indicated that NHCs with a low steric demand could be used to support the desired metal hydrides, and that varying the size of the amide ligand yielded subtle changes to the coordination at the magnesium center and requisite reaction conditions.

The fourth portion of this doctoral research focused on the reduction chemistry of zwitterionic carbene–CO_2 adducts known as "carbene-2-carboxylates." Electrochemical reduction studies (section 4.1) indicated that the π–system of the CAAC–CO_2 core is able to accept an electron at milder overpotentials than free CO_2. Additionally, the one-electron reduced species was able to react irreversibly *in situ* with carbon dioxide under CO_2 saturation conditions to yield CO_3^{2-} and a $^{CAAC}C{=}C{=}O$ adduct in THF and MeCN. Using the information gained during these electrochemical experiments, the reduction of a CAAC-2-carboxylate adduct with alkali metal reductants $Li_{(s)}$, $Na_{(s)}$, and $K_{(s)}$ was subsequently studied. The aforementioned reduction resulted in a diverse array of singly- and doubly-reduced CAAC–CO_2–alkali clusters which were hydrocarbon soluble, stable in solution at room temperature under inert atmosphere, and isolable as crystalline solids. The electronic structure of the clusters were studied with a combination of experimental and computational methods. Notably, the singlet-triplet gap of the doubly reduced clusters proved to be close enough in energy to have thermally accessible excited states. At room temperature, it was observed that the doubly-reduced clusters were both NMR and EPR silent, which led us to conclude, with support from computational data, that at room temperature there is significant population of both possible electron configurations (i.e., singlet and triplet-diradical).

5.2. Extensions Beyond Completed Work and Outlook on the Field

From the results described in chapter 2, it is clear that the cooperativity between the π-acidic carbene and π-basic diimine confers unusual electronic structures to molecules such as (CAAC)Mg($^{\mathrm{Dipp}}$DAB)(**2.9**). Future investigations would need to uncover the reactivity profiles of these complexes as either reagents or catalysts. Fortunately there are reports that hint at the reactivity of reduced Mg–diimine functionalities (without a coordinated carbene) in redox-neutral sigma bond metatheses/deprotonation events[88, 89, 115, 116] and in electron-transfer events such as dioxygen reduction.[51] Although the electronic structures of the related compounds presented in this work are notably different, the aforementioned investigations offer a good foundation for developing a reactivity profile.

In chapter 3, the observed structural differences between the “HMDS” and “ASCP” amide ligands, as well as their effects on temperatures required to synthesize a magnesium hydride complex should allow for further development of magnesium precursors that allow ultra-mild temperature synthetic protocols. In an industrial setting, even a decrease in reaction temperature of 20 °C (similar to that observed between the HMDS and ASCP precursors in Ch. 3) would translate to dramatic energy and overhead cost savings at production scale. Further work using the hydrides from chapter 3 could optimize the combination of carbene and amide ligand to obtain an even more hydride-rich complex (e.g. carbene–MgH_2), and additionally study the viability of compounds **3.4-3.5** as molecular catalysts.[43] Alkaline hydrides have demonstrated high competency in a variety of catalytic transformations including hydrogenations of small molecules such as simple alkenes and imines[30, 49, 50, 233, 234] or carbon dioxide.[30, 57] It remains to be discovered whether carbene-coordinated alkaline earth hydrides can participate in similar transformations.

For reduced carbene-2-carboxylates of the type described in chapter 4, there is much to learn regarding the electron-transfer abilities of these compounds. Traditionally, organic bi- and diradicals[228, 230, 231] have found numerous applications in both carbon–carbon bond formation reactions and materials applications. Given that the natures of the highest energy orbitals in the reduced CAAC–CO_2 clusters are closely dependent on the counterion (e.g., Li, Na, or K), the replacement of these ions with other metals such as Zn, Mg, Cu, etc. should yield dramatic variation in the electronic nature of the organic orbitals. These variations could lead to a number of new applications for carbene-2-carboxylates that are now available thanks to the research conducted as a part of this doctoral work.

Appendices and Supporting Information

Appendix I – Experimental Details

General Considerations

All manipulations were carried out with the rigorous exclusion of air and moisture under an atmosphere of argon using standard Schlenk techniques or a MBRAUN LABmaster glovebox operating at <0.1 ppm H_2O and O_2 and equipped with a −39 °C freezer. All glassware used for experiments or measurements was oven-dried at 190 °C overnight before use. All reaction solvents were distilled over sodium/benzophenone and stored over 3 Å molecular seives. Deuterated acetonitrile was purchased from Cambridge Isotope Laboratories and purified by heating over calcium hydride for at least 48 h under followed by distillation under an argon atmosphere. NMR spectra were recorded at room temperature on a Bruker Avance 600 MHz (^1H: 600.13 MHz, ^{13}C: 150.90 MHz). Proton and carbon chemical shifts are reported in ppm and are referenced using the residual proton and carbon signals of the deuterated solvent (^1H; CD_3CN, δ 1.94, ^{13}C; CD_3CN, δ 1.32). Continuous wave (CW) EPR spectra were collected at room temperature using an X-band Bruker EMX spectrometer equipped with an ER 4123D dielectric resonator. Solid-state FTIR spectra were recorded on an Agilent Cary 630 FT-IR equipped with a diamond ATR unit in an argon-filled glovebox. Combustion microanalyses were performed using a PerkinElmer Series 2400 II CHNS/O Analyzer. Crystallographic data for **1**-**5** are summarized in Table S1. CO_2 used for the synthesis of **1** was purchased from Praxair (99.9% purity, part no. CD 3.0-T) and used as recieved without any further drying or purification. Diethyl- and cyclohexyl-substituted cyclic (alkyl)(amino) carbene (^{Et2}CAAC and ^{Cy}CAAC) was prepared according to literature[235] and recrystallized from hexanes before use. Phenylsilane ($PhSiH_3$) was purchased from Millipore Sigma and used as received. Free I^iPr^{Me2} was prepared according to a literature procedure and recrystallized from *n*-hexane prior to use.[236] In cases where alkali metals are used, shavings were taken off of commercially available metal ingots or rods by removing the oxidized outer layer and shaving the fresh surface as finely as possible with a blade.

Synthetic Methodology

Chapter 2.

Synthesis of IPrMgCl$_2$·THF (2.2). In a 100 mL Schlenk flask, a solution of IPr (2.05 g, 5.15 mmol) was prepared in freshly distilled THF (50 mL). To this solution, MgCl$_2$ (0.5 g, 5.15 mmol) was added and allowed to react for 16 hours at room temperature until a homogenous, pale yellow solution was obtained. All volatiles were removed under vacuum to yield sticky yellow solids. Hexanes (30 mL) was added and the resulting suspension stirred for 16 hours. This suspension was filtered over medium frit, and the hexane trituration repeated once more to yield **1** as a white powder (2.33 g, 80% yield). Crystals suitable for X-ray diffraction were obtained by layering a saturated THF solution of **1** with hexanes (2:1 THF/hexanes). ^{1}H NMR (800.13 MHz, THF-d_8, 298 K) δ 7.35 (t, J=7.7 Hz, 1H) 7.25 (d, J=7.7 Hz, 4H) 7.18 (s, 2H, backbone C*H*) 3.62 (m, 4H, THF) 2.81 (hept, J=6.8 Hz, 4H, Dipp-(CH$_3$)$_2$C*H*) 1.77 (m, 4H, THF) 1.18 (d, J=6.9 Hz, 6H, Dipp-CH_3) 1.16 (d, J=6.1 Hz, 6H, Dipp-CH_3) ^{13}C{^{1}H} NMR (201.193 MHz, THF, 298 K) δ 220.8 (C$_{carbene}$), 146.5 (C$_{ipso}$), 129.0, 125.2 (C$_{backbone}$) 123.7, 122.3, 67.2 (THF), 29.0 (C$_{methyl}$), 25.1 (THF), 23.6 (C$_{methyl}$). Satisfactory elemental analysis results could not be obtained (see note in general procedures).

Synthesis of [IPrMgCl$_2$]$_2$ (2.3). In a 100 mL Schlenk flask, a solution of IPr (1.04 g, 2.70 mmol) was prepared in freshly distilled toluene (75 mL). To this solution, MgCl$_2$ (0.245 g, 2.57 mmol) was added and allowed to react for 5 days at room temperature. All volatiles were removed under vacuum to yield yellow solids. Hexanes (30 mL) was added and the resulting suspension was allowed to stir overnight. This suspension was filtered over medium frit, and the hexane trituration repeated once more to yield **2** as a white powder (1.20 g, 96% yield). Crystals suitable for X-ray diffraction were obtained by extracting the product with refluxing toluene, filtering through a 0.45 μm PTFE syringe filter, and cooling slowly to room temperature. NMR data could not be obtained due to the poor solubility of the complex in non-donor solvents. Upon addition of **2** to THF-*d*$_8$ the complex slowly dissolves and converts to **1** with coordinated THF-d$_8$. The NMR spectrum of the resulting solution shows the same resonances for **1** without the presence of coordinated protio-THF (Figure S4). Anal. Calcd. for $C_{27}H_{32}Cl_2MgN_2$: C, 67.59; H, 6.72; N, 5.84%. Found: C, 69.07; H, 7.60; N, 5.79%. Note: compounds **1** and **2** exhibit extreme water sensitivity, notably more so than the free carbene. In the presence of any trace proton source such as residual H_2O in solvents, or trace amounts of HCl impurities in the MgCl$_2$ starting material, complexes **1** and **2** decompose into a protonated product of the type $[IPrH]^+[MgCl_3]^-$. This side product exhibits similar solubility to **1** and **2**, and crystallizes out under similar conditions as colorless, needle-like crystals. In THF, this complex adopts the structure shown in Figure S1. The protonated salt was observed as the primary side product in all reactions to form complexes **1** and **2**.

*Synthesis of (^{Et2}CAAC)MgBr$_2$ (2.4)***.** Free ^{Et2}CAAC (500 mg, 1.580 mmol) and anhydrous MgBr$_2$ (292 mg, 1.580 mmol) were combined in a 100 mL round-bottom flask. Dry toluene (80 mL) was added and the suspension was stirred for 16 h at r.t. The resulting mixture was filtered through a pad of Celite to remove the small amount of insoluble material. The filtrate was concentrated to incipient crystallization of solids before *n*-hexane (50 mL) was added, precipitating white solids which were collected via filtration to yield the product as an off-white solid (583 mg, 74%). ^{1}H NMR (600 MHz, C_6D_6) δ 7.19 (t, *J* = 7.7 Hz, 1H, H_{para}-Dipp), 7.07 (d, *J* = 7.7 Hz, 2H, H_{meta}-Dipp), 2.78 (hept, *J* = 6.8 Hz, 2H, C*H*$(CH_3)_2$-Dipp), 2.23 (m, 4H, C$H_2$$CH_3$), 1.60 (d, *J* = 6.7 Hz, 6H, CH_3-Dipp), 1.35 (s, 2H, CH_2(backbone)), 1.04 (d, *J* = 6.6 Hz, 6H, CH_3-Dipp), 0.95 (t, *J* = 7.4 Hz, 6H, CH_2CH_3), 0.85 (s, 6H, $(CH_3)_2$). ^{13}C NMR (150.9 MHz, C_6D_6) δ 257.5 ($C_{carbene}$), 145.0, 134.8, 130.4, 125.9, 82.6, 66.1, 41.1, 31.3, 29.2, 29.1, 28.3, 24.0, 10.5.

Synthesis of (SIPr)MgBr$_2$ (2.5). To a solution of SIPr (250 mg, 0.640 mmol) in dry toluene (85 mL) was added anhydrous $MgBr_2$ (120 mg, 0.652 mmol). The resulting mixture was stirred vigorously at r.t. for 16 h and filtered through a Celite pad. The volume of the resulting pale bronze filtrate was reduced under vacuum to incipient crystallization, then hexanes were added (approx. 50 mL) precipitating a white solid. These solids were collected via filtration, washed with hexanes (15 mL) and dried under vacuum to yield the product as an off-white solid (235 mg, 68%). Colorless plate-like crystals suitable for X-ray diffraction were obtained from a saturated toluene solution at –37 °C. ^{1}H NMR (600 MHz, C_6D_6, 333 K) δ 7.13 (m, 2H, H_{ortho}-Dipp), 7.05 (m, 4H, H_{meta}-Dipp), 3.48 (s, 4H, CH_2–*backbone*), 3.27 (hept, *J* = 6.20 Hz, 4H, C*H*$(CH_3)_2$), 1.59 (d, 12H, CH(CH_3)$_2$), 1.06 (d, 12H, CH(CH_3)$_2$); ^{13}C NMR (150.9 MHz, C_6D_6, 333 K) δ 206.93 ($C_{carbene}$), 147.4, 134.9, 130.2, 125.1, 124.9, 54.3, 29.1, 28.9, 26.4, 25.1, 24.8, 24.5.

Synthesis of (SIPr)BeCl$_2$. To a 20 mL scintillation vial, $(Et_2O)_2BeCl_2$ (292 mg, 1.28 mmol) was stirred in dry toluene (5 mL). A solution of SIPr (500 mg, 1.28 mmol) dissolved in toluene (5 mL) was added dropwise to the stirring solution, which formed a white precipitate immediately upon addition. After filtration and drying *in vacuo*, compound **4** was isolated as an air- and moisture-sensitive yellow solid (505 mg, 84% yield). Colorless plate-like crystals suitable for X-ray diffraction were obtained from a saturated toluene solution at –37 °C. ^{1}H NMR (500.13 MHz, C_6D_6, 298 K) δ 7.13 (m, 2H, H_{ortho}-Dipp), 7.03 (m, 4H, H_{meta}-Dipp), 3.51 (s, 4H, CH_2–*backbone*), 3.26 (hept, *J* = 6.7 Hz, 4H, C*H*(CH_3)$_2$), 1.51 (d, *J* = 6.8 Hz, 12H, CH(CH_3)$_2$), 1.11(d, *J* = 6.8 Hz 12H, CH(CH_3)$_2$); ^{13}C NMR (150.9 MHz, C_6D_6) δ 188.1 ($C_{carbene}$), 146.9, 133.3, 130.3, 124.8, 53.8, 28.9, 26.1, 23.7; ^{9}Be NMR (84.28 MHz, C_6D_6) δ 10.0.

Synthesis of (^{Et2}CAAC)MgBr(^{Dipp}DAB) (2.7). Compound **1** (100 mg, 0.200 mmol) and ^{Dipp}DAB (75 mg, 0.200 mmol) were combined in a scintillation vial and dissolved in toluene, yielding a homogeneous yellow solution. KC_8 (28 mg, 0.210 mmol) was added at RT and the vial was stirred at for 16 h. The resulting bright orange suspension was filtered, and the filtrate reduced to incipient recrystallization under vacuum and kept at -37 °C. The resulting solids were collected to yield bright orange crystals of the product suitable for X-ray diffraction (45 mg, 28 %). EPR (X-band) 3515 G (m, $a_N = a_H = 2.54$ G).

Synthesis of (^{Et2}CAAC)MgBr(bpy) (2.8). Procedure followed for the preparation of **5**, using 1.1 eq of KC_8 (28 mg, 0.210 mmol) and 2,2-bipyridyl (31 mg, 0.200 mmol) instead of ^{Dipp}DAB. The reaction mixture and subsequent filtrate exhibits a deep cabernet-red color characteristic of **6**.

The toluene filtrate was not reduced under vacuum, but instead recrystallized directly after filtering at -37 °C, yielding dark red needle-like crystals of **7** suitable for X-ray diffraction (66 mg, 67%). EPR (X-band) 3515 G (m, $a_N = a_H = 2.98$ G).

Synthesis of (^{Et2}*CAAC)Mg(*^{Dipp}*DAB) (2.9).* Compound **1** (100 mg, 0.200 mmol) and ^{Dipp}DAB (75 mg, 0.200 mmol) were combined in a scintillation vial and dissolved in toluene, yielding a homogeneous yellow solution. KC_8 (56 mg, 0.420 mmol) was added while the solution was at r.t., and the vial was stirred at r.t. for 16 h. The resulting dark green suspension was filtered, and the dark green filtrate reduced to incipient recrystallization under vacuum and kept at -37 °C. The resulting dark green solids were collected and washed with *n*-hexane (2 mL) to yield the product as a dark green solid (85 mg, 60%). Single crystals suitable for X-ray diffraction were obtained from a saturated hexane mixture at -37 °C. ^{1}H NMR (600 MHz, C_6D_6) δ 7.26 (d, J = 7.5 Hz, 4H, H_{meta}-Dipp(DAB)), 7.19 (m, 2H), 7.13 (m, 1H), 7.03 (m, 3H), 6.82 (d, J = 7.8 Hz, 2H), 5.80 (s, 2H, CH(DAB backbone)), 3.80 (hept, J = 6.9 Hz, 4H, CH(CH_3)$_2$-Dipp(DAB)), 2.54 (hept, J = 6.8 Hz, 2H, CH(CH_3)$_2$-Dipp(CAAC)), 1.56 (m, 2H, C$H_2$$CH_3$), 1.51 (d, J = 6.8 Hz, 12H, CH_3-Dipp(DAB)), 1.41 (m, 2H, C$H_2$$CH_3$), 1.25 (d, J = 7.0 Hz, 12H, CH_3-Dipp(DAB)), 1.14 (s, 2H, CH_2(CAAC backbone)), 0.98 (d, J = 6.7 Hz, 6H, CH_3-Dipp(CAAC)), 0.87 (d, J = 6.8 Hz, 6H, CH_3-Dipp(CAAC)), 0.62 (s, 6H, (CH_3)$_2$), 0.59 (t, J = 7.4 Hz, 6H, CH_2CH_3(CAAC)). ^{13}C NMR (151 MHz, C_6D_6) δ 234.5 ($C_{carbene}$), 154.2, 145.2, 144.5, 130.5, 128.9, 128.1, 124.5, 122.3, 121.7, 121.0, 83.6, 63.9, 39.5, 29.3, 28.9, 28.1, 27.0, 25.8, 23.7, 21.5, 8.8.

Synthesis of (^{Et2}CAAC)Be(bpy). (^{Et2}CAAC)BeCl$_2$ (127 mg, 0.320 mmol) and bpy (50 mg, 0.320 mmol) were combined in a scintillation vial and dissolved in toluene, yielding a blue solution. KC$_8$ (95 mg, 0.704 mmol) was added while the solution was at r.t., and the vial was stirred at r.t. overnight. The resulting dark purple suspension was filtered, and the dark purple filtrate reduced to incipient recrystallization under vacuum and kept at -37 °C. The resulting dark purple solid were collected and washed with *n*-hexane (2 mL) to yield the product as a dark purple solid (110 mg, 72%). Single crystals suitable for X-ray diffraction were obtained from a saturated toluene/hexane mixture at -37 °C. ^{1}H NMR (500.13 MHz, C_6D_6, 298K) δ 7.27 (m, 2H, *H*-Bpy), 7.22 (m, 1H, H_{para}-Dipp), 7.10 (m, 2H, H_{meta}-Dipp), 6.49 (m, 2H, *H*-Bpy), 6.14 (m, 2H, *H*-Bpy), 5.70 (m, 2H, *H*-Bpy) 2.88 (hept, *J* = 6.7 Hz, 2H, C*H*(CH$_3$)$_2$-Dipp), 2.02 (m, 4H, C*H*$_2$CH$_3$), 1.54 (s, 2H, C*H*$_2$(CAAC backbone)), 1.08 (m, 12H, C*H*$_3$-Dipp(CAAC)), 0.92 (s, 6H, (C*H*$_3$)$_2$), 0.87 (t, *J* = 7.4 Hz, 6H(C*H*$_3$)$_2$); ^{13}C NMR (150.9 MHz, C_6D_6) δ 246.0 ($C_{carbene}$), 148.5, 140.1, 136.2, 129.6, 128.1, 126.5, 125.4, 120.4, 114.3, 105.8, 78.6, 62.0, 43.5, 29.7, 29.4, 29.2, 25.4, 23.3, 9.7; ^{9}Be NMR (84.28 MHz, C_6D_6) δ 4.8.

Synthesis of (SIPr)Be(bpy). Compound **4** (151 mg, 0.320 mmol) and bpy (50 mg, 0.320 mmol) were combined in a scintillation vial and dissolved in toluene, yielding a pink solution. KC$_8$ (95 mg, 0.704 mmol) was added while the solution was at r.t., and the vial was stirred at r.t. overnight. The resulting dark red suspension was filtered, and the dark red filtrate reduced to incipient recrystallization under vacuum and kept at –37 °C. The resulting dark red solids were collected and washed with *n*-hexane (2 mL) to yield the product as a dark red solid (124 mg, 70%). Single crystals suitable for X-ray diffraction were obtained from a saturated toluene/hexane mixture at -37 °C. ^{1}H NMR (500.13 MHz, C_6D_6, 298K) δ 7.04 (m, 6H, Aryl), 5.88 (m, 4H, Aryl), 5.24 (m, 2H, Aryl), 3.36 (s, 4H, C*H*$_2$–*backbone*), 3.11 (hept, *J* = 6.7 Hz, 4H, C*H*(CH$_3$)$_2$-Dipp), 1.17 (d, *J* = 6.9 Hz, 12H, CH(C*H*$_3$)$_2$), 1.10 (d, J = 6.9 Hz, 12H, CH(C*H*$_3$)$_2$); ^{13}C NMR (150.9 MHz, C_6D_6) δ 185.1($C_{carbene}$), 146.5, 138.3, 135.3, 129.9, 125.1, 122.6, 119.6, 112.1, 102.5, 54.4, 28.9, 25.0, 23.2; ^{9}Be NMR (84.28 MHz, C_6D_6) δ 4.5.

Chapter 3.

Synthesis of $[Mg(N(SiMe_3)_2)_2]_2$ - Hexamethyldisilazane (25 mL, 120 mmol) was added to a 250 mL Schlenk round-bottomed flask fitted with a reflux condenser. To this flask, a 1.0 M solution of di-*n*-butylmagnesium (60 mL, 60 mmol) was added slowly at RT. The resulting solution was stirred vigorously and heated to 75 °C for 3 d. All volatiles were removed under vacuum at 40 °C (to remove as much unreacted amine and heptane as possible) until a sticky white solid was obtained. The solid was redissolved in minimal *n*-hexane and kept at –39 °C, yielding the product as a highly pure, completely colorless crystalline solid. Further reduction in volume and recrystallization of the supernatant was necessary to retrieve remaining product (13.455 g, 65%). ^{1}H NMR (600 MHz, C_6D_6) δ 0.45 (s, 36H), 0.37 (s, 36H).

Synthesis of $[Mg(N[SiMe_2(CH_2)]_2)_2]_2$, *(**3.1**)* – Compound **3.1** was prepared via a similar procedure to $[Mg(N(SiMe_3)_2)_2]_2$, using 2 eq of $HN[SiMe_2(CH_2)]_2)_2$ (10 mL, 52.83 mmol). The product was obtained after recrystallization from hexane at –39 °C as a colorless crystalline solid. Further reduction in volume and recrystallization of the supernatant was necessary to retrieve remaining product (6.296 g, 70%). ^{1}H NMR (600 MHz, C_6D_6) δ 0.95 (s, 8H,

$Si(CH_3)_2(CH_2)_2$), 0.81 (s, 8H, $Si(CH_3)_2(C\mathit{H}_2)_2$), 0.36 (s, 24H, $Si(C\mathit{H}_3)_2(CH_2)_2$) 0.32 (s, 24H, $Si(C\mathit{H}_3)_2(CH_2)_2$); ^{13}C NMR (150.90 MHz, C_6D_6) δ 12.0, 10.0, 5.8, 5.2. m.p.: 138-140 °C.

*Synthesis of (I^iPr^{Me2})Mg(HMDS)$_2$ (**3.2**)* - Crystalline I^iPr^{Me2} (0.523 g, 2.9 mmol) and $Mg(HMDS)_2$ (1.000 g, 2.9 mmol) were combined in a 100 mL Schlenk round-bottomed flask, dissolved in a minimal amount of *n*-hexane (approx. 40 mL), yielding a colorless solution which was stirred for 16 h at RT. All volatiles were removed under vacuum and the resulting solids collected, yielding the product (1.305 g, 86% yield) as a bright white free-flowing powder. ^{1}H NMR (600 MHz, C_6D_6) δ 5.25 (hept, 2H, $(CH_3)_2C\mathit{H}$), 1.49 (s, 6H, $C_{backbone}(C\mathit{H}_3)$), 1.23 (d, 12H, $(C\mathit{H}_3)CH$), 0.29 (s, 36H, $Si(C\mathit{H}_3)_3$); ^{13}C NMR (150.90 MHz, C_6D_6) δ 179.7 ($C_{carbene}$), 125.5, 53.0, 22.4, 10.0, 6.5. m.p.: 116-118 °C.

*Synthesis of (I^iPr^{Me2})Mg(ASCP)$_2$ (**3.3**)* - Crystalline I^iPr^{Me2} (0.500 g, 2.77 mmol) and **3.1** (0.946 g, 2.77 mmol) were combined in a 100 mL Schlenk round-bottomed flask, dissolved in a minimal amount of *n*-hexane (approx. 40 mL), yielding a colorless solution which was stirred for 16 h at RT. All volatiles were removed under vacuum and the resulting solids collected, yielding the product (1.278 g, 89% yield) as a bright white free-flowing powder. ^{1}H NMR (600 MHz, C_6D_6) δ 4.19 (hept, *J*= 6.8 Hz, 2H, $(CH_3)_2C\mathit{H}$), 1.41 (s, 6H, $C_{backbone}(C\mathit{H}_3)$), 1.30 (d, *J* = 6.8 Hz, 12H, $(C\mathit{H}_3)CH$), 1.07 (s, 8H, $Si(CH_3)_2(C\mathit{H}_2)_2$), 0.32 (s, 24H, $Si(C\mathit{H}_3)_2(CH_2)_2$); ^{13}C NMR (150.90 MHz, C_6D_6) δ 177.0 ($C_{carbene}$), 125.0, 51.8, 23.3, 12.3, 9.1, 5.1. m.p.: 149-151 °C.

Synthesis of [(I^{i}Pr^{Me2})Mg(μ-H)(HMDS)]$_2$ ***(3.4)*** – Compound **3.2** (133 mg, 0.25 mmol) was added to a small Schlenk pressure tube equipped with a stir bar and dissolved in minimal *n*-hexane (8 mL). $PhSiH_3$ (58 mg, 0.54 mmol) was added at RT, and the tube was sealed before heating at 65 C for 16 h. A small amount of white precipitate was observed, which was removed via filtration through a 0.45 μm PTFE syringe filter. The filtrate was kept at –39 °C to yield clear, colorless, rectangular block-like crystals of the product suitable for X-ray diffraction (68 mg, 73%). ^{1}H NMR (600 MHz, C_6D_6) δ 5.30 (hept, *J*= 6.9 Hz, 4H, $(CH_3)_2CH$), 4.29 (s, 2H, Mg*H*), 1.64 (s, 12H, $C_{backbone}(CH_3)$), 1.42 (d, *J* = 7.0 Hz, 36H, $(CH_3)CH$) 0.37 (s, 36H, $Si(CH_3)_3$); ^{13}C NMR (150.90 MHz, C_6D_6) δ 182.0 ($C_{carbene}$), 125.0, 53.4, 22.6, 9.9, 6.4. m.p.: 178-180 °C.

Synthesis of [(I^{i}Pr^{Me2})Mg(μ-H)(ASCP)]$_2$ ***(3.5)*** – Compound **3.3** (521 mg, 1.00 mmol) was added to a Schlenk pressure tube along with a stir bar and dissolved in a minimal amount of n-hexane (approx. 25 mL). $PhSiH_3$ (217 mg, 2.00 mmol) was added to the solution at RT. The flask was sealed and heated while stirring at 40 °C for 16 h, yielding a bright white precipitate. The suspension was filtered over a medium frit and the solids were collected, yielding the product as a highly pure, bright white powder (241 mg, 66%). Clear, colorless, rhombohedral single crystals suitable for X-ray diffraction were obtained by keeping the filtrate at –39 °C. ^{1}H NMR (600 MHz, C_6D_6) δ 4.93 (hept, *J* = 6.8 Hz, 4H, $(CH_3)_2CH$), 4.31 (s, 2H, Mg*H*), 1.59 (s, 12H, $C_{backbone}(CH_3)$), 1.45 (d, *J* = 7.0 Hz, 24H, $(CH_3)CH$), 1.10 (s, 8H, $Si(CH_3)_2(CH_2)_2$)), 0.22 (s, 24H, $Si(CH_3)_2(CH_2)_2$); ^{13}C NMR (150.90 MHz, C_6D_6) δ 180.9 ($C_{carbene}$), 124.8, 52.9, 23.0, 12.6, 9.6, 4.7. m.p.: 218-220 °C.

Chapter 4.

Synthesis of $^{Cy}CAACCO_2$ ***(4.1)*** – In a Schlenk round bottomed flask under argon, a solution of ^{Cy}CAAC (0.500 g, 1.54 mmol) was prepared in freshly distilled Et_2O (20 mL) to yield a clear, colorless solution. The flask sidearm was opened to a flow of argon. CO_2 was allowed to bubble rapidly into the solution for 30 minutes via a balloon fitted with a needle adapter, which was purged with argon 3 times prior to being filled. The flask sidearm remained open to the Schlenk manifold during the entire reaction to maintain approximately 1 atm of pressure and air-free conditions. White precipitate immediately began to form upon the initial introduction of CO_2 and continued over the course of the reaction. The resulting white solids were filtered via cannula, washed with hexanes (20 mL) and dried under vacuum to yield **1** as a bright white solid. Single crystals suitable for Xray diffraction were obtained by cooling a saturated THF solution of the product to -37 °C (0.375 g, 66%). ^{1}H NMR (800 MHz, CD_2Cl_2) δ 7.44 (t, *J* = 7.8 Hz, 1H, $C\boldsymbol{H}_{para}$) 7.29 (d, *J* = 7.8 Hz, 2H, $C\boldsymbol{H}_{meta}$) 2.74 (hept, *J* = 6.4 Hz, 2H, $C\boldsymbol{H}_{methine}$) 2.33 (s, 2H, $(C\boldsymbol{H}_2)_{backbone}$) 2.16 (td, *J* = 13.3, 3.3 Hz, 2H, $(C\boldsymbol{H}_2)_{Cy}$) 1.88 (d, *J* = 12.2 Hz, 2H, $(C\boldsymbol{H}_2)_{Cy}$) 1.83 (dt, *J* = 13.2, 2.9 Hz, 2H, $(C\boldsymbol{H}_2)_{Cy}$) 1.73 (d, *J* = 12.4 Hz, 1H, $(C\boldsymbol{H}_2)_{Cy}$) 1.46 (s, 6H, $(C\boldsymbol{H}_3)_{backbone}$) 1.41 (m, 2H, $(C\boldsymbol{H}_2)_{Cy}$) 1.36 (m, 1H, $(C\boldsymbol{H}_2)_{Cy}$) 1.32 (d, *J* = 6.5 Hz, 6H, $(C\boldsymbol{H}_3)_{Dipp}$) 1.29 (d, *J* = 6.7 Hz, 6H, $(C\boldsymbol{H}_3)_{Dipp}$) ^{13}C NMR (201 MHz, CD_2Cl_2) δ 193.4 ($\mathbf{C}_{C=N}$), 158.6 ($\mathbf{C}_{CO2}$), 146.3 ($\mathbf{C}_{ipso}$), 130.9, 129.5, 125.9, 79.6, 53.8, 53.1, 45.5, 36.2, 30.1, 29.6, 26.5, 25.0, 24.5, 22.2. Anal. Calcd. for $CyCAACCO_2{\cdot}0.5THF$: C, 76.99; H, 9.69; N, 3.45. Found: C, 76.84; H, 9.48; N, 3.65.

Synthesis of $^{Cy}CAAC{=}C{=}O$ ***(4.2)*** *and Decay Experiment*

A solution of ^{Cy}CAAC (30 mg, 92 μmol) in THF (1 mL) was prepared in a Schlenk pressure tube under an argon atmosphere. The clear solution was completely frozen in a bath of liquid N_2, and the flask headspace was evacuated. A balloon of CO was attached to the sidearm via a glass three-way valve, allowing rigorously air-free conditions to be maintained during the introduction of CO. The balloon and flask sidearm were opened, allowing the CO to refill the evacuated headspace of the pressure tube. Once pressure had equilibrated, the pressure tube was sealed completely, and the cold bath removed. No reaction was observed until the contents of the tube had thawed, at which point the solution rapidly gained a deep blue color, which exactly matched that of the reported ^{menthyl}CAAC[171] of compound **4.2** (a photograph of this solution immediately after thawing is shown in Figure A1.1A). At temperatures above the freezing point of THF (-108.4 °C), the blue color is extremely short lived, and fades over the course of minutes. This short lifetime precluded the isolation of a pure sample of **4.2**, so its presence was confirmed, and decay monitored, via solution-phase IR spectroscopy. The solution of **4.2** was immediately brought into a glovebox and transferred to an Omnicell with CaF_2 windows and PTFE spacer. The IR spectrum of this solution showed a characteristic band for the C=O stretch of **4.2** at 2056 cm^{-1}, the disappearance of which was monitored over the course of 8 min at intervals of 2 min. (these data are given in supporting information of the original publication).[177] ^{1}H NMR of the decay products in THF-d_8 showed multiple carbene-containing products, none of which were free ^{Cy}CAAC, further supporting the existence of multiple active decomposition pathways for **4.2**.

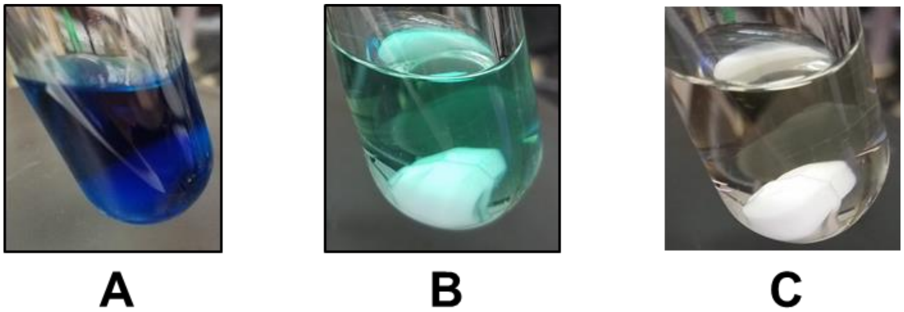

Figure A1.1 (A) Solution of **2** in THF under a CO atmosphere at t = 0 min after preparation. (B) The same solution of **4.2** in THF at t = 4 min after preparation. (C) Same solution of **4.2** in THF at t = 10 min after preparation.

Synthesis of tetrabutyl-n-ammonium oxalate $[(TBA)_2(ox)]$

A round bottom flask equipped with a stir bar was charged with 1.00 g of oxalic acid dihydrate and 10.4 ml of tetrabutylammonium hydroxide and stirred for 45 minutes. The resulting solution was condensed under reduced pressure at 65-70 ˚C for 30 mins and then dried under vacuum at 70 ˚C for 48 hours to yield a white solid. Due to the hygroscopic nature of this material a yield was not obtained. The acetonitrile solution IR spectrum gave strong absorbances at 1552 cm^{-1} and 1288 cm^{-1} and the THF solution IR gave a weak absorbance at 1550 cm^{-1} and 1286 cm^{-1}. ^{13}C NMR (600 MHz, $(CD_3)_2SO$) δ 174.8 ($\mathbf{C}_{C=O}$), 57.3, 23.1, 19.0 ($\mathbf{C}_{-CH2-}$), 13.3 ($\mathbf{C}_{-CH3}$), Anal. Calcd. for $[(TBA)_2(ox)]$: C, 71.21; H, 12.67; N, 4.89. Found: C, 70.99; H, 12.48; N, 4.29.

Synthesis of $^{Et2}CAACCO_2$ ***(4.3)*** – Free diethyl CAAC (0.867 g, 2.77 mmol) was added to a 100 mL Schlenk tube and dissolved in a minimal amount of freshly dried THF (approx. 30 mL). The flask sidearm was attached directly to a mineral oil bubbler via flexible PVC tubing. A small gas sample bag was purged thoroughly with CO_2 before being filled with CO_2 fitted with a stainless-steel needle long enough to easily reach the solution. The needle was introduced through the septum of the Schlenk flask, the flask sidearm was opened, and CO_2 was allowed to bubble into the solution while maintaining steady positive pressure within the system (as indicated by the oil bubbler). Almost immediately after the introduction of the CO_2, a fine, bright-white precipitate was observed. Upon the depletion of the entire sample bag (approximately 5 min), the flask sidearm was closed, the needle was removed, and the flask connected to a Schlenk manifold. The white precipitate was isolated via cannula filtration, washed with dry hexanes (approx. 30 mL) and dried completely under reduced pressure. The remaining solids were collected yielding the product (0.800 g, 81%) as a highly pure white solid which is insoluble in non-polar hydrocarbon solvents, but increasingly soluble in THF, MeCN and CH_2Cl_2, respectively. Colorless, plate-like single crystals of the product suitable for X-ray diffraction were obtained by keeping a saturated THF solution of **4.3** at –39 °C. ^{1}H NMR: (600 MHz, CD_3CN) δ 1.13 (t, J = 7.3 Hz, 6H, $C(CH_2CH_3)_2$), 1.29 (t, J = 6 Hz, 12H, $CH(CH_3)_2$), 1.45 (s, 6H, $C(CH_3)_2$), 1.89 (m, 2H, $C(CH_2CH_3)_2$), 2.02 (m, 2H, $C(CH_2CH_3)_2$), 2.27 (s, 2H, backbone-CH_2), 2.80 (hept, J = 6.2 Hz, 2H, $CH(CH_3)_2$), 7.35 (d, J = 7.8 Hz, 2H, *meta*-H), 7.47 (t, J = 7.9 Hz, 1H, *para*-H); ^{13}C NMR (150.90 MHz, CD_3CN) δ 195.3, 159.2, 147.0, 131.5, 130.7, 126.6, 80.7, 57.5, 42.0, 32.2, 30.5, 29.5, 26.5, 24.6, 9.6; FTIR (solid state): ν 2968, 2925, 2874, 1664 (s), 1600 (m), 1470, 1353 (m), 1144, 1055 (w), 898 (w), 805 (s), 751 (m), 682 (w). Anal. Calc'd. for $C_{23}H_{35}NO_2$ (MW: 357.54 g mol^{-1}): C, 77.27; H, 9.87; N, 3.92; Found: 77.47, 10.11, 3.87. m.p.: 106 °C – 115 °C.

*Synthesis of $(THF)_3Li_2(CAACCO_2)_2$ (**4.4**)* – Compound **4.3** (150 mg, 0.420 mmol) was added to a 20 mL scintillation vial along with a stir bar and suspended in dry THF (approx. 15 mL). Freshly cut Li shavings (3.5 mg, 0.504 mmol) were added at RT and the resulting mixture was stirred vigorously for 36 h. The red-orange reaction mixture was filtered through a 0.45 μm PTFE syringe filter and the filtrate concentrated to a dark red oil under reduced pressure. The residue was dissolved in hexanes (approx. 3 mL) and stored in a -37 ^{o}C freezer yielding X-ray quality red block-like crystals after 2 days. After removal of supernatant, the crystals were dried under vacuum to yield **2** as paramagnetic crystalline red solids (103 mg, 52%). NOTE: This reaction is *highly* sensitive to the amount of reductant used. Precise control of the stoichiometry in this reaction is extremely important to ensure the successful isolation of pure product. EPR (CW, X-band) g = 1.99782 (a_{13C} = 2.24 G); FTIR (solid state): ν 2958, 2867, 1533 (s), 1341 (s), 1233 (s), 1196 (s), 1151(s), 1053 (s), 1053 (s), 911 (m), 798 (s), 742 (m). Anal. Calc'd. for $Li_2C_{58}H_{94}N_2O_7$ (MW: 945.28 g mol^{-1}): C, 73.70; H, 10.02; N, 2.96; Found: 73.07, 10.14, 3.02. m.p.: 73 °C – 82 °C.

*Synthesis of (THF)$_4$Na$_4$(CAACCO$_2$)$_4$ (**4.5**)* – Compound **4.3** (75 mg, 0.210 mmol) was added to a 20 mL scintillation vial along with a stir bar and dissolved in dry THF (approx. 8 mL). Sodium metal shavings (5.3 mg, 0.231 mmol) were added at RT, and the resulting mixture was stirred vigorously at RT for 16 h. The bright orange reaction mixture was filtered through a 0.45 μm PTFE syringe filter, and the resulting filtrate concentrated under reduced pressure until orange precipitate was observed. This precipitate was redissolved by agitation and gentle warming. The resulting saturated bright orange solution was kept at –39 °C to yield large, bright orange crystals of the product (43 mg, 45%). NOTE: This reaction is extremely sensitive to the amount of reductant used. Precise control of the stoichiometry in this reaction is extremely important to ensure the successful isolation of pure product. EPR (CW, X-band) g = 1.99782 (a_{13C} = 2.24 G);

FTIR (solid state): ν 2964, 2867, 1517 (s), 1465 (m), 1297 (m), 1222 (m), 1055 (s), 902 (m), 798 (m), 743 (m); Anal. Calc'd for $NaC_{27}H_{43}NO_3$ (MW: 452.63 g mol^{-1}): C, 71.65; H, 9.58; N, 3.09; Found: C, 71.14; H, 9.91; N, 2.92. m.p.: 74 °C – 80 °C.

*Synthesis of $(THF)_4K_4(CAACCO_2)_4$ (**4.6**)* – Compound **4.3** (75 mg, 0.210 mmol) was added to a 20 mL scintillation vial along with a stir bar and dissolved in dry THF (approx. 8 mL). KC_8 flakes (34 mg, 0.252 mmol) were added at RT, and the resulting mixture was stirred vigorously for 36 h. The purple-red mixture was filtered through a 0.45 μm PTFE syringe filter and concentrated to *ca.* 3 mL under reduced pressure. Hexanes (approx. 1 mL) were added and the mixture subsequently filtered. Red block-like crystals suitable for X-ray diffraction studies were obtained from keeping the filtrate at RT. The supernatant was stored at -37 ºC yielding a second crop of crystals which were recovered after 3 days and dried under vacuum (total isolated yield: 84 mg, 85%). NOTE: This reaction is extremely sensitive to the amount of reductant used. Precise control of the stoichiometry in this reaction is extremely important to ensure the successful isolation of pure product. FTIR (solid state): ν 2958, 2863, 1517 (s), 1463 (m), 1297 (s), 1226 (s), 1153 (m), 1055 (m), 926 (w), 798 (m), 742 (m). Satisfactory elemental analysis results could not be obtained for this compound. m.p.: 94 °C – 99 °C.

*Synthesis of $(THF)_nLi_2(CAACCO_2)$ $0<n<0.333$ [**4.7** ($n=0.333$) and **4.8** ($n=0.0$)]* – Compound **4.3** (100 mg, 0.280 mmol) was added to a Schlenk tube along with a stir bar and dissolved in dry THF (approx. 20 mL). Lithium metal shavings (7.8 mg, 1.12 mmol) were added at RT, and the resulting mixture was stirred vigorously at RT for 3 d, yielding a deep red/orange solution. The reaction mixture was dried to a sticky residue under reduced pressure, extracted with toluene (10 mL) and filtered. The deep red/orange extract was dried completely under reduced pressure and triturated twice with hexanes (2 x 4 mL) to yield a deep red/orange glassy solid which was collected and confirmed to be an inseperable mixture of **5** and **6**. This mixture apparently results from the incomplete removal of THF from the molecular structure of the product. This mixture can be accurately described as one species with the general formula $(THF)_nLi_2(CAACCO_2)$ $0<n<0.333$ with a molar mass between 371.422 g/mol (n = 0) and 395.456 g/mol (n = 0.333). The true amount of THF (value of n) in this bulk sample was analyzed by elemental analysis. The results of this analysis gave an experimental CHN content closer to the expected values for $(THF)_{0.333}Li_2(CAACCO_2)$ (77 mg, 70 %). FTIR (solid state): ν 2960, 2930, 2865, 1679 (m), 1599 (s), 1467 (s), 1438 (s), 1381 (s), 1250 (s), 1176 (s), 1129 (s), 1051 (s), 803 (s), 754 (s); Anal. Calc'd for $C_{76}H_{113}Li_6N_3O_8$ (MW: 1238.26 g mol^{-1}): C, 73.49; H, 9.69; N, 3.34; Found: C, 72.06; H, 9.77; N, 3.53; m.p.: 118 °C – 125 °C.

Synthesis of $Na_{12}(CAACCO_2)_6$ ***(4.9)*** – Compound **4.3** (100 mg, 0.280 mmol) was added to a Schlenk tube along with a stir bar and dissolved in dry THF (approx. 20 mL). Sodium metal shavings (26 mg, 1.12 mmol) were added, and the resulting mixture was stirred vigorously for 16 h, yielding a dark orange solution. The reaction mixture was dried completely under reduced pressure and extracted with hexane (15 mL). The filtrate was dried completely under vacuum to yield the product as a dark orange crystalline solid. A saturated hexane solution of the product was kept at –39 °C to yield orange plate-like crystals of the product suitable for X-ray diffraction (97 mg, 86%). NOTE: This reaction can also be performed successfully using a 5% sodium dispersion on sodium chloride (5 wt. % Na/NaCl) reported by Jones *et al.*[237] in place of sodium shavings. FTIR (solid state): ν 2956, 2923, 2865, 1584 (m), 1433 (s), 1246 (s), 1120 (s), 1062 (s), 799 (m), 753 (m). Anal. Calc'd for $Na_2C_{23}H_{35}NO_2$ (MW: 403.52 g mol^{-1}): C, 68.46; H, 8.74; N, 3.47; Found: C, 68.16; H, 8.74; N, 3.22; m.p.: decomposition at 151 °C.

Synthesis of $K_{10}(CAACCO_2)_5$ ***(4.10)*** – Compound **4.3** (100 mg, 0.280 mmol) was added to a Schlenk tube along with a stir bar and dissolved in dry THF (approx. 20 mL). Potassium metal shavings (33 mg, 0.836 mmol) were added, and the resulting mixture was stirred vigorously for 6 h, yielding a dark red-purple solution. The reaction mixture was dried completely under reduced pressure and extracted with hexane (15 mL). The filtrate was dried completely under vacuum to yield the product as a dark red-purple crystalline solid. A saturated hexane solution of the product was kept at –39 °C to yield dark red-purple plate-like crystals of the product suitable for X-ray diffraction (116 mg, 96%). NOTE: This reaction can also be performed successfully using potassium graphite (KC_8) in place of potassium shavings with comparable yields. FTIR (solid state): ν 2956, 2927, 2863, 1502 (m), 1461 (m), 1431 (m), 1246 (s), 1062 (s), 796 (m), 751 (m); Anal. Calc'd for $K_2C_{23}H_{35}NO_2$ (MW: 435.73 g mol^{-1}): C, 63.40; H, 8.10; N, 3.21; Found: C, 62.90; H, 8.59; N, 2.94; m.p.: 162 °C – 171 °C.

Appendix II – Molecular Structures

Molecular Structure Data

Chapter 2

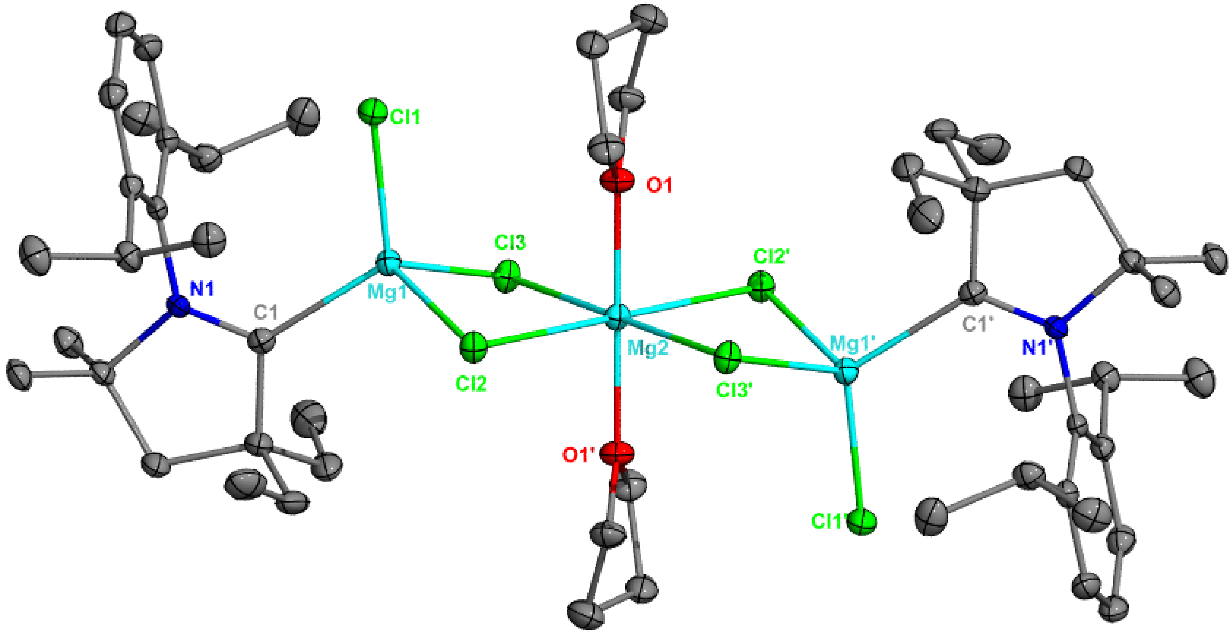

Figure A2.1 Molecular structure of compound 2.1. (thermal ellipsoids set at 50% probability, H atoms omitted for clarity). Selected bond distances (Å) and angles (deg): Cl1-Mg1: 2.2772(9); Cl2-Mg1: 2.3767(9); Cl2-Mg2: 2.5489(6); Mg1-C1: 2.234(2); Mg2-O1: 2.0573(15); N1-C1: 1.301(3); Mg1-Cl2-Mg2: 86.91(2); C1-Mg1-Cl1: 118.67(7); C1-Mg1-Cl2: 110.85(7); Cl2-Mg1-Cl3: 93.75(3).

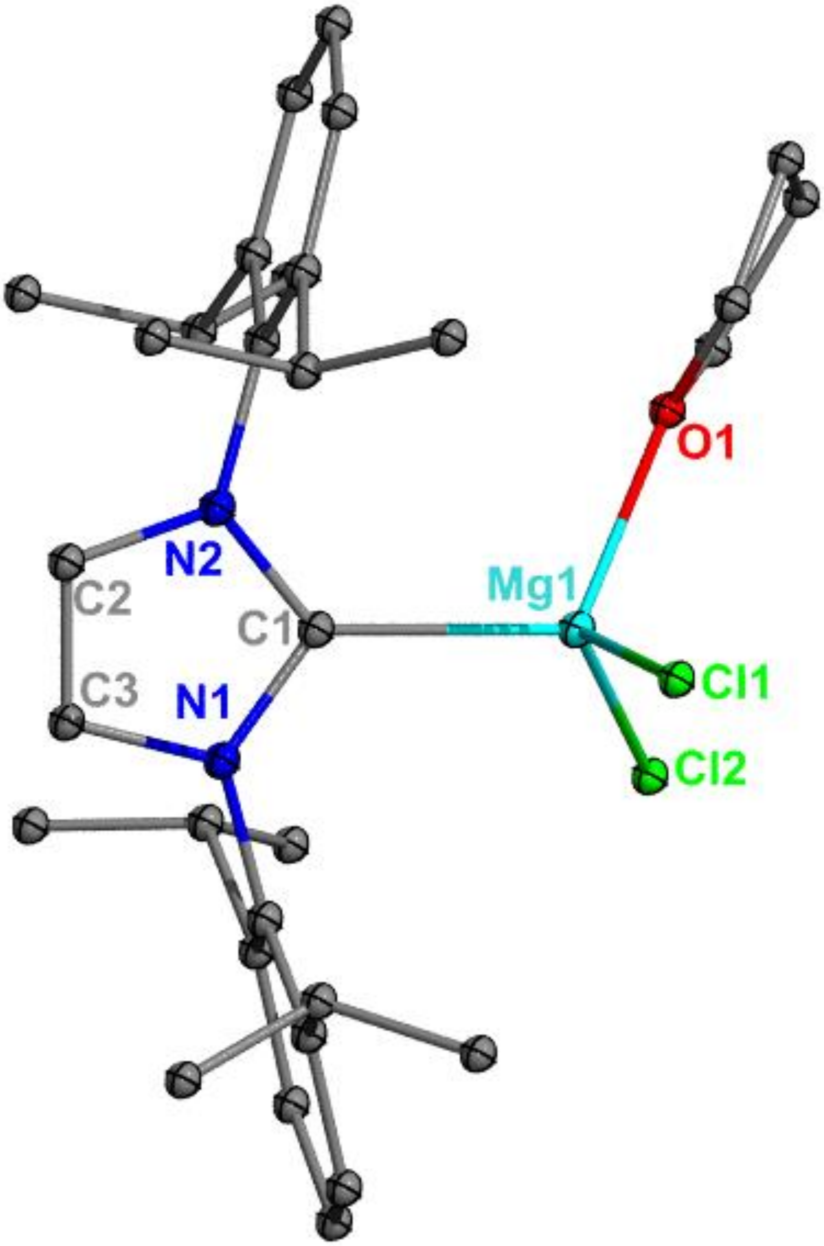

Figure A2.2 Molecular structure of 2.2. (thermal ellipsoids set at 50% probability). Only one of the two chemically equivalent but crystallographically distinct molecules is shown. H atoms and two cocrystallized THF molecules are omitted for clarity. Selected bond distances (Å) and angles (deg): C1–Mg1: 2.202(6); C1–N1: 1.350(8); C1–N2: 1.377(8); Mg1–Cl1: 2.270(3); Mg1–Cl2: 2.310(4); Mg1–O1: 2.018(5); N1–C1–Mg1: 125.7(4); C1–Mg1–Cl1: 105.66(17); C1–Mg1–Cl2: 110.32(19); Cl1–Mg1–Cl2: 122.43(16).

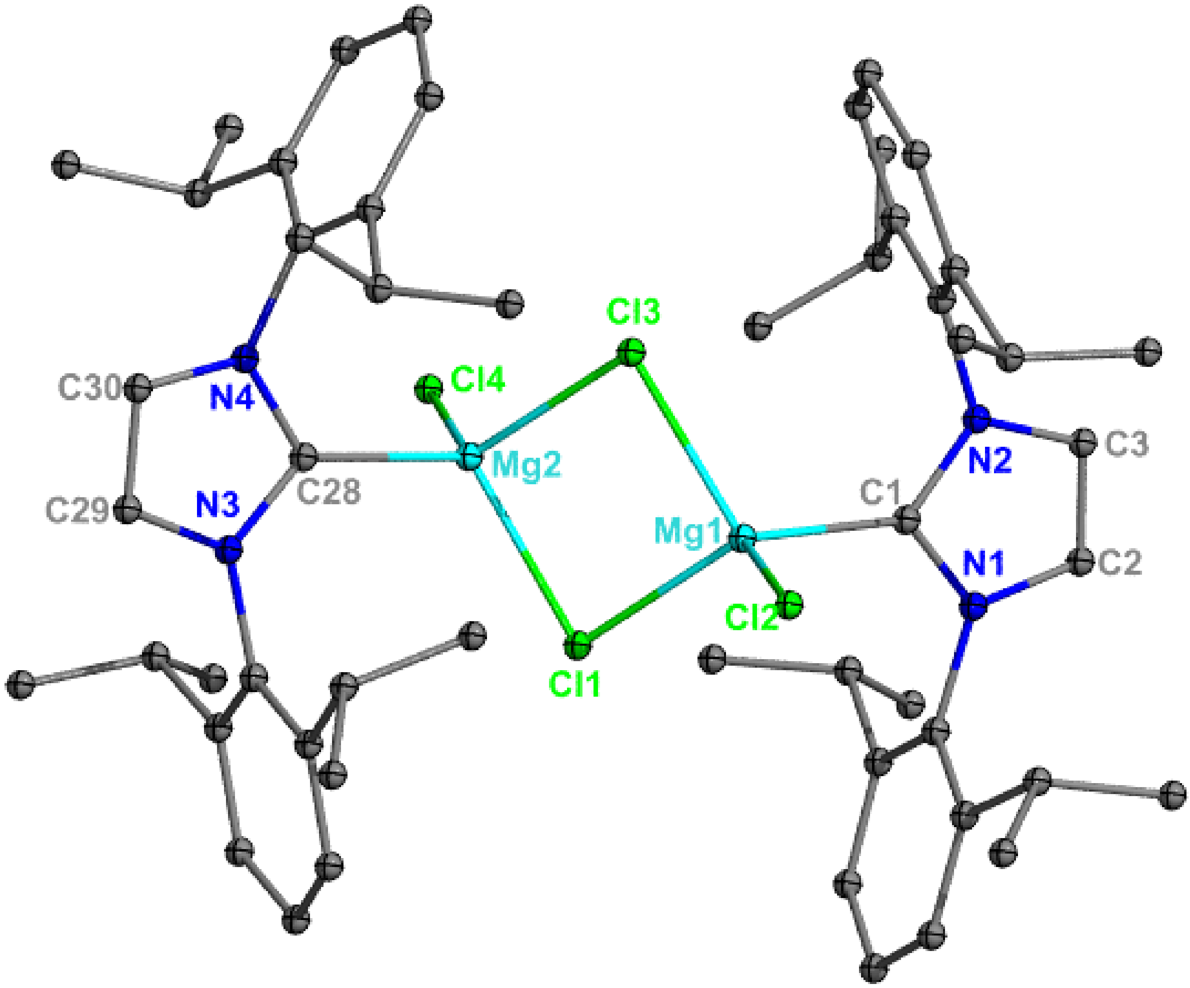

Figure A2.3. Molecular structure of 2.3. (thermal ellipsoids set at 50% probability, H atoms and three cocrystallized toluene molecules omitted for clarity). Selected bond distances (Å) and angles (deg): C1–Mg1: 2.213(4); C1–N1: 1.373(5); C1–N2: 1.371(5); Mg1–Cl1: 2.403(2); Mg1–Cl2: 2.2912(19); Mg1–Cl3: 2.408(2); Mg2–Cl4: 2.2855(19); N1–C1–Mg1: 129.9(3); C1–Mg1–Cl1: 115.98(13); Cl1–Mg1–Cl2: 113.42(8).

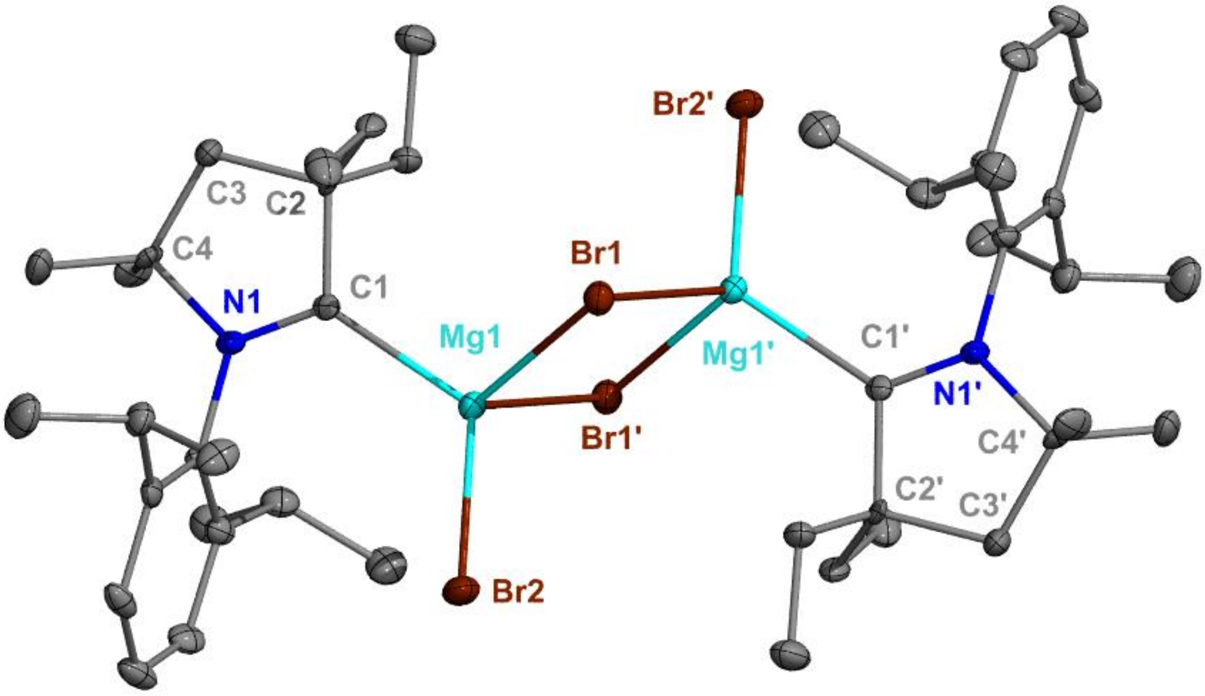

Figure A2.4. Molecular structure of 2.4. (thermal ellipsoids set at 50% probability, H atoms omitted for clarity). Selected bond distances (Å) and angles (deg): C1–Mg1:2.231(3); C1–N1:1.293(4); Mg1–Br1:2.5531(12); Mg1–Br2:2.4249(12); Mg1–Br1′: 2.5800(12); C1–Mg1–Br1:110.90(10); C1–Mg1–Br2:123.19(9); Br1–Mg1–Br2:107.82(5); Br1–Mg1–Br1′: 93.16(4).

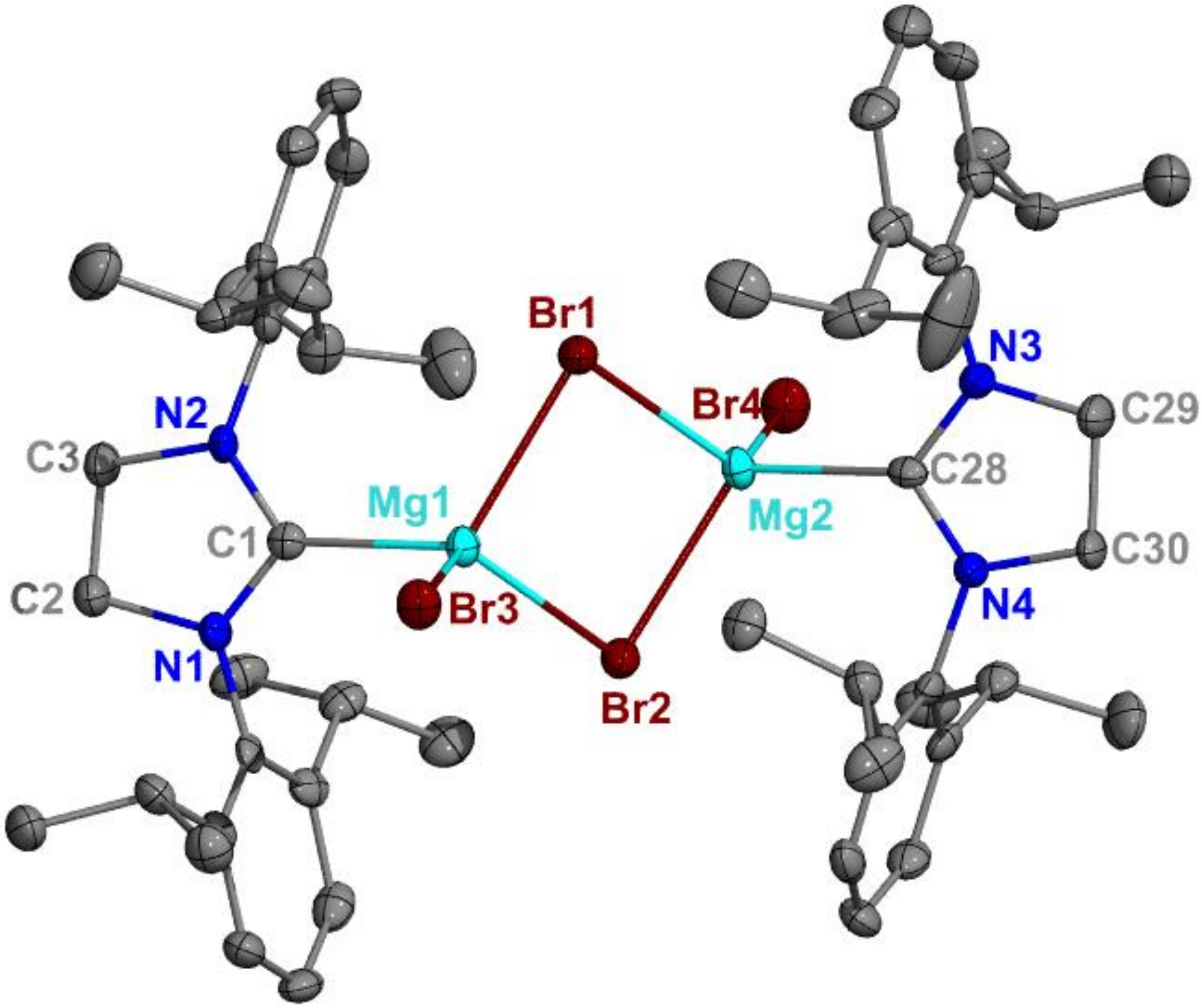

Figure A2.5. Molecular structure of 2.5. (thermal ellipsoids set at 50% probability, H atoms omitted for clarity). Selected bond distances (Å) and angles (deg): C1–Mg1: 2.2102(45); C1–N1: 1.3361(54); Mg1–Br1: 2.5574(16); Mg1–Br2: 2.5324(16); Mg1–Br3: 2.4272(15); C1–Mg1–Br3: 101.17(12); C1–Mg1–Br2:118.02(12); Br1–Mg1–Br2:93.359(51).

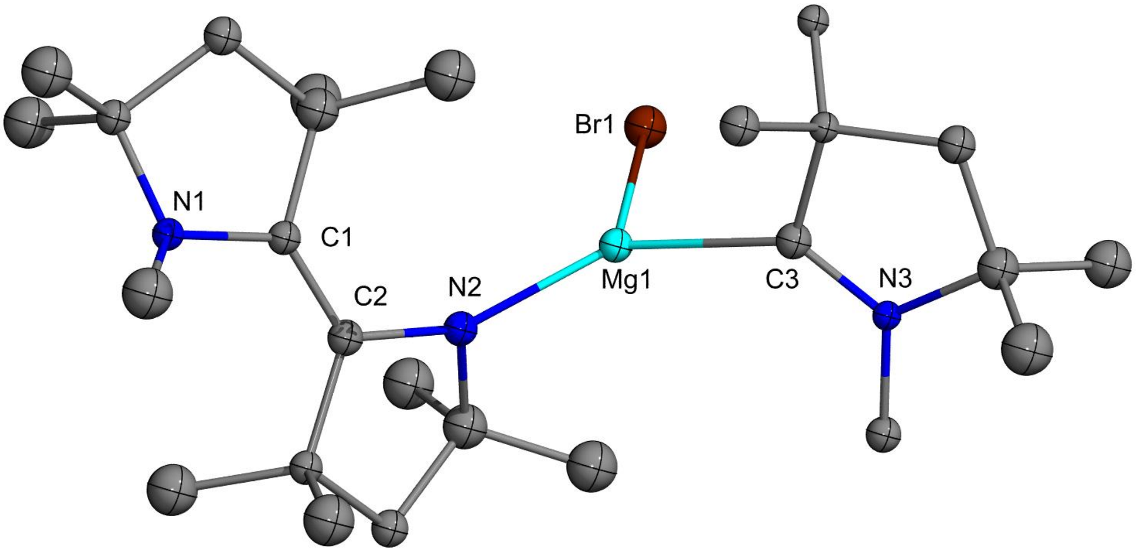

Figure A2.6. Preliminary solution to the X-ray crystallographic data showing the molecular structure of 2.6 (Dipp groups attached to N1 and N3 and CAAC-ethyl groups omitted for clarity) Due to the low crystal quality, the accuracy of interatomic distances/angles is too low to merit meaningful discussion. The attachments do, however, support the existence of the structure described in chapter 2, section 3.

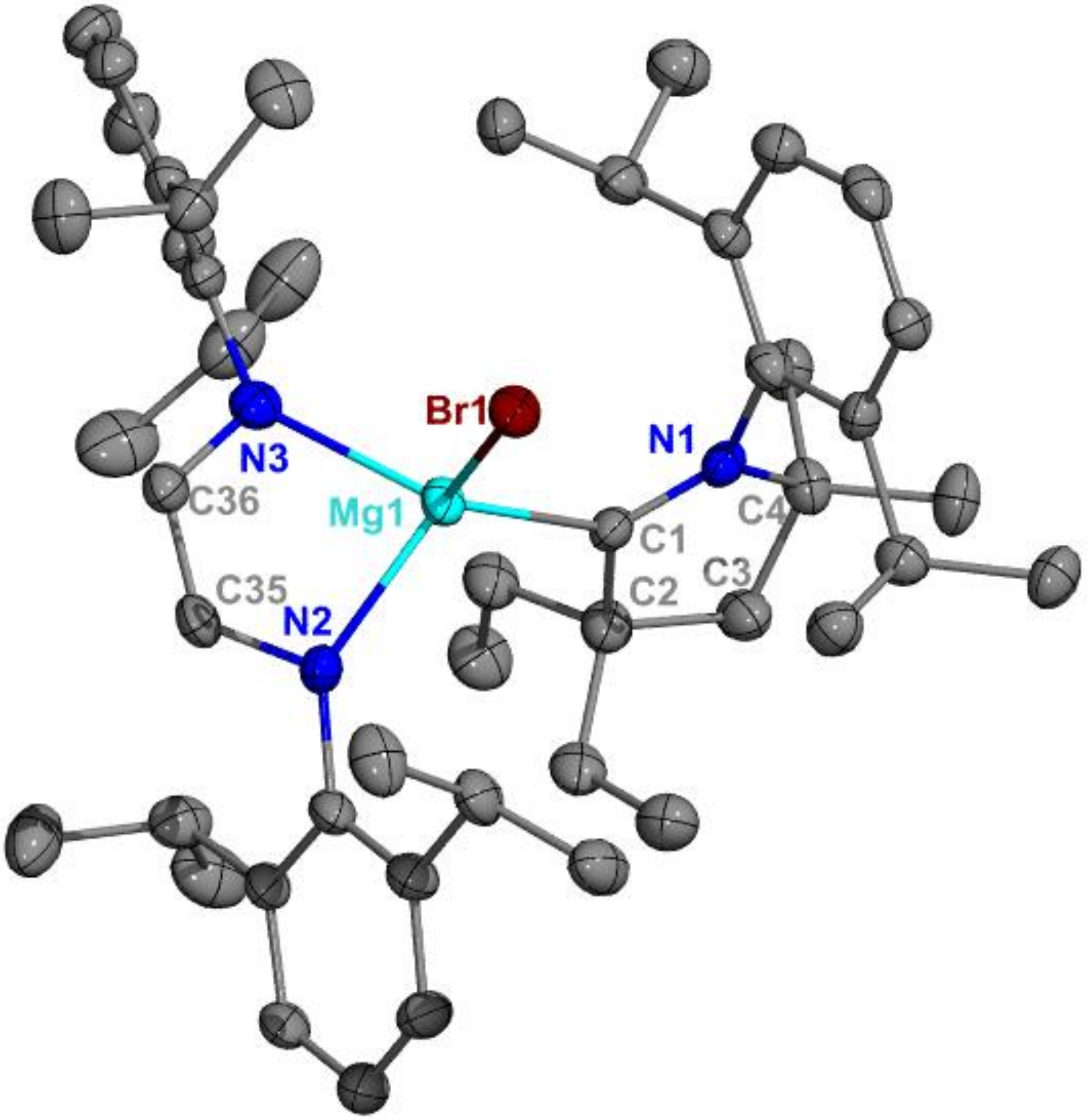

Figure A2.7. Molecular structure of 2.7 (thermal ellipsoids set at 50% probability, H atoms omitted for clarity). Selected bond distances (Å) and angles (deg): Mg1–C1: 2.293(5); C1–N1: 1.3000(6); Mg1–Br1: 2.4642(14); Mg1–N2: 2.097(4); Mg1–N3: 2.140(5); C35–N2: 1.341(7); C36–N3: 1.347(4); C35–C36: 1.404(7); C1–Mg1–Br1: 114.68(12); C35–N2–Mg1: 105.6(3).

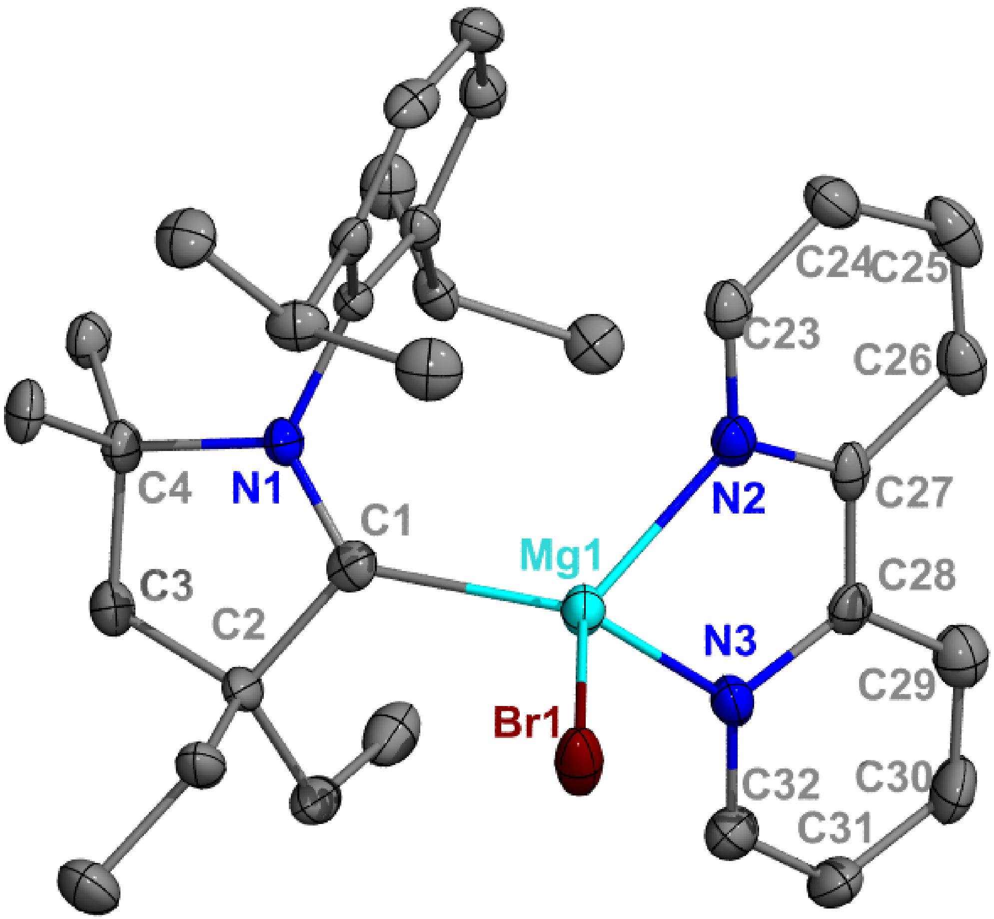

Figure A2.8. Molecular Structure of **2.8** (thermal ellipsoids set at 50% probability, H atoms omitted for clarity). Selected bond distances (Å) and angles (deg): Mg1–C1: 2.246(4); C1–N1: 1.301(5); Mg1–Br1: 2.4724(15); Mg1–N2: 2.073(4); Mg1–N3: 2.069(4); C27–N2: 1.383(5); C28–N3: 1.389(5); C27–C28: 1.409(6); C1–Mg1–Br1: 108.92(11); C27–N2–Mg1: 112.8(3).

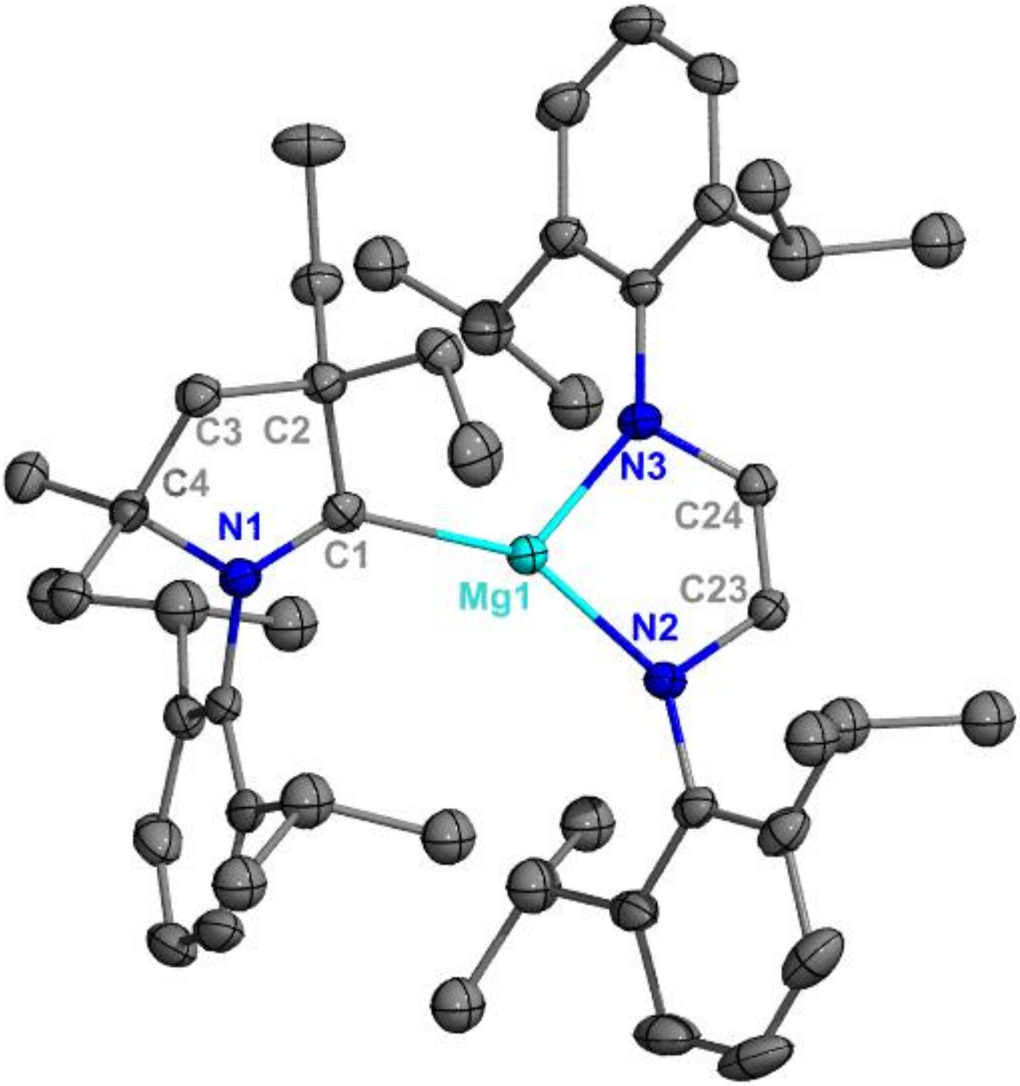

Figure A2.9. Molecular Structure of **2.9** (thermal ellipsoids set at 50% probability, H atoms omitted for clarity). Selected bond distances (Å) and angles (deg): Mg1–C1: 2.194(2); Mg1–N2: 1.9644(16); Mg1–N3: 1.9682(16); C23–N2: 1.410(2); C24–N3: 1.410(2); C23–C24: 1.342(3); C1–Mg1–N2: 144.38(7); N2–Mg1–N3: 90.79(7).

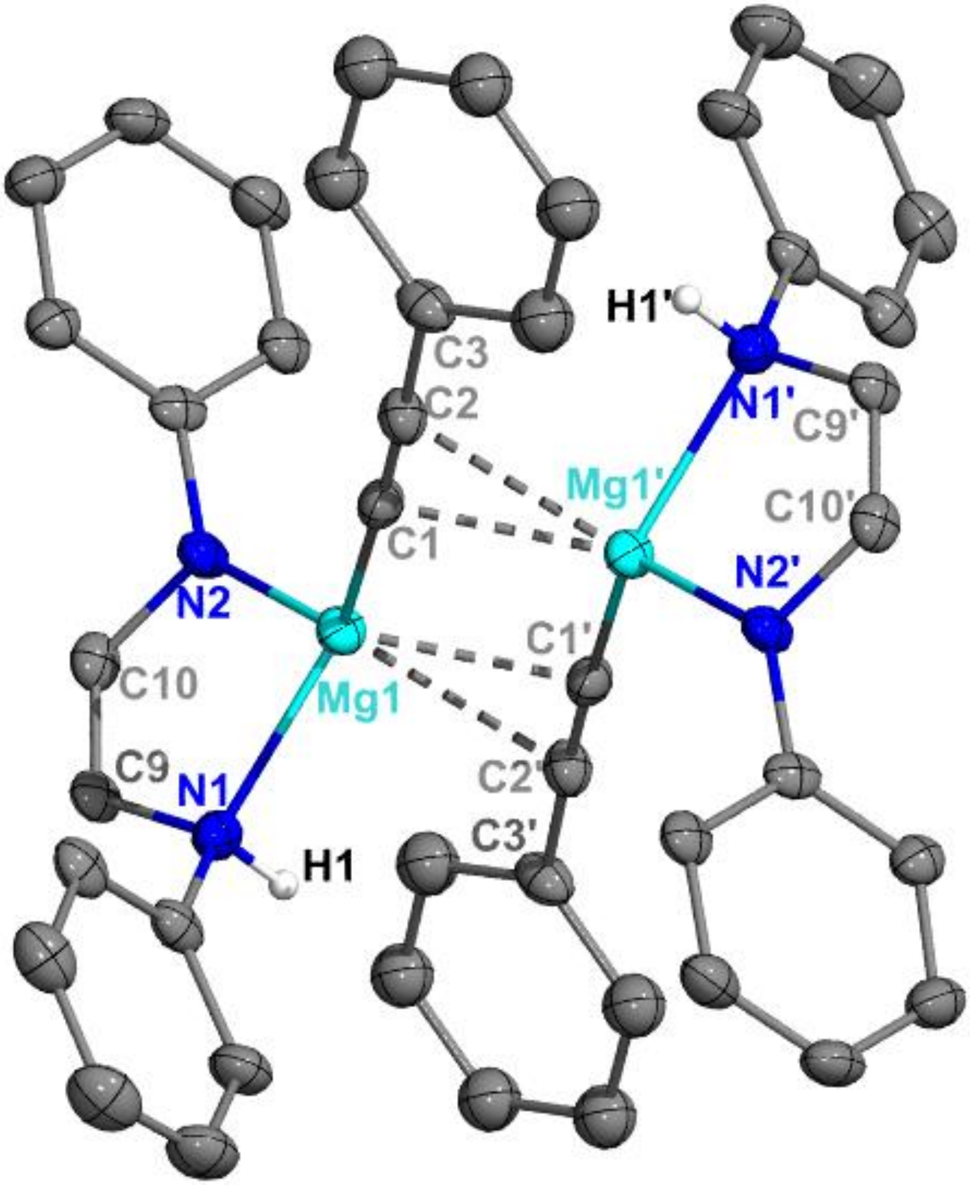

Figure A2.10. Molecular Structure of **2.10** (thermal ellipsoids set at 50% probability, H atoms omitted for clarity). Selected bond distances (Å) and angles (deg): Mg1–N2: 2.000(2); Mg1–N1: 2.157(2); Mg1–C1: 2.138(3); Mg1–C1’: 2.284(3); Mg1–C2: 2.629(3); Mg1–Mg1’: 3.1017(16); N2–Mg1–N1: 85.02(8); N2–Mg1–C1: 120.65(9).

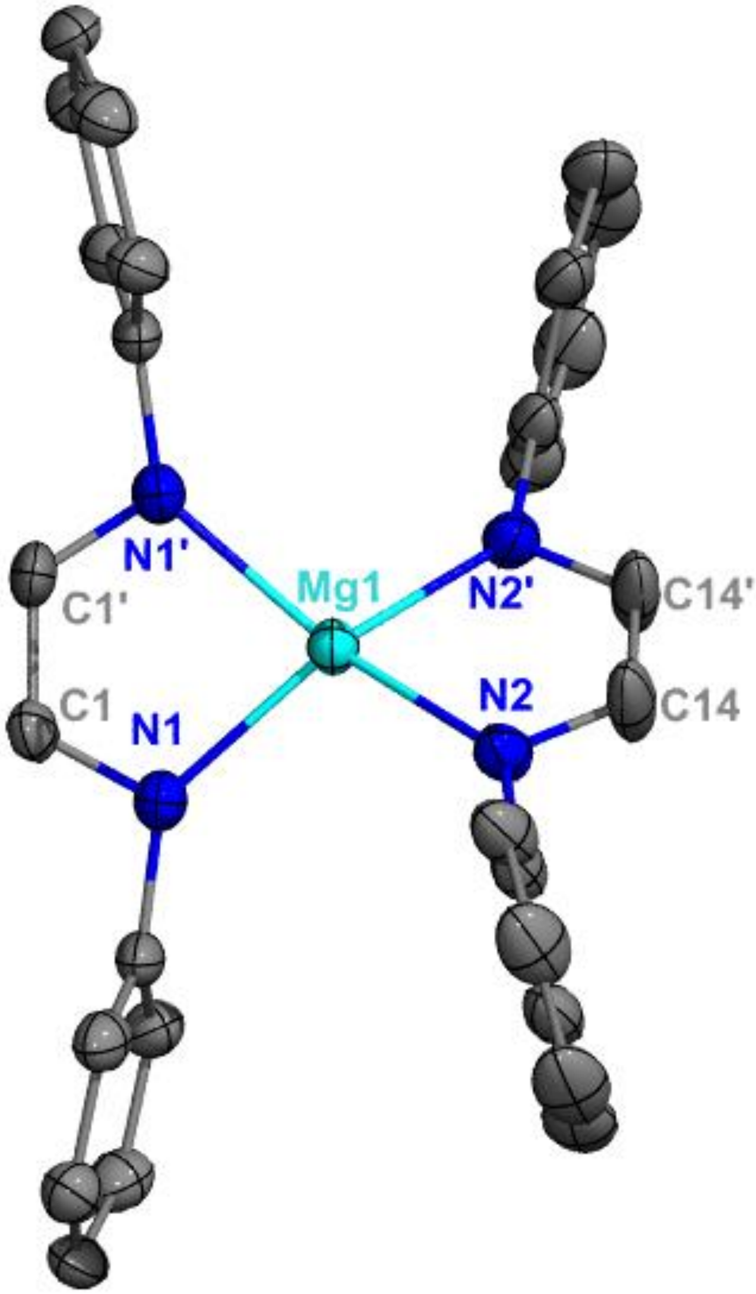

Figure A2.11. Molecular Structure of **2.11** (thermal ellipsoids set at 50% probability, H atoms and Dipp-isopropyl groups omitted for clarity). Selected bond distances (Å) and angles (deg): Mg1–N1: 2.085(2); Mg1–N2: 2.080(2); N1–C1: 1.381(10); C14–C14’: 1.400(6); N2–Mg1–N2: 82.36(12); N2–Mg1–N1: 146.87(9); N2–Mg1–N1: 106.80(8).

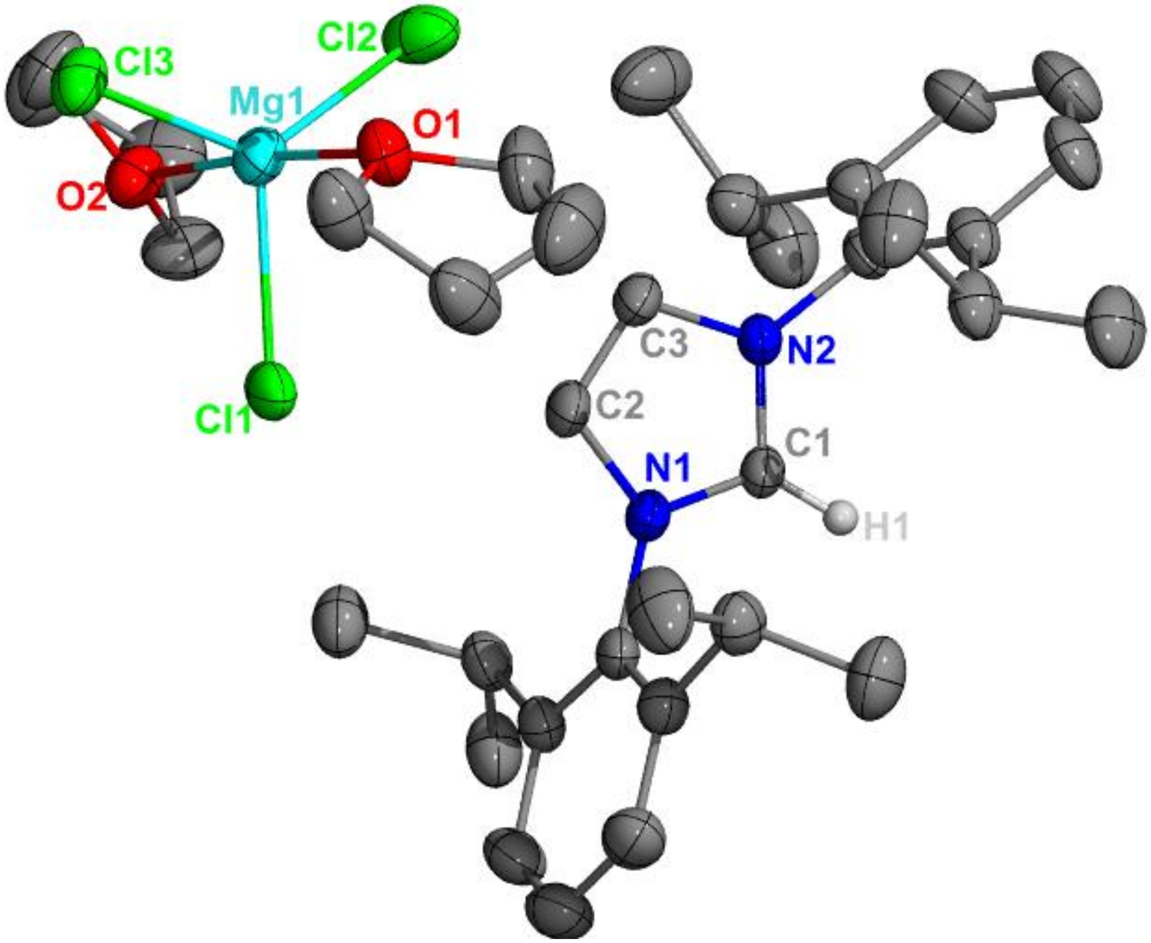

Figure A2.12. Molecular structure of compound 2.X., [(IPrH)][(THF$_2$)MgCl$_3$] (thermal ellipsoids set at 30% probability)

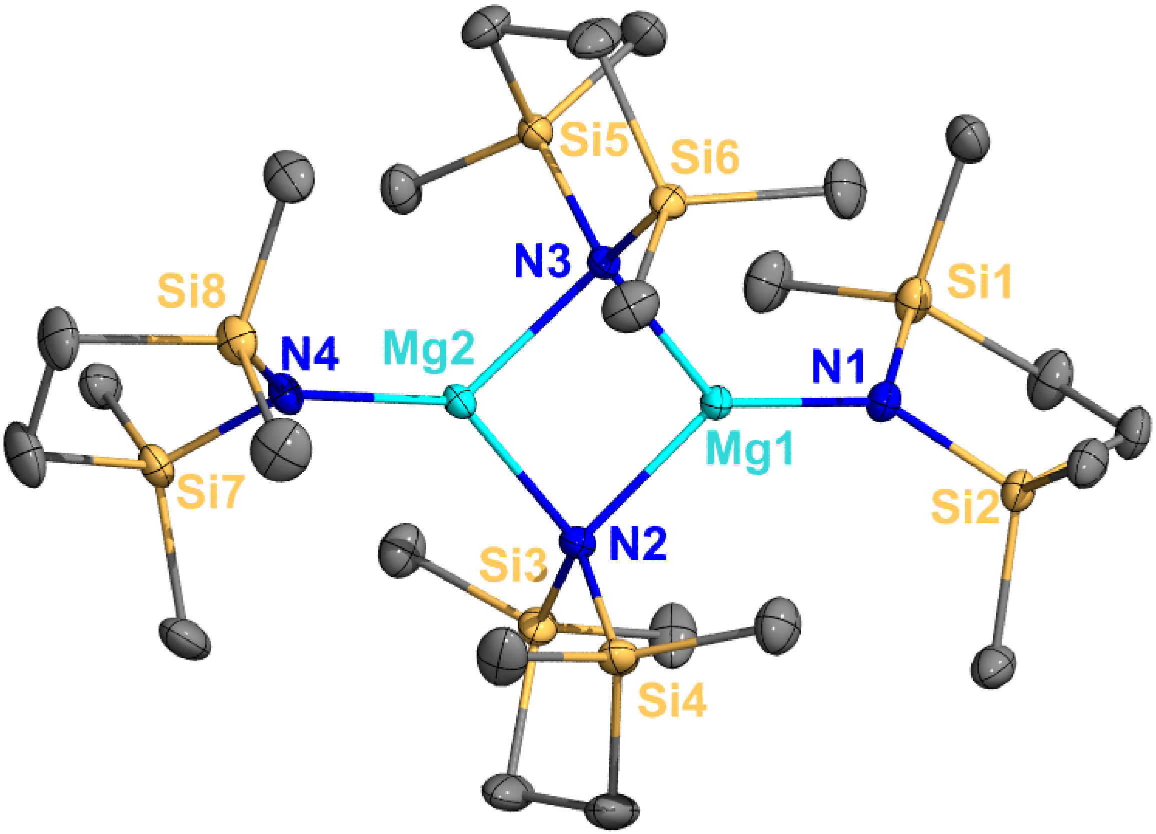

Figure A2.13. Molecular Structure of **3.1** (thermal ellipsoids set at 50% probability, H atoms omitted for clarity.)

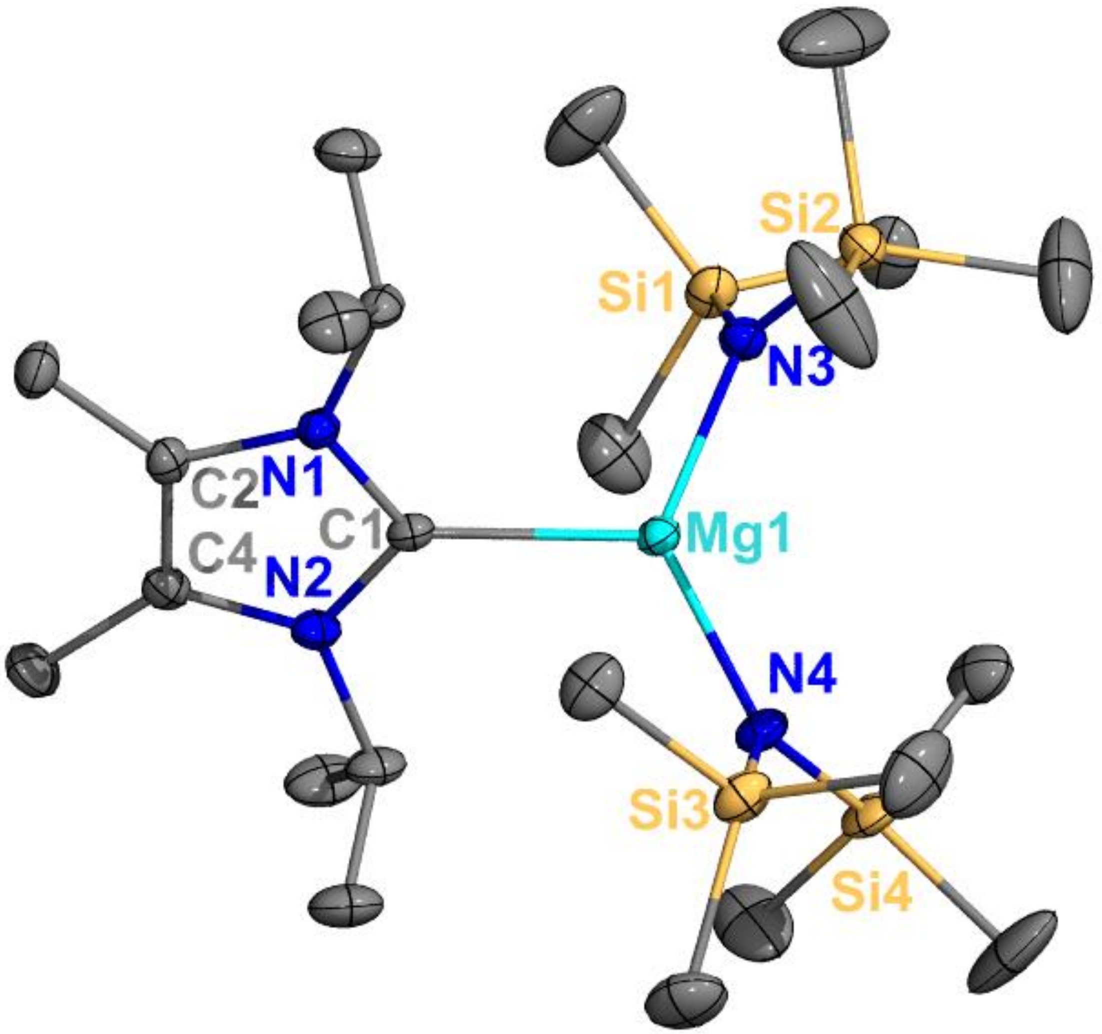

Figure A2.14. Molecular structure of **3.2** (thermal ellipsoids at 50% probability; H atoms omitted for clarity Selected bond distances (Å) and angles (deg): Mg1–C1: 2.2120(19); Mg1–N3: 1.9920(16); Mg1–N4: 1.9944(16); C1–N1: 1.360(2); C1–N2: 1.361(2); N3–Mg1–C1: 111.75(7); N4–Mg1–C1: 117.82(7); N4–Mg1–N3: 130.27(7).

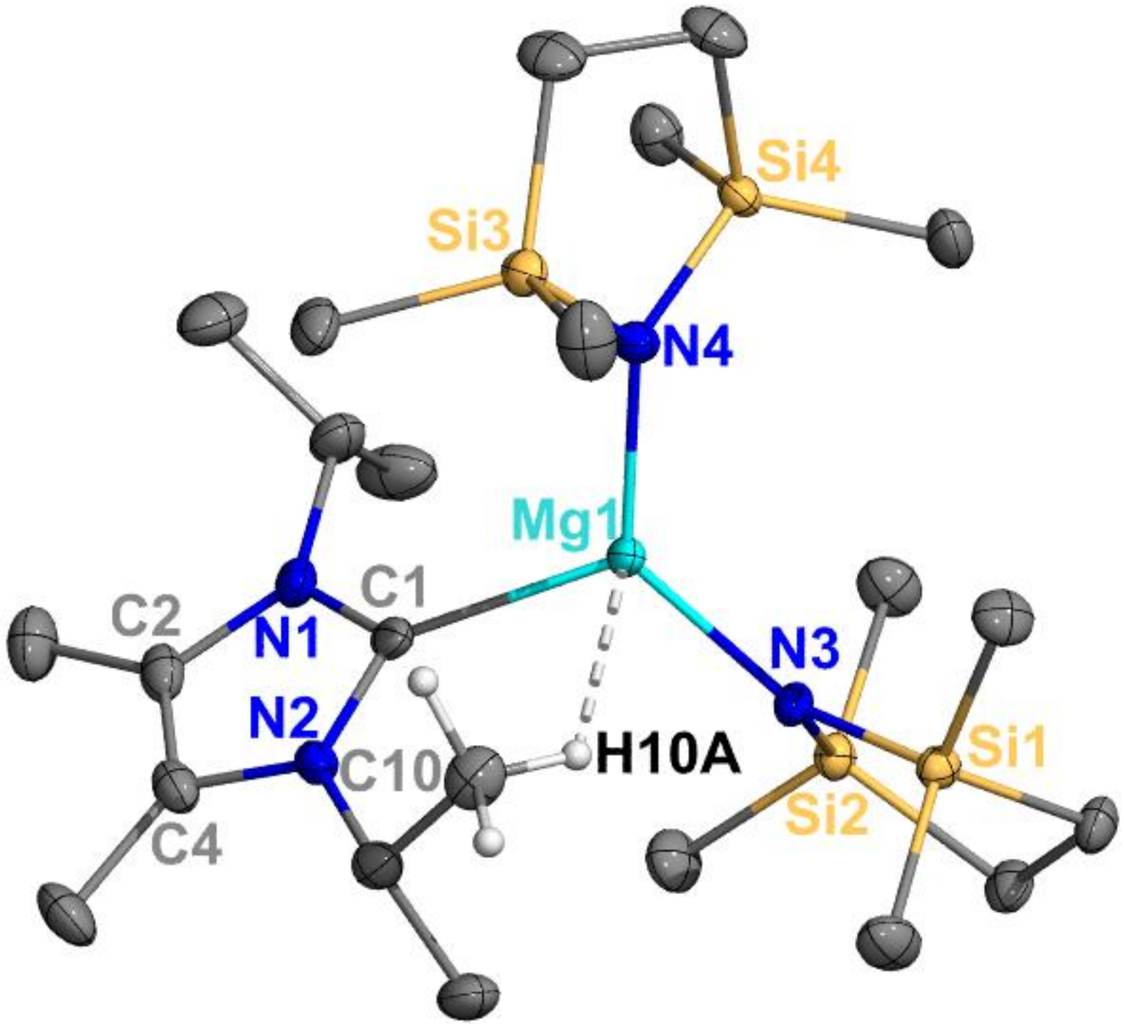

Figure A2.15. Molecular structure of **3.3** (thermal ellipsoids at 50% probability; H atoms omitted for clarity with the exception of those located on C10). Only the major occupied position is shown for disordered *N*-isopropyl substituents. Selected bond distances (Å) and angles (deg): Mg1–C1: 2.2118(13); Mg1–H10A: 2.429(16); Mg1–N3: 1.9855(10); Mg1–N4: 1.9755(11); C1–N1: 1.3572(16); C1–N2: 1.3583(15); N3–Mg1–C1: 113.92(4); N4–Mg1–C1: 115.06(4); N4–Mg1–N3: 130.62(4); C1–Mg1–H10A: 78.4(4); C10–H10A–Mg1: 121.1(11).

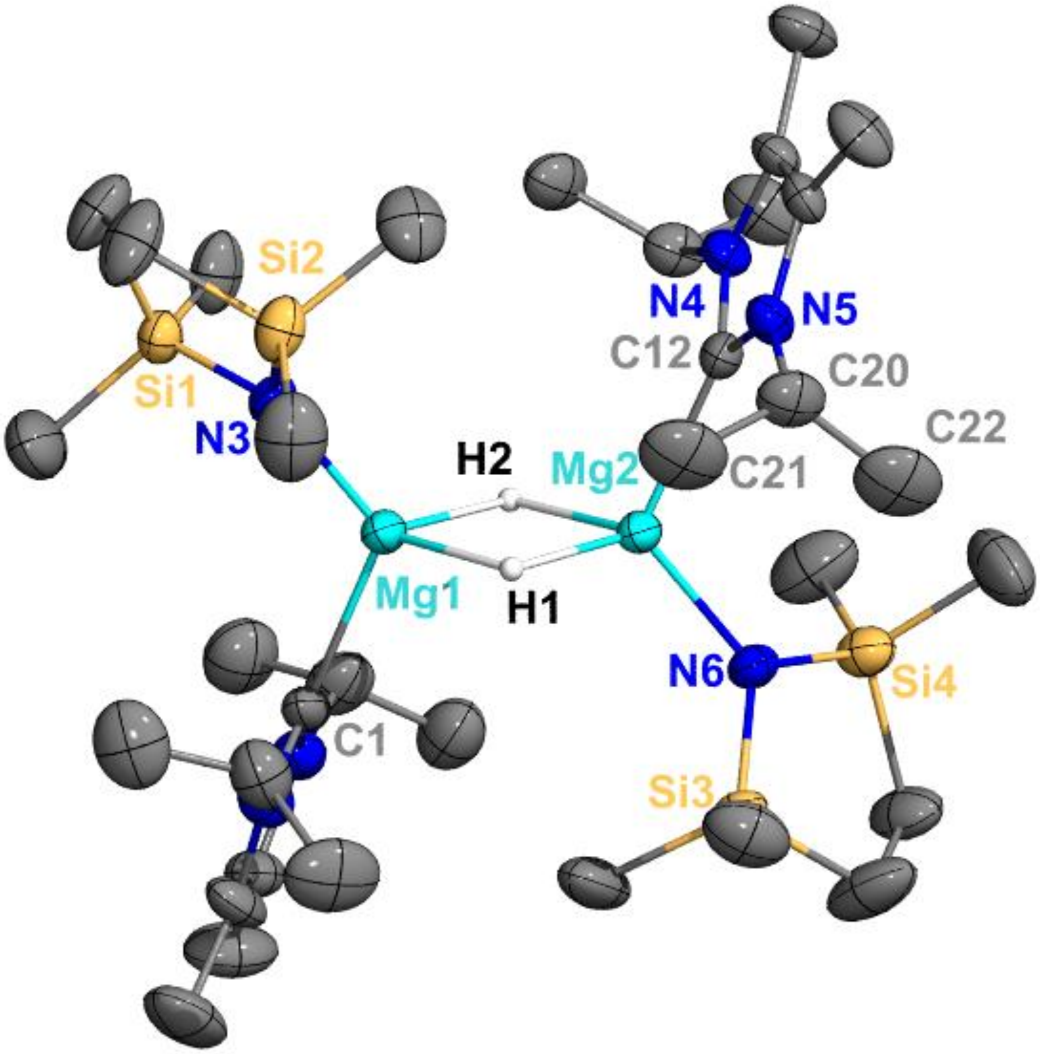

Figure A2.16. Molecular Structures of **3.4** (thermal ellipsoids set at 50%; H atoms omitted for clarity with the exception of H1 and H2 which were isotropically refined). Selected bond distances (Å) and angles (deg): Mg1–C1: 2.2239(17); Mg2–C18: 2.2250(16); Mg1–H1: 1.828(18); Mg1–H2: 1.933(18); Mg2–H1: 1.861(17); Mg2–H2: 1.865(18); Mg1–Mg2 2.8269(9); Mg1–N3: 2.0098(14); Mg2–N6: 2.0144(14); N3–Mg1–C1: 118.02(6); C1–Mg1–H1: 105.3(6); H1–Mg1–H2: 81.4(8).

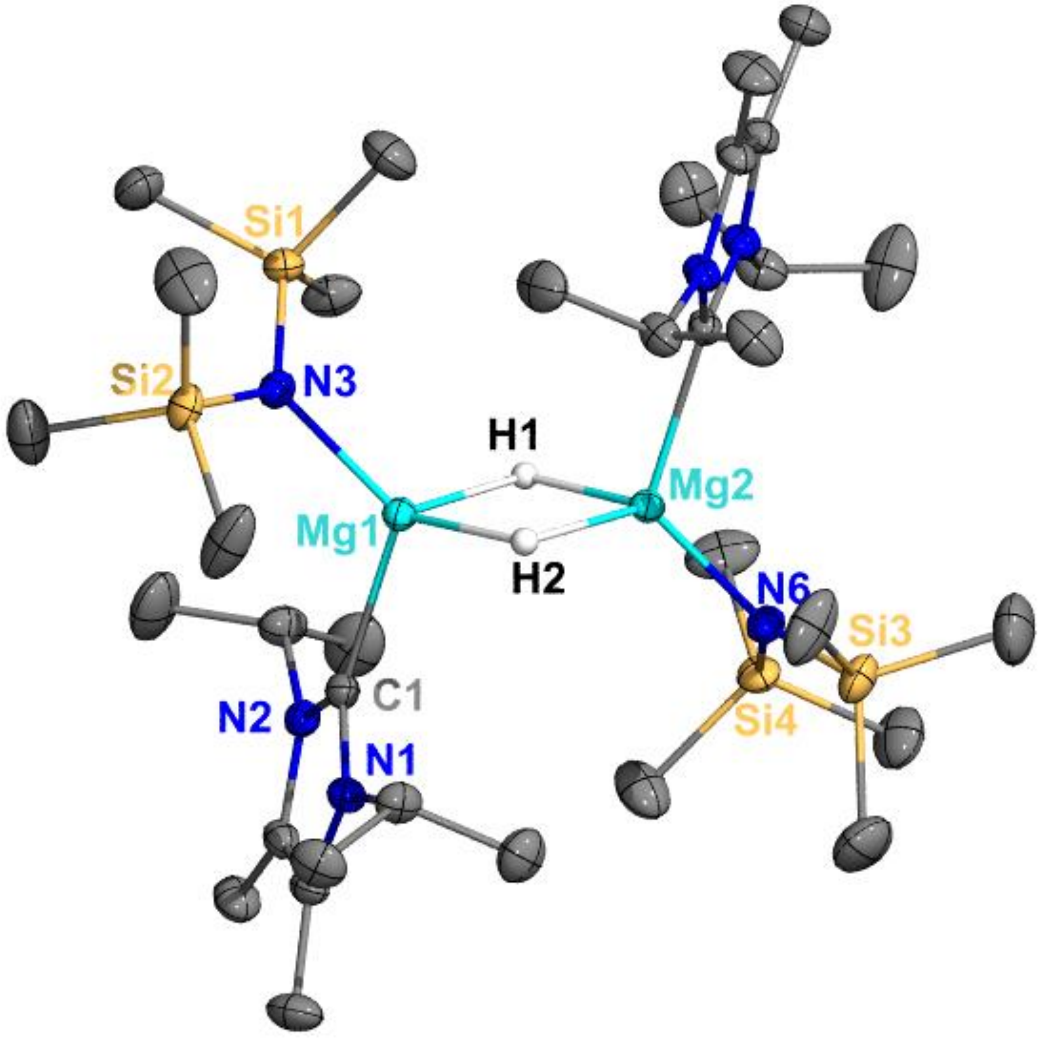

Figure A2.17. Molecular structure of **3.5** (thermal ellipsoids set at 50%; H atoms omitted for clarity with the exception of H1 and H2 which were isotropically refined. Only the major occupied position is shown for disordered *N*-isopropyl substituents.) Selected bond distances (Å) and angles (deg): Mg1–C1: 2.230(4); Mg2–C12: 2.228(4); Mg1–H1: 1.93(4); Mg1–H2: 1.93(4); Mg2–H1: 1.97(4); Mg2–H2: 1.82(4); Mg1–Mg2; 2.8163(19); Mg1–N3: 1.994(4); Mg2–N6: 2.000(4); N3–Mg1–C1: 119.27(16); C1–Mg1–H1: 107.1(12); H1–Mg1–H2: 84.4(17).

Chapter 4

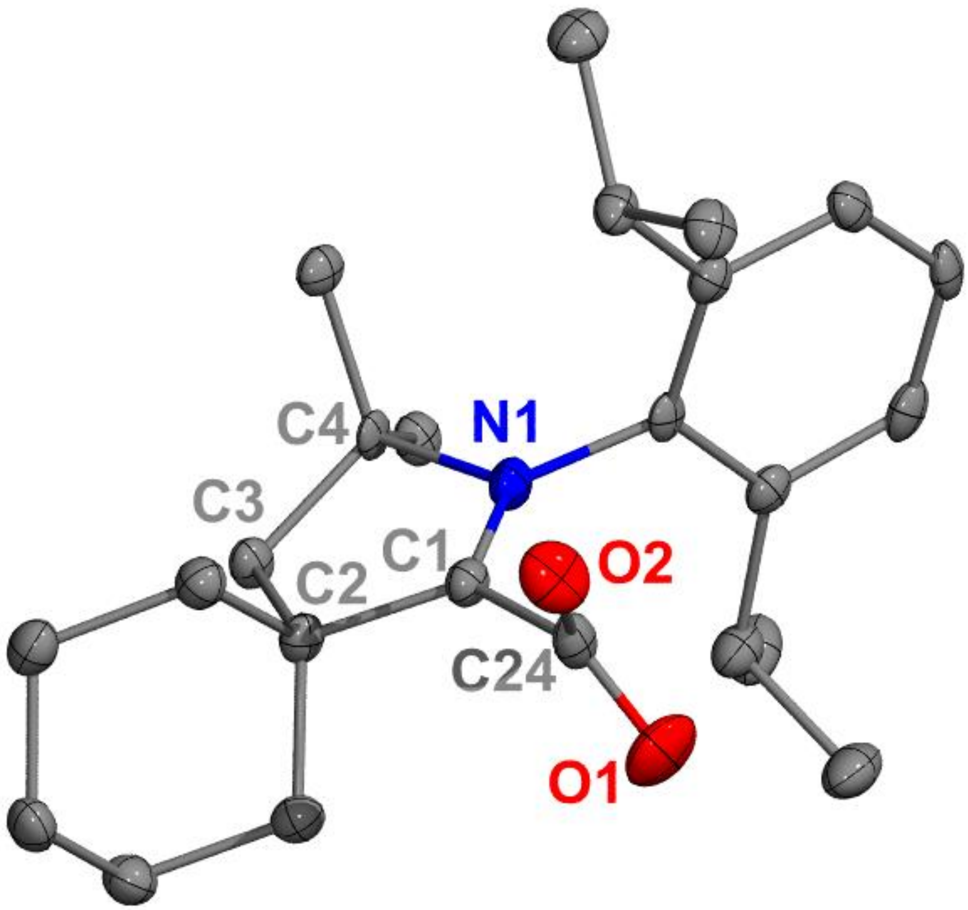

Figure A2.18. Molecular structure of compound **4.1** (thermal ellipsoids at 40% probability; only one of the two chemically equivalent but crystallographically distinct molecules is shown). H atoms and co-crystallized THF solvent molecules omitted for clarity. Selected bond distances (Å) bond angles (°) and torsion angles (°): C1–C24: 1.526(4); C1–N1: 1.297(4); O1–C24 1.236(4); O2–C24: 1.234(4); N1–C1–C24: 123.9(3); O2–C24–O1: 131.5(3); O1–C24–C1: 113.7(3); N1–C1–C24–O2: 101.2(4).

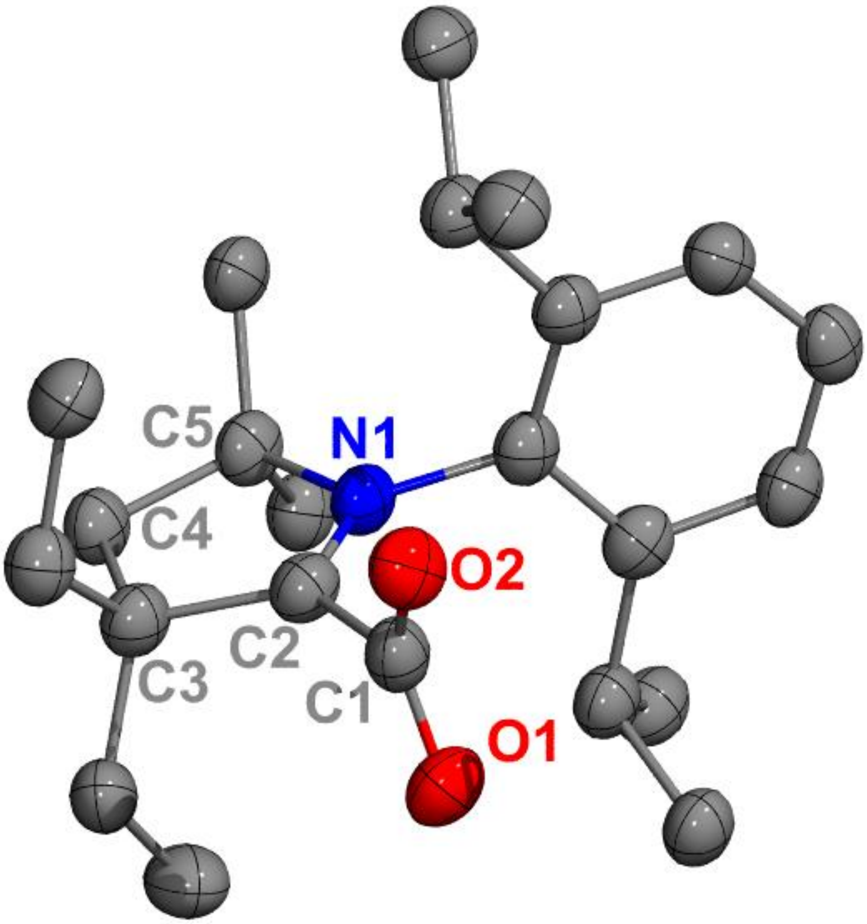

Figure A2.19. Molecular Structure of **4.3** (thermal ellipsoids set at 50% probability, H atoms omitted for clarity). Selected bond distances (Å) bond angles (°) and torsion angles (°): O1–C1: 1.236(5); O2–C1: 1.248(5); C1–C2: 1.516(5); N1–C2: 1.282(5); C2–N1–C5: 114.8(3); O1–C1–O2: 131.9(4); O1–C1–C2: 112.9(4); N1–C2–C3: 113.2(4); O2–C1–C2–N1: 86.5(5); O1–C1–C2–N1: –95.4(5).

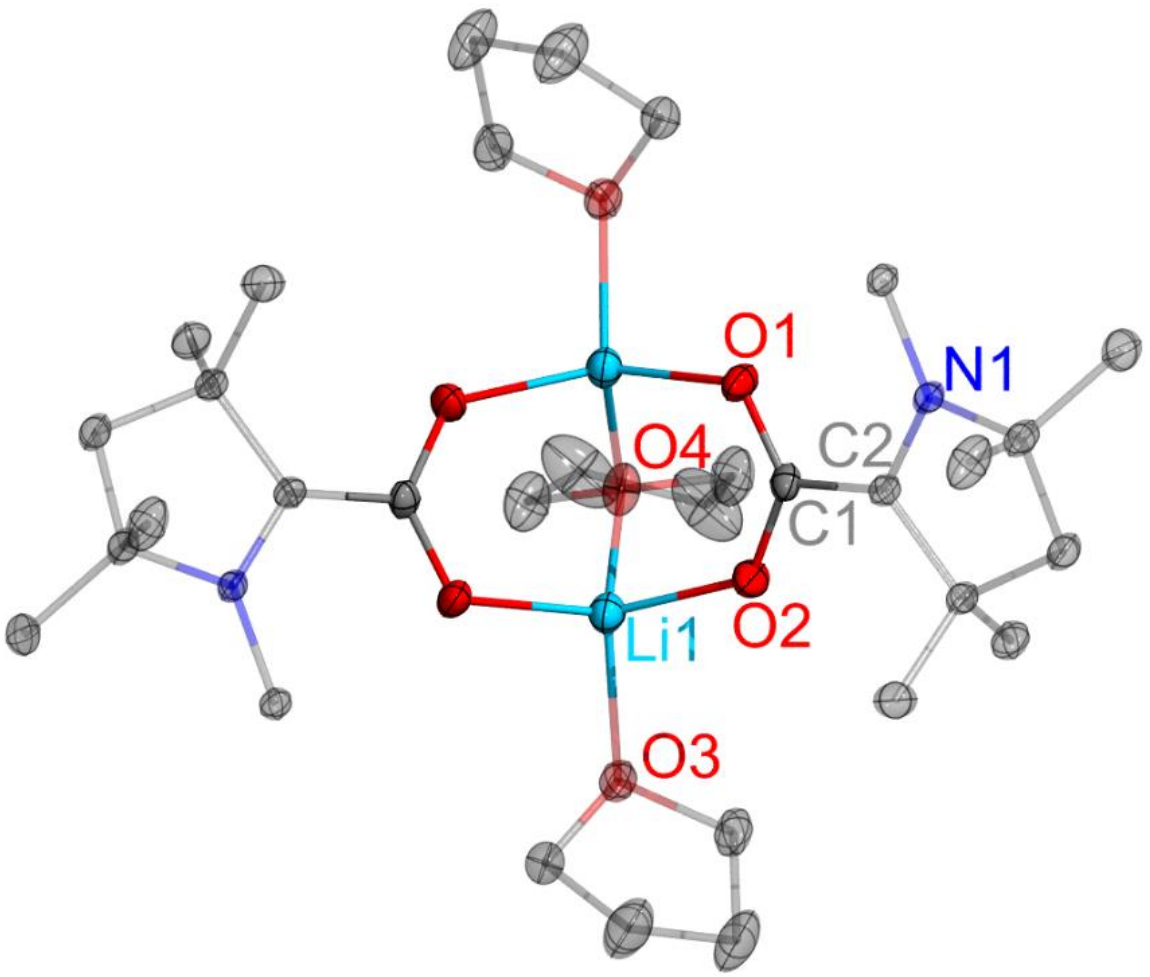

Figure A2.20. Solid state molecular structures of **4.4** (All H atoms and carbon atoms not directly attached to the CAAC core ring are omitted for clarity). Selected bond distances (Å) and angles (deg): O1–C1: 1.2732(12); O2–C1: 1.2778(12); C1–C2: 1.4533(13); N1–C2: 1.3802(12); O1–C1–O2: 123.71(9); O1–C1–C2: 119.84(9); O2–C1–C2: 116.45(9); N1–C2–C1: 124.85(9); N1–C2–C3: 110.81(8).

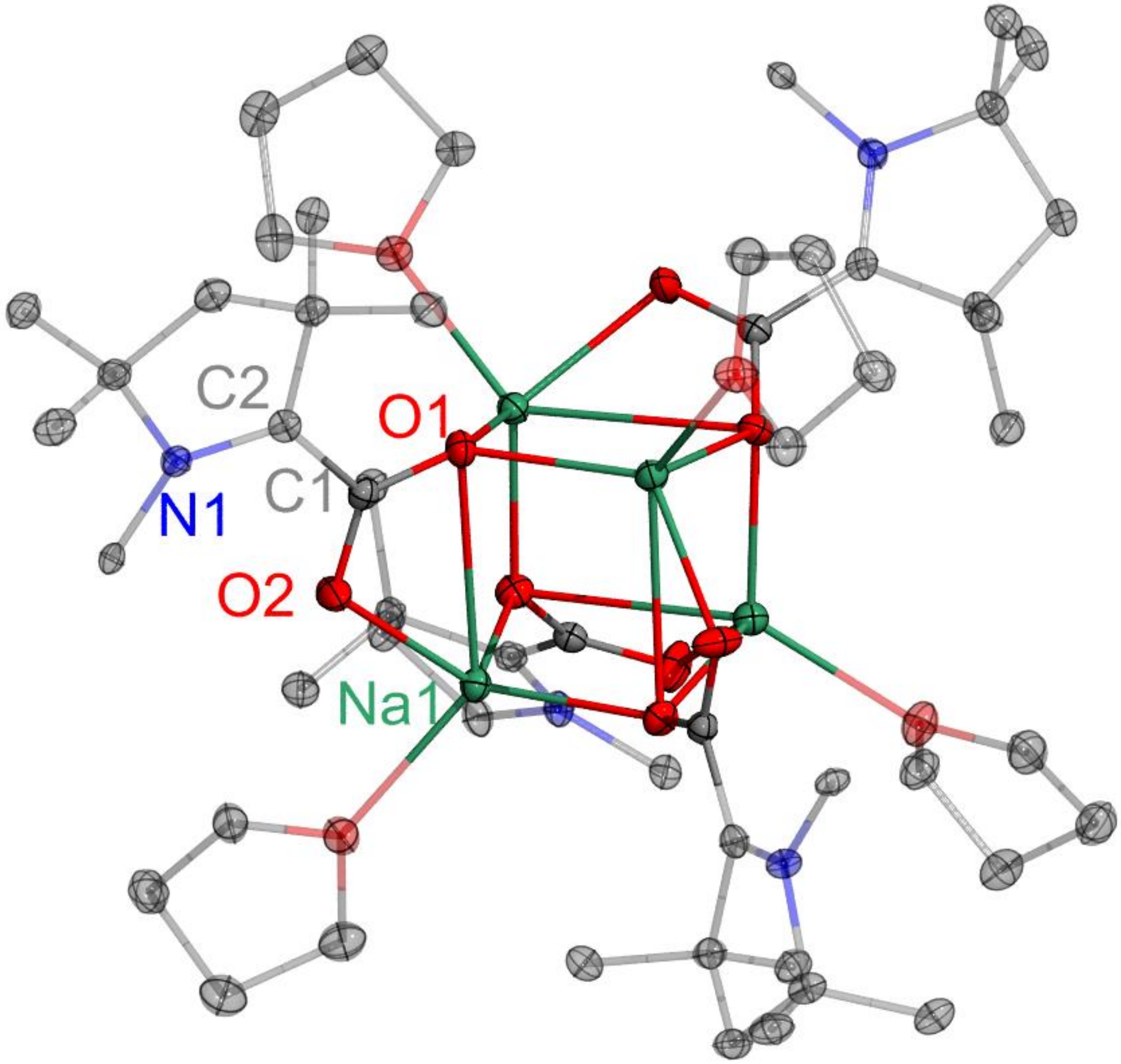

Figure A2.21. Solid state molecular structures of **4.5** (All H atoms and carbon atoms not directly attached to the CAAC core ring are omitted for clarity). Selected bond distances (Å) and angles (deg): O1–C1: 1.286(3); O2–C1: 1.266(3); C1–C2: 1.458(3); N1–C2: 1.385(3); O2–C1–O1: 122.9(2); O2–C1–C2: 118.7(2); O1–C1–C2: 118.3(2); N1–C2–C1: 124.7(2); N1–C2–C3: 109.7(2).

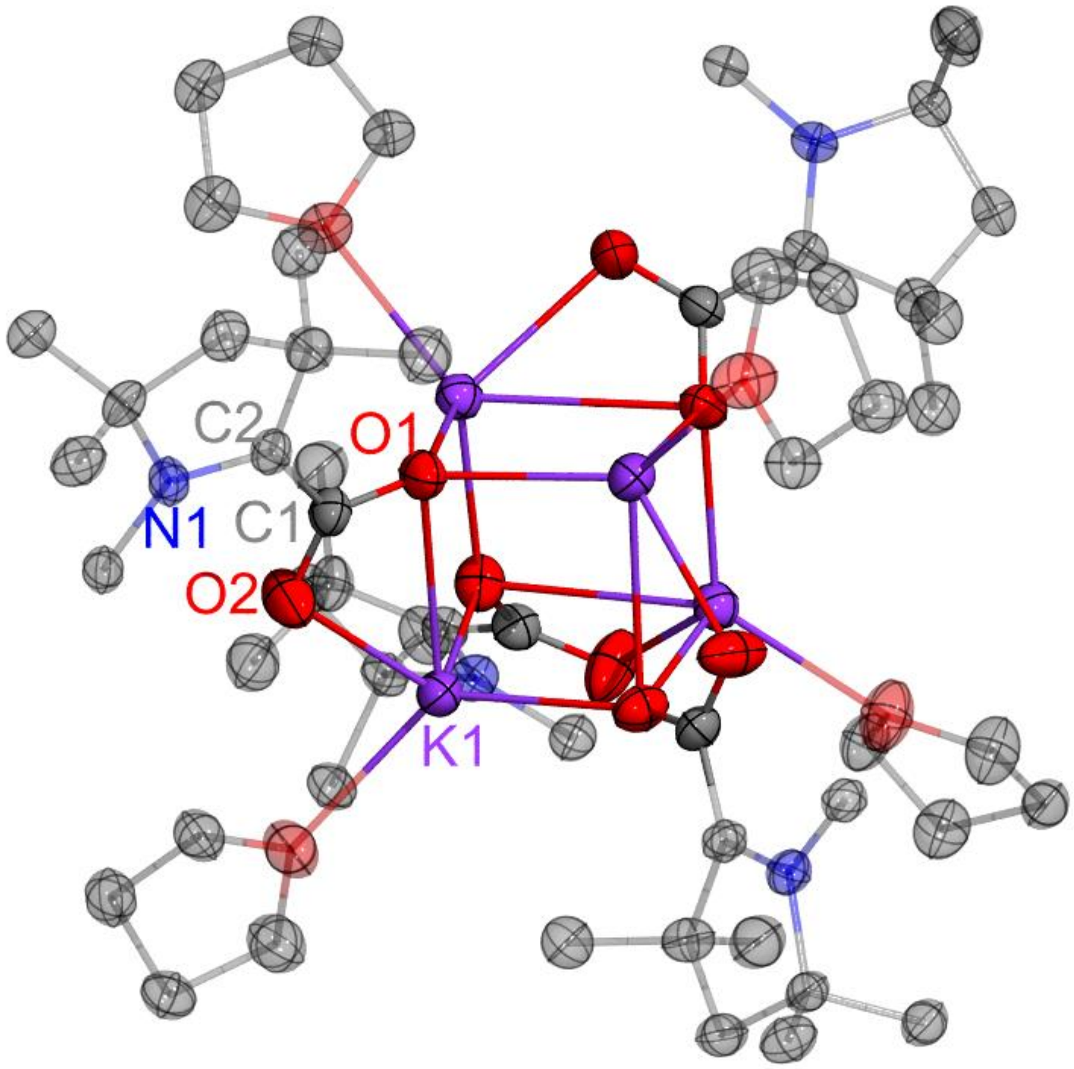

Figure A2.22. Solid state molecular structures of **4.6** (All H atoms and carbon atoms not directly attached to the CAAC core ring are omitted for clarity). Selected bond distances (Å) and angles (deg): O1–C1: 1.276(6); O2–C1: 1.265(7); C1–C2: 1.451(7); N1–C2: 1.384(6); O2–C1–O1: 123.0(5); O2–C1–C2: 119.1(5); O1–C1–C2: 117.9(5); N1–C2–C1: 123.3(5); N1–C2–C3: 110.2(4).

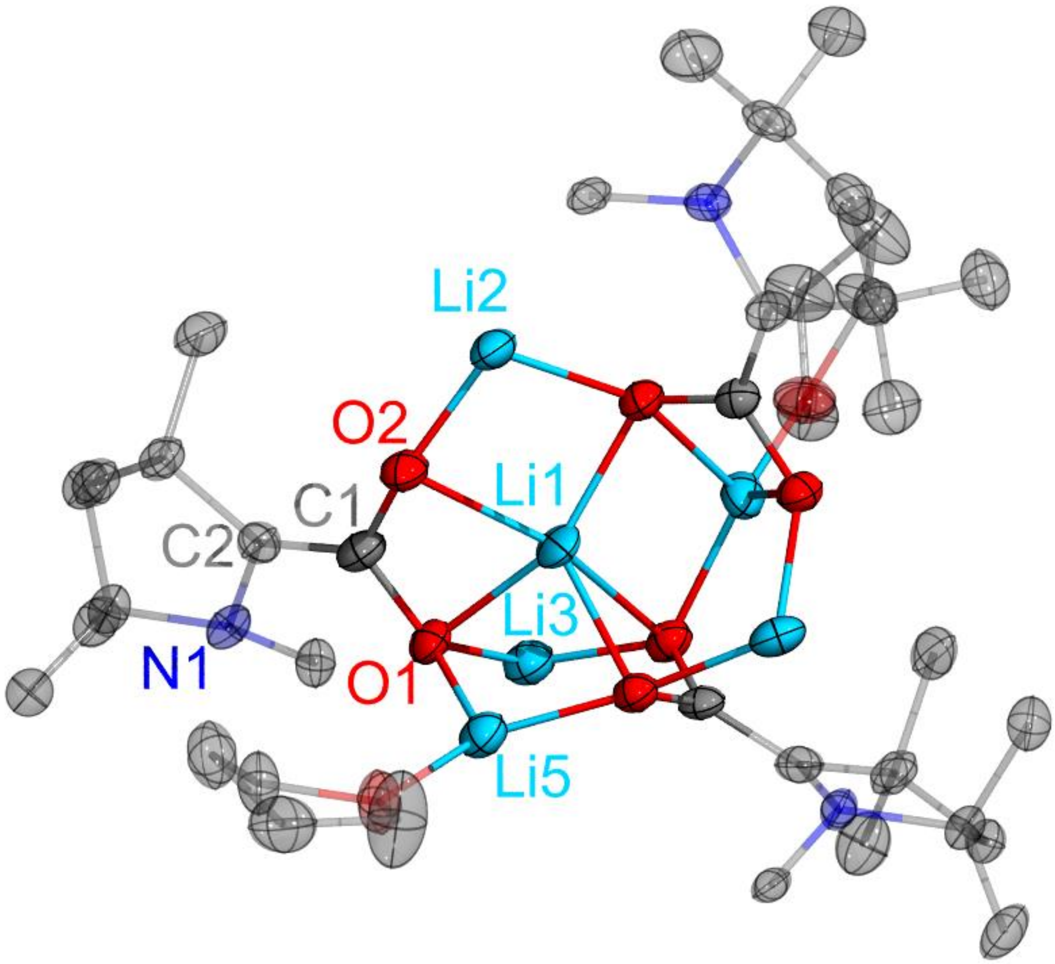

Figure A2.23. Solid state molecular structure of **4.7** (All H atoms and carbon atoms not directly attached to the CAAC core ring are omitted for clarity). Selected bond distances (Å) and angles (deg): O1–C1: 1.354(7); O2–C1: 1.332(7); C1–C2: 1.379(8); N1–C2: 1.463(7); O2–C1–O1: 114.1(5); O1–C1–C2: 121.2(5); O2–C1–C2: 124.6(5); C1–C2–N1: 120.0(5); N1–C2–C3: 109.6(5).

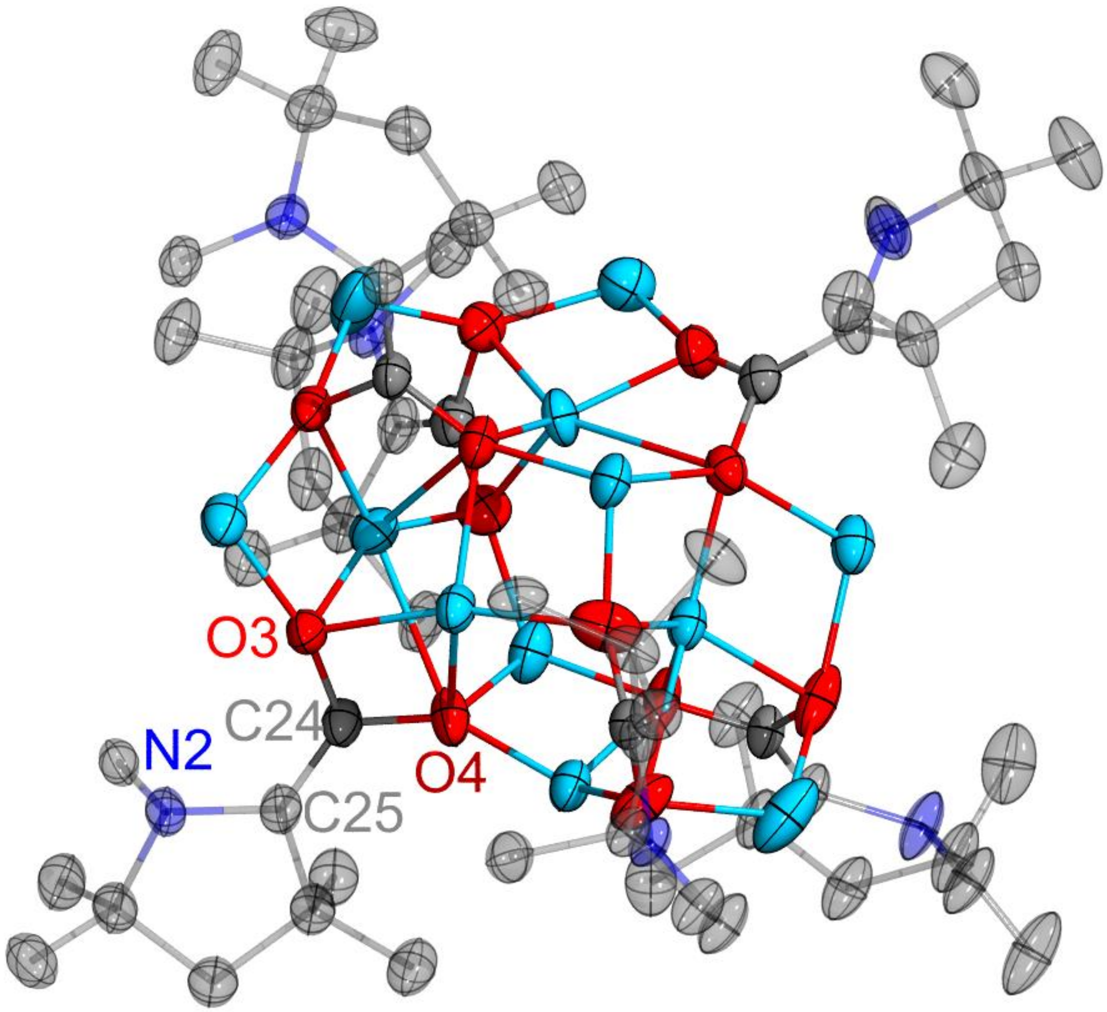

Figure A2.24. Solid state molecular structure of **4.8** (All H atoms and carbon atoms not directly attached to the CAAC core ring are omitted for clarity). Selected bond distances (Å) and angles (deg): O1–C1: 1.365(2); O2–C1: 1.360(2); C1–C2: 1.343(3); N1–C2: 1.452(2); O2–C1–O1: 114.20(15); C2–C1–O1: 120.63(16); C2–C1–O2: 125.16(16); C1–C2–N1: 121.20(16); N1–C2–C3: 110.58(15).

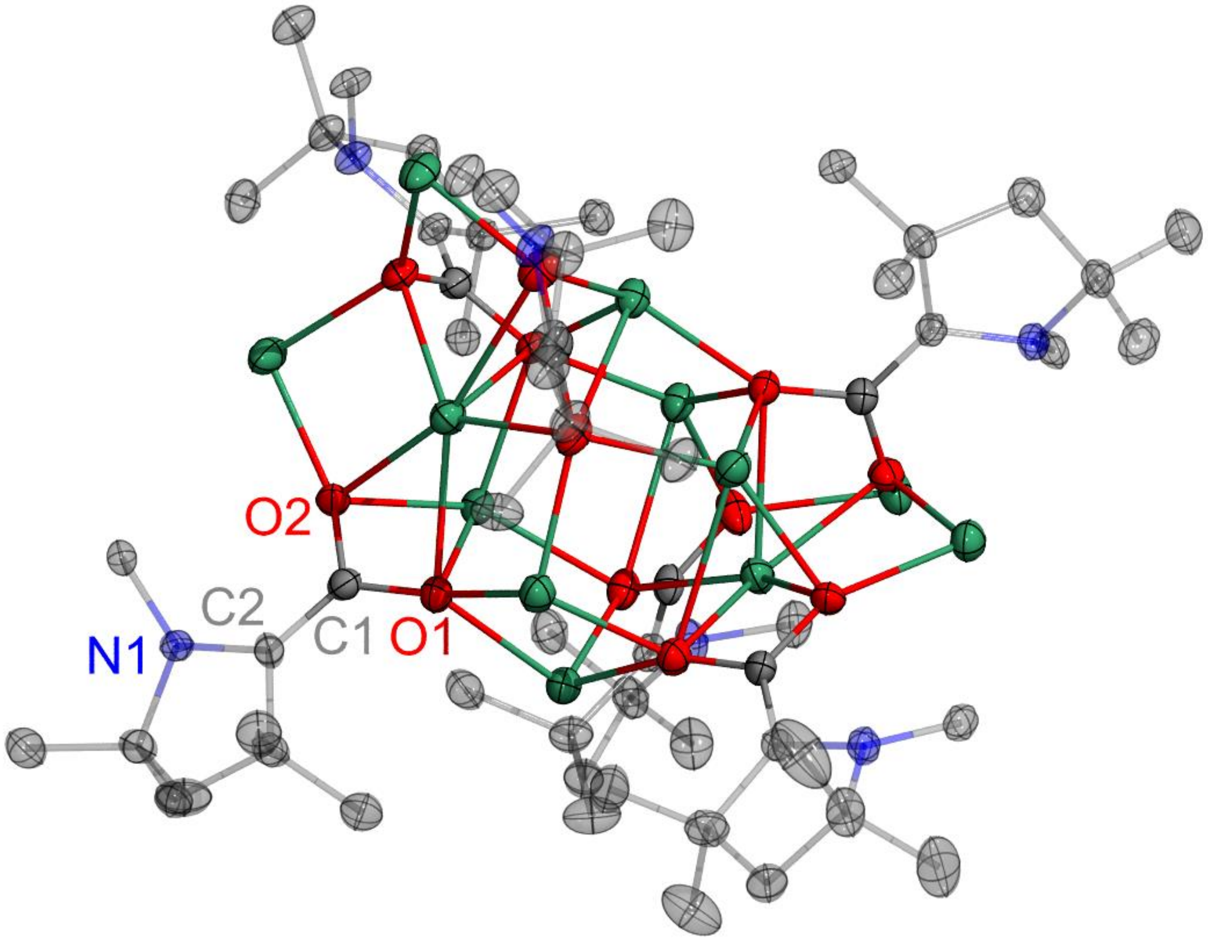

Figure A2.25. Solid state molecular structure of **4.9**. All H atoms and all carbon atoms not directly attached to the CAAC core ring are omitted for clarity. Selected bond distances (Å) and angles (deg): O1–C1: 1.364(4); O2–C1: 1.336(4); C1–C2: 1.365(5); N1–C2: 1.452(4); O2–C1–O1: 113.4(3); O1–C1–C2: 124.0(3); C1–C2–N1: 122.9(3); N1–C2–C3: 107.9(3).

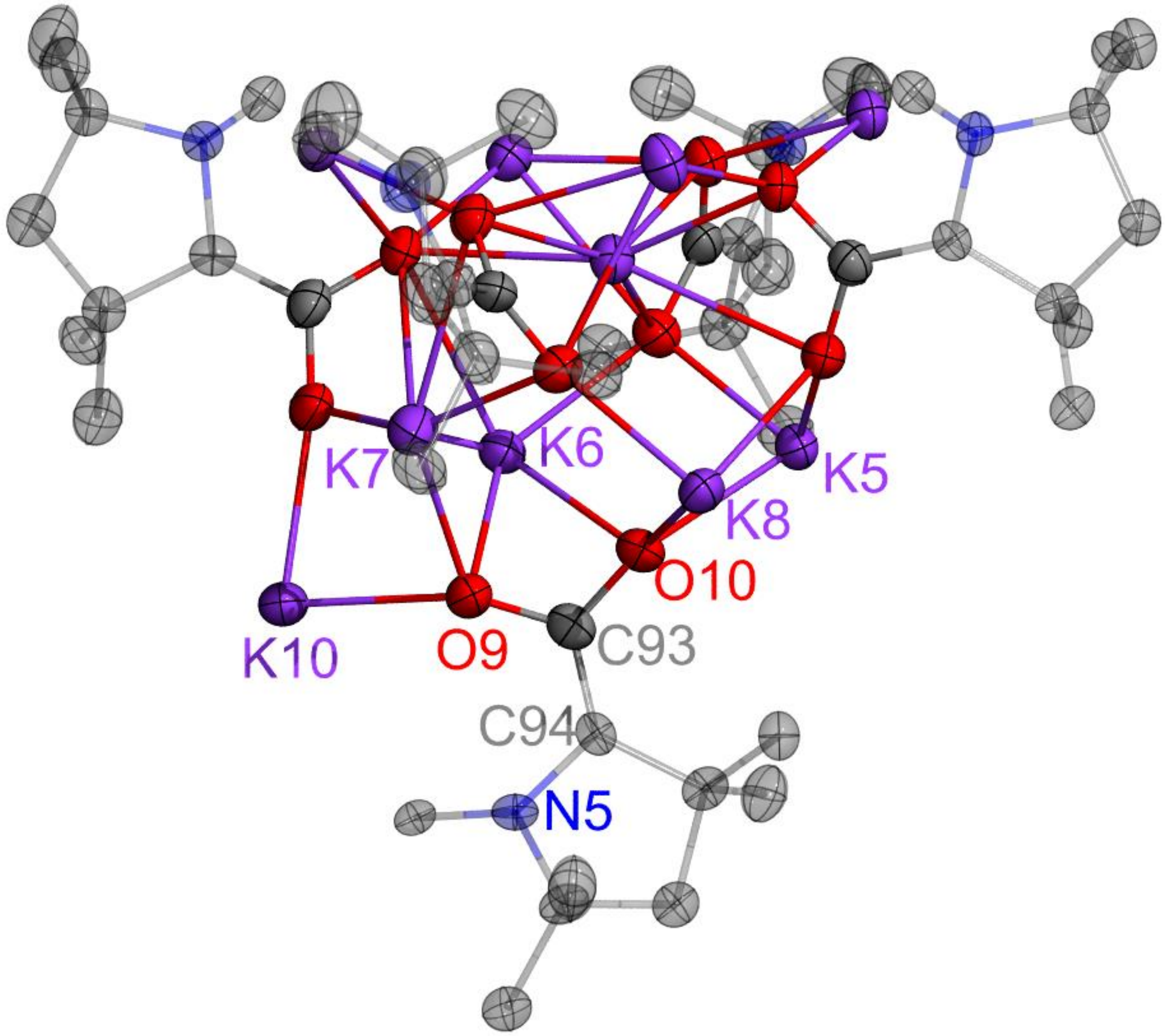

Figure A2.26. Solid state molecular structure of **4.10**. All H atoms and all carbon atoms not directly attached to the CAAC core ring are omitted for clarity. Selected bond distances (Å) and angles (deg): O9–C93: 1.342(10); O10–C93: 1.304(9); C93–C94: 1.385(11); N5–C94: 1.455(9); O10–C93–O9: 115.8(7); O9–C93–C94: 120.0(7); C93–C94–N5: 119.5(6); N5–C94–C95: 108.7(6).

Appendix III – Spectral Data

Nuclear Magnetic Resonance (NMR) Data

Chapter 2.

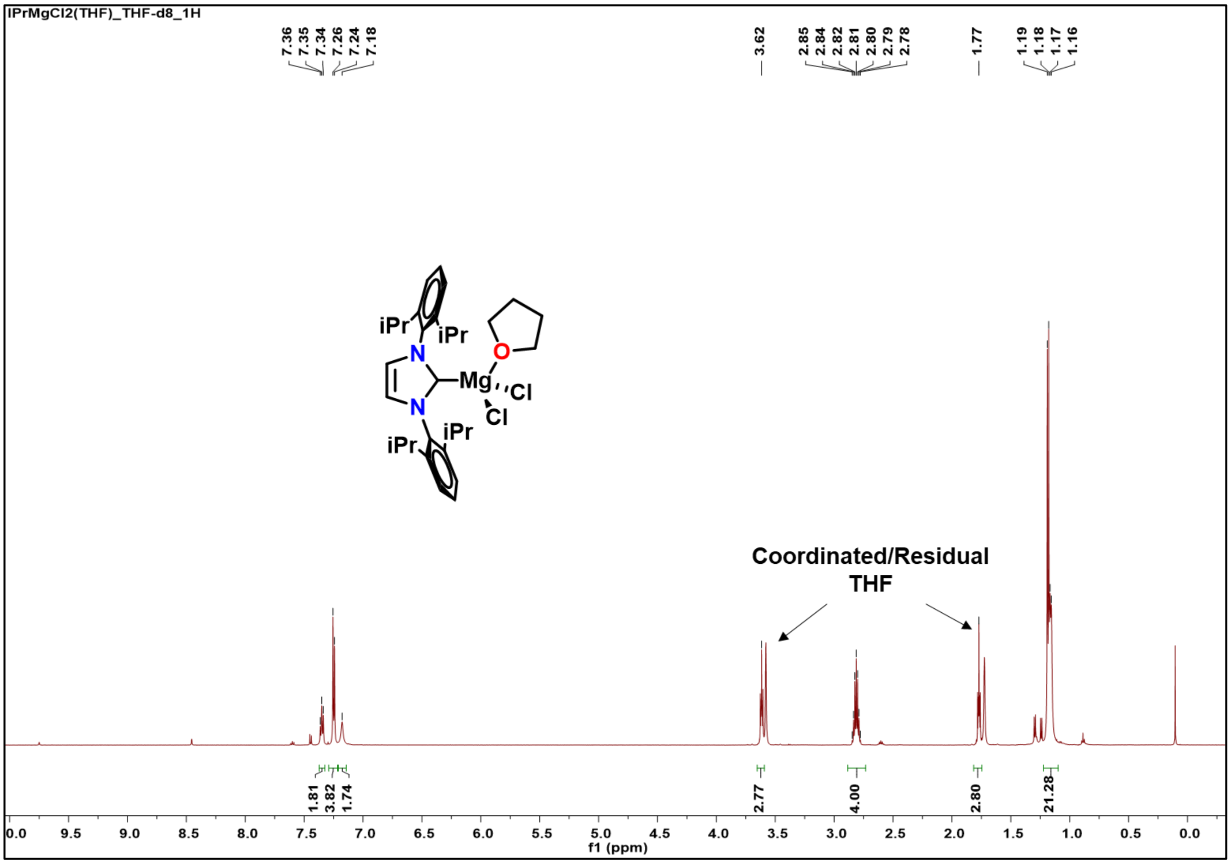

Figure A3.1. ^{1}H NMR spectrum of **2.2** in (600 MHz, THF-d_8, 298 K) showing stoichiometric THF-H_8 coordination.

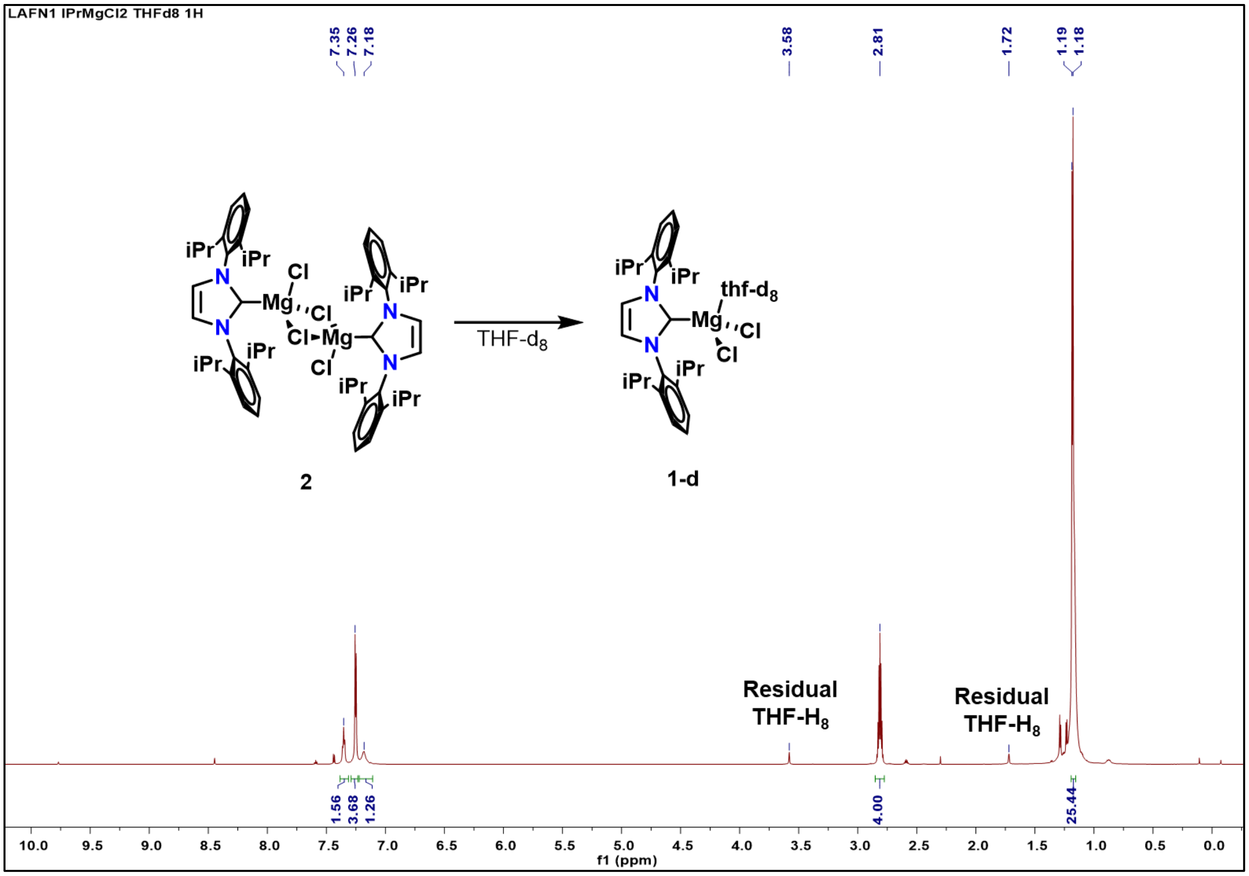

Figure A3.2. ^{1}H NMR spectrum of a sample of complex **2.3** dissolved in THF-*d8* (600 MHz, 298 K) showing identical peaks to complex **2.2** in the same solvent (figure S3). This supports the tendency for **2.3** to convert to **2.2** in the presence of THF.

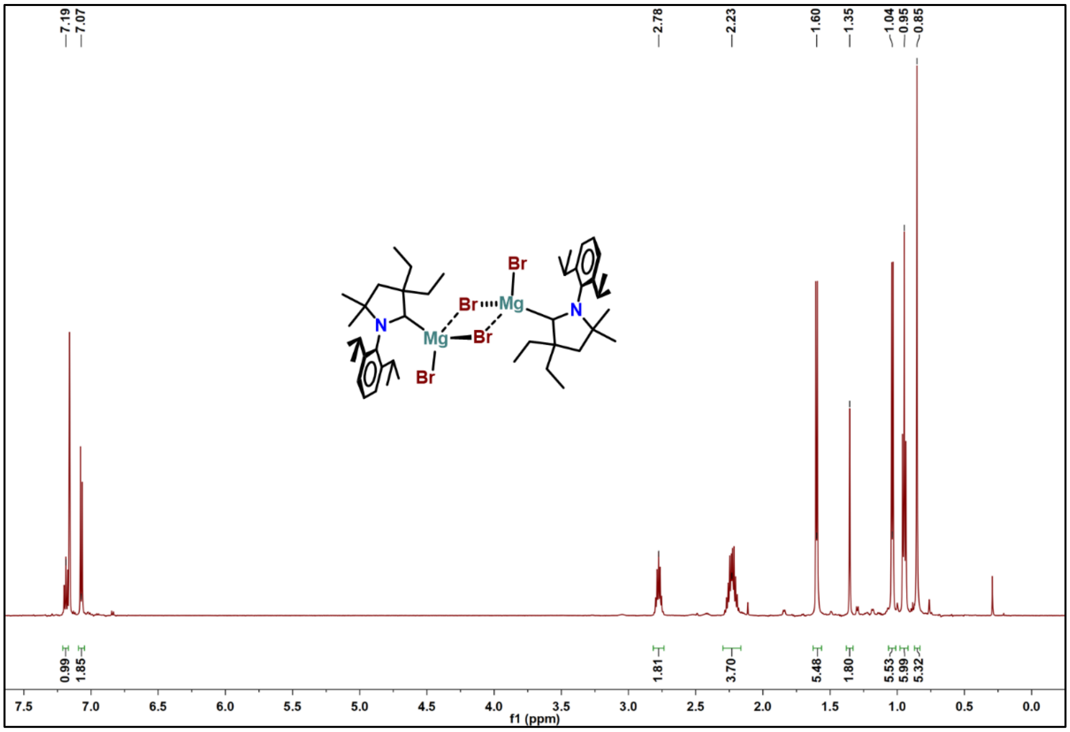

Figure A3.3. ^{1}H NMR spectrum (600 MHz, C_6D_6, 298 K) of compound **2.4**.

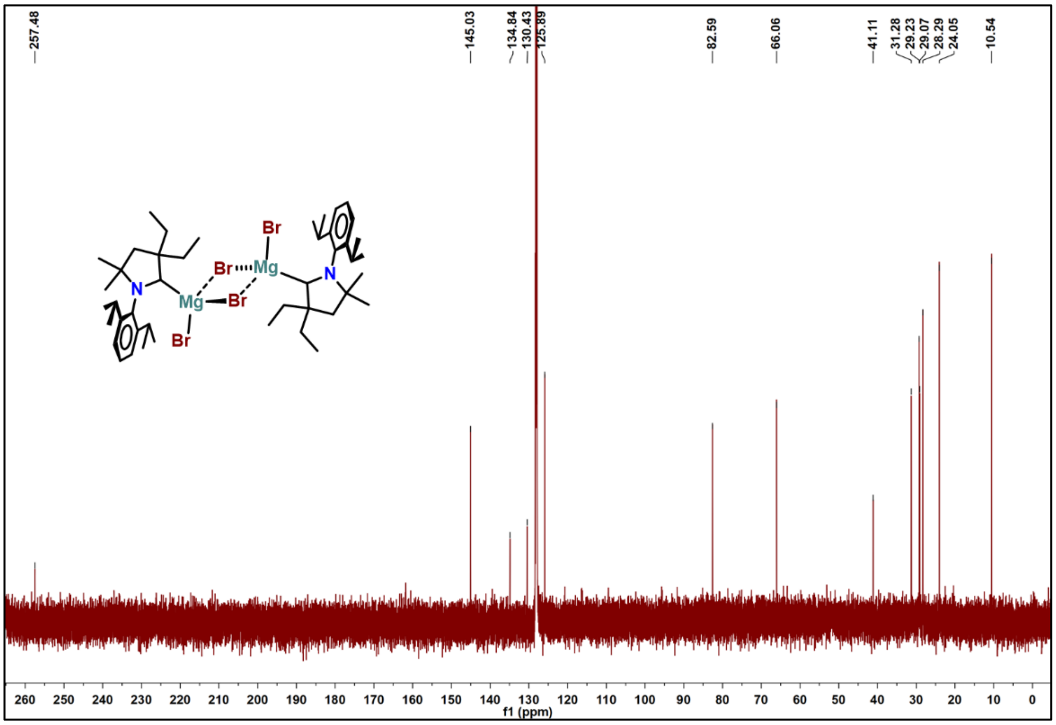

Figure A3.4. $^{13}C\{^{1}H\}$NMR (150.9 MHz, C_6D_6, 298 K) of compound **2.4**.

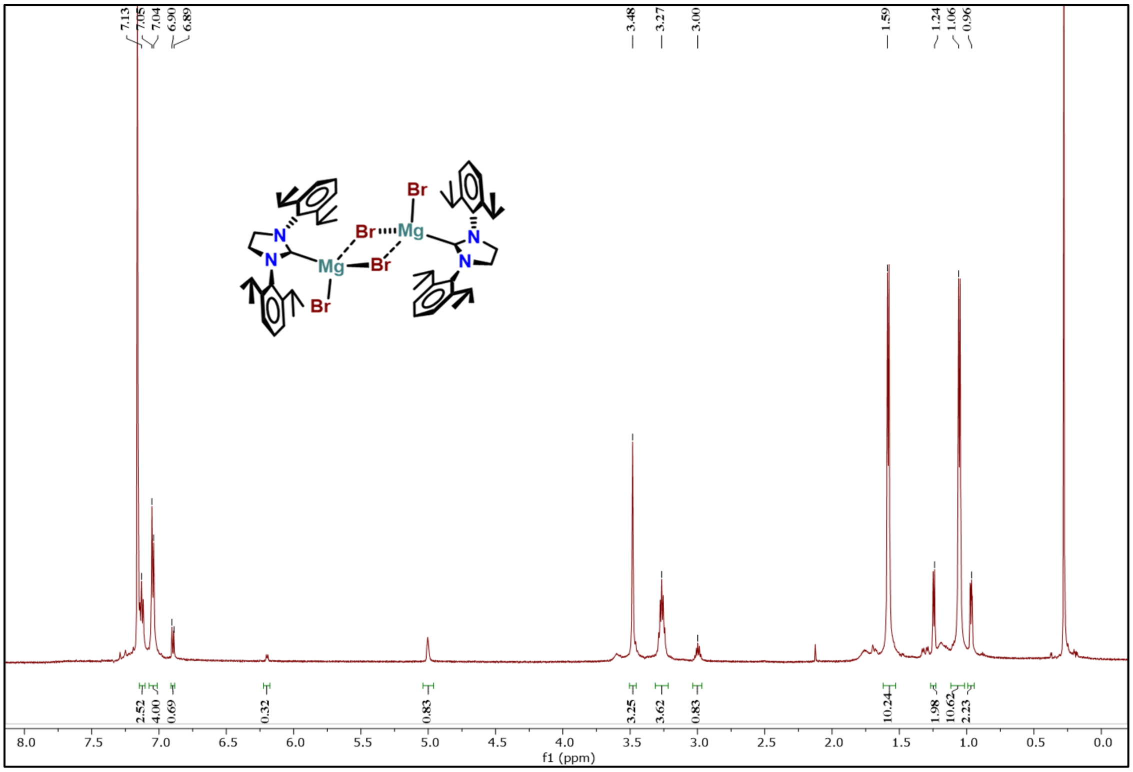

Figure A3.5. ^{1}H NMR spectrum (600 MHz, C_6D_6, 333 K) of compound **2.5.**

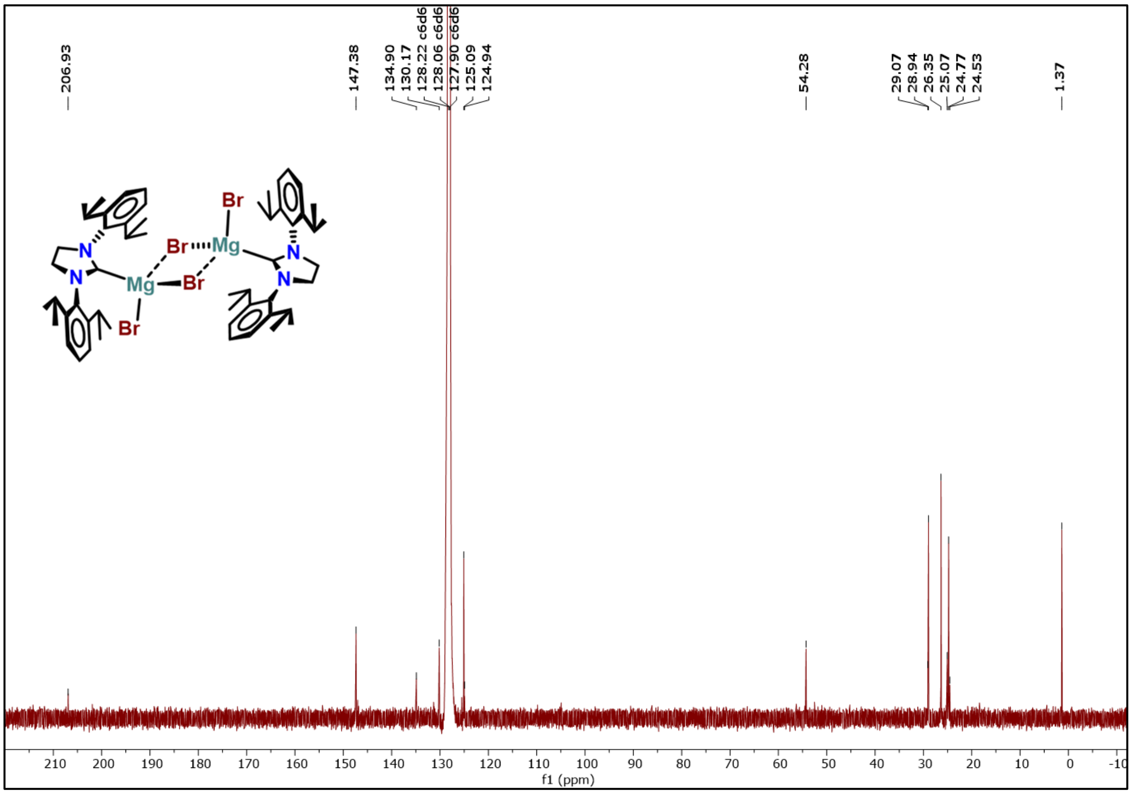

Figure A3.6. $^{13}C\{^{1}H\}$ NMR (150.9 MHz, C_6D_6, 333 K) of compound **2.5**.

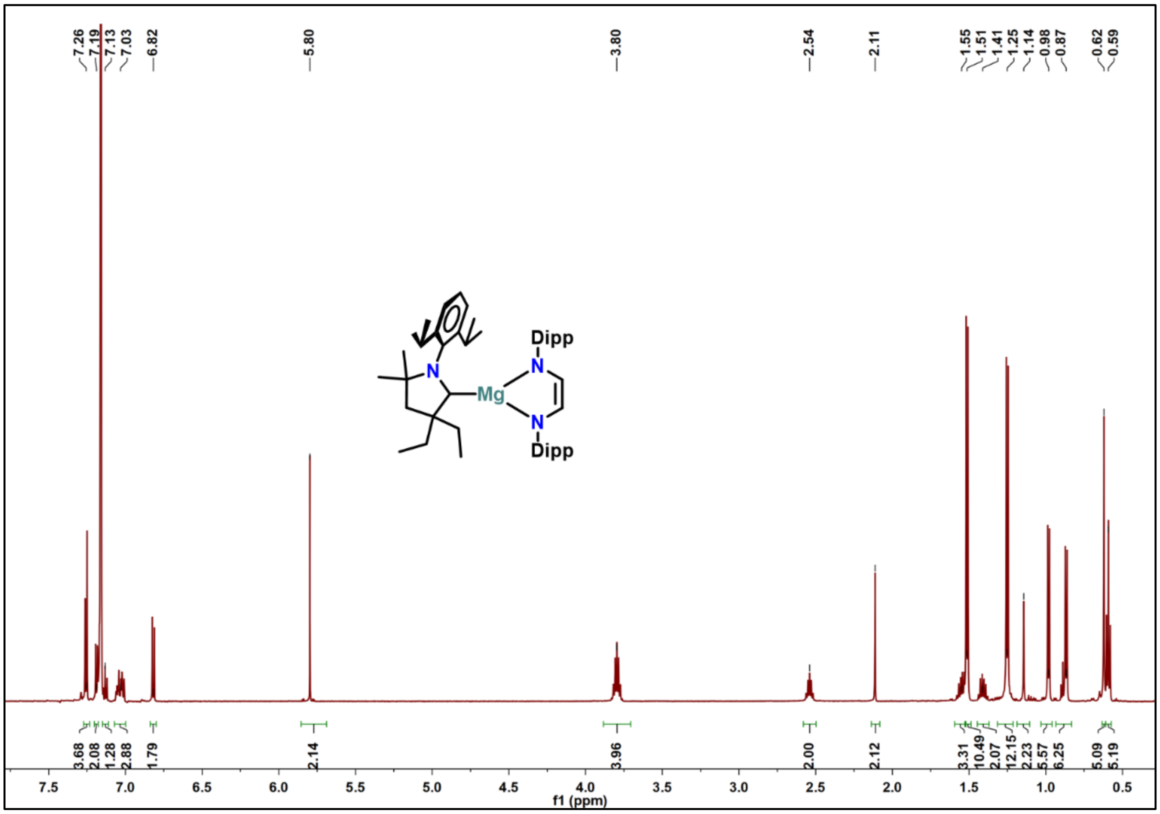

Figure A3.7. ^{1}H NMR spectrum (600 MHz, C_6D_6, 298 K) of compound **2.9.**

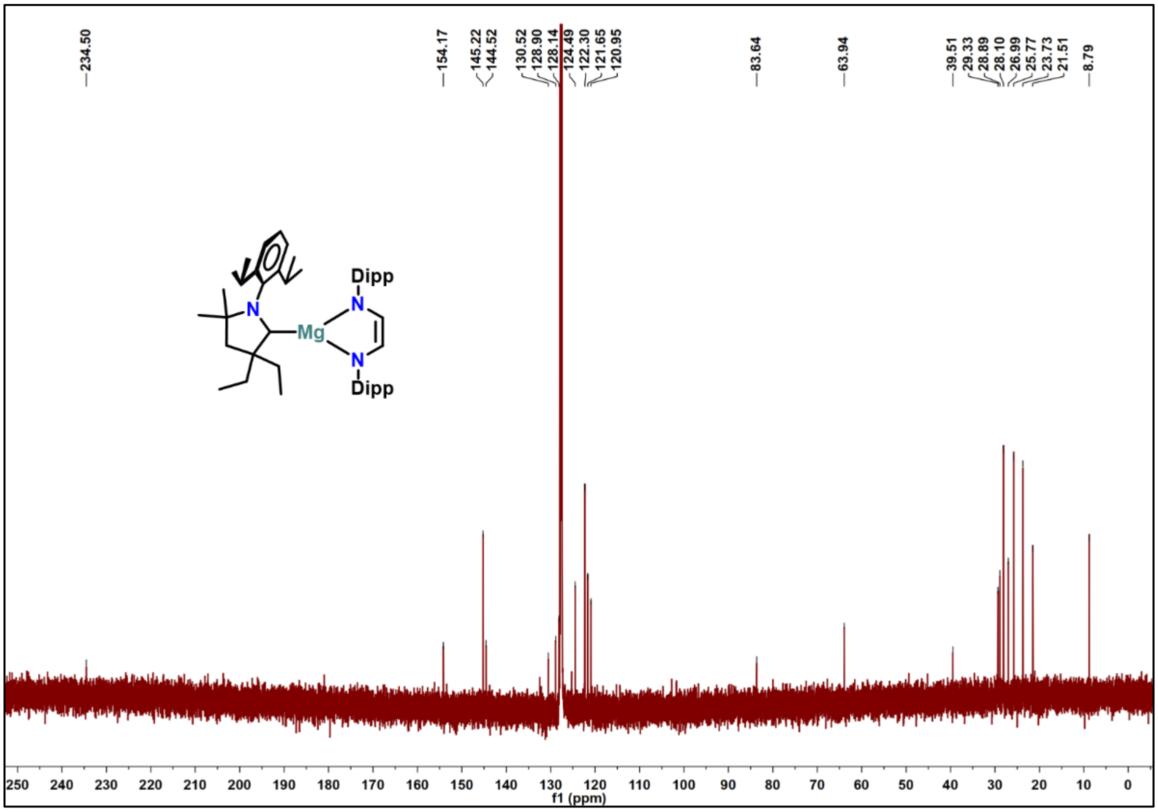

Figure A3.8. $^{13}C\{^1H\}$ NMR (150.9 MHz, C_6D_6, 298 K) of compound **2.9**.

Chapter 3.

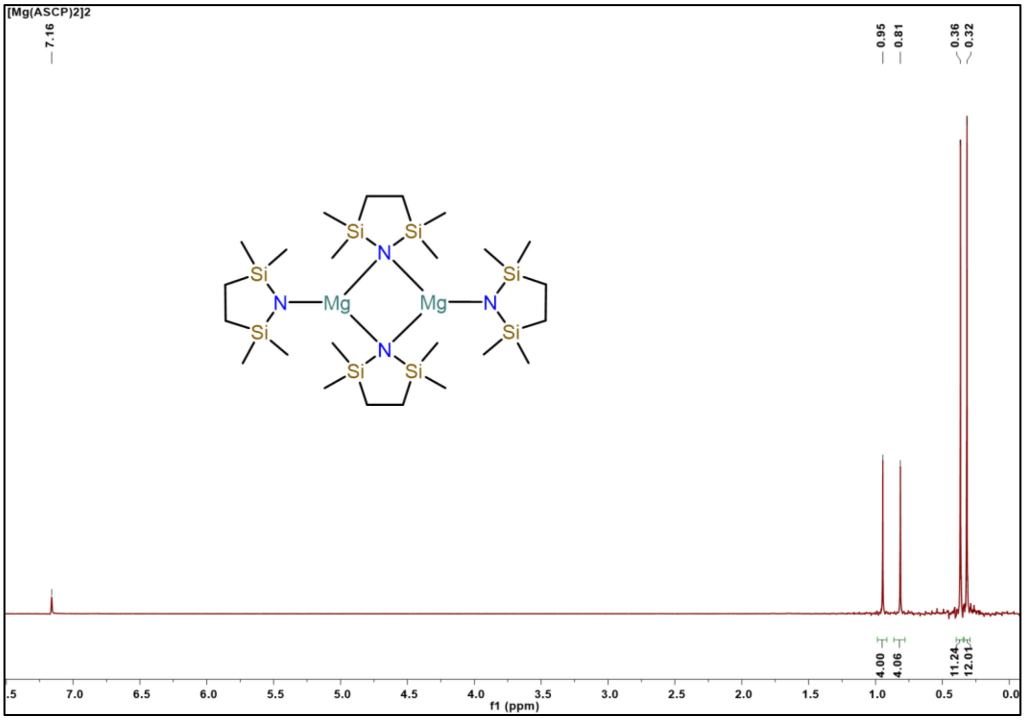

Figure A3.9. ^{1}H NMR spectrum of **3.1** in C_6D_6 at 298 K.

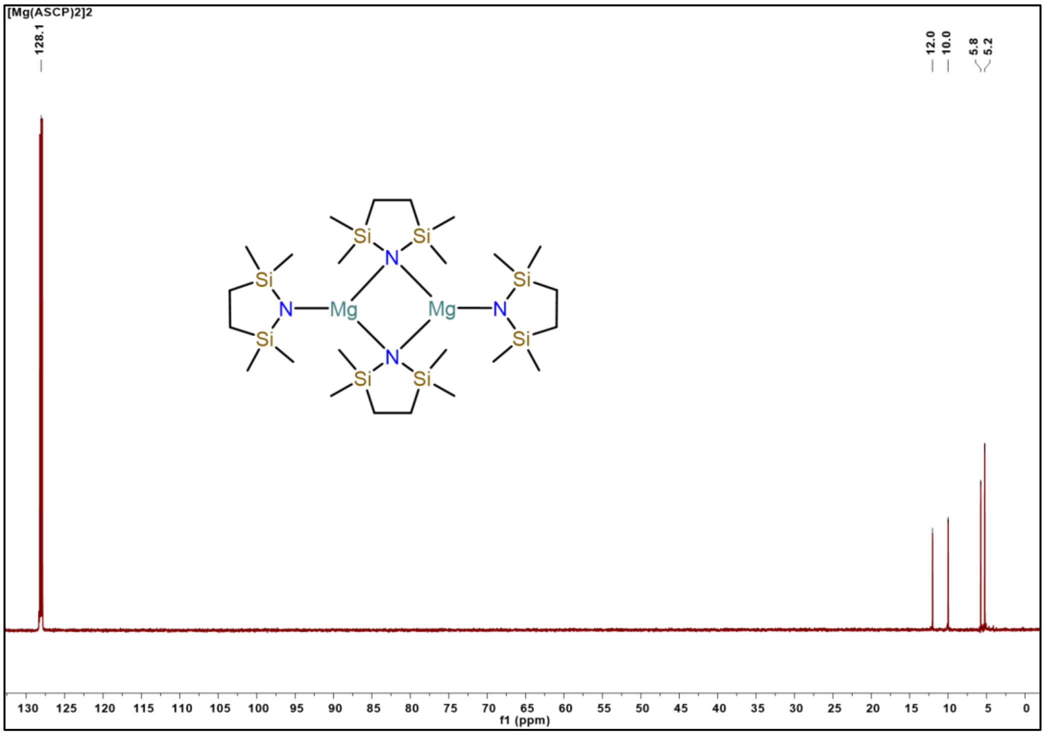

Figure A3.10. ^{13}C{^{1}H} NMR spectrum of **3.1** in C_6D_6 at 298 K.

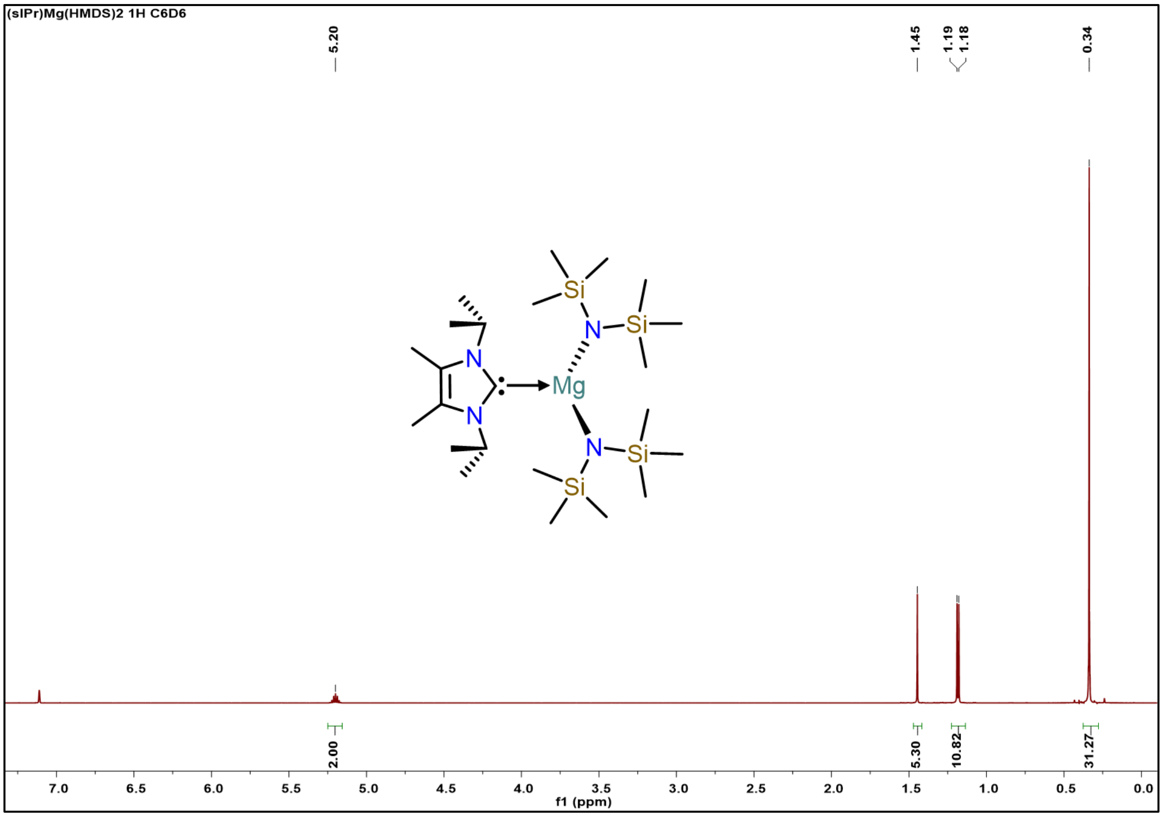

Figure A3.11. ^{1}H NMR spectrum of **3.2** in C_6D_6 at 298 K.

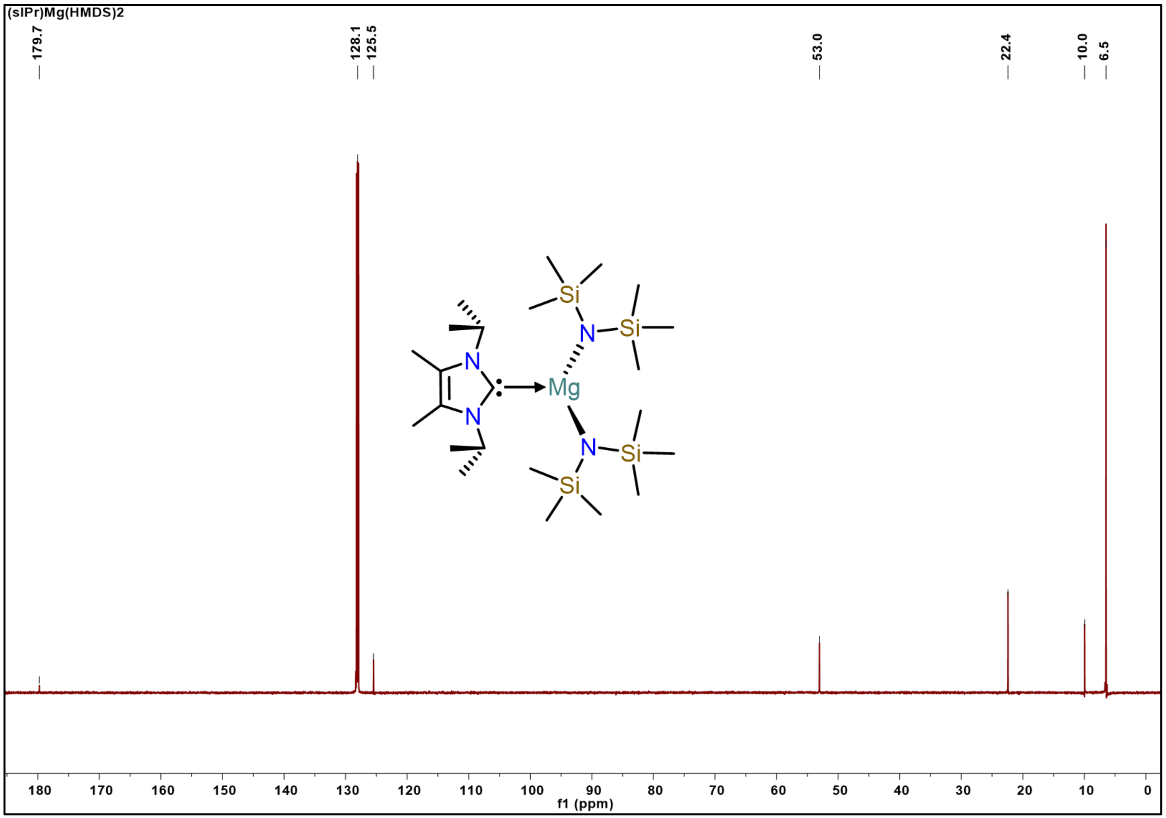

Figure A3.12. ^{13}C NMR spectrum of **3.2** in C_6D_6 at 298 K.

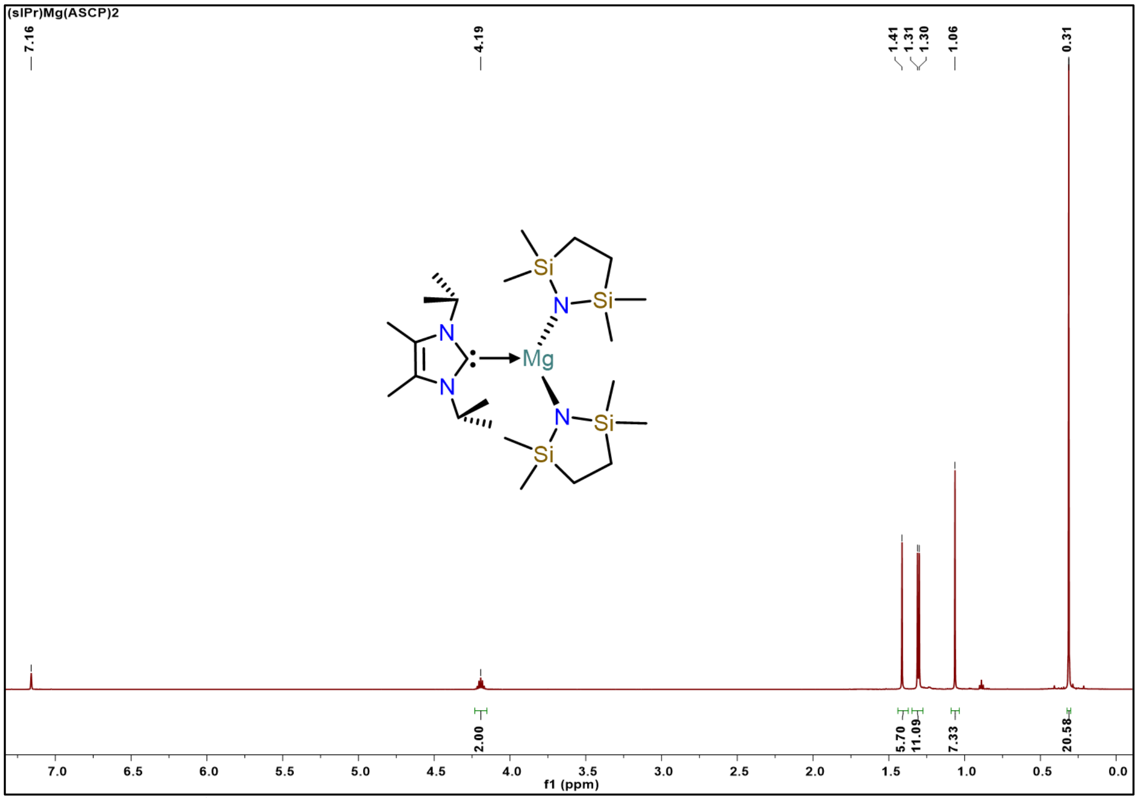

Figure A3.13. ^{1}H NMR spectrum of **3.3** in C_6D_6 at 298 K.

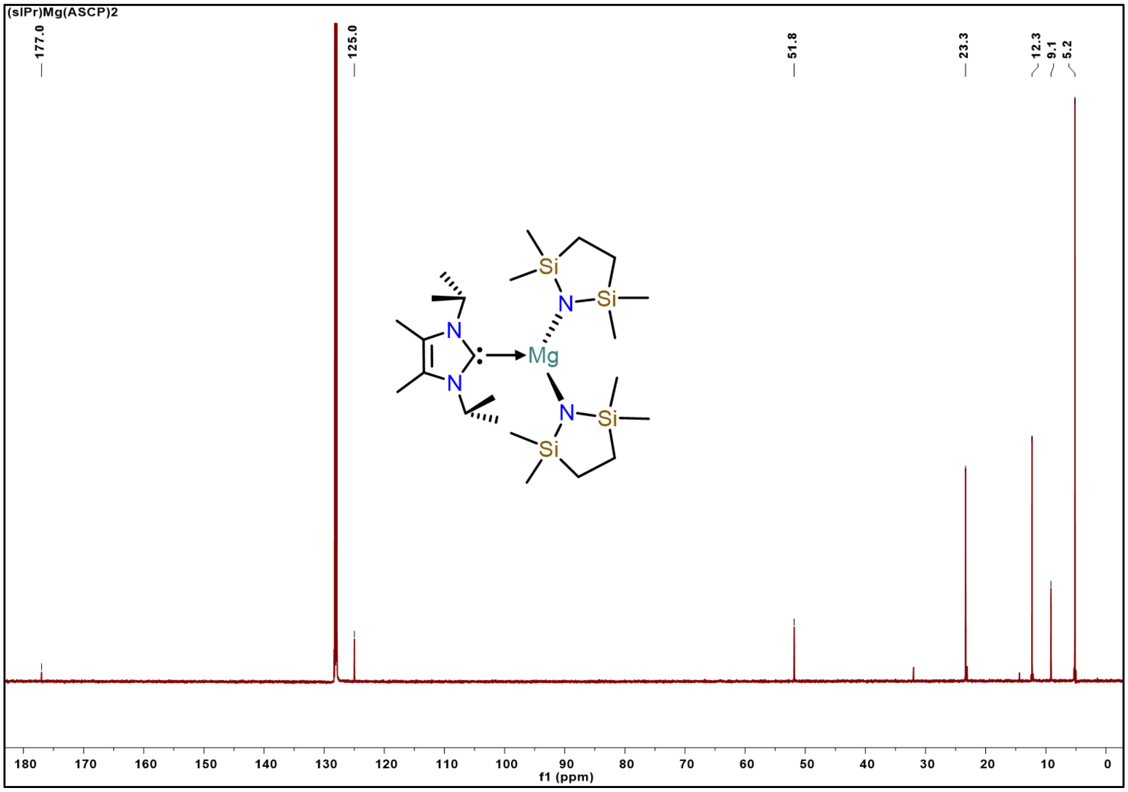

Figure A3.14. ^{13}C{^{1}H} NMR spectrum of **3.3** in C_6D_6 at 298 K.

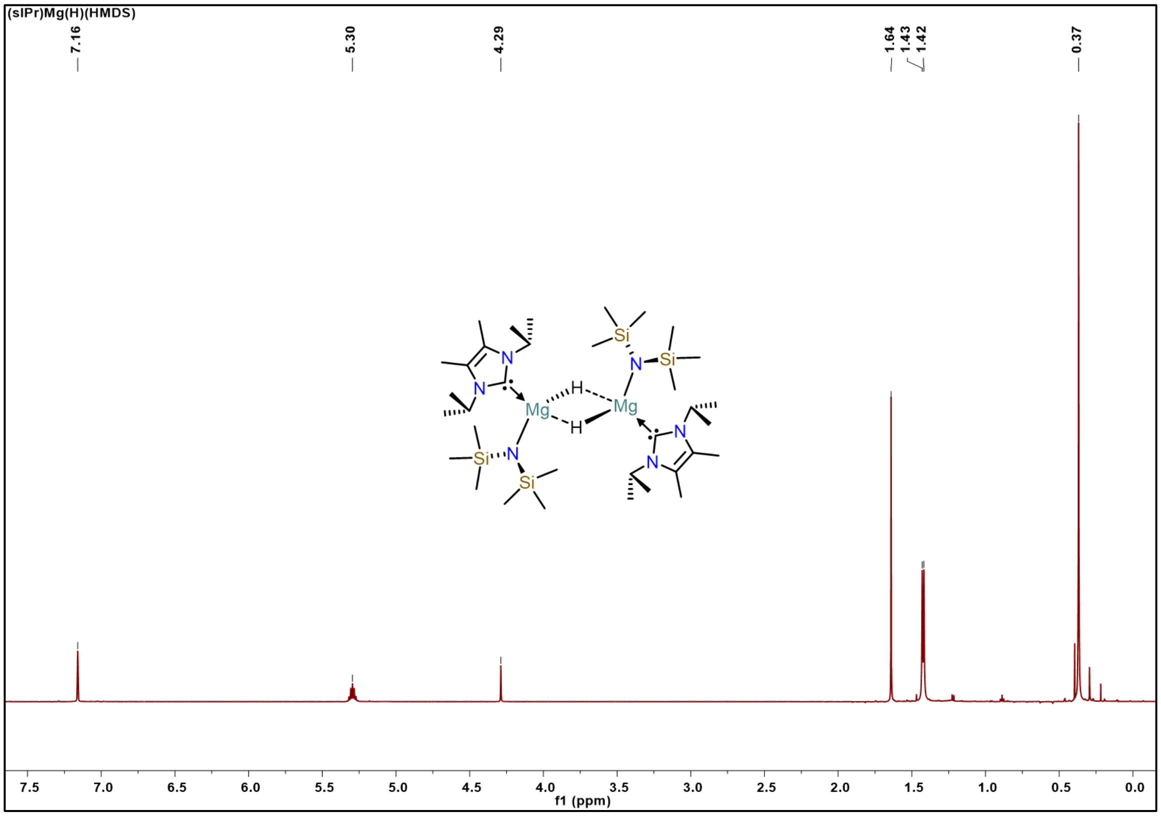

Figure A3.15. ^{1}H NMR spectrum of **3.4** in C_6D_6 at 298 K.

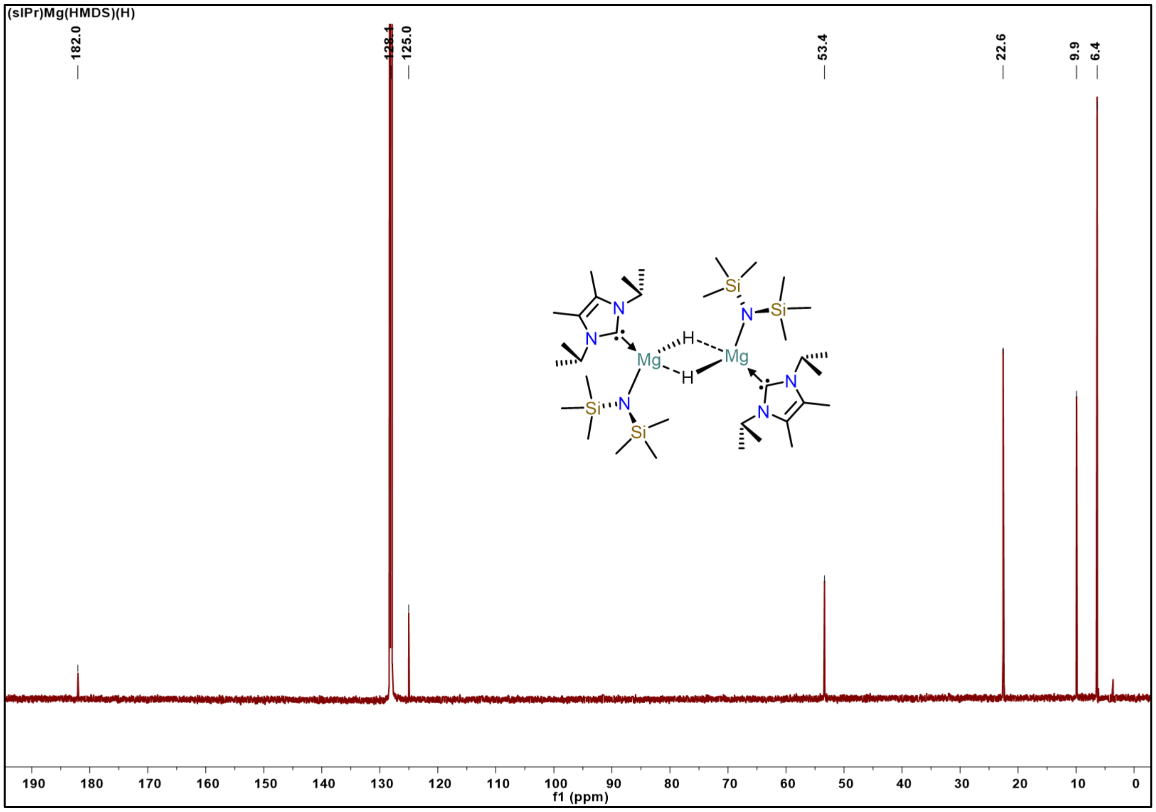

Figure A3.16. ^{13}C NMR spectrum of **3.4** in C_6D_6 at 298 K.

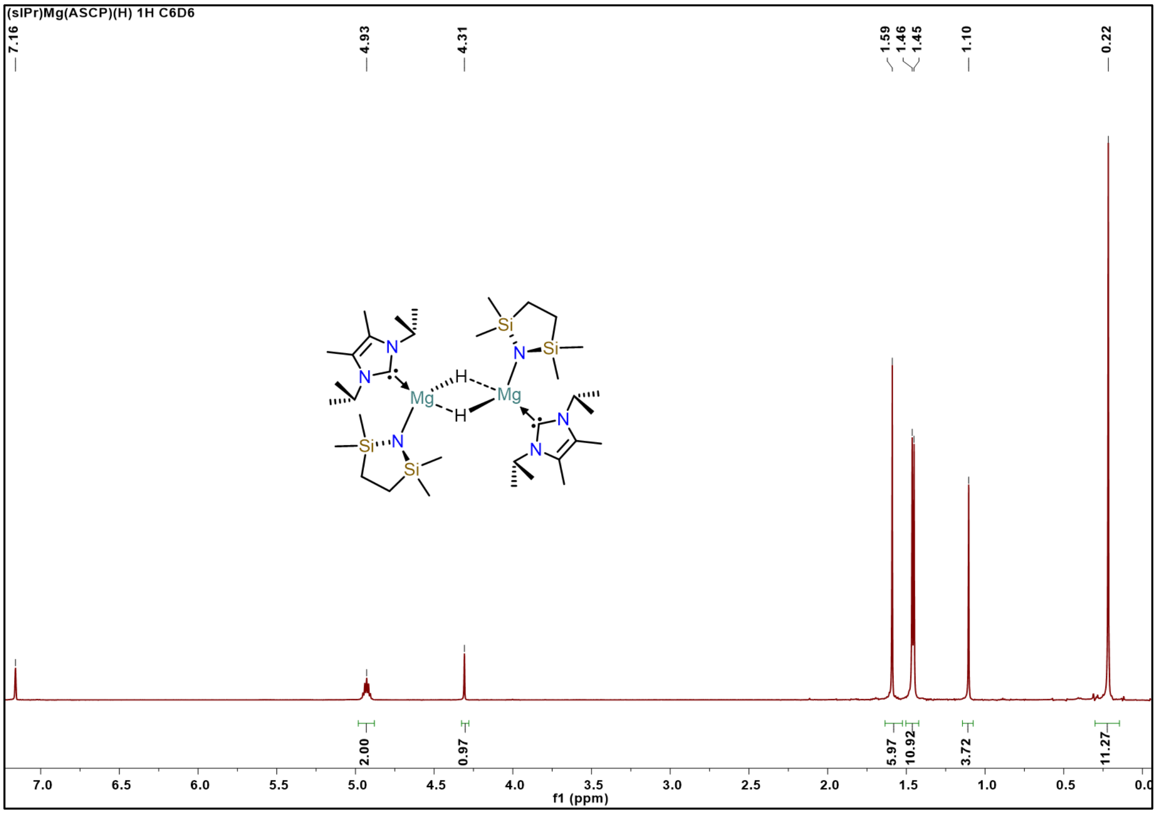

Figure A3.17. ^{1}H NMR spectrum of **3.5** in C_6D_6 at 298 K.

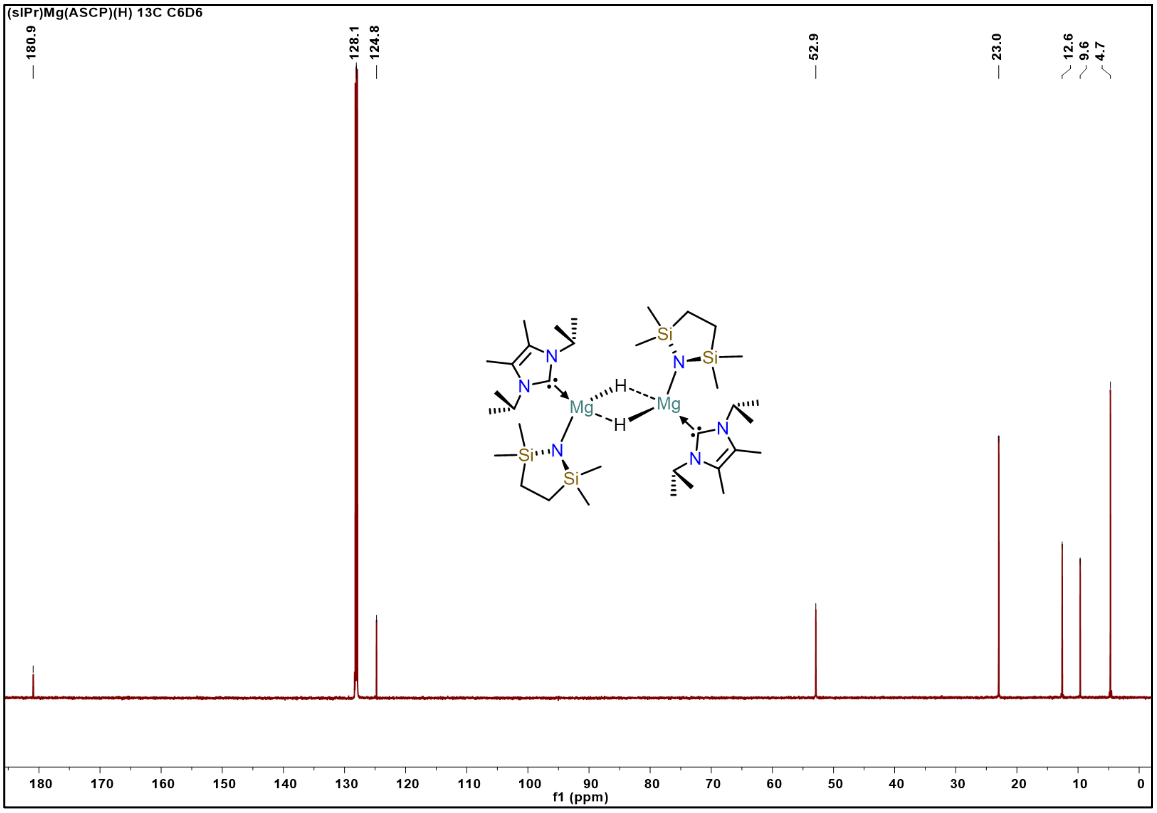

Figure A3.18. ^{13}C NMR spectrum of **3.5** in C_6D_6 at 298 K.

Chapter 4.

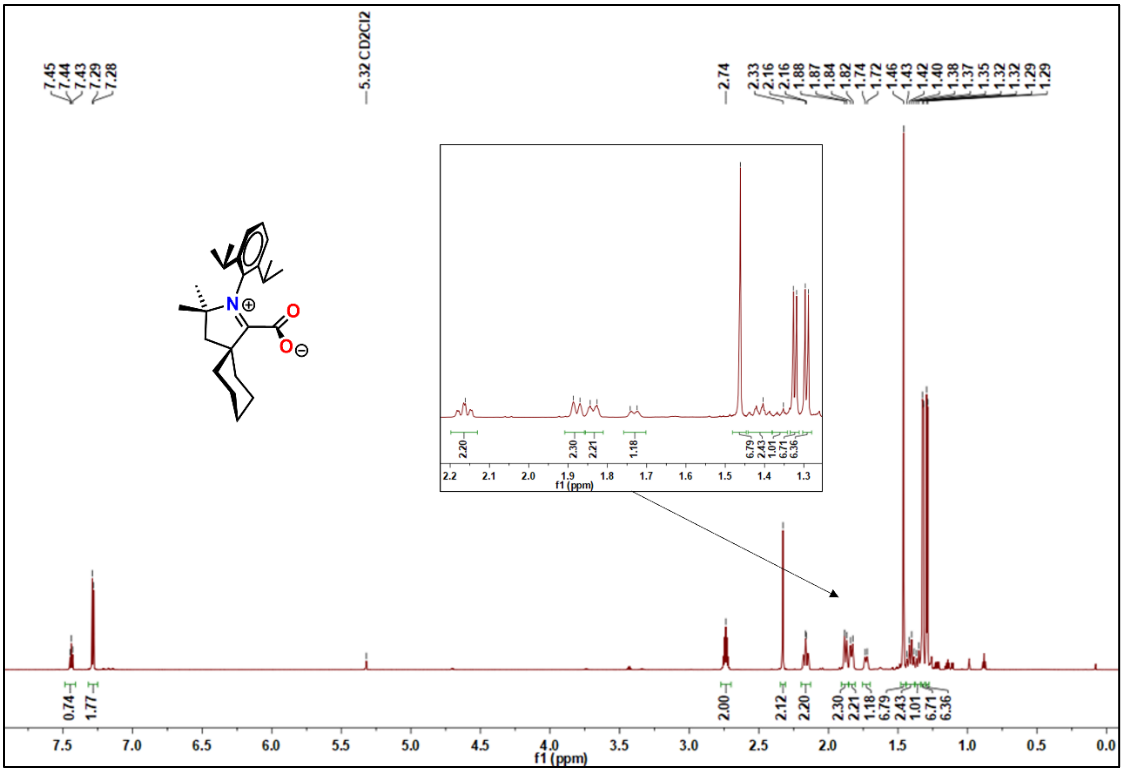

Figure A3.19. ^{1}H NMR spectrum of **4.1** in CD$_3$CN at 298 K.

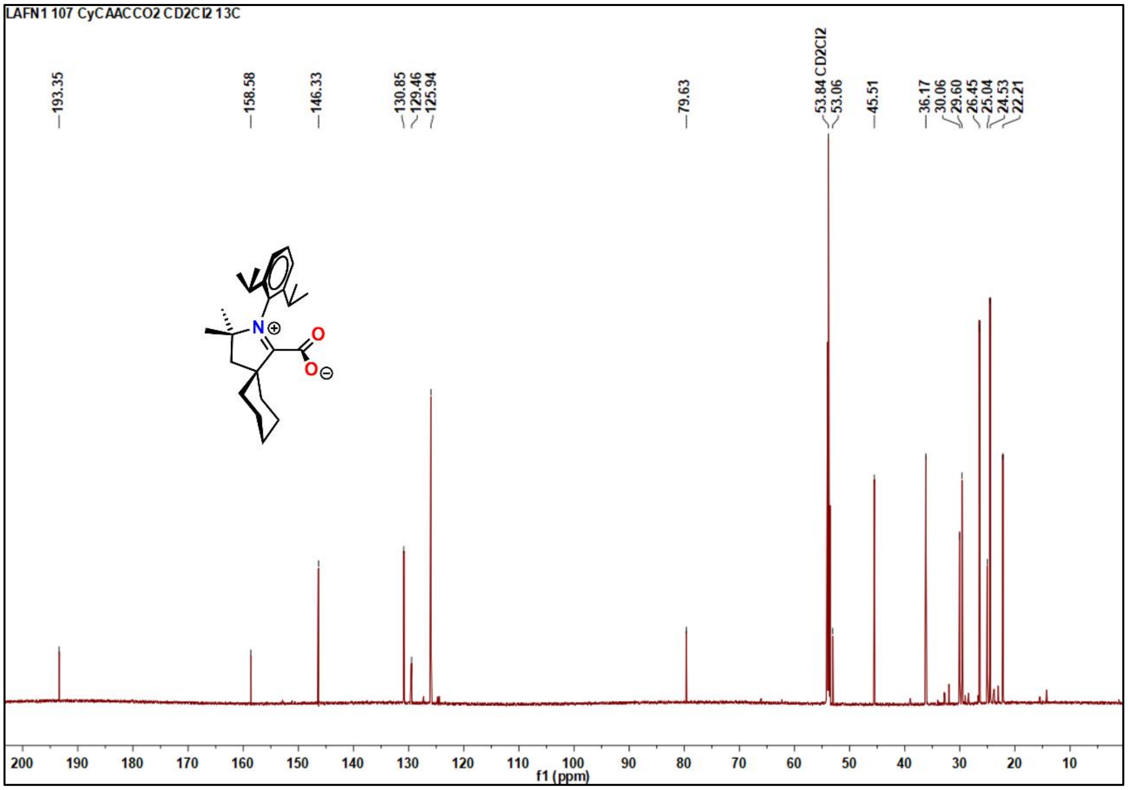

Figure A3.20. ^{1}H NMR spectrum of **4.1** in CD_3CN at 298 K.

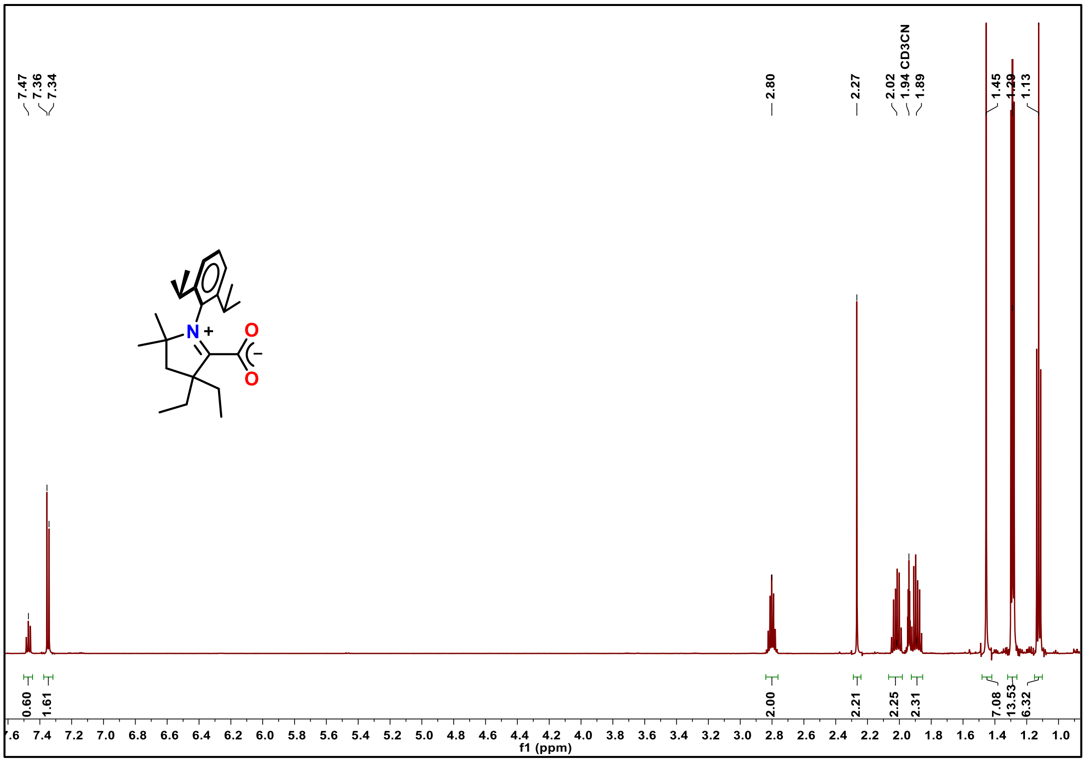

Figure A3.21. ^{1}H NMR spectrum of **4.3** in CD_3CN at 298 K.

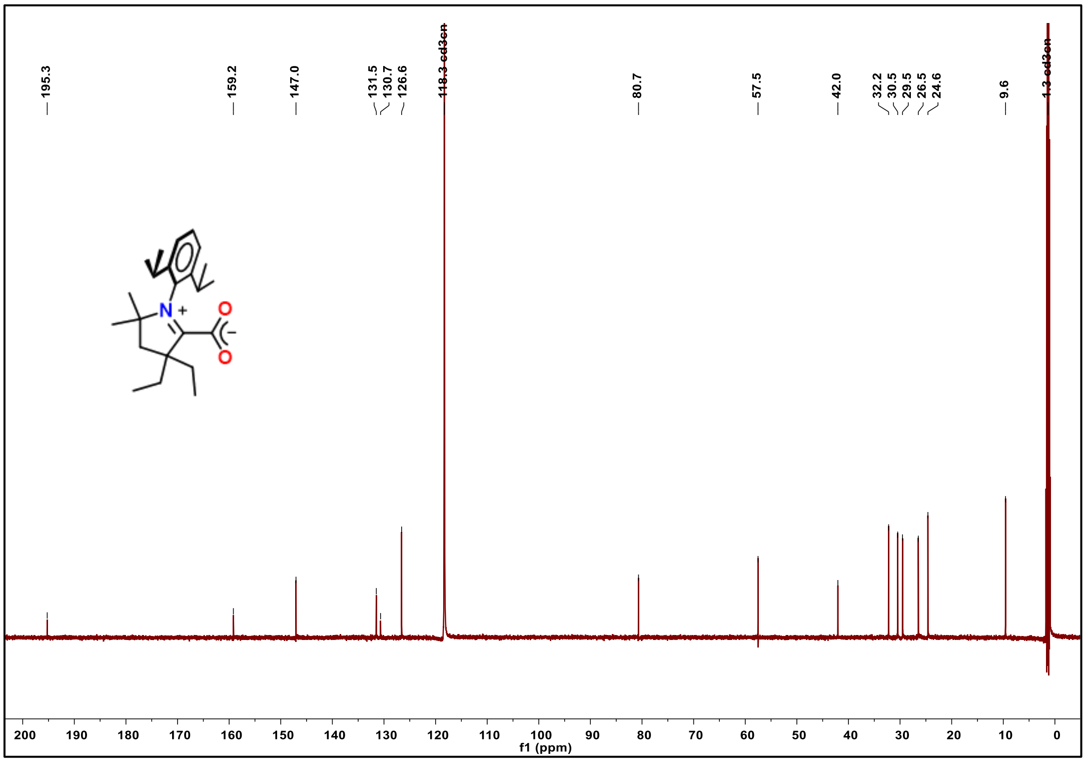

Figure A3.22. $^{13}C\{^{1}H\}$ NMR spectrum of **4.3** in CD_3CN at 298 K.

EPR Spectra

Chapter 4.

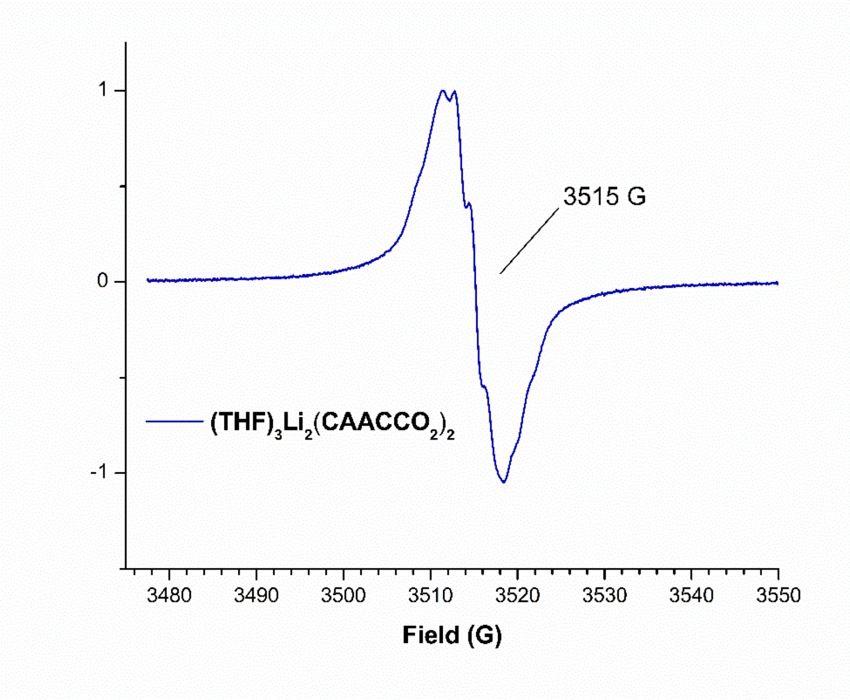

Figure A3.23. EPR spectrum of **4.4** in toluene solution at 298 K.

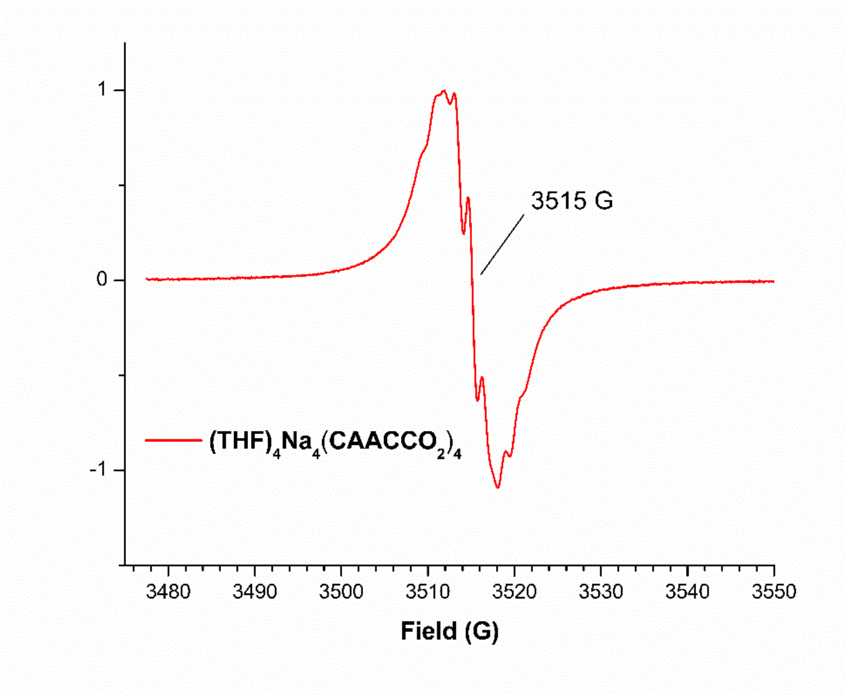

Figure A3.24. EPR spectrum of **4.5** in toluene solution at 298 K.

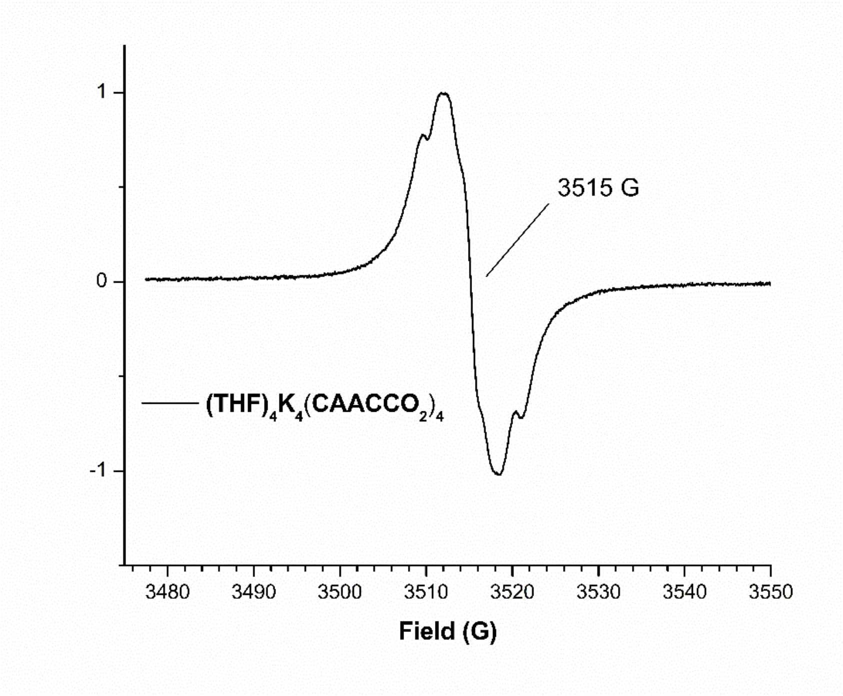

Figure A3.25. EPR spectrum of **4.6** in toluene solution at 298 K.

FTIR Spectra

Chapter 2

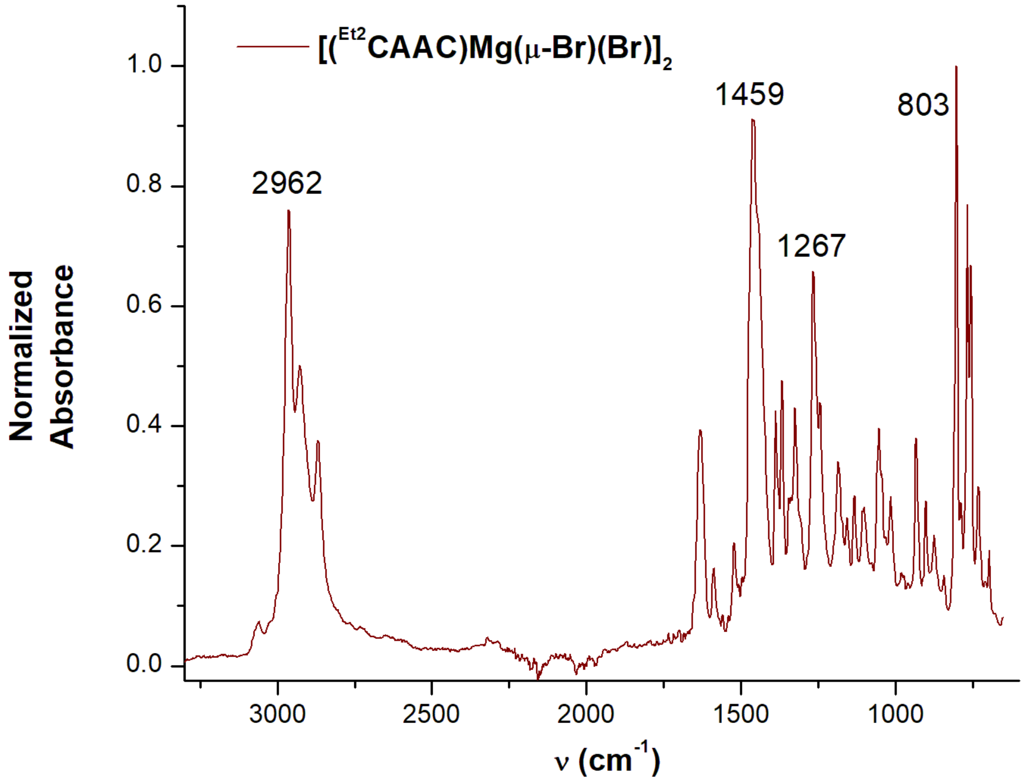

Figure A3.26. FTIR spectrum of compound **2.4.**

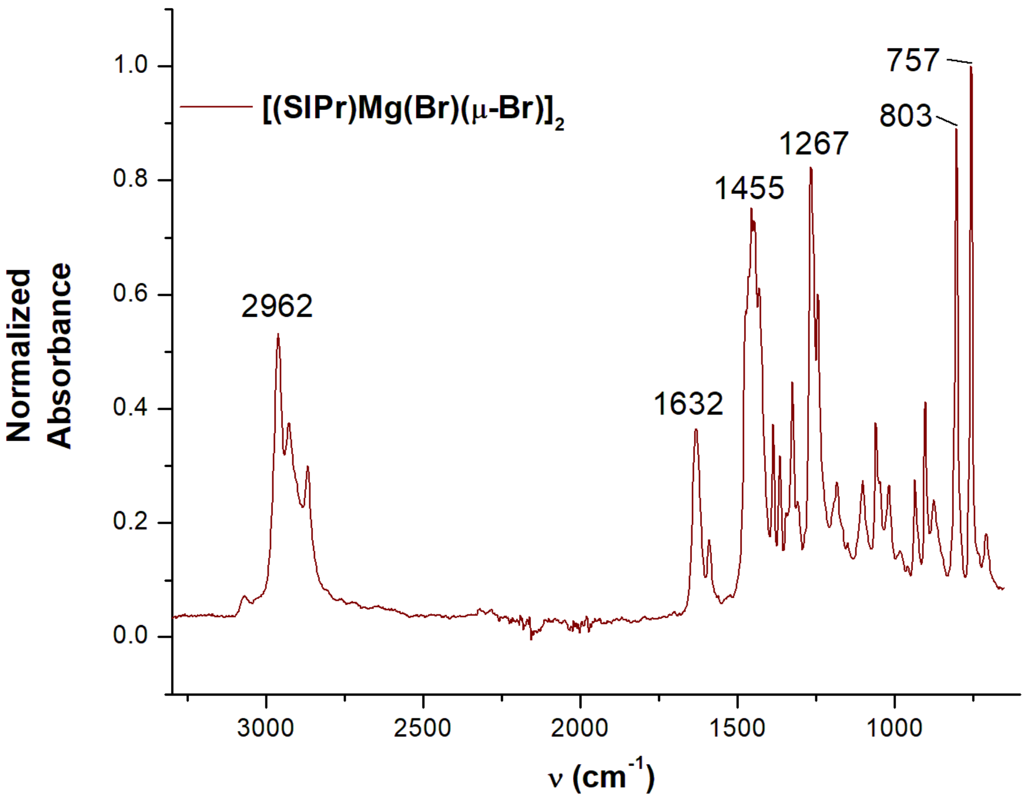

Figure A3.27. FTIR spectrum of compound **2.5.**

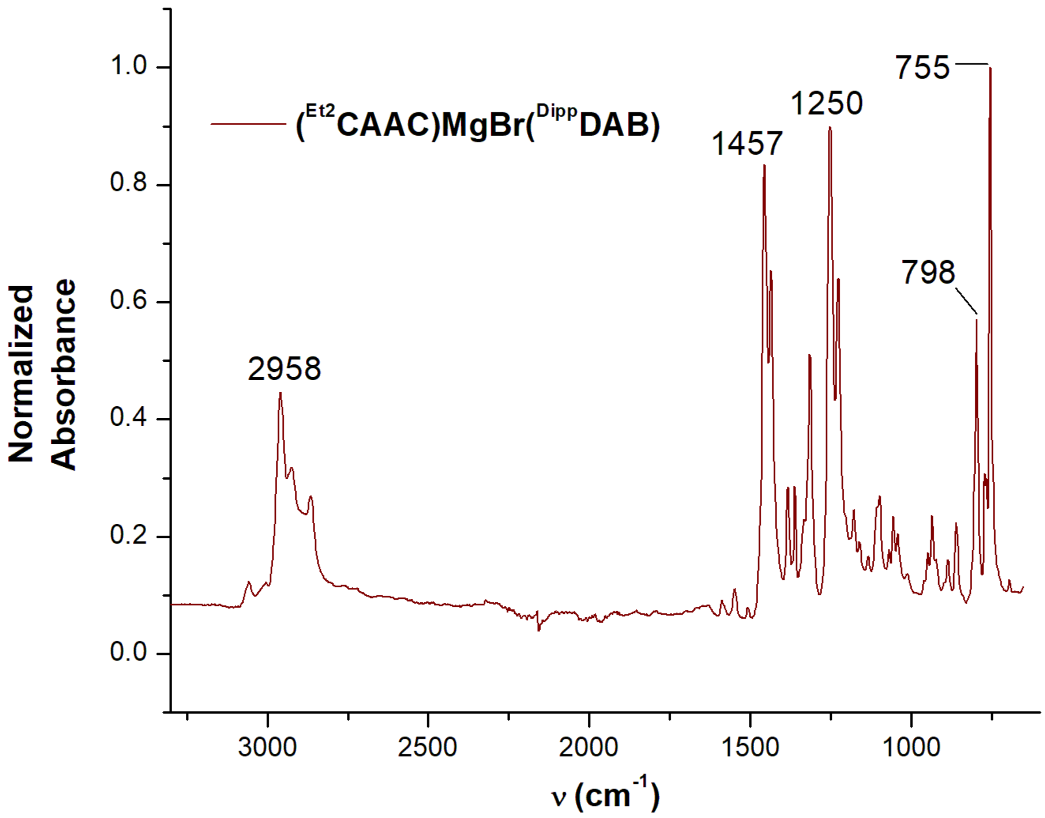

Figure A3.28. FTIR spectrum of compound **2.7.**

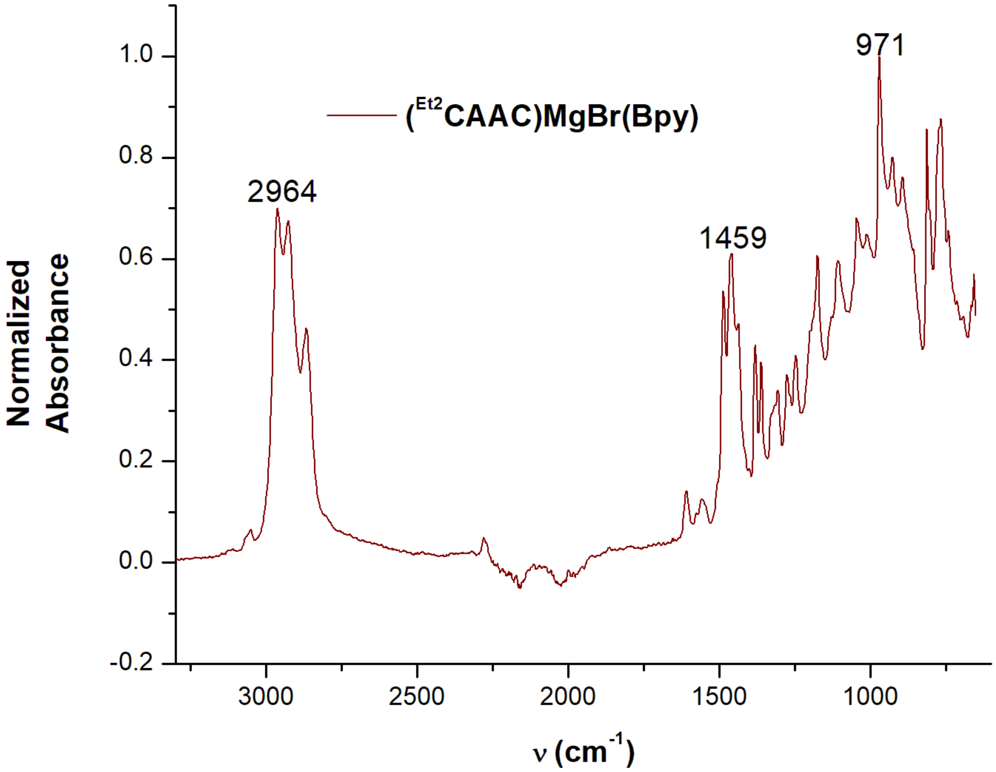

Figure A3.29. FTIR spectrum of compound **2.8.**

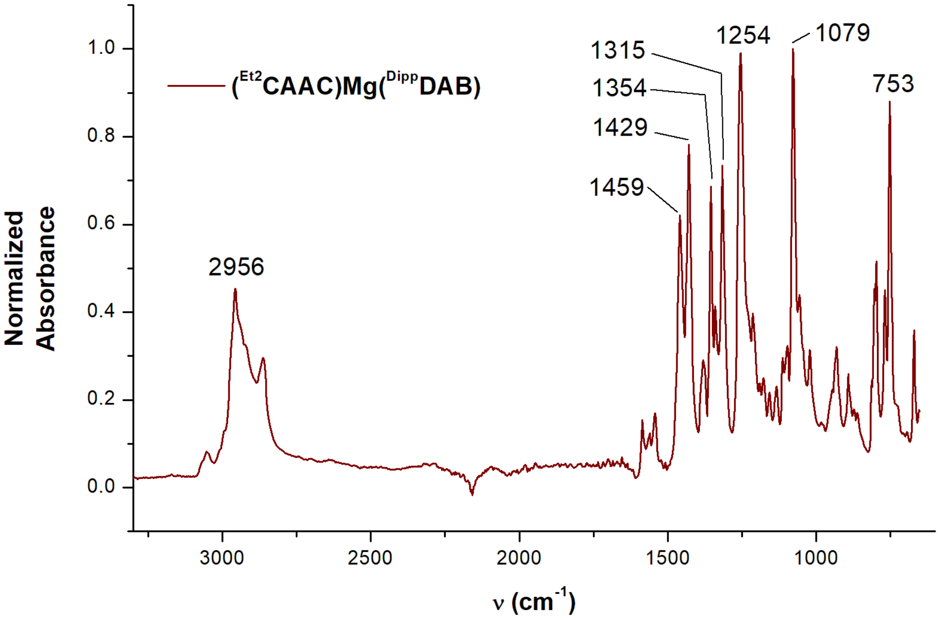

Figure A3.30. FTIR spectrum of compound **2.9.**

Chapter 3.

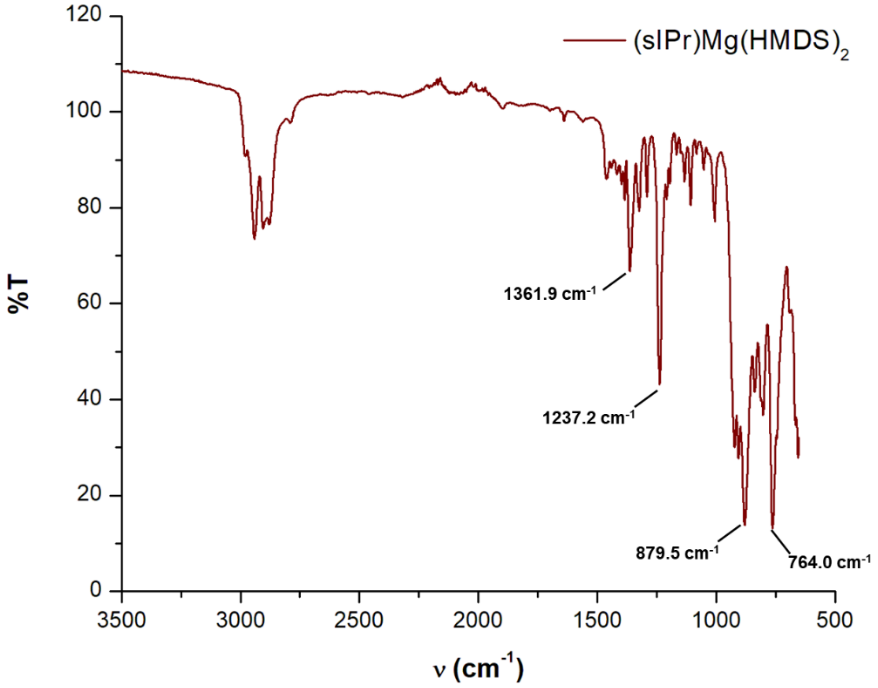

Figure A3.31. FTIR spectrum of **3.2**.

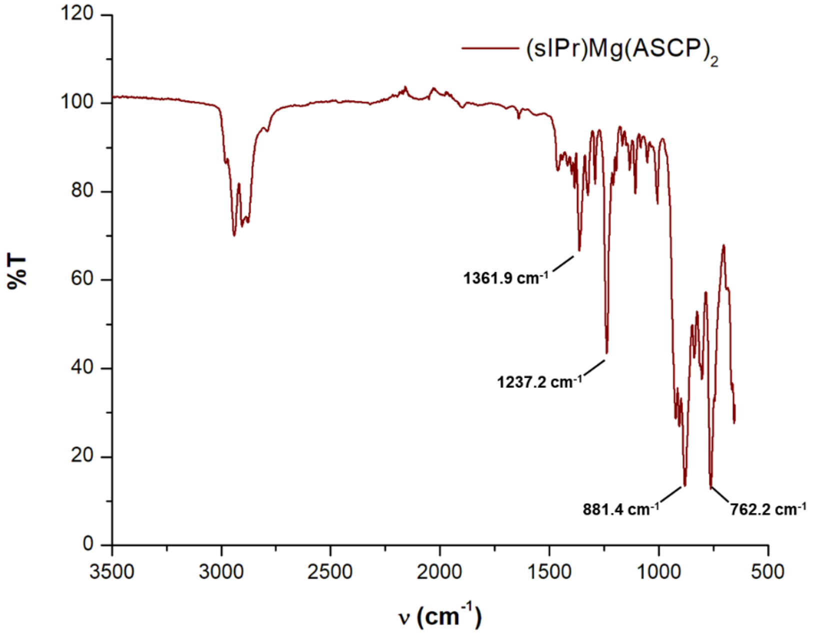

Figure A3.32. FTIR spectrum of **3.3**.

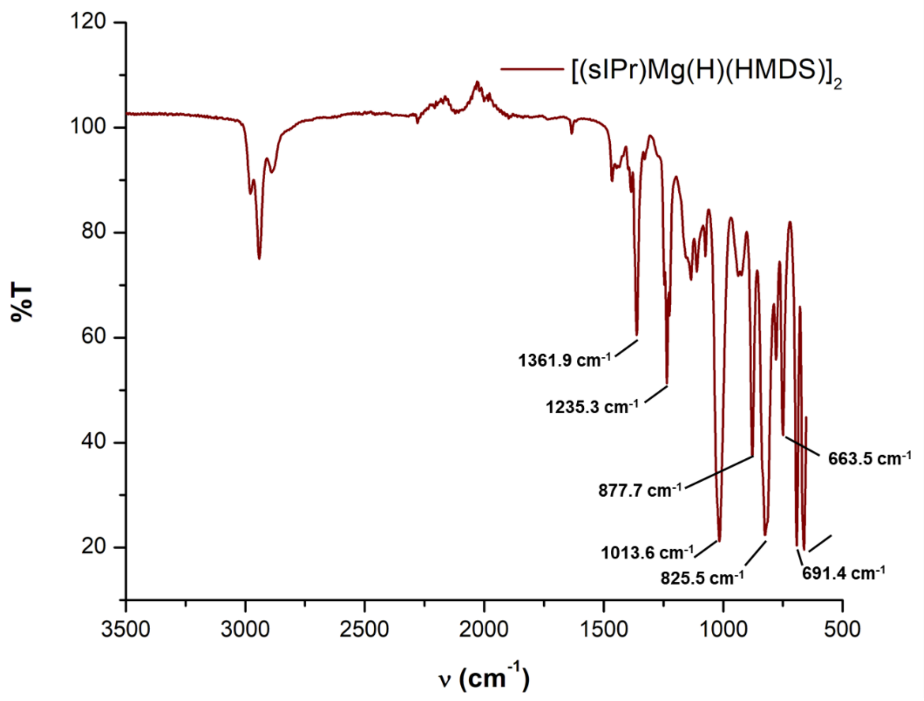

Figure A3.33. FTIR spectrum of **3.4.**

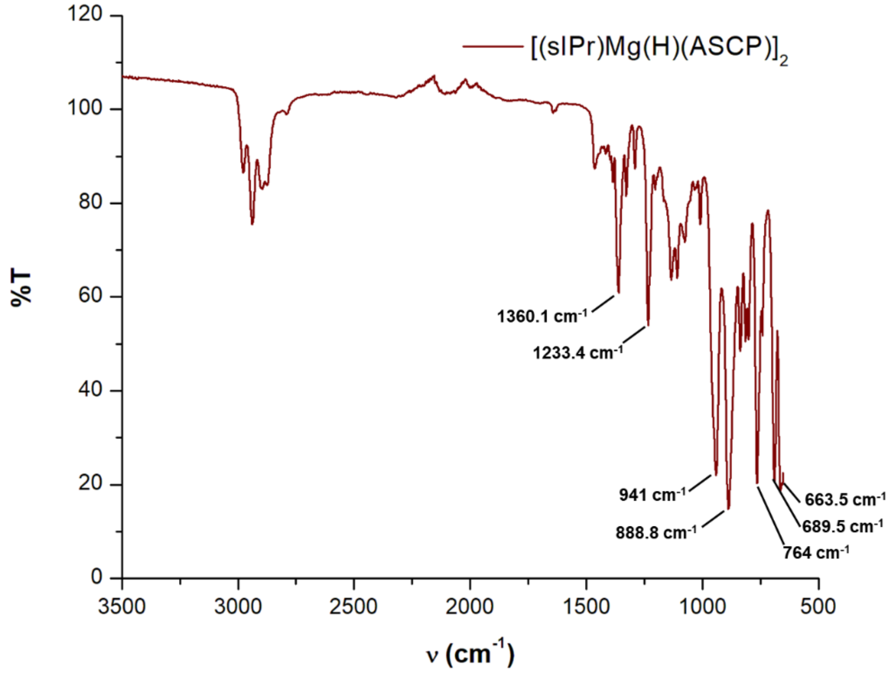

Figure A3.34. FTIR spectrum of **3.5.**

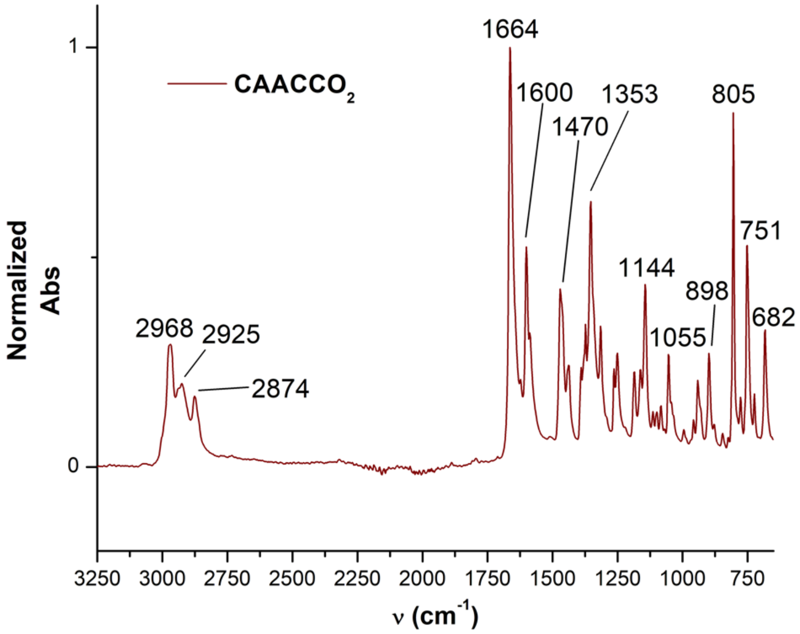

Figure A3.35. FTIR (solid state) of **4.3** at 298 K.

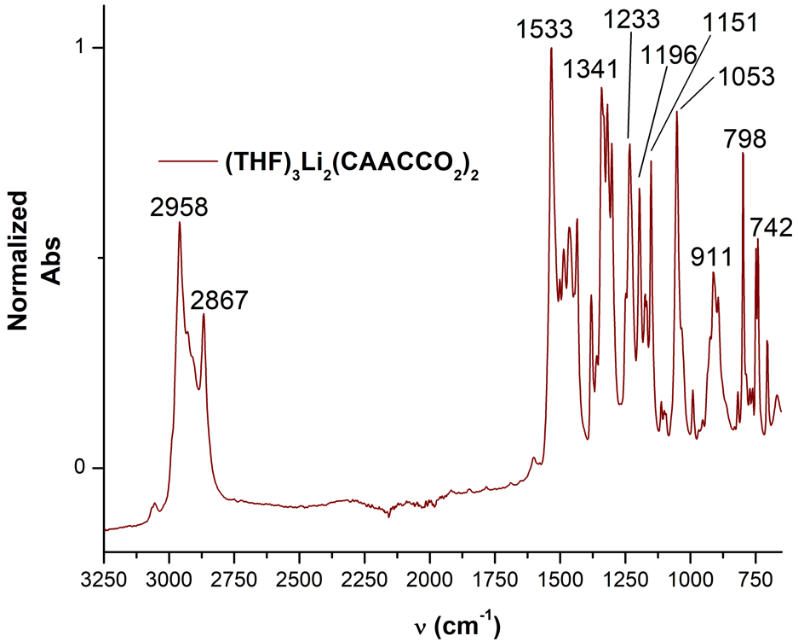

Figure A3.36. FTIR (solid state) of **4.4** at 298 K.

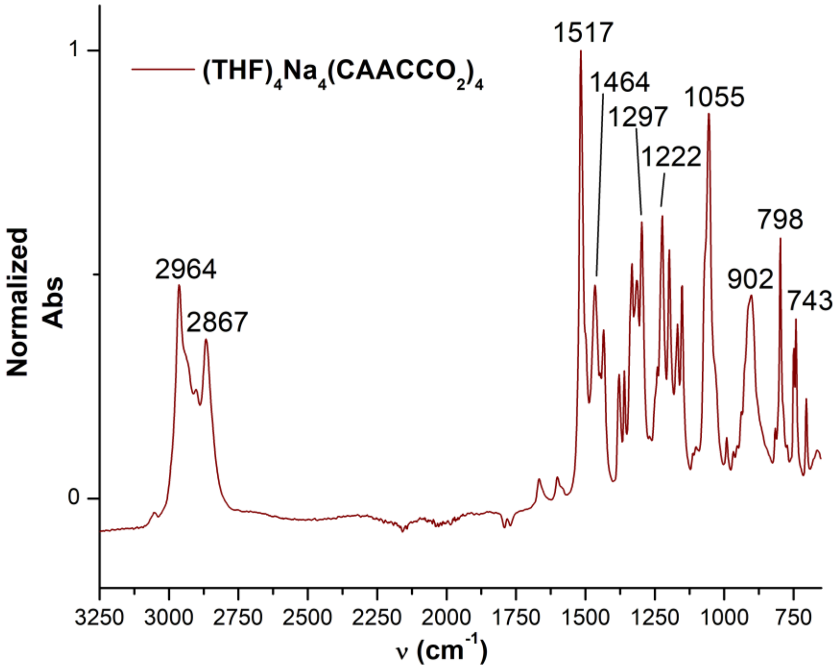

Figure A3.37. FTIR (solid state) of **4.5** at 298 K.

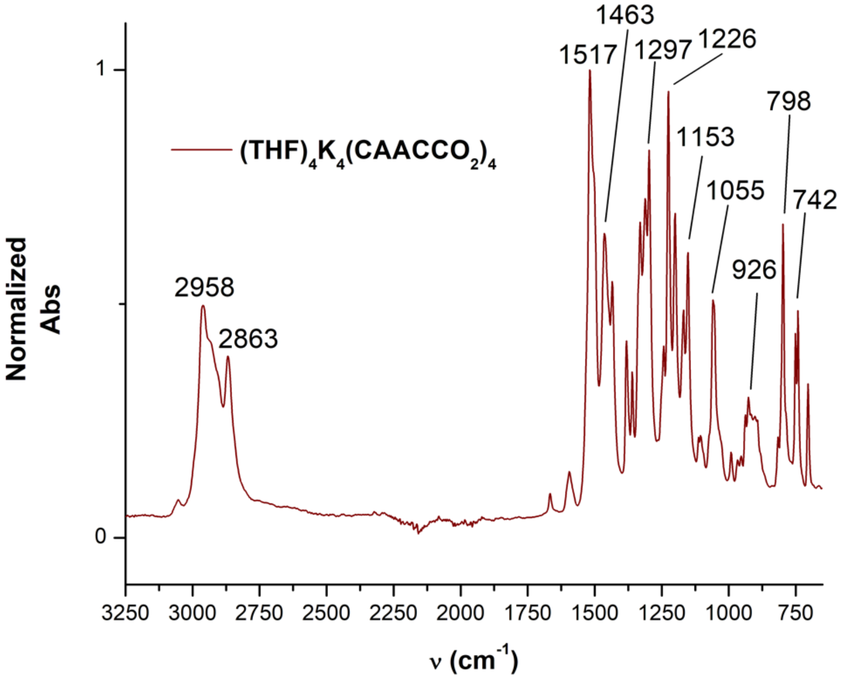

Figure A3.38. FTIR (solid state) of **4.6** at 298 K.

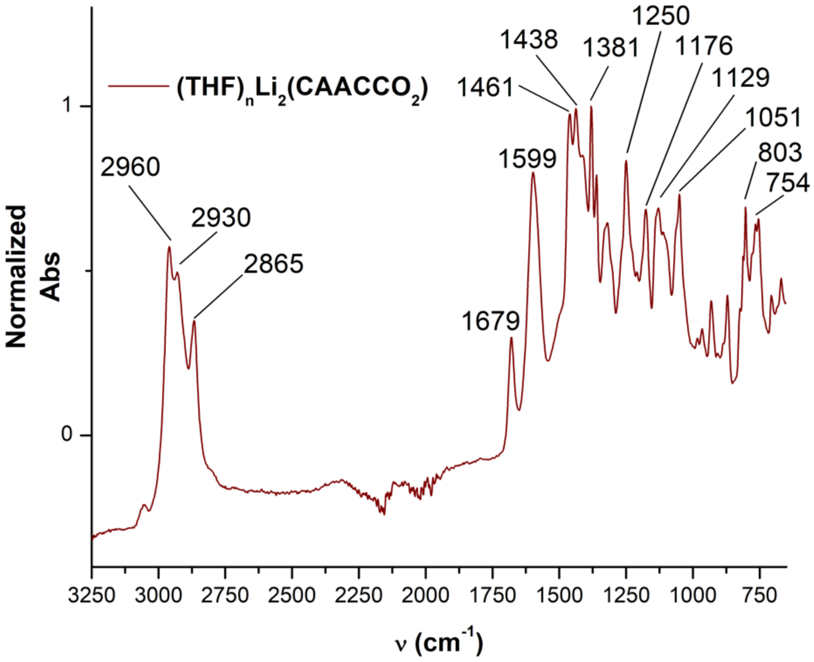

Figure A3.39. FTIR (solid state) of mixture of **4.7** (n=0.333) and **4.8** (n=0.0**)** at 298 K.

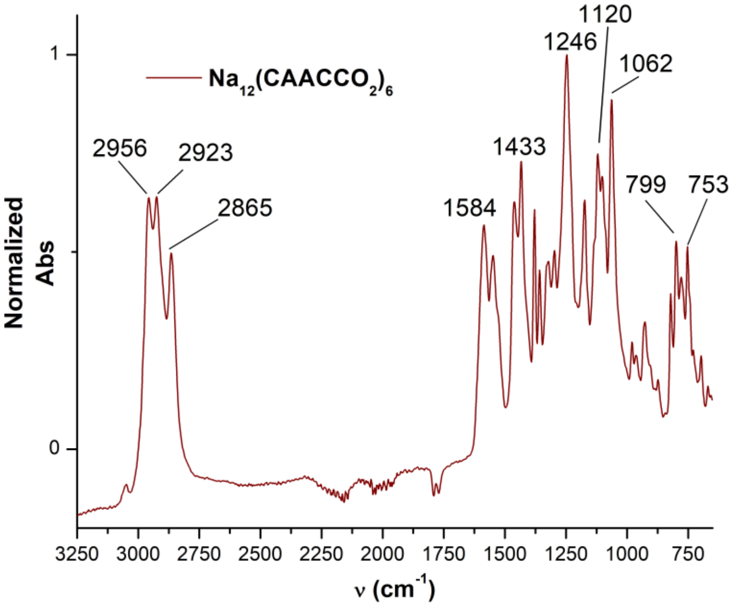

Figure A3.40. FTIR (solid state) of **4.9** at 298 K.

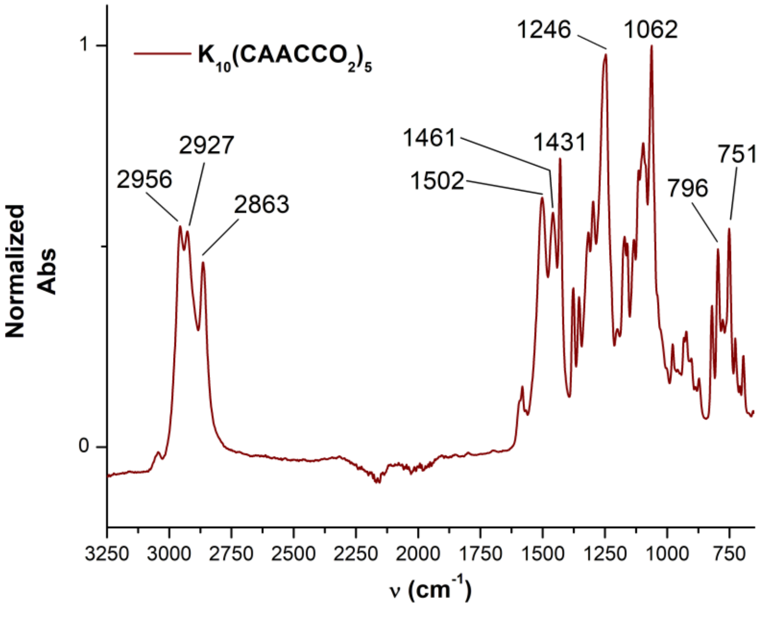

Figure A3.41. FTIR (solid state) of **4.10** at 298 K.

Electronic Absorption (UV/Vis) Spectra

Chapter 2.

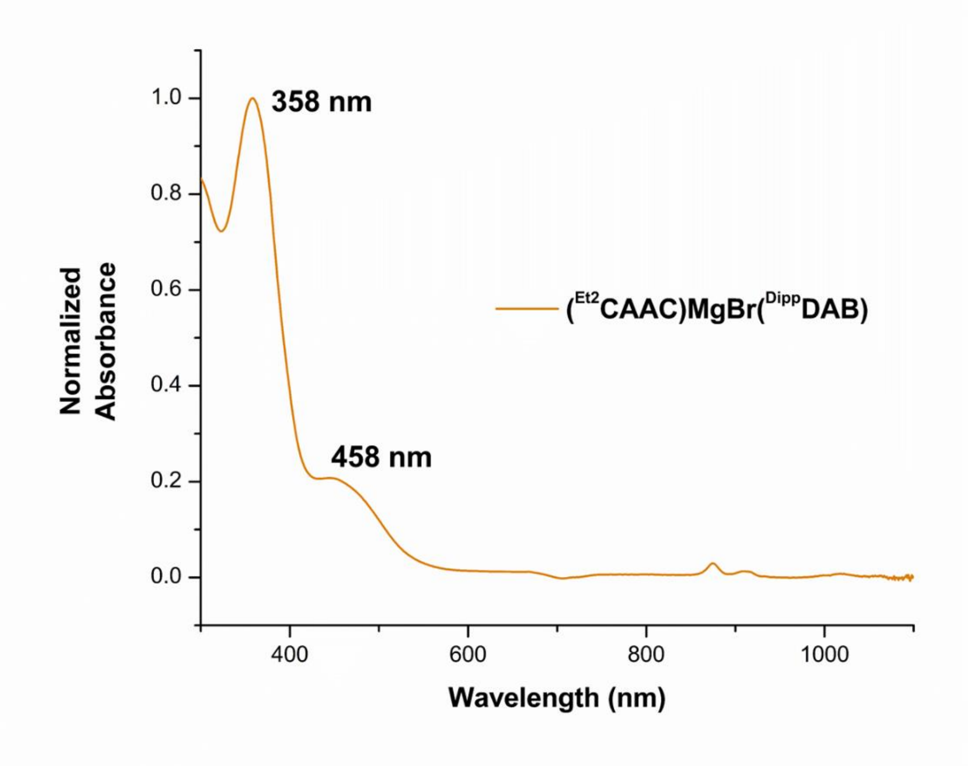

Figure A3.42. Normalized electronic absorption spectrum of compound **2.7** in toluene (0.1 mg mL^{-1}).

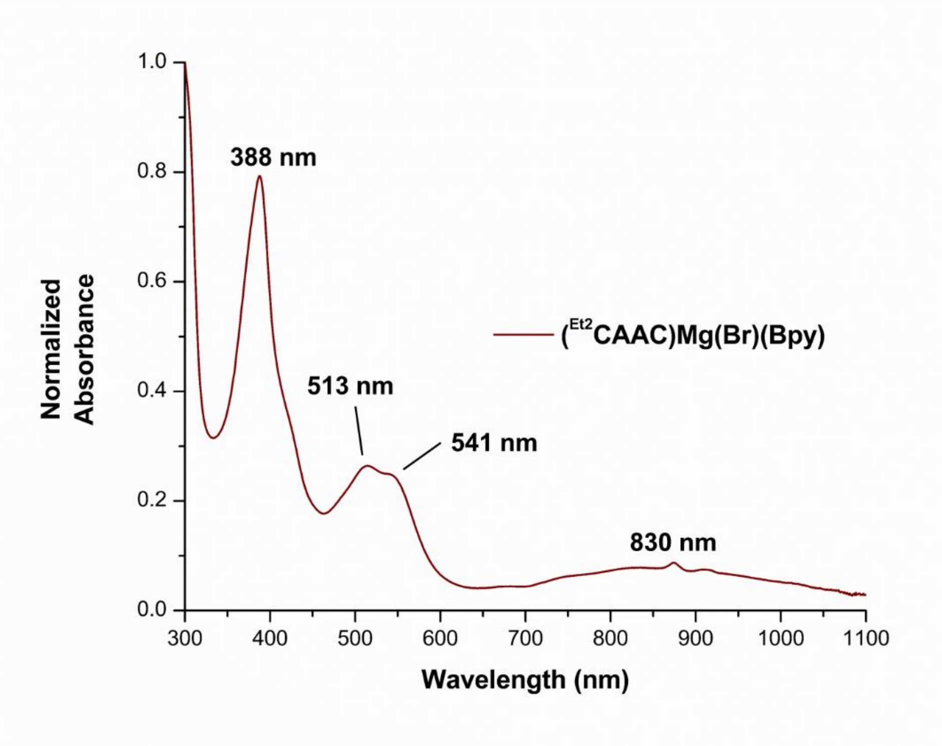

Figure A3.43. Normalized electronic absorption spectrum of compound **2.8** in toluene (0.1 mg mL^{-1}).

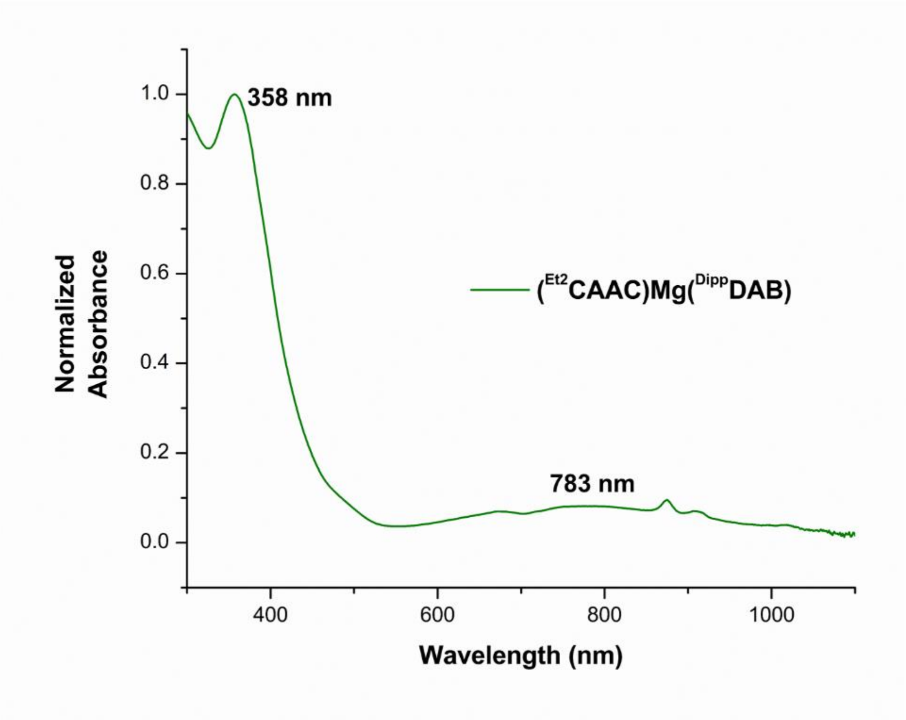

Figure A3.44. Normalized electronic absorption spectrum of compound **2.9** in toluene (0.1 mg mL^{-1}).

Chapter 4.

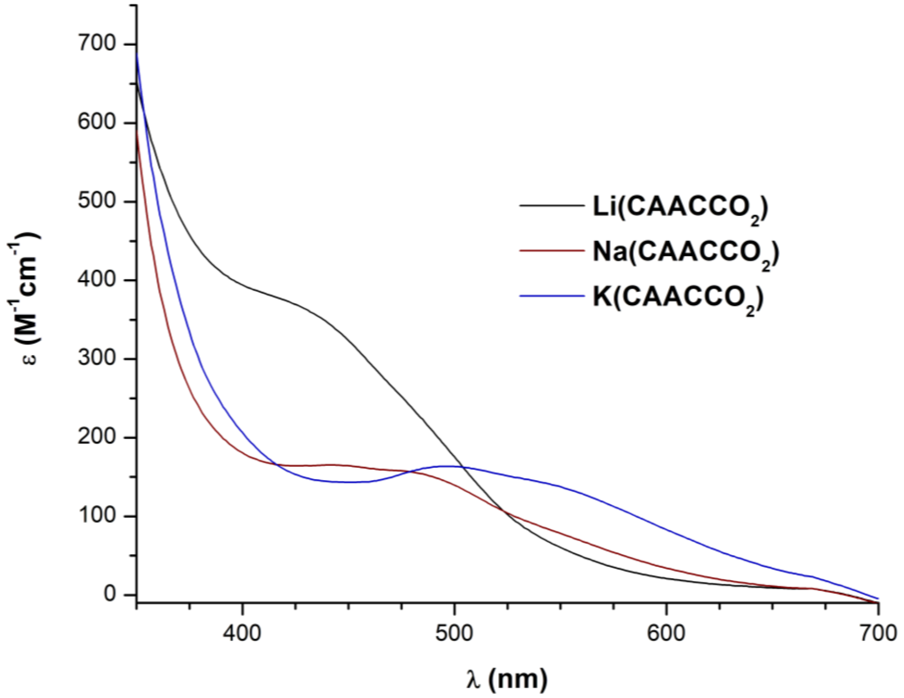

Figure A3.45. Stacked electronic absorption spectra of compounds **4.4-4.6** in toluene (0.5 mg/mL).

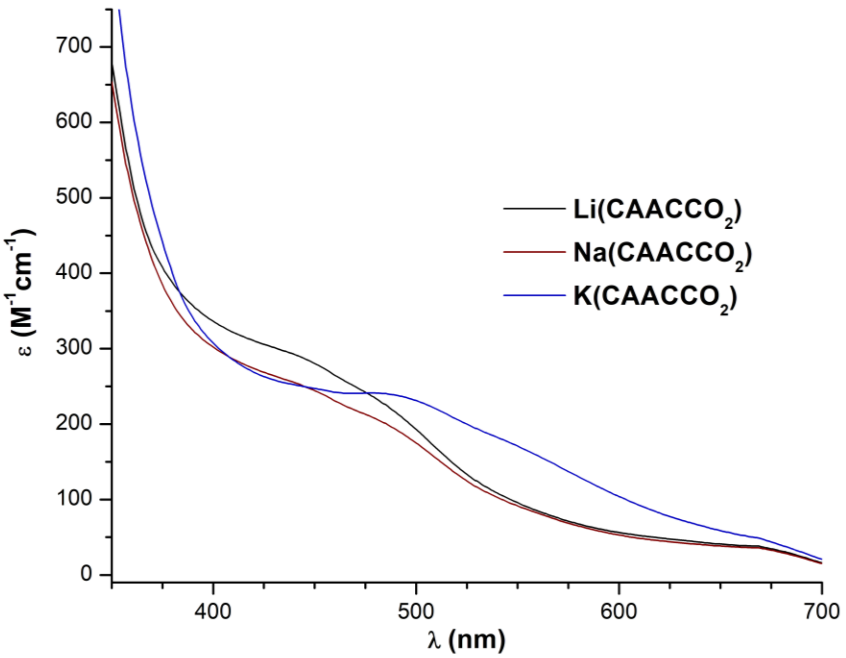

Figure A3.46. Stacked electronic absorption spectra of compounds **4.4-4.6** in THF (0.5 mg/mL).

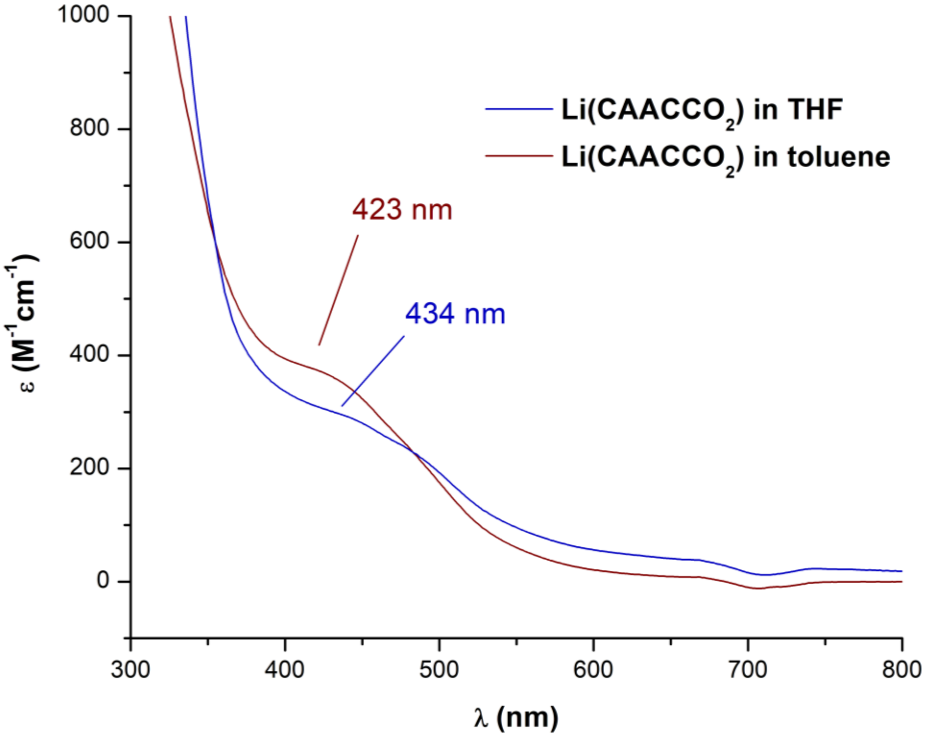

Figure A3.47. Stacked electronic absorption spectra of **4.4** in toluene and THF (0.5 mg/mL).

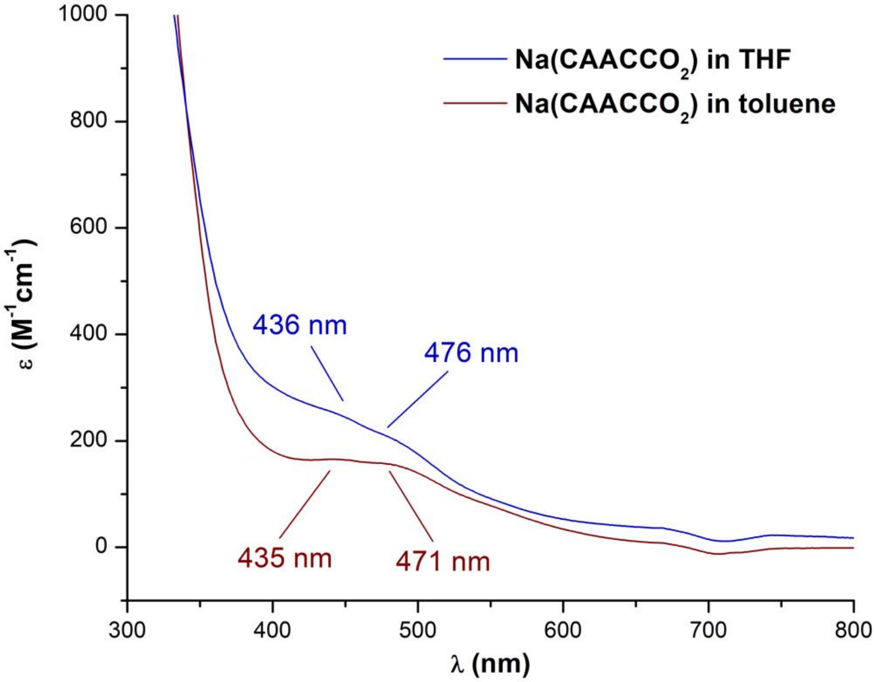

Figure A3.48. Stacked electronic absorption spectra of **4.5** in toluene and THF (0.5 mg/mL).

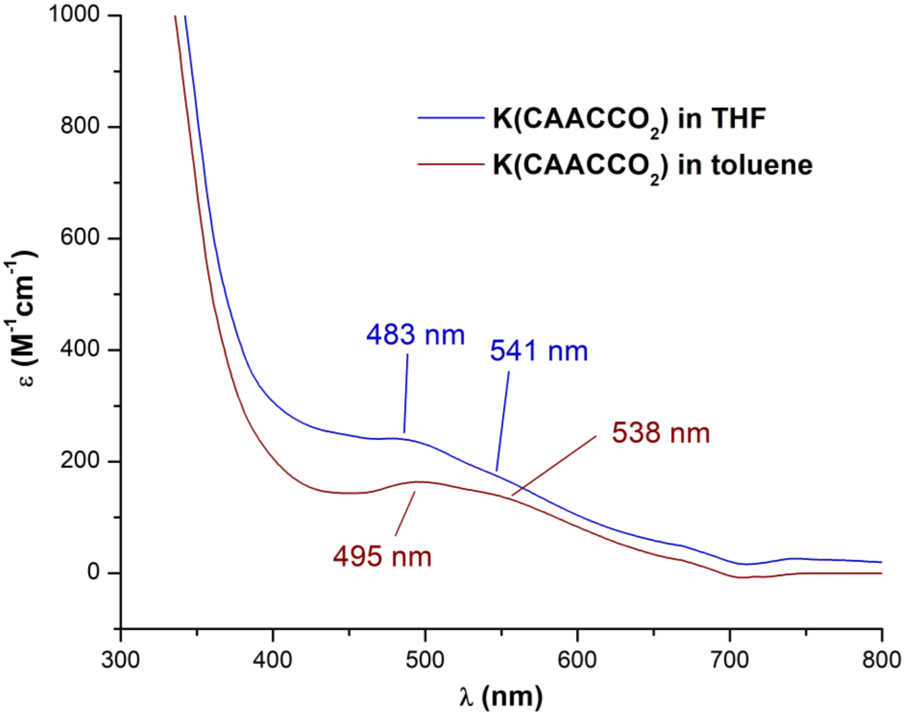

Figure A3.49. Stacked electronic absorption spectra of **4.6** in toluene and THF (0.5 mg/mL).

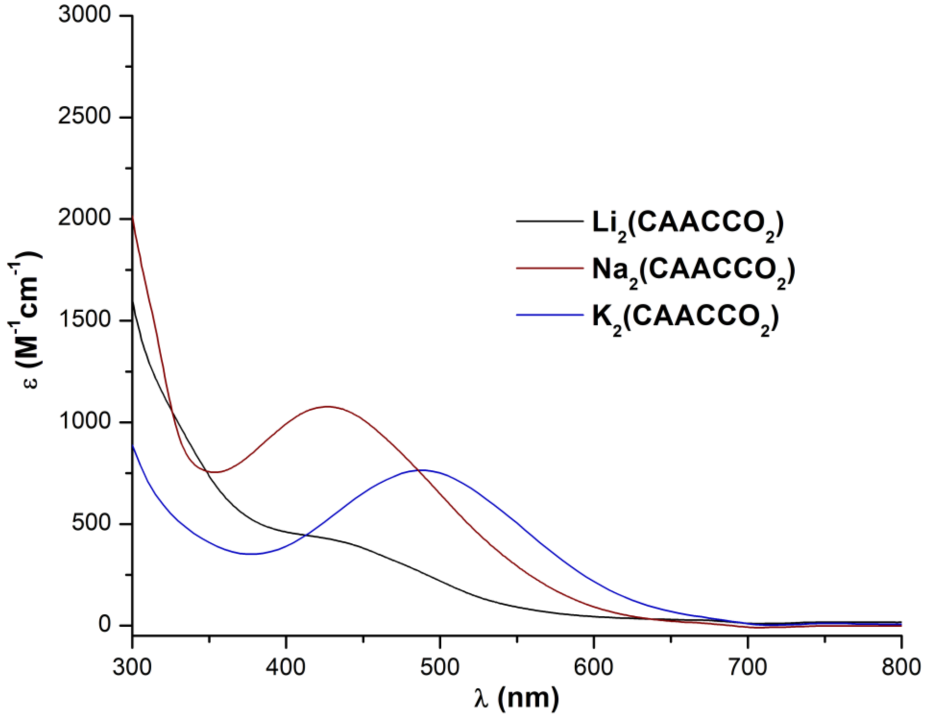

Figure A3.50. Stacked electronic absorption spectra of compounds **4.7-4.10** in toluene (0.5 mg/mL).

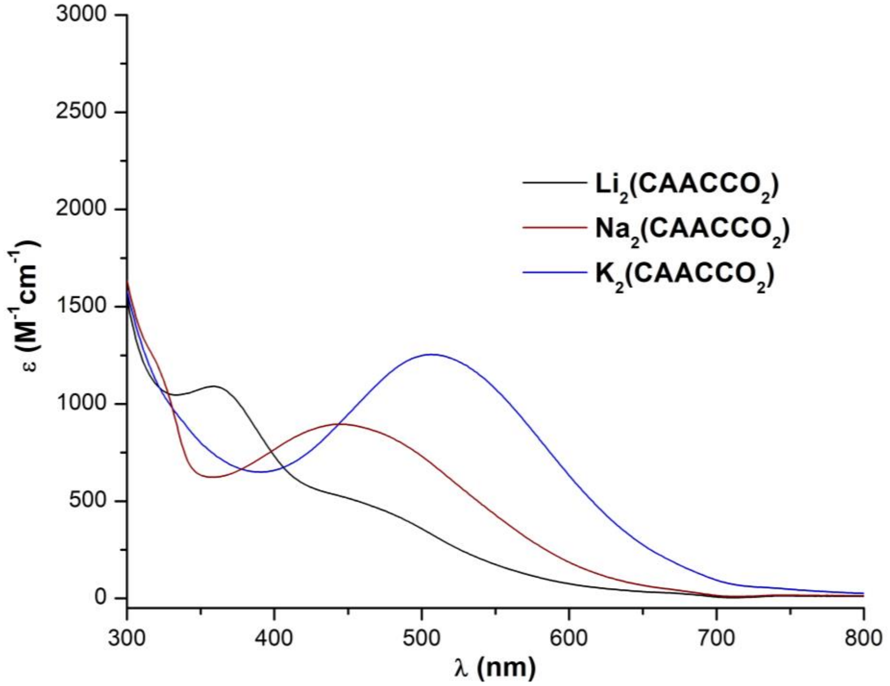

Figure A3.51. Stacked electronic absorption spectra of compounds **4.7-4.10** in THF (0.5 mg/mL).

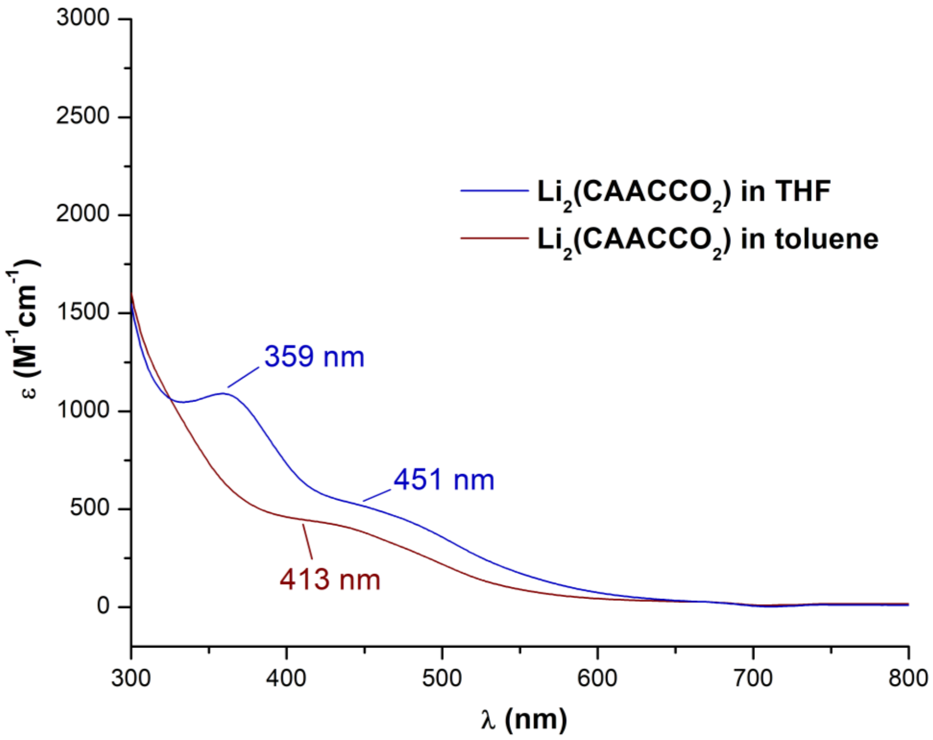

Figure A3.52. Stacked electronic absorption spectra of **4.7/4.8** in toluene and THF (0.5 mg/mL).

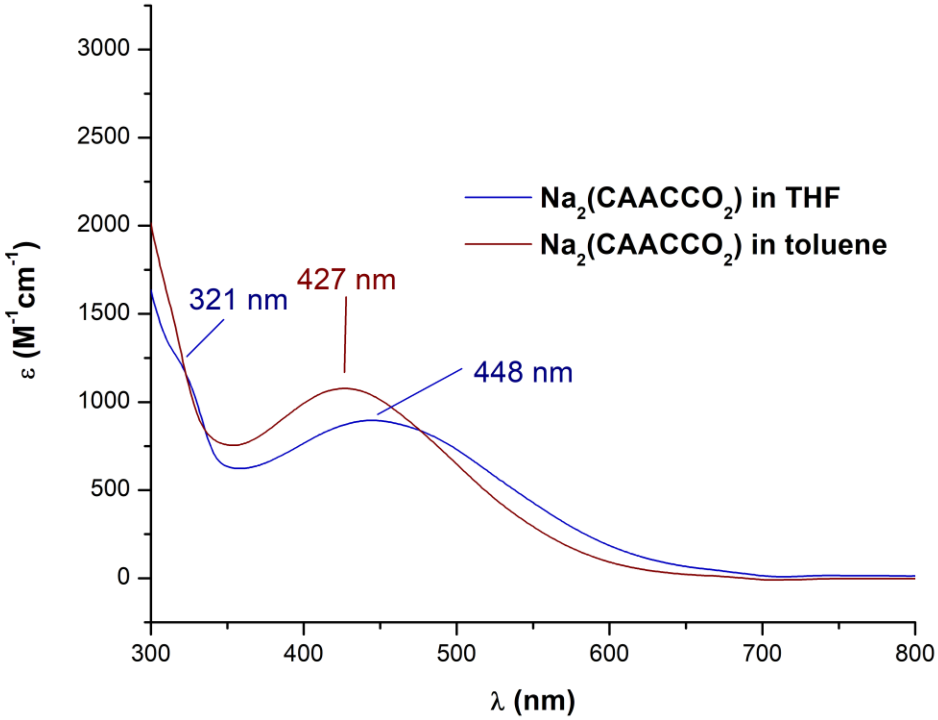

Figure A3.53. Stacked electronic absorption spectra of **4.9** in toluene and THF (0.5 mg/mL).

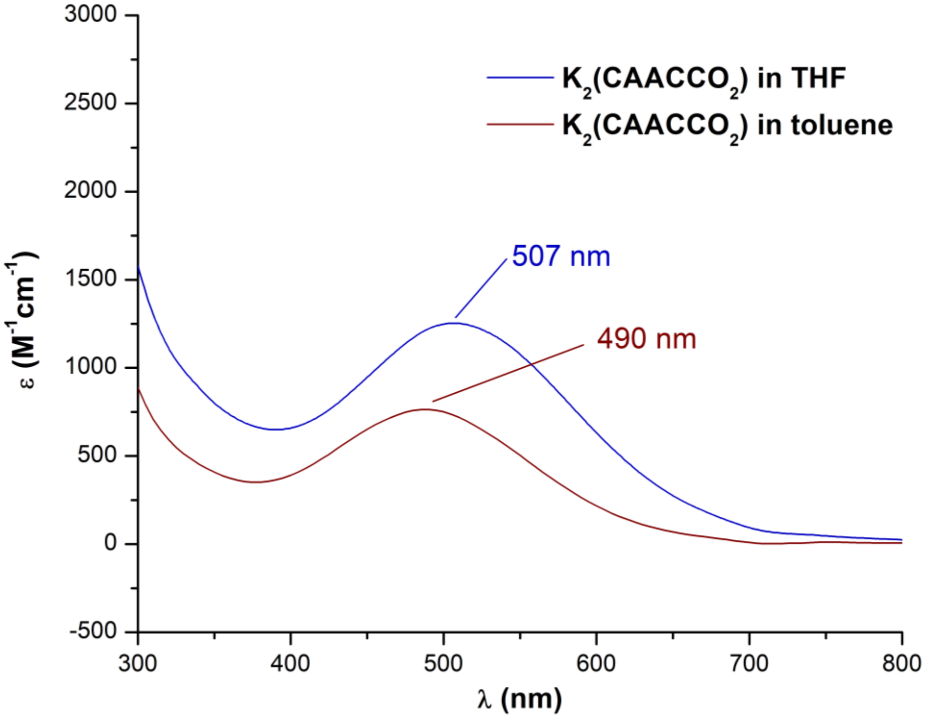

Figure A3.54. Stacked electronic absorption spectra of **4.10** in toluene and THF (0.5 mg/mL).

Appendix IV. Computational Data

Chapter 2.

All computational data given herein were obtained, analyzed and prepared by Andrew Molino and David Wilson at La Trobe University in Melbourne, Australia. Further information on calculated atomic coordinates, bond distances, WBI values, Mulliken charges, etc. can be found in the original manuscript.[123] All calculations were performed using Gaussian 16 revision A.03 unless noted.[238] Geometry optimizations were performed using the B3LYP density functionals utilizing both def2-SVP and def2-TZVP basis sets.[239-241] Grimme's D3 dispersion with Becke-Johnson damping was included, labelled D3(BJ).[242] A restricted-open-shell formalism was employed for open-shell systems. Harmonic vibrational frequencies were computed at the same level of theory in order to characterise the stationary points as minima on the potential energy surface. Calculations were computed with the inclusion of solvent effects using the polarisable continuum model (IEF-PCM) with Truhlar's SMD model with parameters for toluene ($\varepsilon = 2.3741$).[243] NBO analysis was performed using NBO 6.0.[244] TD-DFT calculations were carried out to elucidate the UV-Vis absorbance profile using the ωB97XD/def2-TZVP level of theory in an unrestricted formalism and inclusive of toluene solvation. EDA analysis was conducted using the ADF package at the BP86-D3(BJ)/DZP level of theory (including ZORA relativistic effects).[245]

Calculated Molecular Orbitals

Compound 2.7	
LUMO	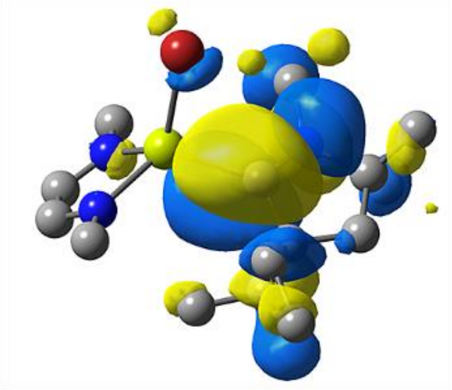
SOMO	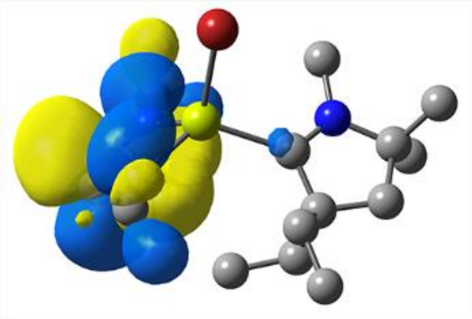
SOMO-1	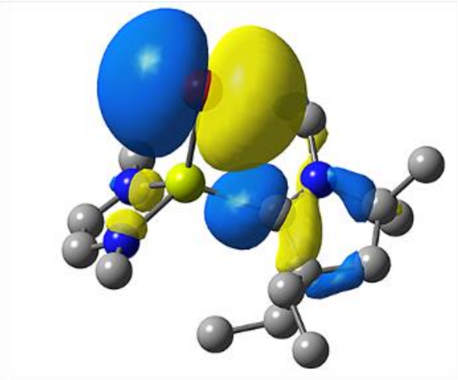

Figure A4.1. Calculated frontier molecular orbitals (along with the SOMO-1) of compound **2.7**.

Compound 2.8	
LUMO	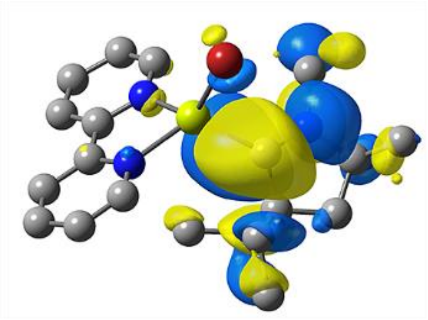
SOMO	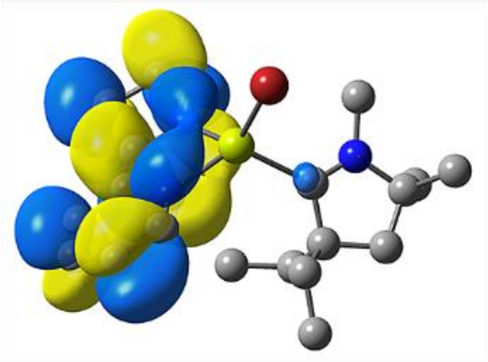

SOMO-1	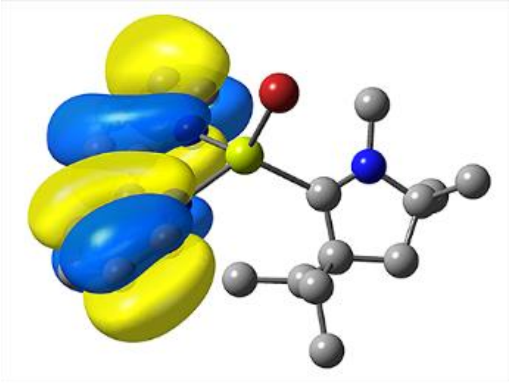

Figure A4.2. Calculated frontier molecular orbitals (along with the SOMO-1) of compound **2.8**.

Compound 7	
LUMO	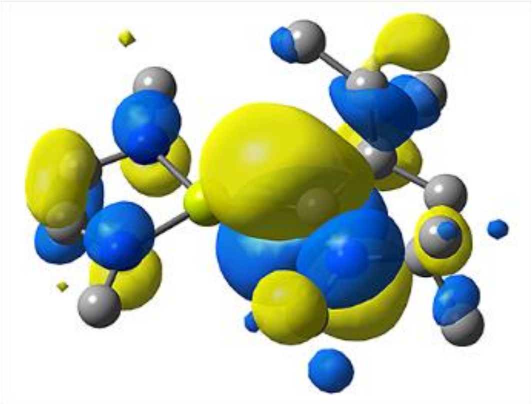

HOMO	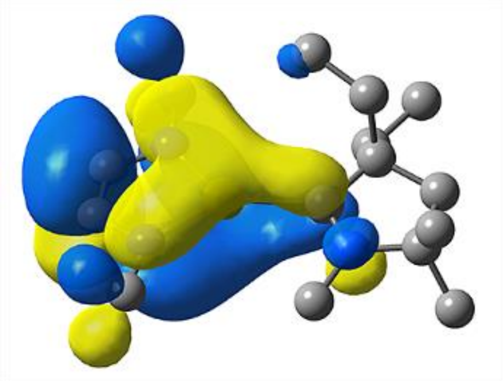
HOMO-1	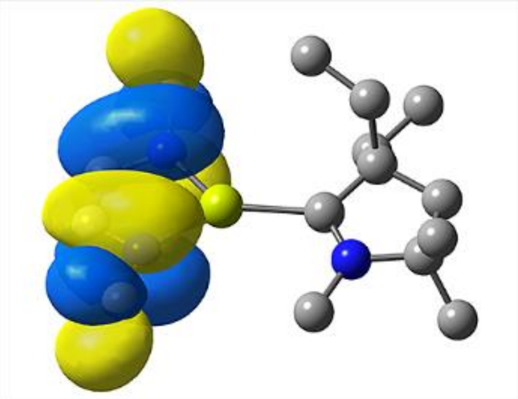

Figure A4.3. Calculated frontier molecular orbitals (along with the HOMO-1) of compound **2.9**.

Chapter 4.

All computational data given herein were obtained, analyzed and prepared by Andrew Molino and David Wilson at La Trobe University in Melbourne, Australia. Further information on calculated coordinates of optimized geometries, etc. can be found in the original manuscript.[225]

Geometry Optimizations and population analyses were performed using Gaussian 16 rev. A.03.[238] Hybrid quantum mechanics/molecular mechanics (QM/MM) optimizations using B3LYP-D3(BJ)/def2-SVP for QM and universal force field (UFF) parameters for MM. All core CAAC-CO_2 and M (M = Li, Na, K) atoms were treated in the QM domain, while Dipp groups and explicit THF molecules were treated in the MM domain UFF. All calculations were inclusive of solvent effects using the polarizable continuum model (IEF-PCM) with Truhlar's SMD model with parameters for THF ($\varepsilon = 7.25$).

All subsequent property and electronic structure calculations employed the QM/MM optimized geometries with a full QM treatment of the entire system. Molecular orbital (MO) and intrinsic bonding orbital (IBO) analysis was performed using single-point B3LYP-D3(BJ)/def2-SVP calculations (inclusive of THF solvation). Hyperfine couplings (HFC) were computed using ORCA 4.2.1 at the B3LYP-D3(BJ)/EPR-II level of theory inclusive of solvent (CPCM(THF)).[246] X-band EPR spectra were simulated with EasySpin 6.0.0-dev.26, using the esfit least-squares fitting function. The Nelder/Mead downhill simplex local optimization algorithm was employed, with an integral target function varying parameters for $\boldsymbol{a}_{\mathbf{iso}}$, and $\boldsymbol{g}$, starting with theoretically computed values, fitting to the experimental spectra.

Spin Populations

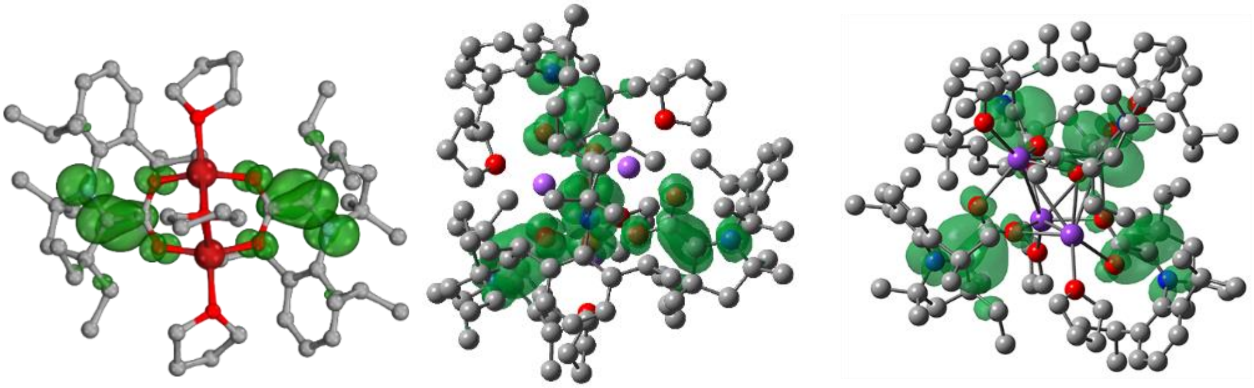

4.4 (Li) **4.5 (Na)** **4.7 (K)**

Figure A4.4. Spin density surface plots of compounds **4.4-4.6**. B3LYP-D3(BJ)/def2-SVP//B3LYP-D3(BJ)/def2-SVP/UFF inclusive of THF solvent model.

	2(Li)		**3(Na)**		**4(K)**	
	Atoms	Fragment	Atoms	Fragment	Atoms	Fragment
CAAC Carbon	51%	73%	61%	76%	58%	78%
CAAC Nitrogen	22%		16%		13%	
CO2 Carbon	4%	18%	6%	19%	8%	18%
CO2 Oxygen	14%		14%		15%	
Alkali Metal	0.4%		0.5%		0.6%	
Sum (Heavy Atoms)	97%		99.6%		99.2%	

Figure A4.5. Computed spin population percentages of singly reduced **4.4-4.6** for specific atoms and summed for CAAC (except Dipp) and CO2 fragments. The remaining spin population is located on the Dipp (N_{CAAC}) substituents.

Simulated EPR Spectra

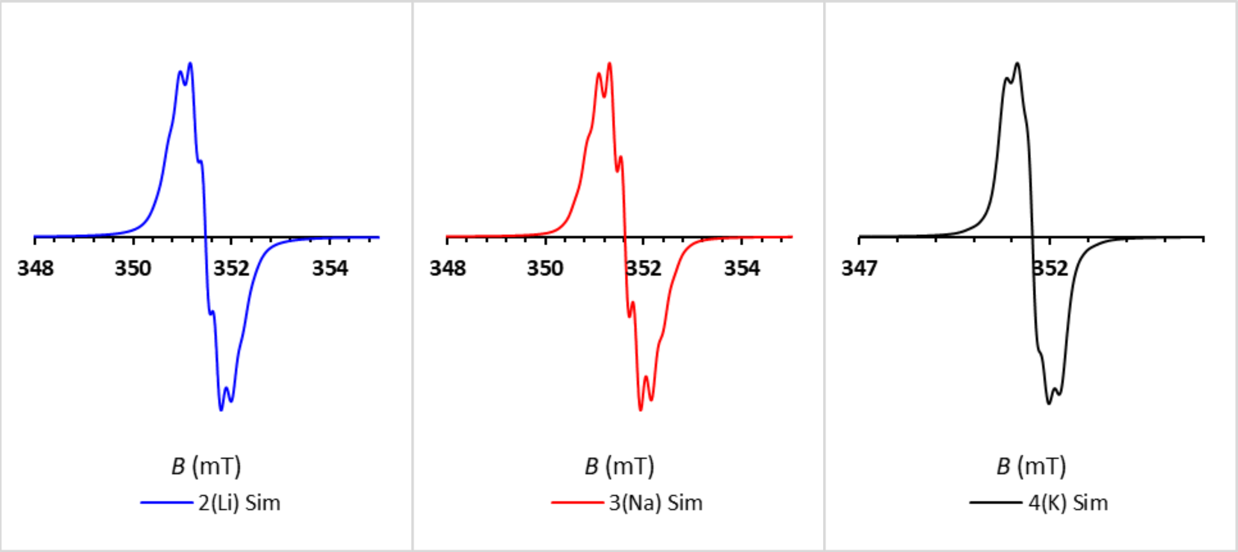

Figure A4.6. Simulated EPR spectra for **4.4 (Li)**, **4.5 (Na)** and **4.6 (K)**.

Molecular Orbitals

2(Li)	**3(Na)**	**4(K)**
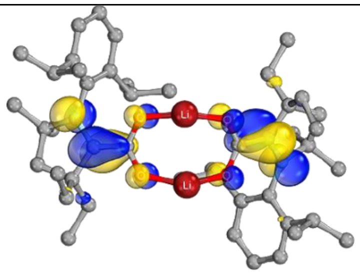	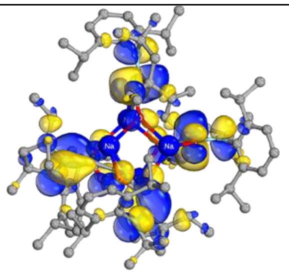	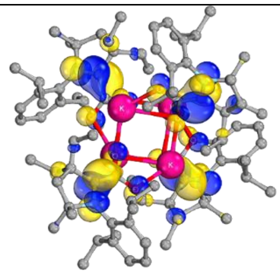
SOMO	SOMO	SOMO
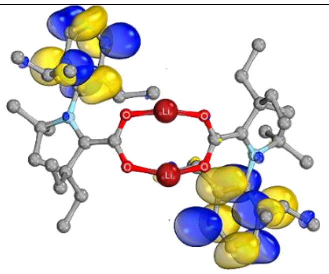	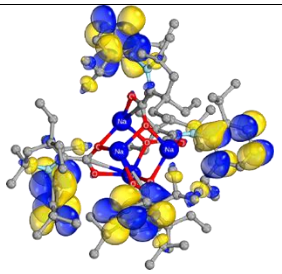	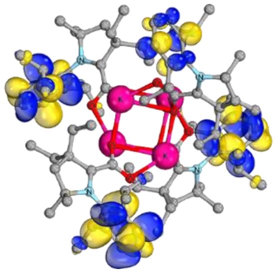
LUMO	LUMO	LUMO

Figure A4.7. Frontier molecular orbitals of compounds **4.4-4.6**. B3LYP-D3(BJ)/def2-SVP//B3LYP-D3(BJ)/def2-SVP/UFF inclusive of THF solvent model.

Intrinsic Bonding Orbitals (IBOs)

4.4 Singly-Reduced	**4.7** Doubly-Reduced
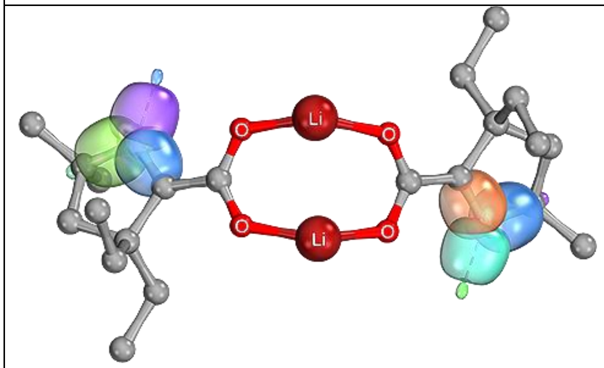	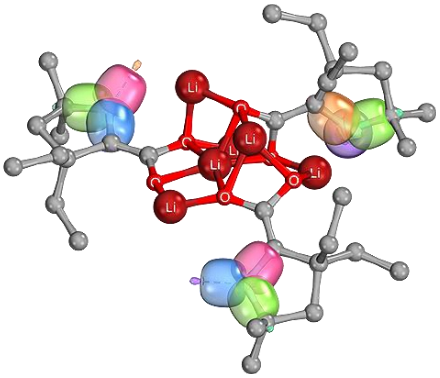
$\mathrm{N_{CAAC}}$ sigma bonds N1- $\mathrm{C_{Carbene}}$ σ (N1=1.169; $\mathrm{C_{Carbene}}$=0.813) N1- $\mathrm{C_{Dipp}}$ σ (N1=1.128; $\mathrm{C_{Dipp}}$=0.855) N1- $\mathrm{C_{CAAC}}$ σ (N1=1.143; $\mathrm{C_{CAAC}}$=0.819)	$\mathrm{N_{CAAC}}$ sigma bonds N1- $\mathrm{C_{Carbene}}$ σ (N1=1.099; $\mathrm{C_{Carbene}}$=0.873) N1- $\mathrm{C_{Dipp}}$ σ (N1=1.156; $\mathrm{C_{Dipp}}$=0.818) N1- $\mathrm{C_{CAAC}}$ σ (N1=1.042; $\mathrm{C_{CAAC}}$=0.930)
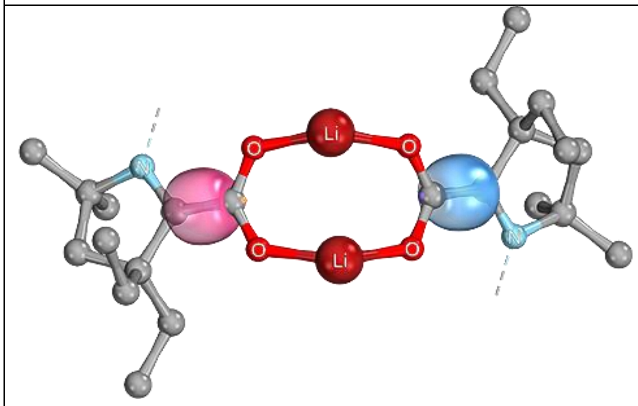	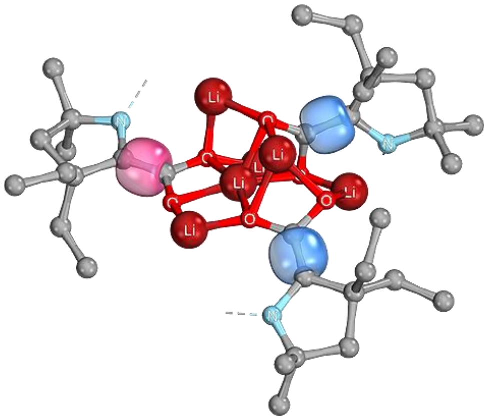
C-C sigma bond $\mathrm{C_{Carbene}}$-$\mathrm{C_{CO2}}$ σ ($\mathrm{C_{Carbene}}$ =1.020; $\mathrm{C_{CO2}}$=0.962)	C-C sigma bond $\mathrm{C_{Carbene}}$-$\mathrm{C_{CO2}}$ σ ($\mathrm{C_{Carbene}}$ =1.008; $\mathrm{C_{CO2}}$=0.973)

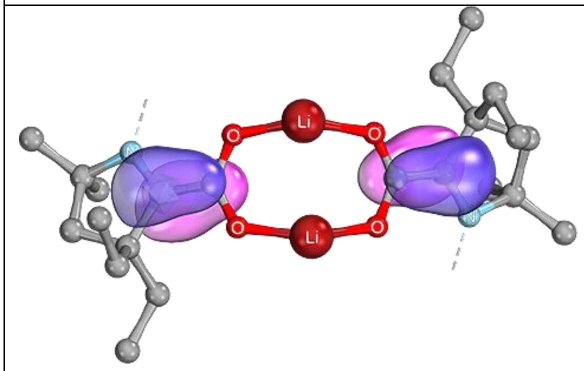	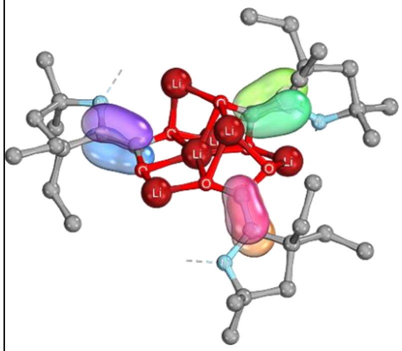
C-C pi bond C_{Carbene}-C_{CO2} π (C_{Carbene} =1.386; C_{CO2}=0.503)	C-C pi bond C_{Carbene}-C_{CO2} π (C_{Carbene} =1.199; C_{CO2}=0.768)
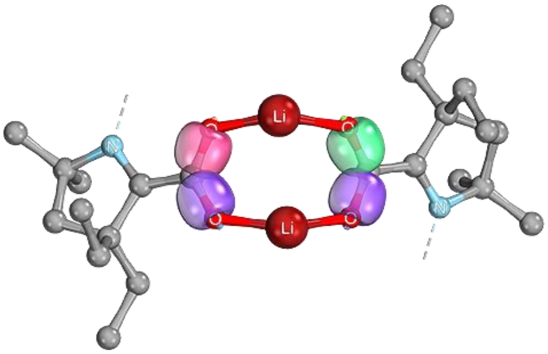	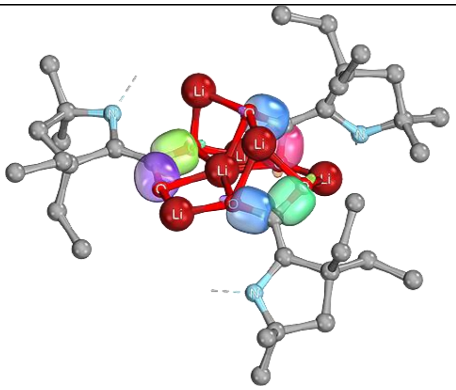
C-O sigma bond C_{CO2}-O_{CO2} π (C_{CO2} =1.223; O_{CO2}=0.771)	C-O sigma bond C_{CO2}-O_{CO2} π (C_{CO2} =1.177; O_{CO2}=0.812)

Figure A4.8. Carbene and CO_2 IBOs of compounds **4.4** and **4.7**. B3LYP-D3(BJ)/def2-SVP//B3LYP-D3(BJ)/def2-SVP/UFF inclusive of THF solvent model.

References.

1. Anastas, P. T.; Kirchhoff, M. M., Origins, current status, and future challenges of green chemistry. *Acc. Chem. Res.* **2002,** *35* (9), 686-694.

2. Heiserman, D., *Exploring chemical elements and their compounds*. McGraw-Hill: 1991.

3. Harder, S., Molecular early main group metal hydrides: synthetic challenge, structures and applications. *Chem. Commun.* **2012,** *48* (91), 11165-11177.

4. Silverman, G. S.; Rakita, P. E., *Handbook of Grignard reagents*. CRC Press: 1996.

5. Westerhausen, M., 100 Years after Grignard: Where Does the Organometallic Chemistry of the Heavy Alkaline Earth Metals Stand Today? *Angew. Chem. Int. Ed.* **2001,** *40* (16), 2975-2977.

6. Westerhausen, M.; Langer, J.; Krieck, S.; Fischer, R.; Görls, H.; Köhler, M., Heavier Group 2 Grignard Reagents of the Type Aryl-Ae(L) n -X (Post-Grignard Reagents). In *Alkaline-*

Earth Metal Compounds: Oddities and Applications, Harder, S., Ed. Springer Berlin Heidelberg: Berlin, Heidelberg, 2013; pp 29-72.

7. Westerhausen, M.; Koch, A.; Görls, H.; Krieck, S., Heavy Grignard Reagents: Synthesis, Physical and Structural Properties, Chemical Behavior, and Reactivity. *Chem. Eur. J.* **2016,** *23* (7), 1456-1483.

8. Westerhausen, M.; Koch, A.; Görls, H.; Krieck, S., Heavy Grignard Reagents: Synthesis, Physical and Structural Properties, Chemical Behavior, and Reactivity. *Chem. Eur. J.* **2017,** *23* (7), 1456-1483.

9. Seyferth, D., Zinc Alkyls, Edward Frankland, and the Beginnings of Main-Group Organometallic Chemistry. *Organometallics* **2001,** *20* (14), 2940-2955.

10. Seyferth, D., Alkyl and Aryl Derivatives of the Alkali Metals: Useful Synthetic Reagents as Strong Bases and Potent Nucleophiles. 1. Conversion of Organic Halides to Organoalkali-Metal Compounds. *Organometallics* **2006,** *25* (1), 2-24.

11. Wisniak, J., François Auguste Victor Grignard. *Educación química* **2004,** *15*, 4.

12. Schlenk, W.; Schlenk jun, W., Über die Konstitution der Grignardschen Magnesiumverbindungen. *Berichte der deutschen chemischen Gesellschaft (A and B Series)* **1929,** *62* (4), 920-924.

13. Seyferth, D., Alkyl and Aryl Derivatives of the Alkali Metals: Strong Bases and Reactive Nucleophiles. 2. Wilhelm Schlenk's Organoalkali-Metal Chemistry. The Metal Displacement and the Transmetalation Reactions. Metalation of Weakly Acidic Hydrocarbons. Superbases. *Organometallics* **2009,** *28* (1), 2-33.

14. Luisi, R.; Capriati, V., *Lithium compounds in organic synthesis: from fundamentals to applications*. John Wiley & Sons: 2014.

15. Tamao, K.; Sumitani, K.; Kumada, M., Selective carbon-carbon bond formation by cross-coupling of Grignard reagents with organic halides. Catalysis by nickel-phosphine complexes. *J. Am. Chem. Soc.* **1972,** *94* (12), 4374-4376.

16. Tamao, K.; Kiso, Y.; Sumitani, K.; Kumada, M., Alkyl group isomerization in the cross-coupling reaction of secondary alkyl Grignard reagents with organic halides in the presence of nickel-phosphine complexes as catalysts. *J. Am. Chem. Soc.* **1972,** *94* (26), 9268-9269.

17. Huang, J.; Nolan, S. P., Efficient Cross-Coupling of Aryl Chlorides with Aryl Grignard Reagents (Kumada Reaction) Mediated by a Palladium/Imidazolium Chloride System. *J. Am. Chem. Soc.* **1999,** *121* (42), 9889-9890.

18. Tamura, M.; Kochi, J. K., Vinylation of Grignard reagents. Catalysis by iron. *J. Am. Chem. Soc.* **1971,** *93* (6), 1487-1489.

19. Tamura, M.; Kochi, J., Coupling of Grignard Reagents with Organic Halides. *Synthesis* **1971,** *1971* (06), 303-305.

20. Ali, S. H.; Deacon, G. B.; Junk, P. C.; Hamidi, S.; Wiecko, M.; Wang, J., Lanthanoid Pseudo-Grignard Reagents: A Major Untapped Resource. *Chem. Eur. J.* **2018,** *24* (1), 230-242.

21. Harder, S.; Piers, W. E., Organometallic and coordination chemistry of the s-block metals. *Dalton Trans.* **2018,** *47* (36), 12491-12492.

22. Krieck, S.; Westerhausen, M., Kudos and Renaissance of s-Block Metal Chemistry. *Inorganics* **2017,** *5* (1).

23. Graetz, J., New approaches to hydrogen storage. *Chem. Soc. Rev.* **2009,** *38* (1), 73-82.

24. Grochala, W.; Edwards, P. P., Thermal Decomposition of the Non-Interstitial Hydrides for the Storage and Production of Hydrogen. *Chem. Rev.* **2004,** *104* (3), 1283-1316.

25. Orimo, S.-i.; Nakamori, Y.; Eliseo, J. R.; Züttel, A.; Jensen, C. M., Complex Hydrides for Hydrogen Storage. *Chem. Rev.* **2007,** *107* (10), 4111-4132.

26. Yang, J.; Sudik, A.; Wolverton, C.; Siegel, D. J., High capacity hydrogen storage materials: attributes for automotive applications and techniques for materials discovery. *Chem. Soc. Rev.* **2010,** *39* (2), 656-675.

27. Schnitzler, S.; Spaniol, T. P.; Maron, L.; Okuda, J., Formation and Reactivity of a Molecular Magnesium Hydride with a Terminal Mg□H Bond. *Chem. Eur. J.* **2015,** *21* (32), 11330-11334.

28. Arrowsmith, M.; Hill, M. S.; MacDougall, D. J.; Mahon, M. F., A Hydride-Rich Magnesium Cluster. *Angew. Chem. Int. Ed.* **2009,** *48* (22), 4013-4016.

29. Mukherjee, D.; Okuda, J., Molecular Magnesium Hydrides. *Angew. Chem. Int. Ed.* **2017,** *57* (6), 1458-1473.

30. Rauch, M.; Ruccolo, S.; Parkin, G., Synthesis, Structure, and Reactivity of a Terminal Magnesium Hydride Compound with a Carbatrane Motif, [TismPriBenz]MgH: A Multifunctional Catalyst for Hydrosilylation and Hydroboration. *J. Am. Chem. Soc.* **2017,** *139* (38), 13264-13267.

31. Bonyhady, S. J.; Jones, C.; Nembenna, S.; Stasch, A.; Edwards, A. J.; McIntyre, G. J., β-Diketiminate-Stabilized Magnesium(I) Dimers and Magnesium(II) Hydride Complexes: Synthesis, Characterization, Adduct Formation, and Reactivity Studies. *Chem. Eur. J.* **2010,** *16* (3), 938-955.

32. Maitland, B.; Wiesinger, M.; Langer, J.; Ballmann, G.; Pahl, J.; Elsen, H.; Färber, C.; Harder, S., A Simple Route to Calcium and Strontium Hydride Clusters. *Angew. Chem. Int. Ed.* **2017,** *56* (39), 11880-11884.

33. Causero, A.; Ballmann, G.; Pahl, J.; Zijlstra, H.; Färber, C.; Harder, S., Stabilization of Calcium Hydride Complexes by Fine Tuning of Amidinate Ligands. *Organometallics* **2016,** *35* (19), 3350-3360.

34. Wilson, A. S. S.; Hill, M. S.; Mahon, M. F.; Dinoi, C.; Maron, L., Organocalcium-mediated nucleophilic alkylation of benzene. *Science* **2017,** *358* (6367), 1168.

35. Arrowsmith, M.; Hill, M. S.; Kociok-Köhn, G.; MacDougall, D. J.; Mahon, M. F., Beryllium-Induced C□N Bond Activation and Ring Opening of an N-Heterocyclic Carbene. *Angew. Chem. Int. Ed.* **2012,** *51* (9), 2098-2100.

36. Jones, C., Dimeric magnesium(I) β-diketiminates: a new class of quasi-universal reducing agent. *Nat. Rev. Chem.* **2017,** *1*, 0059.

37. Green, S. P.; Jones, C.; Stasch, A., Stable Magnesium(I) Compounds with Mg-Mg Bonds. *Science* **2007,** *318* (5857), 1754.

38. Westerhausen, M., Molecular Magnesium(I) Compounds: From Curiosity to Kudos. *Angew. Chem. Int. Ed.* **2008,** *47* (12), 2185-2187.

39. Boutland, A. J.; Carroll, A.; Alvarez Lamsfus, C.; Stasch, A.; Maron, L.; Jones, C., Reversible Insertion of a C═C Bond into Magnesium(I) Dimers: Generation of Highly Active 1,2-Dimagnesioethane Compounds. *J. Am. Chem. Soc.* **2017,** *139* (50), 18190-18193.

40. Green, S. P.; Jones, C.; Stasch, A., Stable Adducts of a Dimeric Magnesium(I) Compound. *Angew. Chem. Int. Ed.* **2008,** *47* (47), 9079-9083.

41. Gentner, T. X.; Rösch, B.; Ballmann, G.; Langer, J.; Elsen, H.; Harder, S., Low Valent Magnesium Chemistry with a Super Bulky β-Diketiminate Ligand. *Angew. Chem. Int. Ed.* **2019,** *58* (2), 607-611.

42. Arrowsmith, M.; Hill, M. S.; Hadlington, T.; Kociok-Köhn, G.; Weetman, C., Magnesium-Catalyzed Hydroboration of Pyridines. *Organometallics* **2011,** *30* (21), 5556-5559.

43. Hill, M. S.; Liptrot, D. J.; Weetman, C., Alkaline earths as main group reagents in molecular catalysis. *Chem. Soc. Rev.* **2016,** *45* (4), 972-988.

44. Brinkmann, C.; Barrett, A. G. M.; Hill, M. S.; Procopiou, P. A., Heavier Alkaline Earth Catalysts for the Intermolecular Hydroamination of Vinylarenes, Dienes, and Alkynes. *J. Am. Chem. Soc.* **2012,** *134* (4), 2193-2207.

45. Nifant'ev, I. E.; Shlyakhtin, A. V.; Tavtorkin, A. N.; Ivchenko, P. V.; Borisov, R. S.; Churakov, A. V., Monomeric and dimeric magnesium mono-BHT complexes as effective ROP catalysts. *Catal. Comm.* **2016,** *87*, 106-111.

46. Barrett, A. G. M.; Crimmin, M. R.; Hill, M. S.; Procopiou, P. A., Heterofunctionalization catalysis with organometallic complexes of calcium, strontium and barium. *Proceedings of the Royal Society A: Mathematical, Physical and Engineering Science* **2010,** *466* (2116), 927-963.

47. Harder, S., From Limestone to Catalysis: Application of Calcium Compounds as Homogeneous Catalysts. *Chem. Rev.* **2010,** *110* (7), 3852-3876.

48. Datta, S.; Roesky, P. W.; Blechert, S., Aminotroponate and Aminotroponiminate Calcium Amides as Catalysts for the Hydroamination/Cyclization Catalysis. *Organometallics* **2007,** *26* (18), 4392-4394.

49. Bauer, H.; Thum, K.; Alonso, M.; Fischer, C.; Harder, S., Alkene Transfer Hydrogenation with Alkaline-Earth Metal Catalysts. *Angew. Chem. Int. Ed. Engl.* **2019,** *58* (13), 4248-4253.

50. Bauer, H.; Alonso, M.; Färber, C.; Elsen, H.; Pahl, J.; Causero, A.; Ballmann, G.; De Proft, F.; Harder, S., Imine hydrogenation with simple alkaline earth metal catalysts. *Nat. Catal.* **2018,** *1* (1), 40-47.

51. Ren, W.; Gu, D., An Azobenzenyl Anion Radical Complex of Magnesium: Synthesis, Structure, and Reactivity Studies. *Inorg. Chem.* **2016,** *55* (22), 11962-11970.

52. Wilson, A. S. S.; Dinoi, C.; Hill, M. S.; Mahon, M. F.; Maron, L., Heterolysis of Dihydrogen by Nucleophilic Calcium Alkyls. *Angew. Chem. Int. Ed. Engl.* **2018,** *57* (47), 15500-15504.

53. Anker, M. D.; Kefalidis, C. E.; Yang, Y.; Fang, J.; Hill, M. S.; Mahon, M. F.; Maron, L., Alkaline Earth-Centered CO Homologation, Reduction, and Amine Carbonylation. *J. Am. Chem. Soc.* **2017,** *139* (29), 10036-10054.

54. Raghavendra, B.; Shashank, P. V. S.; Pandey, M. K.; Reddy, N. D., CO2/Epoxide Coupling and the ROP of ε-Caprolactone: Mg and Al Complexes of γ-Phosphino-ketiminates as Dual-Purpose Catalysts. *Organometallics* **2018,** *37* (11), 1656-1664.

55. Kember, M. R.; Williams, C. K., Efficient Magnesium Catalysts for the Copolymerization of Epoxides and CO2; Using Water to Synthesize Polycarbonate Polyols. *J. Am. Chem. Soc.* **2012,** *134* (38), 15676-15679.

56. Anker, M. D.; Arrowsmith, M.; Bellham, P.; Hill, M. S.; Kociok-Köhn, G.; Liptrot, D. J.; Mahon, M. F.; Weetman, C., Selective reduction of CO2 to a methanol equivalent by B(C6F5)3-activated alkaline earth catalysis. *Chem. Sci.* **2014,** *5* (7), 2826-2830.

57. Rauch, M.; Parkin, G., Zinc and Magnesium Catalysts for the Hydrosilylation of Carbon Dioxide. *J. Am. Chem. Soc.* **2017,** *139* (50), 18162-18165.

58. Rösch, B.; Gentner, T. X.; Elsen, H.; Fischer, C. A.; Langer, J.; Wiesinger, M.; Harder, S., Nucleophilic Aromatic Substitution at Benzene with Powerful Strontium Hydride and Alkyl Complexes. *Angew. Chem. Int. Ed.* **2019,** *58* (16), 5396-5401.

59. Kambe, N.; Iwasaki, T.; Terao, J., Pd-catalyzed cross-coupling reactions of alkyl halides. *Chem. Soc. Rev.* **2011,** *40* (10), 4937-4947.

60. Small, B. L.; Brookhart, M.; Bennett, A. M. A., Highly Active Iron and Cobalt Catalysts for the Polymerization of Ethylene. *J. Am. Chem. Soc.* **1998,** *120* (16), 4049-4050.

61. Nakamura, M.; Matsuo, K.; Ito, S.; Nakamura, E., Iron-Catalyzed Cross-Coupling of Primary and Secondary Alkyl Halides with Aryl Grignard Reagents. *J. Am. Chem. Soc.* **2004,** *126* (12), 3686-3687.

62. Bolm, C.; Legros, J.; Le Paih, J.; Zani, L., Iron-Catalyzed Reactions in Organic Synthesis. *Chem. Rev.* **2004,** *104* (12), 6217-6254.

63. Wenger, O. S., Is Iron the New Ruthenium? *Chem. Eur. J.* **2019,** *0* (0).

64. Amatore, C.; Jutand, A., Anionic Pd(0) and Pd(II) Intermediates in Palladium-Catalyzed Heck and Cross-Coupling Reactions. *Acc. Chem. Res.* **2000,** *33* (5), 314-321.

65. Jones, C., Open questions in low oxidation state group 2 chemistry. *Communications Chemistry* **2020,** *3* (1), 159.

66. Lide, R. D., Ed., *CRC Handbook of Chemistry and Physics*. 77 ed.; CRC Press: Boca Raton, FL: 1993.

67. Krieck, S.; Görls, H.; Yu, L.; Reiher, M.; Westerhausen, M., Stable "Inverse" Sandwich Complex with Unprecedented Organocalcium(I): Crystal Structures of [(thf)2Mg(Br)-C6H2-2,4,6-Ph3] and [(thf)3Ca{μ-C6H3-1,3,5-Ph3}Ca(thf)3]. *J. Am. Chem. Soc.* **2009,** *131* (8), 2977-2985.

68. Arrowsmith, M.; Braunschweig, H.; Celik, M. A.; Dellermann, T.; Dewhurst, R. D.; Ewing, W. C.; Hammond, K.; Kramer, T.; Krummenacher, I.; Mies, J.; Radacki, K.; Schuster, J. K., Neutral zero-valent s-block complexes with strong multiple bonding. *Nat. Chem.* **2016,** *8*, 890.

69. Naglav, D.; Neumann, A.; Bläser, D.; Wölper, C.; Haack, R.; Jansen, G.; Schulz, S., Bonding situation in Be[N(SiMe3)2]2 – an experimental and computational study. *Chem. Commun.* **2015,** *51* (18), 3889-3891.

70. R.A. Kemp, A. M. F., CCDC 661034: Experimental Structure Determination. 2008.

71. Westerhausen, M., Synthesis and spectroscopic properties of bis(trimethylsilyl)amides of the alkaline-earth metals magnesium, calcium, strontium, and barium. *Inorg. Chem.* **1991,** *30* (1), 96-101.

72. Henderson, K. W.; Kerr, W. J., Magnesium Bisamides as Reagents in Synthesis. *Chem. Eur. J.* **2001,** *7* (16), 3430-3437.

73. Westerhausen, M.; Greul, J.; Hausen, H.-D.; Schwarz, W., Synthese von substituierten Calcium-bis(disilylamiden) mittels der Transmetallierung von Zinn(II)- und Zinn(IV)-amiden. *Z.A.A.C.* **1996,** *622* (8), 1295-1305.

74. Hill, M. S.; Hodgson, M.; Liptrot, D. J.; Mahon, M. F., Stoichiometric reactivity of dialkylamine boranes with alkaline earth silylamides. *Dalton Trans.* **2011,** *40* (30), 7783-7790.

75. Speight, I. R.; Chmely, S. C.; Hanusa, T. P.; Rheingold, A. L., Mechanochemically directed metathesis in group 2 chemistry: calcium amide formation without solvent. *Chem. Commun.* **2019,** *55* (15), 2202-2205.

76. Naglav, D.; Neumann, A.; Bläser, D.; Wölper, C.; Haack, R.; Jansen, G.; Schulz, S., Bonding situation in Be[N(SiMe3)2]2 – an experimental and computational study. *Chem. Commun.* **2015,** *51*, 3889-3891.

77. Power, P. P., Main-group elements as transition metals. *Nature* **2010,** *463*, 171.

78. Wang, Y.; Xie, Y.; Wei, P.; King, R. B.; Schaefer, H. F.; von R. Schleyer, P.; Robinson, G. H., A Stable Silicon(0) Compound with a Si=Si Double Bond. *Science* **2008,** *321* (5892), 1069-1071.

79. Braunschweig, H.; Dewhurst, R. D.; Hammond, K.; Mies, J.; Radacki, K.; Vargas, A., Ambient-temperature isolation of a compound with a boron-boron triple bond. *Science* **2012,** *336* (6087), 1420-1422.

80. Wang, Y.; Xie, Y.; Abraham, M. Y.; Gilliard, R. J.; Wei, P.; Schaefer, H. F.; Schleyer, P. v. R.; Robinson, G. H., Carbene-Stabilized Parent Phosphinidene. *Organometallics* **2010,** *29* (21), 4778-4780.

81. Melancon, K. M.; Gildner, M. B.; Hudnall, T. W., Synthesis, Spectroscopic Characterization, and Redox Reactivity of a Cyclic (Alkyl) Amino Carbene-Derived Arsamethine Cyanine Dye. *Chem. Eur. J.* **2018,** *24* (37), 9264-9268.

82. Kretschmer, R.; Ruiz, D. A.; Moore, C. E.; Rheingold, A. L.; Bertrand, G., One-, Two-, and Three-Electron Reduction of a Cyclic Alkyl (amino) carbene–SbCl3 Adduct. *Angew. Chem. Int. Ed.* **2014,** *53* (31), 8176-8179.

83. Wang, G.; Freeman, L. A.; Dickie, D. A.; Mokrai, R.; Benkő, Z.; Gilliard Jr, R. J., Isolation of Cyclic(Alkyl)(Amino) Carbene–Bismuthinidene Mediated by a Beryllium(0) Complex. *Chem. Eur. J.* **2019,** *25* (17), 4335-4339.

84. Jones, D. D. L.; Douair, I.; Maron, L.; Jones, C., Photochemically Activated Dimagnesium(I) Compounds: Reagents for the Reduction and Selective C−H Bond Activation of Inert Arenes. *Angew. Chem. Int. Ed.* **2021,** *60* (13), 7087-7092.

85. Wang, G.; Walley, J. E.; Dickie, D. A.; Pan, S.; Frenking, G.; Gilliard, R. J., A Stable, Crystalline Beryllium Radical Cation. *J. Am. Chem. Soc.* **2020,** *142* (10), 4560-4564.

86. Czernetzki, C.; Arrowsmith, M.; Fantuzzi, F.; Gärtner, A.; Tröster, T.; Krummenacher, I.; Schorr, F.; Braunschweig, H., A Neutral Beryllium(I) Radical. *Angew. Chem. Int. Ed.* **2021,** *60* (38), 20776-20780.

87. Rösch, B.; Gentner, T. X.; Eyselein, J.; Langer, J.; Elsen, H.; Harder, S., Strongly reducing magnesium(0) complexes. *Nature* **2021,** *592* (7856), 717-721.

88. Fedushkin, I. L.; Khvoinova, N. M.; Skatova, A. A.; Fukin, G. K., Oxidative Addition of Phenylacetylene through C□H Bond Cleavage To Form the MgII–dpp-bian Complex: Molecular Structure of [Mg{dpp-bian(H)}(C□CPh)(thf)2] and Its Diphenylketone Insertion Product [Mg(dpp-bian).−{OC(Ph2)C□CPh}(thf)]. *Angew. Chem. Int. Ed.* **2003,** *42* (42), 5223-5226.

89. Fedushkin, I. L.; Morozov, A. G.; Rassadin, O. V.; Fukin, G. K., Addition of Nitriles to Alkaline Earth Metal Complexes of 1,2-Bis[(phenyl)imino]acenaphthenes. *Chem. Eur. J.* **2005,** *11* (19), 5749-5757.

90. Voutchkova, A. M.; Feliz, M.; Clot, E.; Eisenstein, O.; Crabtree, R. H., Imidazolium Carboxylates as Versatile and Selective N-Heterocyclic Carbene Transfer Agents: Synthesis, Mechanism, and Applications. *J. Am. Chem. Soc.* **2007,** *129* (42), 12834-12846.

91. Van Ausdall, B. R.; Glass, J. L.; Wiggins, K. M.; Aarif, A. M.; Louie, J., A Systematic Investigation of Factors Influencing the Decarboxylation of Imidazolium Carboxylates. *The Journal of Organic Chemistry* **2009,** *74* (20), 7935-7942.

92. Delaude, L., The Chemistry of Azolium-Carboxylate Zwitterions and Related Compounds: a Survey of the Years 2009–2020. *Advanced Synthesis & Catalysis* **2020,** *n/a* (n/a).

93. Jones, C., Bulky guanidinates for the stabilization of low oxidation state metallacycles. *Coord. Chem. Rev.* **2010,** *254* (11), 1273-1289.

94. de Bruin-Dickason, C. N.; Sutcliffe, T.; Alvarez Lamsfus, C.; Deacon, G. B.; Maron, L.; Jones, C., Kinetic stabilisation of a molecular strontium hydride complex using an extremely bulky amidinate ligand. *Chem. Commun.* **2018,** *54* (7), 786-789.

95. Arrowsmith, M.; Maitland, B.; Kociok-Köhn, G.; Stasch, A.; Jones, C.; Hill, M. S., Mononuclear Three-Coordinate Magnesium Complexes of a Highly Sterically Encumbered β-Diketiminate Ligand. *Inorg. Chem.* **2014,** *53* (19), 10543-10552.

96. Barrett, A. G. M.; Casely, I. J.; Crimmin, M. R.; Hill, M. S.; Lachs, J. R.; Mahon, M. F.; Procopiou, P. A., β-Diketiminato Calcium and Magnesium Amides; Model Complexes for Hydroamination Catalysis. *Inorg. Chem.* **2009,** *48* (10), 4445-4453.

97. Gibson, V. C.; Segal, J. A.; White, A. J. P.; Williams, D. J., Novel Mono-alkyl Magnesium Complexes Stabilized by a Bulky β-Diketiminate Ligand: Structural Characterization of a Coordinatively Unsaturated Trigonal System. *J. Am. Chem. Soc.* **2000,** *122* (29), 7120-7121.

98. Kennedy, A. R.; Mulvey, R. E.; Robertson, S. D., N-Heterocyclic carbene stabilized adducts of alkyl magnesium amide, bisalkyl magnesium and Grignard reagents: trapping oligomeric organo s-block fragments with NHCs. *Dalton Trans.* **2010,** *39* (38), 9091-9099.

99. Turner, Z. R.; Buffet, J.-C., Group 1 and 2 cyclic (alkyl)(amino)carbene complexes. *Dalton Trans.* **2015,** *44* (29), 12985-12989.

100. Turner, Z. R., Chemically Non-Innocent Cyclic (Alkyl)(Amino)Carbenes: Ligand Rearrangement, C−H and C−F Bond Activation. *Chem. Eur. J.* **2016,** *22* (32), 11461-11468.

101. Arduengo, A. J.; Davidson, F.; Krafczyk, R.; Marshall, W. J.; Tamm, M., Adducts of Carbenes with Group II and XII Metallocenes†. *Organometallics* **1998,** *17* (15), 3375-3382.

102. Mungur, S. A.; Liddle, S. T.; Wilson, C.; Sarsfield, M. J.; Arnold, P. L., Bent metal carbene geometries in amido N-heterocyclic carbene complexes. *Chem. Commun.* **2004,** (23), 2738-2739.

103. Stasch, A.; Sarish, S. P.; Roesky, H. W.; Meindl, K.; Dall'Antonia, F.; Schulz, T.; Stalke, D., Synthesis and Characterization of Alkynyl Complexes of Groups 1 and 2. *Chem. Asian J.* **2009,** *4* (9), 1451-1457.

104. Stasch, A., Synthesis of a Dimeric Magnesium(I) Compound by an MgI/MgII Redox Reaction. *Angew. Chem. Int. Ed.* **2014,** *53* (38), 10200-10203.

105. Baishya, A.; Peddarao, T.; Nembenna, S., Organomagnesium amide catalyzed cross-dehydrocoupling of organosilanes with amines. *Dalton Trans.* **2017,** *46* (18), 5880-5887.

106. Wong, Y. O.; Freeman, L. A.; Agakidou, A. D.; Dickie, D. A.; Webster, C. E.; Gilliard, R. J., Two Carbenes versus One in Magnesium Chemistry: Synthesis of Terminal Dihalide, Dialkyl, and Grignard Reagents. *Organometallics* **2019,** *38* (3), 688-696.

107. Baillie, S. E.; Clegg, W.; García-Álvarez, P.; Hevia, E.; Kennedy, A. R.; Klett, J.; Russo, L., Synthesis and characterization of an infinite sheet of metal–alkyl bonds: unfolding the elusive structure of an unsolvated alkali-metal trisalkylmagnesiate. *Chem. Commun.* **2011,** *47* (1), 388-390.

108. Hernán-Gómez, A.; Uzelac, M.; Baillie, S. E.; Armstrong, D. R.; Kennedy, A. R.; Fuentes, M. Á.; Hevia, E., Molecular Manipulations of a Utility Nitrogen–Heterocyclic Carbene by Sodium Magnesiate Complexes and Transmetallation Chemistry with Gold Complexes. *Chem. Eur. J.* **2018,** *24* (41), 10541-10549.

109. Uzelac, M.; Kennedy, A. R.; Hernán-Gómez, A.; Fuentes, M. Á.; Hevia, E., Heavier Alkali-metal Gallates as Platforms for Accessing Functionalized Abnormal NHC Carbene-Gallium Complexes. *Z.A.A.C.* **2016,** *642* (22), 1241-1244.

110. Martínez-Martínez, A. J.; Fuentes, M. Á.; Hernán-Gómez, A.; Hevia, E.; Kennedy, A. R.; Mulvey, R. E.; O'Hara, C. T., Alkali-Metal-Mediated Magnesiations of an N-Heterocyclic Carbene: Normal, Abnormal, and “Paranormal” Reactivity in a Single Tritopic Molecule. *Angew. Chem. Int. Ed.* **2015,** *54* (47), 14075-14079.

111. Robertson, S. D.; Uzelac, M.; Mulvey, R. E., Alkali-Metal-Mediated Synergistic Effects in Polar Main Group Organometallic Chemistry. *Chem. Rev.* **2019,** *119* (14), 8332-8405.

112. Thiele, K.-H.; Lorenz, V.; Thiele, G.; Zönnchen, P.; Scholz, J., [Be(dad)2]: Synthesis and Structure of a Diazabutadieneberyllium Complex. *Angew. Chem. Int. Ed. Engl.* **1994,** *33* (13), 1372-1373.

113. Liu, S.-F.; Wu, Q.; Schmider, H. L.; Aziz, H.; Hu, N.-X.; Popović, Z.; Wang, S., Syntheses, Structures, and Electroluminescence of New Blue/Green Luminescent Chelate Compounds: Zn(2-py-in)2(THF), BPh2(2-py-in), Be(2-py-in)2, and BPh2(2-py-aza) [2-py-in = 2-(2-pyridyl)indole; 2-py-aza = 2-(2-pyridyl)-7-azaindole]. *J. Am. Chem. Soc.* **2000,** *122* (15), 3671-3678.

114. Arrowsmith, M.; Hill, M. S.; Kociok-Köhn, G., Activation of N-Heterocyclic Carbenes by {BeH2} and {Be(H)(Me)} Fragments. *Organometallics* **2015,** *34* (3), 653-662.

115. Fedushkin, I. L.; Chudakova, V. A.; Skatova, A. A.; Khvoinova, N. M.; Kurskii, Y. A.; Glukhova, T. A.; Fukin, G. K.; Dechert, S.; Hummert, M.; Schumann, H., Monomeric Magnesium and Calcium Complexes containing the Rigid, Dianionic 1, 2-Bis[(2, 5-di-tert-butylphenyl)imino]acenaphthene (dtb-BIAN) and 1, 2-Bis[(2-biphenyl)imino]acenaphthene (bph-BIAN) Ligands. *Z.A.A.C.* **2004,** *630* (4), 501-507.

116. Fedushkin, I. L.; Chudakova, V. A.; Skatova, A. A.; Fukin, G. K., Solvent-free alkali and alkaline earth metal complexes of di-imine ligands. *Heteroatom Chemistry* **2005,** *16* (7), 663-670.

117. Bailey, P. J.; Dick, C. M.; Fabre, S.; Parsons, S.; Yellowlees, L. J., Complexation of dimethylmagnesium with α-diimines; structural and EPR characterisation of single electron and alkyl transfer products. *Dalton Trans.* **2006,** (13), 1602-1610.

118. Ma, M.; Wang, H.; Wang, J.; Shen, L.; Zhao, Y.; Xu, W. H.; Wu, B.; Yang, X. J., Mg-Mg-bonded compounds with N,N'-dipp-substituted phenanthrene-diamido and o-phenylene-diamino ligands. *Dalton Trans* **2019,** *48* (7), 2295-2299.

119. Anga, S.; Bhattacharjee, J.; Harinath, A.; Panda, T. K., Synthesis, structure and reactivity study of magnesium amidinato complexes derived from carbodiimides and N,N′-bis(2,6-diisopropylphenyl)-1,4-diaza-butadiene ligands. *Dalton Trans.* **2015,** *44* (3), 955-965.

120. Gao, J.; Liu, Y.; Zhao, Y.; Yang, X.-J.; Sui, Y., Syntheses and Structures of Magnesium Complexes with Reduced α-Diimine Ligands. *Organometallics* **2011,** *30* (22), 6071-6077.

121. Walley, J. E.; Breiner, G.; Wang, G.; Dickie, D. A.; Molino, A.; Dutton, J. L.; Wilson, D. J. D.; Gilliard, J. R. J., s-Block carbodicarbene chemistry: C(sp3)–H activation and cyclization mediated by a beryllium center. *Chem. Commun.* **2019,** *55* (13), 1967-1970.

122. Connelly, N. G.; Geiger, W. E., Chemical Redox Agents for Organometallic Chemistry. *Chem. Rev.* **1996,** *96* (2), 877-910.

123. Freeman, L. A.; Walley, J. E.; Obi, A. D.; Wang, G.; Dickie, D. A.; Molino, A.; Wilson, D. J. D.; Gilliard, R. J., Stepwise Reduction at Magnesium and Beryllium: Cooperative Effects of Carbenes with Redox Non-Innocent α-Diimines. *Inorg. Chem.* **2019,** *58* (16), 10554-10568.

124. Kaes, C.; Katz, A.; Hosseini, M. W., Bipyridine: The Most Widely Used Ligand. A Review of Molecules Comprising at Least Two 2,2‘-Bipyridine Units. *Chem. Rev.* **2000,** *100* (10), 3553-3590.

125. Su, Y.; Zhao, Y.; Gao, J.; Dong, Q.; Wu, B.; Yang, X.-J., Alkali Metal and Zinc Complexes of a Bridging 2,5-Diamino-1,4-Benzoquinonediimine Ligand. *Inorg. Chem.* **2012,** *51* (10), 5889-5896.

126. Liu, Y.; Li, S.; Yang, X.-J.; Yang, P.; Gao, J.; Xia, Y.; Wu, B., Synthesis and Structure of a Zinc−Zinc-Bonded Compound with a Monoanionic α-Diimine Ligand, [LZn−ZnL] (L = [(2,6-iPr2C6H3)NC(Me)]2−). *Organometallics* **2009,** *28* (17), 5270-5272.

127. Cole, B. E.; Wolbach, J. P.; Dougherty, W. G.; Piro, N. A.; Kassel, W. S.; Graves, C. R., Synthesis and Characterization of Aluminum-α-diimine Complexes over Multiple Redox States. *Inorg. Chem.* **2014,** *53* (7), 3899-3906.

128. Vaughan, B. A.; Webster-Gardiner, M. S.; Cundari, T. R.; Gunnoe, T. B., A rhodium catalyst for single-step styrene production from benzene and ethylene. *Science* **2015,** *348* (6233), 421.

129. Lawson, J. R.; Wilkins, L. C.; André, M.; Richards, E. C.; Ali, M. N.; Platts, J. A.; Melen, R. L., Synthesis and reactivity of N,N′-1,4-diazabutadiene derived borocations. *Dalton Trans.* **2016,** *45* (41), 16177-16181.

130. Chahkandi, M.; Bhatti, M. H.; Yunus, U.; Rehman, N.; Nadeem, M.; Tahir, M. N.; Zakria, M., Novel cocrystal of N-phthaloyl-β-alanine with 2,2–bipyridyl: Synthesis, computational and free radical scavenging activity studies. *J. Mol. Structure* **2018,** *1152*, 1-10.

131. Laine, T. V. K., Martti; Maaninen, Arto; Aitola, Erkki; Leskelä, Markku, Effect of Metal on the Ethylene Polymerization Behavior of a Diimine-Based Homogeneous Late Transition Metal Catalyst System. *Acta Chem. Scand.* **1999,** *53*, 968-973.

132. Bordwell, F. G., Equilibrium acidities in dimethyl sulfoxide solution. *Acc. Chem. Res.* **1988,** *21* (12), 456-463.

133. Obi, A. D.; Freeman, L. A.; Dickie, D. A.; Gilliard, R. J., N-Heterocyclic Carbene-Mediated Ring Opening of Reduced Diazamagnesacycles. *Organometallics* **2020,** *39* (24), 4575-4583.

134. Harder, S.; Spielmann, J.; Intemann, J.; Bandmann, H., Hydrogen Storage in Magnesium Hydride: The Molecular Approach. *Angew. Chem. Int. Ed.* **2011,** *50* (18), 4156-4160.

135. Sakintuna, B.; Lamari-Darkrim, F.; Hirscher, M., Metal hydride materials for solid hydrogen storage: A review. *International Journal of Hydrogen Energy* **2007,** *32* (9), 1121-1140.

136. Rusman, N. A. A.; Dahari, M., A review on the current progress of metal hydrides material for solid-state hydrogen storage applications. *International Journal of Hydrogen Energy* **2016,** *41* (28), 12108-12126.

137. Satyapal, S.; Petrovic, J.; Read, C.; Thomas, G.; Ordaz, G., The U.S. Department of Energy's National Hydrogen Storage Project: Progress towards meeting hydrogen-powered vehicle requirements. *Catal. Today* **2007,** *120* (3), 246-256.

138. Aldridge, S.; Downs, A. J., Hydrides of the Main-Group Metals: New Variations on an Old Theme. *Chem. Rev.* **2001,** *101* (11), 3305-3366.

139. Aldridge, S.; Jones, C., Modern main group chemistry. *Chem. Soc. Rev.* **2016,** *45* (4), 763-764.

140. Stampfer, J. F.; Holley, C. E.; Suttle, J. F., The Magnesium-Hydrogen System1-3. *J. Am. Chem. Soc.* **1960,** *82* (14), 3504-3508.

141. Stander, C. M.; Pacey, R. A., The lattice energy of magnesium hydride. *Journal of Physics and Chemistry of Solids* **1978,** *39* (8), 829-832.

142. Zachariasen, W. H.; Holley, C. E.; Stamper, J. F., Jnr, Neutron diffraction study of magnesium deuteride. *Acta Crystallographica* **1963,** *16* (5), 352-353.

143. Intemann, J.; Spielmann, J.; Sirsch, P.; Harder, S., Well-Defined Molecular Magnesium Hydride Clusters: Relationship between Size and Hydrogen-Elimination Temperature. *Chem. Eur. J.* **2013,** *19* (26), 8478-8489.

144. Wagemans, R. W. P.; van Lenthe, J. H.; de Jongh, P. E.; van Dillen, A. J.; de Jong, K. P., Hydrogen Storage in Magnesium Clusters: Quantum Chemical Study. *J. Am. Chem. Soc.* **2005,** *127* (47), 16675-16680.

145. For the sake of brevity, only a few examples are given here of the diverse range of ligand types used in group II hydride chemistry. For a comprehensive review of all structurally characterized molecular magnesium hydride complexes categorized by stabizing ligand see reference 4b.

146. Ruspic, C.; Harder, S., Big Ligands for Stabilization of Small Functionalities in Calcium Chemistry. *Inorg. Chem.* **2007,** *46* (24), 10426-10433.

147. Nesterov, V.; Reiter, D.; Bag, P.; Frisch, P.; Holzner, R.; Porzelt, A.; Inoue, S., NHCs in Main Group Chemistry. *Chem. Rev.* **2018,** *118* (19), 9678-9842.

148. Bellemin-Laponnaz, S.; Dagorne, S., Group 1 and 2 and Early Transition Metal Complexes Bearing N-Heterocyclic Carbene Ligands: Coordination Chemistry, Reactivity, and Applications. *Chem. Rev.* **2014,** *114* (18), 8747-8774.

149. Bruyere, J.-C.; Gourlaouen, C.; Karmazin, L.; Bailly, C.; Boudon, C.; Ruhlmann, L.; de Frémont, P.; Dagorne, S., Synthesis and Characterization of Neutral and Cationic Magnesium Complexes Supported by NHC Ligands. *Organometallics* **2019,** *38* (14), 2748-2757.

150. Stewart, C. A.; Dickie, D. A.; Parkes, M. V.; Saria, J. A.; Kemp, R. A., Reactivity of Bis(2,2,5,5-tetramethyl-2,5-disila-1-azacyclopent-1-yl)tin with CO2, OCS, and CS2 and

Comparison to That of Bis[bis(trimethylsilyl)amido]tin. *Inorg. Chem.* **2010,** *49* (23), 11133-11141.

151. Felix, A. M.; Boro, B. J.; Dickie, D. A.; Tang, Y.; Saria, J. A.; Moasser, B.; Stewart, C. A.; Frost, B. J.; Kemp, R. A., Insertion of CO 2 into divalent group 2 and 12 bis (silylamides). *Main Group Chemistry* **2012,** *11* (1), 13-29.

152. Westerhausen, M.; Schwarz, W., Molekül- und Kristallstruktur des Dimeren Magnesium-bis[bis(trimethylsilyl)amids]. *Z.A.A.C.* **1992,** *609* (3), 39-44.

153. Engelhardt, L.; Jolly, B.; Junk, P.; Raston, C.; Skelton, B.; White, A., Highly Hindered Amido-Lithium and Amido-Magnesium Complexes. Crystal-Structures of [Li(Mu-N(SiMe3)2)(Tetrahydrofuran)]2 and [MgBu^s(Mu-N(SiMe₃)₂)]2. *Aust. J. Chem.* **1986,** *39* (9), 1337-1345.

154. Wannagat, U.; Autzen, H.; Kuckertz, H.; Wismar, H.-J., Beiträge zur Chemie der Silicium–Stickstoff-Verbindungen. CXIII. Tetrakis(trimethylsilyl)-magnesiumdiamid. *Z.A.A.C.* **1972,** *394* (3), 254-262.

155. Brookhart, M.; Green, M. L. H.; Parkin, G., Agostic interactions in transition metal compounds. *Proc. Natl. Acad. Sci. U.S.A.* **2007,** *104* (17), 6908.

156. Wiesinger, M.; Maitland, B.; Elsen, H.; Pahl, J.; Harder, S., Stabilizing Magnesium Hydride Complexes with Neutral Ligands. *Eur. J. Inorg. Chem.* **2019,** *2019* (41), 4433-4439.

157. Bonyhady, S. J.; Collis, D.; Frenking, G.; Holzmann, N.; Jones, C.; Stasch, A., Synthesis of a stable adduct of dialane(4) (Al2H4) via hydrogenation of a magnesium(I) dimer. *Nat. Chem.* **2010,** *2*, 865.

158. Schnitzler, S.; Cui, P.; Spaniol, T. P.; Okuda, J., Molecular magnesium hydrides supported by an anionic triazacyclononane-type ligand. *Dalton Trans.* **2017,** *46* (6), 1761-1765.

159. Gallagher, D. J.; Henderson, K. W.; Kennedy, A. R.; O'Hara, C. T.; Mulvey, R. E.; Rowlings, R. B., Hydride encapsulation in s-block metal inverse crown chemistry. *Chem. Commun.* **2002,** (4), 376-377.

160. Lemmerz, L. E.; Mukherjee, D.; Spaniol, T. P.; Wong, A.; Ménard, G.; Maron, L.; Okuda, J., Cationic magnesium hydride [MgH]+ stabilized by an NNNN-type macrocycle. *Chem. Commun.* **2019,** *55* (22), 3199-3202.

161. Welz, E.; Böhnke, J.; Dewhurst, R. D.; Braunschweig, H.; Engels, B., Unravelling the Dramatic Electrostructural Differences Between N-Heterocyclic Carbene- and Cyclic (Alkyl)(amino)carbene-Stabilized Low-Valent Main Group Species. *J. Am. Chem. Soc.* **2018,** *140* (39), 12580-12591.

162. Holzmann, N.; Andrada, D. M.; Frenking, G., Bonding situation in silicon complexes [(L)2(Si2)] and [(L)2(Si)] with NHC and cAAC ligands. *Journal of Organometallic Chemistry* **2015,** *792*, 139-148.

163. Mondal, K. C.; Roesky, H. W.; Schwarzer, M. C.; Frenking, G.; Tkach, I.; Wolf, H.; Kratzert, D.; Herbst-Irmer, R.; Niepötter, B.; Stalke, D., Conversion of a Singlet Silylene to a stable Biradical. *Angewandte Chemie International Edition* **2012,** *52* (6), 1801-1805.

164. Rozenberg, I.; Eivgi, O.; Frenklah, A.; Butilkov, D.; Kozuch, S.; Goldberg, I.; Lemcoff, N. G., Synthesis and Catalytic Properties of Sulfur-Chelated Ruthenium Benzylidenes Bearing a Cyclic (Alkyl)(amino)carbene Ligand. *ACS Catalysis* **2018,** *8* (9), 8182-8191.

165. Bawari, D.; Goswami, B.; R, S. V.; Thakur, S. K.; Varun Tej, R. V.; Roy Choudhury, A.; Singh, S., Neutral and cationic cyclic (alkyl)(amino)carbene mercury [cAAC–Hg(ii)] complexes: scope of hydroamination of alkynes with organomercury compounds. *Dalton Transactions* **2018,** *47* (18), 6274-6278.

166. Eichhorn, A. F.; Kuehn, L.; Marder, T. B.; Radius, U., Facile insertion of a cyclic alkyl(amino) carbene carbon into the B–B bond of diboron(4) reagents. *Chemical Communications* **2017,** *53* (85), 11694-11696.

167. Soleilhavoup, M.; Bertrand, G., Cyclic (Alkyl)(Amino)Carbenes (CAACs): Stable Carbenes on the Rise. *Acc. Chem. Res.* **2015,** *48* (2), 256-266.

168. Melaimi, M.; Jazzar, R.; Soleilhavoup, M.; Bertrand, G., Cyclic (Alkyl)(amino)carbenes (CAACs): Recent Developments. **2017,** *56* (34), 10046-10068.

169. Lavallo, V.; Canac, Y.; Präsang, C.; Donnadieu, B.; Bertrand, G., Stable Cyclic (Alkyl)(Amino)Carbenes as Rigid or Flexible, Bulky, Electron-Rich Ligands for Transition-Metal Catalysts: A Quaternary Carbon Atom Makes the Difference. **2005,** *44* (35), 5705-5709.

170. Lavallo, V.; Canac, Y.; Präsang, C.; Donnadieu, B.; Bertrand, G., Stable Cyclic (Alkyl)(Amino)Carbenes as Rigid or Flexible, Bulky, Electron-Rich Ligands for Transition-Metal Catalysts: A Quaternary Carbon Atom Makes the Difference. **2005,** *117* (35), 5851-5855.

171. Lavallo, V.; Canac, Y.; Donnadieu, B.; Schoeller, W. W.; Bertrand, G., CO Fixation to Stable Acyclic and Cyclic Alkyl Amino Carbenes: Stable Amino Ketenes with a Small HOMO–LUMO Gap. **2006,** *45* (21), 3488-3491.

172. Luca, O. R.; McCrory, C. C. L.; Dalleska, N. F.; Koval, C. A., The Selective Electrochemical Conversion of Preactivated CO2 to Methane. **2015,** *162* (7), H473-H476.

173. Riduan, S. N.; Zhang, Y.; Ying, J. Y., Conversion of Carbon Dioxide into Methanol with Silanes over N-Heterocyclic Carbene Catalysts. **2009,** *48* (18), 3322-3325.

174. Riduan, S. N.; Zhang, Y.; Ying, J. Y., Conversion of Carbon Dioxide into Methanol with Silanes over N-Heterocyclic Carbene Catalysts. **2009,** *121* (18), 3372-3375.

175. Singh, A. P.; Samuel, P. P.; Roesky, H. W.; Schwarzer, M. C.; Frenking, G.; Sidhu, N. S.; Dittrich, B., A Singlet Biradicaloid Zinc Compound and Its Nonradical Counterpart. *J. Am. Chem. Soc.* **2013,** *135* (19), 7324-7329.

176. Savéant, J. M., Coupling of Electrode Electron Transfers with Homogeneous Chemical Reactions. In *Elements of Molecular and Biomolecular Electrochemistry*, John Wiley & Sons, Inc.: 2006.

177. Lieske, L. E.; Freeman, L. A.; Wang, G.; Dickie, D. A.; Gilliard, R. J., Jr.; Machan, C. W., Metal-Free Electrochemical Reduction of Carbon Dioxide Mediated by Cyclic(Alkyl)(Amino) Carbenes. *Chem. Eur. J.* **2019,** *25* (24), 6098-6101.

178. Machan, C. W.; Sampson, M. D.; Chabolla, S. A.; Dang, T.; Kubiak, C. P., Developing a Mechanistic Understanding of Molecular Electrocatalysts for CO2 Reduction using Infrared Spectroelectrochemistry. *Organometallics* **2014,** *33* (18), 4550-4559.

179. Zavarine, I. S.; Kubiak, C. P., A versatile variable temperature thin layer reflectance spectroelectrochemical cell. *J. Electroanal. Chem.* **2001,** *495* (2), 106–109.

180. Del Bene, J. E.; Alkorta, I.; Elguero, J., Carbenes as Electron-Pair Donors To CO2 for C⋯C Tetrel Bonds and C–C Covalent Bonds. *J. Phys. Chem. A* **2017,** *121* (20), 4039-4047.

181. Alecu, I. M.; Zheng, J.; Zhao, Y.; Truhlar, D. G., Computational Thermochemistry: Scale Factor Databases and Scale Factors for Vibrational Frequencies Obtained from Electronic Model Chemistries. *Journal of Chemical Theory and Computation* **2010,** *6* (9), 2872-2887.

182. Lavallo, V.; Canac, Y.; Donnadieu, B.; Schoeller, W. W.; Bertrand, G., CO Fixation to Stable Acyclic and Cyclic Alkyl Amino Carbenes: Stable Amino Ketenes with a Small HOMO–LUMO Gap. **2006,** *118* (21), 3568-3571.

183. Glendening, E. D.; Landis, C. R.; Weinhold, F., NBO 6.0: Natural bond orbital analysis program. **2013,** *34* (16), 1429-1437.

184. Glendening, E.; Badenhoop, J.; Reed, A.; Carpenter, J.; Bohmann, J.; Morales, C.; Landis, C.; Weinhold, F. J. T. C. I., University of Wisconsin, Madison, WI, Natural bond orbital analysis program: NBO 6.0. **2013**.

185. Moss, R. A.; Platz, M.; Jones, M., *Reactive intermediate chemistry*. Wiley Online Library: 2004.

186. Chen, H.; Armand, M.; Courty, M.; Jiang, M.; Grey, C. P.; Dolhem, F.; Tarascon, J.-M.; Poizot, P., Lithium Salt of Tetrahydroxybenzoquinone: Toward the Development of a Sustainable Li-Ion Battery. *J. Am. Chem. Soc.* **2009,** *131* (25), 8984-8988.

187. Cordes, H. F.; Richter, H. P.; Heller, C. A., Mass spectrometric evidence for the existence of 1, 2-dioxetanedione (carbon dioxide dimer). Chemiluminescent intermediate. *J. Am. Chem. Soc.* **1969,** *91* (25), 7209-7209.

188. Lackner, K. S.; Wendt, C. H.; Butt, D. P.; Joyce, E. L.; Sharp, D. H., Carbon dioxide disposal in carbonate minerals. *Energy* **1995,** *20* (11), 1153-1170.

189. Paparo, A.; Silvia, J. S.; Kefalidis, C. E.; Spaniol, T. P.; Maron, L.; Okuda, J.; Cummins, C. C., A Dimetalloxycarbene Bonding Mode and Reductive Coupling Mechanism for Oxalate Formation from CO2. *Angew. Chem. Int. Ed.* **2015,** *54* (31), 9115-9119.

190. Paparo, A.; Okuda, J., Carbonite, the dianion of carbon dioxide and its metal complexes. *J. Organomet. Chem.* **2018,** *869*, 270-274.

191. von Baczko, K., *Kohlenstoff: Chemisches Verhalten von CO und CO2. Teil C2*. Verlag Chemie: 1972.

192. Hauge, R. H.; Margrave, J. L.; Kauffman, J. W.; Rao, N. A.; Konarski, M. M.; Bell, J. P.; Billups, W. E., Matrix isolation studies on the lithium-induced reductive coupling of carbon dioxide. *J. Chem. Soc. Chem. Commun.* **1981,** (24), 1258-1260.

193. Kafafi, Z. H.; Hauge, R. H.; Billups, W. E.; Margrave, J. L., Carbon dioxide activation by alkali metals. 2. Infrared spectra of M+CO2- and M22+CO22- in argon and nitrogen matrixes. *Inorg. Chem.* **1984,** *23* (2), 177-183.

194. Arduengo, A. J.; Harlow, R. L.; Kline, M., A stable crystalline carbene. *J. Am. Chem. Soc.* **1991,** *113* (1), 361-363.

195. Lavallo, V.; Canac, Y.; Präsang, C.; Donnadieu, B.; Bertrand, G., Stable Cyclic (Alkyl)(Amino)Carbenes as Rigid or Flexible, Bulky, Electron-Rich Ligands for Transition-Metal Catalysts: A Quaternary Carbon Atom Makes the Difference. *Angew. Chem.* **2005,** *117* (35), 5851-5855.

196. Melaimi, M.; Jazzar, R.; Soleilhavoup, M.; Bertrand, G., Cyclic (Alkyl)(amino)carbenes (CAACs): Recent Developments. *Angew. Chem. Int. Ed.* **2017,** *56* (34), 10046-10068.

197. Marion, N.; Nolan, S. P., N-Heterocyclic carbenes in gold catalysis. *Chem. Soc. Rev.* **2008,** *37* (9), 1776-1782.

198. Díez-González, S.; Marion, N.; Nolan, S. P., N-Heterocyclic Carbenes in Late Transition Metal Catalysis. *Chem. Rev.* **2009,** *109* (8), 3612-3676.

199. Herrmann, W. A., N-Heterocyclic Carbenes: A New Concept in Organometallic Catalysis. *Angew. Chem. Int. Ed.* **2002,** *41* (8), 1290-1309.

200. Hopkinson, M. N.; Richter, C.; Schedler, M.; Glorius, F., An overview of N-heterocyclic carbenes. *Nature* **2014,** *510*, 485.

201. Riduan, S. N.; Zhang, Y.; Ying, J. Y., Conversion of Carbon Dioxide into Methanol with Silanes over N-Heterocyclic Carbene Catalysts. *Angew. Chem. Int. Ed.* **2009,** *48* (18), 3322-3325.

202. Frey, G. D.; Lavallo, V.; Donnadieu, B.; Schoeller, W. W.; Bertrand, G., Facile Splitting of Hydrogen and Ammonia by Nucleophilic Activation at a Single Carbon Center. *Science* **2007,** *316* (5823), 439.

203. Phillips, E. M.; Reynolds, T. E.; Scheidt, K. A., Highly Diastereo- and Enantioselective Additions of Homoenolates to Nitrones Catalyzed by N-Heterocyclic Carbenes. *J. Am. Chem. Soc.* **2008,** *130* (8), 2416-2417.

204. Enders, D.; Niemeier, O.; Henseler, A., Organocatalysis by N-Heterocyclic Carbenes. *Chem. Rev.* **2007,** *107* (12), 5606-5655.

205. Regnier, V.; Romero, E. A.; Molton, F.; Jazzar, R.; Bertrand, G.; Martin, D., What Are the Radical Intermediates in Oxidative N-Heterocyclic Carbene Organocatalysis? *J. Am. Chem. Soc.* **2019,** *141* (2), 1109-1117.

206. Grossmann, A.; Enders, D., N-Heterocyclic Carbene Catalyzed Domino Reactions. *Angew. Chem. Int. Ed.* **2012,** *51* (2), 314-325.

207. Mahoney, J. K.; Regnier, V.; Romero, E. A.; Molton, F.; Royal, G.; Jazzar, R.; Martin, D.; Bertrand, G., The serendipitous discovery of a readily available redox-bistable molecule derived from cyclic(alkyl)(amino)carbenes. *Org. Chem. Front.* **2018,** *5* (13), 2073-2078.

208. Ryan, S. J.; Candish, L.; Lupton, D. W., Acyl anion free N-heterocyclic carbene organocatalysis. *Chem. Soc. Rev.* **2013,** *42* (12), 4906-4917.

209. Li, Z.; Mayer, R. J.; Ofial, A. R.; Mayr, H., From Carbodiimides to Carbon Dioxide: Quantification of the Electrophilic Reactivities of Heteroallenes. *J. Am. Chem. Soc.* **2020,** *142* (18), 8383-8402.

210. Voutchkova, A. M.; Appelhans, L. N.; Chianese, A. R.; Crabtree, R. H., Disubstituted Imidazolium-2-Carboxylates as Efficient Precursors to N-Heterocyclic Carbene Complexes of Rh, Ru, Ir, and Pd. *J. Am. Chem. Soc.* **2005,** *127* (50), 17624-17625.

211. Wang, Y.-B.; Sun, D.-S.; Zhou, H.; Zhang, W.-Z.; Lu, X.-B., CO2, COS and CS2 adducts of N-heterocyclic olefins and their application as organocatalysts for carbon dioxide fixation. *Green Chemistry* **2015,** *17* (7), 4009-4015.

212. Zhou, H.; Zhang, W.-Z.; Liu, C.-H.; Qu, J.-P.; Lu, X.-B., CO2 Adducts of N-Heterocyclic Carbenes: Thermal Stability and Catalytic Activity toward the Coupling of CO2 with Epoxides. *The Journal of Organic Chemistry* **2008,** *73* (20), 8039-8044.

213. Theuergarten, E.; Bannenberg, T.; Walter, M. D.; Holschumacher, D.; Freytag, M.; Daniliuc, C. G.; Jones, P. G.; Tamm, M., Computational and experimental investigations of CO2 and N2O fixation by sterically demanding N-heterocyclic carbenes (NHC) and NHC/borane FLP systems. *Dalton Trans.* **2014,** *43* (4), 1651-1662.

214. Talapaneni, S. N.; Buyukcakir, O.; Je, S. H.; Srinivasan, S.; Seo, Y.; Polychronopoulou, K.; Coskun, A., Nanoporous Polymers Incorporating Sterically Confined N-Heterocyclic Carbenes for Simultaneous CO2 Capture and Conversion at Ambient Pressure. *Chem. Mat.* **2015,** *27* (19), 6818-6826.

215. Finn, C.; Schnittger, S.; Yellowlees, L. J.; Love, J. B., Molecular approaches to the electrochemical reduction of carbon dioxide. *Chem. Commun.* **2012,** *48* (10), 1392-1399.

216. Kuchenbeiser, G.; Soleilhavoup, M.; Donnadieu, B.; Bertrand, G., Reactivity of Cyclic (Alkyl)(amino)carbenes (CAACs) and Bis(amino)cyclopropenylidenes (BACs) with Heteroallenes: Comparisons with their N-Heterocyclic Carbene (NHCs) Counterparts. *Chem. Asian J.* **2009,** *4* (11), 1745-1750.

217. Hans, M.; Delaude, L.; Rodriguez, J.; Coquerel, Y., N-Heterocyclic Carbene Catalyzed Carba-, Sulfa-, and Phospha-Michael Additions with NHC·CO2 Adducts as Precatalysts. *The Journal of Organic Chemistry* **2014,** *79* (6), 2758-2764.

218. Tolentino, D. R.; Neale, S. E.; Isaac, C. J.; Macgregor, S. A.; Whittlesey, M. K.; Jazzar, R.; Bertrand, G., Reductive Elimination at Carbon under Steric Control. *J. Am. Chem. Soc.* **2019,** *141* (25), 9823-9826.

219. Luca, O. R.; McCrory, C. C. L.; Dalleska, N. F.; Koval, C. A., The Selective Electrochemical Conversion of Preactivated CO2to Methane. *Journal of The Electrochemical Society* **2015,** *162* (7), H473-H476.

220. Luca, O. R.; Fenwick, A. Q., Organic reactions for the electrochemical and photochemical production of chemical fuels from CO2 – The reduction chemistry of carboxylic acids and derivatives as bent CO2 surrogates. *Journal of Photochemistry and Photobiology B: Biology* **2015,** *152*, 26-42.

221. Wakefield, B. J., *The chemistry of organolithium compounds*. Elsevier: 2013.

222. Kaufmann, E.; Sieber, S.; Schleyer, P. v. R., Carboxylation of lithium compounds: ab initio mechanisms. *J. Am. Chem. Soc.* **1989,** *111* (11), 4005-4008.

223. Bresciani, G.; Biancalana, L.; Pampaloni, G.; Marchetti, F., Recent Advances in the Chemistry of Metal Carbamates. *Molecules* **2020,** *25* (16).

224. Kennedy, A. R.; Mulvey, R. E.; Oliver, D. E.; Robertson, S. D., Lithium and aluminium carbamato derivatives of the utility amide 2,2,6,6-tetramethylpiperidide. *Dalton Trans.* **2010,** *39* (27), 6190-6197.

225. Freeman, L. A.; Obi, A. D.; Machost, H. R.; Molino, A.; Nichols, A. W.; Dickie, D. A.; Wilson, D. J. D.; Machan, C. W.; Gilliard, R. J., Soluble, crystalline, and thermally stable alkali CO2− and carbonite (CO22−) clusters supported by cyclic(alkyl)(amino) carbenes. *Chem. Sci.* **2021,** *12* (10), 3544-3550.

226. The bulk mixture of 5 and 6 was analyzed as one product with a varying amount of THF, as discussed in the SI. As such, this yield is given with respect to the chemical formula of the bulk mixture as determined by combustion analysis.

227. Gentner, T. X.; Mulvey, R. E., Alkali-Metal Mediation: Diversity of Applications in Main-Group Organometallic Chemistry. *Angew. Chem. Int. Ed. Engl.* **2021,** *60* (17), 9247-9262.

228. Rajca, A., Organic diradicals and polyradicals: from spin coupling to magnetism? *Chem. Rev.* **1994,** *94* (4), 871-893.

229. Carl Lineberger, W.; Thatcher Borden, W., The synergy between qualitative theory, quantitative calculations, and direct experiments in understanding, calculating, and measuring the energy differences between the lowest singlet and triplet states of organic diradicals. *Physical Chemistry Chemical Physics* **2011,** *13* (25), 11792-11813.

230. Salem, L.; Rowland, C., The Electronic Properties of Diradicals. *Angew. Chem. Int. Ed. Engl.* **1972,** *11* (2), 92-111.

231. Abe, M., Diradicals. *Chem. Rev.* **2013,** *113* (9), 7011-7088.

232. Freeman, L. A.; Walley, J. E.; Dickie, D. A.; Gilliard, R. J., Low-nuclearity magnesium hydride complexes stabilized by N-heterocyclic carbenes. *Dalton Trans.* **2019,** *48* (46), 17174-17178.

233. Buch, F.; Brettar, J.; Harder, S., Hydrosilylation of Alkenes with Early Main-Group Metal Catalysts. *Angew. Chem.* **2006,** *118* (17), 2807-2811.

234. Penafiel, J.; Maron, L.; Harder, S., Early Main Group Metal Catalysis: How Important is the Metal? *Angew. Chem. Int. Ed.* **2015,** *54* (1), 201-206.

235. Lavallo, V.; Canac, Y.; Prasang, C.; Donnadieu, B.; Bertrand, G., Stable cyclic (alkyl)(amino)carbenes as rigid or flexible, bulky, electron-rich ligands for transition-metal catalysts: a quaternary carbon atom makes the difference. *Angew. Chem. Int. Ed.* **2005,** *44* (35), 5705-5709.

236. Kuhn, N.; Kratz, T., Synthesis of Imidazol-2-ylidenes by Reduction of Imidazole-2(3H)-thiones. *Synthesis* **1993,** *1993* (06), 561-562.

237. Hicks, J.; Juckel, M.; Paparo, A.; Dange, D.; Jones, C., Multigram Syntheses of Magnesium(I) Compounds Using Alkali Metal Halide Supported Alkali Metals as Dispersible Reducing Agents. *Organometallics* **2018,** *37* (24), 4810-4813.

238. Frisch, M. J.; Trucks, G. W.; Schlegel, H. B.; Scuseria, G. E.; Robb, M. A.; Cheeseman, J. R.; Scalmani, G.; Barone, V.; Petersson, G. A.; Nakatsuji, H.; Li, X.; Caricato, M.; Marenich, A. V.; Bloino, J.; Janesko, B. G.; Gomperts, R.; Mennucci, B.; Hratchian, H. P.; Ortiz, J. V.; Izmaylov, A. F.; Sonnenberg, J. L.; Williams; Ding, F.; Lipparini, F.; Egidi, F.; Goings, J.; Peng, B.; Petrone, A.; Henderson, T.; Ranasinghe, D.; Zakrzewski, V. G.; Gao, J.; Rega, N.; Zheng, G.; Liang, W.; Hada, M.; Ehara, M.; Toyota, K.; Fukuda, R.; Hasegawa, J.; Ishida, M.; Nakajima, T.; Honda, Y.; Kitao, O.; Nakai, H.; Vreven, T.; Throssell, K.; Montgomery Jr., J. A.; Peralta, J. E.; Ogliaro, F.; Bearpark, M. J.; Heyd, J. J.; Brothers, E. N.; Kudin, K. N.; Staroverov, V. N.; Keith, T. A.; Kobayashi, R.; Normand, J.; Raghavachari, K.; Rendell, A. P.; Burant, J. C.; Iyengar, S. S.; Tomasi, J.; Cossi, M.; Millam, J. M.; Klene, M.; Adamo, C.; Cammi, R.; Ochterski, J. W.; Martin, R. L.; Morokuma, K.; Farkas, O.; Foresman, J. B.; Fox, D. J. *Gaussian 16 Rev. A.03*, Wallingford, CT, 2016.

239. Grimme, S.; Antony, J.; Ehrlich, S.; Krieg, H., A consistent and accurate ab initio parametrization of density functional dispersion correction (DFT-D) for the 94 elements H-Pu. *J. Chem. Phys.* **2010,** *132* (15), 154104.

240. Weigend, F.; Ahlrichs, R., Balanced basis sets of split valence, triple zeta valence and quadruple zeta valence quality for H to Rn: Design and assessment of accuracy. *Phys. Chem. Chem. Phys.* **2005,** *7* (18), 3297-3305.

241. Zhao, Y.; Truhlar, D. G., The M06 suite of density functionals for main group thermochemistry, thermochemical kinetics, noncovalent interactions, excited states, and transition elements: two new functionals and systematic testing of four M06-class functionals and 12 other functionals. *Theor. Chem. Acc.* **2008,** *120* (1), 215-241.

242. Grimme, S.; Ehrlich, S.; Goerigk, L., Effect of the damping function in dispersion corrected density functional theory. *J. Comput. Chem.* **2011,** *32* (7), 1456-1465.

243. Marenich, A. V.; Cramer, C. J.; Truhlar, D. G., Universal Solvation Model Based on Solute Electron Density and on a Continuum Model of the Solvent Defined by the Bulk Dielectric Constant and Atomic Surface Tensions. *J. Phys. Chem. B* **2009,** *113* (18), 6378-6396.

244. Glendening, E. D.; J, K. B.; Reed, A. E.; Carpenter, J. E.; Bohmann, J. A.; Morales, C. M.; Landis, C. R.; Weinhold, F. *NBO 6.0*, Theoretical Chemistry Institute, University of Wisconsin, Madison: 2013.

245. E. J. Baerends, T. Z., J. Autschbach, D. Bashford,; A. Bérces, F. M. B., C. Bo, P. M. Boerrigter,; L. Cavallo, D. P. C., L. Deng, R. M. Dickson, D. E. Ellis,; M. van Faassen, L. F., T. H. Fischer, C. Fonseca Guerra,; A. Ghysels, A. G., S. J. A. van Gisbergen,; A. W. Götz, J. A. G., O. V. Gritsenko, M. Grüning,; S. Gusarov, F. E. H., P. van den Hoek, C. R. Jacob,; H. Jacobsen, L. J., J. W. Kaminski, G. van Kessel,; F. Kootstra, A. K., M. V. Krykunov, E. van Lenthe,; D. A. McCormack, A. M., M. Mitoraj, J. Neugebauer,; V. P. Nicu, L. N., V. P. Osinga, S. Patchkovskii,; P. H. T. Philipsen, D. P., C. C. Pye, W. Ravenek,; J. I. Rodríguez, P. R., P. R. T. Schipper, G. Schreckenbach,; J. S. Seldenthuis, M. S., J. G. Snijders, M. Solà, M. Swart,; D. Swerhone, G. t. V., P. Vernooijs, L. Versluis,; L. Visscher, O. V., F. Wang, T. A. Wesolowski, E. M. van; Wezenbeek, G. W., S. K. Wolff, T. K. Woo and; Yakovlev, A. L. *ADF2012*, SCM: Vrije Universiteit, Amsterdam, The Netherlands.

246. Neese, F., Software update: the ORCA program system, version 4.0. *WIREs Computational Molecular Science* **2018,** *8* (1), e1327.